

**R**  
**ADIOLGY**  
**AND**  
**ONCOLOGY**



**vol.53 no.1**  
**march 2019**

# NOVO

# CABOMETYX®

(kabozantinib) tablete

60 mg | 40 mg | 20 mg

## CABOMETYX® pomembno izboljša PFS, OS in ORR in drugi liniji zdravljenja napredovalega karcinoma ledvičnih celic<sup>1</sup>

### RAZŠIRITEV INDIKACIJE:

Sedaj tudi za zdravljenje napredovalega karcinoma ledvičnih celic (KLC) pri predhodno nezdravljenih odraslih bolnikih s srednje ugodnim ali slabim prognostičnim obetom.<sup>2</sup>

- ✓ PFS<sup>2</sup>
- ✓ OS<sup>2</sup>
- ✓ ORR<sup>2</sup>

ORR: objektivna stopnja odziva; OS: celokupno preživetje; PFS: preživetje brez napredovanja bolezni

#### Referenci:

1. Choueiri TK, Escudier B, Powles T, et al. Cabozantinib versus everolimus in advanced renal cell carcinoma (METEOR): final results from a randomised, open-label, phase 3 trial. *The Lancet Oncology*. 2016;17(7):917-27.
2. Povzetek glavnih značilnosti zdravila Cabometyx.

## Skrajšan povzetek glavnih značilnosti zdravila

**CABOMETYX 20 mg filmsko obložene tablete**  
**CABOMETYX 40 mg filmsko obložene tablete**  
**CABOMETYX 60 mg filmsko obložene tablete**  
(kabozantinib)

**TERAPEVTSKE INDIKACIJE** Zdravljenje napredovalega karcinoma ledvičnih celic (KLC) pri predhodno nezdravljenih odraslih bolnikih s srednje ugodnim ali slabim prognostičnim obetom ter pri odraslih bolnikih po predhodnem zdravljenju, usmerjenem v vaskularni endoteljski rastni faktor (VEGF). V monoterapiji zdravljenje hepatocelularnega karcinoma (HCK) pri odraslih bolnikih, ki so se predhodno že zdravili s sorafenibom. **ODMERJANJE IN NAČIN UPORABE** Pri bolnikih s KLC in HCK je poročen odmerek 60 mg enkrat na dan. Zdravljenje je treba nadaljevati tako dolgo, dokler bolnik več nima kliničnih koristi od terapije ali do pojava nesprejemljive toksičnosti. Pri sumu na neželeno reakcijo na zdravilo bo morda treba zdravljenje začasno prekiniti in/ali zmanjšati odmerek. Če je treba odmerek zmanjšati, se priporoča zmanjšanje na 40 mg na dan in nato na 20 mg na dan. Prekinitev odmerka se priporoča pri obravnavi toksičnosti 3. ali višje stopnje po CTCAE (*common terminology criteria for adverse events*) ali nevzdržni toksičnosti 2. stopnje. Zmanjšanje odmerka se priporoča za dogodke, ki bi lahko čez čas postali resni ali nevzdržni. V primeru pojavnosti neželenih učinkov 1. in 2. stopnje, ki jih bolnik prenaša in jih je možno enostavno obravnavati, prilagoditev odmerjanja običajno ni potrebna. Treba je uvesti podporno oskrbo. V primeru pojavnosti neželenih učinkov 2. stopnje, ki jih bolnik ne prenaša in jih je mogoče obravnavati z zmanjšanjem odmerka ali podporno oskrbo, je treba zdravljenje prekiniti, dokler neželeni učinki ne izzvenijo do ≤ 1. stopnje, uvesti podporno oskrbo in razmisli o ponovni uvedbi zdravljenja z zmanjšanim odmerkom. V primeru pojavnosti neželenih učinkov 3. stopnje je treba zdravljenje prekiniti, dokler neželeni učinki ne izzvenijo do ≤ 1. stopnje, uvesti podporno oskrbo in ponovno uvesti zdravljenje z zmanjšanim odmerkom. V primeru pojavnosti neželenih učinkov 4. stopnje je treba zdravljenje prekiniti, uvesti ustrezno zdravniško oskrbo, in če neželeni učinki izzvenijo do ≤ 1. stopnje, ponovno uvesti zdravljenje z zmanjšanim odmerkom. Če neželeni učinki ne izzvenijo, je treba trajno prenehati z uporabo zdravila. Pri bolnikih z blago ali zmerno ledvično okvaro je treba kabozantinib uporabljati previdno. Uporaba se ne priporoča pri bolnikih s hudo ledvično okvaro. Pri bolnikih z blago okvaro jeter odmerka ni treba prilagajati. Pri bolnikih z zmerno okvaro jeter (Child Pugh B) priporočil za odmerjanje ni možno podati. Pri teh bolnikih je priporočljivo skrbno spremljanje celokupne varnosti. Pri bolnikih s hudo okvaro jeter (Child Pugh C) uporaba kabozantiniba ni priporočljiva. **Način uporabe:** Tablete je treba pogoltniti cele in jih ni dovoljeno drobiti. Bolnikom je treba naročiti, naj vsaj 2 uri pred uporabo zdravila in 1 uro po tem nicesar ne jedo. **KONTRAINDIKACIJE** Preobčutljivost na učinkovino ali katero koli pomožno snov. **POSEBNA OPOZORILA IN PREVIDNOSTNI UKREPI** Večina dogodkov se pojavi zgodaj v teku zdravljenja, zato mora zdravnik bolnika v prvih 8 tednih zdravljenja skrbno spremljati, da oceni, ali je treba odmerek prilagoditi. Dogodki, ki se običajno pojavijo zgodaj, vključujejo hipokalcemijo, hipokaliemijo, trombotično/petehijalno, hipertenzijo, sindrom palmarno-plantarne eritrodisezije (PPES), proteinurijo in gastrointestinalne dogodke (bolečine v trebuhu, vnetje sluznice, zaprtje, driska, bruhanje). Pred uvedbo zdravljenja s kabozantinibom je priporočljivo izvesti preiskave delovanja jeter (ALT, AST in bilirubin), vrednosti skrbno spremljati med zdravljenjem in po potrebi prilagoditi odmerek. Bolnike je treba spremljati glede znakov in simptomov jetrne encelofalopatije. Bolnike, ki imajo vnetno bolezen zvezca (npr. Crohnovo bolezen, ulcerozni kolitis, peritonitis, divertikulitis ali apendicitis), ki imajo tumorsko infiltracijo prebavil ali so imeli pred posegom na prebavnih zapletih (zlasti v povezavi z zapoznelim ali nepopolnim celjenjem), je treba pred uvedbo zdravljenja skrbno oceniti, nato pa natančno spremljati za pojav simptomov perforaciji in fistul, vključno z abscesi in sepsa. Trajna ali

▼ Za to zdravilo se izvaja dodatno spremljanje varnosti. Tako bodo hitreje na voljo nove informacije o njegovi varnosti. Zdravstvene delavce naprošamo, da poročajo o katerem koli domnevnem neželenem učinku zdravila.

ponavljajoča se driska med zdravljenjem je lahko dejavnik tveganja za nastanek analne fistule. Uporaba kabozantiniba je treba pri bolnikih, pri katerih se pojavi gastrointestinalna perforacija ali fistula, ki je ni možno ustrezno obravnavati, prekiniti. Driska, navzea/bruhanje, zmanjšanje apetita in vnetje ustne sluznice/bolečina v ustni votlini so nekateri od najpogostejših poročanih neželenih učinkov na prebavila. Nemudoma je treba uvesti ustrezne medicinske ukrepe, vključno s podpornim zdravljenjem z antiemetiki, antiidiariki ali antacidi, da se prepreči dehidracija, neravnovesje elektrolitov in izguba telesne mase. Če pomembni neželeni učinki na prebavila vztrajajo ali se ponavljajo, je treba presoditi o prekinitvi odmerjanja, zmanjšanju odmerka ali trajni ukinitvi zdravljenja s kabozantinibom. Kabozantinib je treba uporabljati previdno pri bolnikih, pri katerih obstaja tveganje za pojav venske tromboembolije, vključno s pljučno embolijo, in arterijske tromboembolije ali imajo te dogodke v anamnezi. Z uporabo je treba prenehati pri bolnikih, pri katerih se razvije akutni miokardni infarkt ali drugi klinično pomembni znaki zapletov tromboembolije. Kabozantiniba se ne sme dajati bolnikom, ki hudo krvavijo, ali pri katerih obstaja tveganje za hudo krvavitev. Med zdravljenjem s kabozantinibom je treba spremljati vrednosti trombocitov in odmerek prilagoditi glede na resnost trombocitopenije. Zdravljenje s kabozantinibom je treba ustaviti vsaj 28 dni pred načrtovanim kirurškim posegom, vključno z zobozdravstvenim, če je mogoče. Kabozantinib je treba ukiniti pri bolnikih z zapleti s celjenjem rane, zaradi katerih je potrebna zdravniška pomoč. Pred uvedbo kabozantiniba je treba dobro obvladati krvni tlak. Med zdravljenjem je treba vse bolnike spremljati za pojav hipertenzije in jih po potrebi zdraviti s standardnimi antihipertenzivi. V primeru trdovratne hipertenzije, kljub uporabi antihipertenzivov, je treba odmerek kabozantiniba zmanjšati. Z uporabo je treba prenehati, če je hipertenzija resna ali trdovratna kljub zdravljenju z antihipertenzivi in zmanjšanemu odmerku kabozantiniba. V primeru hipertenzijske krize je treba zdravljenje prekiniti. Pri resni PPES je treba razmisliti o prekinitvi zdravljenja. Nadaljevanje zdravljenja naj se začne z nižjim odmerkom, ko se PPES umiri do 1. stopnje. V času zdravljenja je treba redno spremljati beljakovine v urinu. Pri bolnikih, pri katerih se razvije nefrotični sindrom, je treba z uporabo kabozantiniba prenehati. Pri uporabi kabozantiniba so opazili sindrom reverzibilne posteriorne levkoencefalopatije (RPLS), znan tudi kot sindrom posteriorne reverzibilne encelofalopatije (PRES). Na ta sindrom je treba pomisliti pri vseh bolnikih s številnimi prisotnimi simptomi, vključno s epileptičnimi napadi, glavobolom, motnjami vida, zmedenostjo ali spremenjenim mentalnim delovanjem. Pri bolnikih z RPLS je treba zdravljenje prekiniti. Kabozantinib je treba uporabljati previdno pri bolnikih s podaljšanjem intervala QT v anamnezi, pri bolnikih, ki jemljejo antiaritmike, in pri bolnikih z relevantno obstoječo boleznijo srca, bradikardijo ali elektrolitskimi motnjami. Uporaba kabozantiniba je bila povezana z večjo pojavnostjo elektrolitskih nepravilnosti (vključno s hipokaliemijo, hiperkaliemijo, hipomagnezjemijo, hipokalcemijo in hiponatremijo), zato je priporočljivo spremljati biokemijske parametre in po potrebi uvesti ustrezno nadomestno zdravljenje v skladu s standardno klinično prakso. Bolniki z redko dedno intoleranco za galaktozo, lapsonsko obliko zmanjšane aktivnosti laktaze ali malabsorpcijo glukoze/galaktoze ne smejo jemati tega zdravila. **Ploščnosti, posebnosti in dolžine.** Ženskam v rodni dobi je treba svetovati, da v času zdravljenja s kabozantinibom ne smejo zanositi. Zanositev morajo preprečiti tudi ženske partnerice moških bolnikov, ki uporabljajo kabozantinib. Med zdravljenjem in še vsaj 4 mesece po končanju terapije morajo tako bolniki in bolnice kot tudi njihovi partnerji uporabljati zanesljiv način kontracepcije. Kabozantiniba se ne sme uporabljati med nosečnostjo, razen če zdravljenje ni nujno potrebno zaradi kliničnega stanja ženske. Matere med zdravljenjem s kabozantinibom in še 4 mesece po končanju terapije ne smejo dojiti. Zdravljenje s kabozantinibom lahko predstavlja tveganje za plodnost pri moških in ženskah. **INTERAKCIJE** Kabozantinib je substrat za CYP3A4. Pri sočasni uporabi močnih zaviralcev CYP3A4 (npr. ritonavirja, itrakonazola, eritromicina, klaritromicina, soka grenivke) je potrebna previdnost. Kronični sočasni uporabi močnih

induktorjev CYP3A4 (npr. fenitoina, karbamazepina, rifampicina, fenobarbitala ali pripravkov zeliščnega izvora iz šentjanževke) se je treba izogibati. Razmisliti je treba o sočasni uporabi alternativnih zdravil, ki CYP3A4 ne inducirajo in ne zavirajo ali pa inducirajo in zavirajo le neznatno. Pri sočasni uporabi zaviralcev MRP2 (npr. ciklosporin, efavirenz, emtricitabin) je potrebna previdnost, saj lahko povzročijo povečanje koncentracij kabozantiniba v plazmi. Učinka kabozantiniba na farmakokinetiko kontraceptivnih steroidov niso preučili, vendar pa se priporoča dodatna kontracepcijska metoda (pregradna metoda). Zaradi visoke stopnje vezave kabozantiniba na plazemske beljakovine je možna interakcija z varfarinom v obliki izpodrivanja s plazemskih beljakovin, zato je treba spremljati vrednosti INR. Kabozantinib morda lahko poveča koncentracije sočasno uporabljenih substratov P-gp v plazmi. Osebe je treba opozoriti na uporabo substratov P-gp (npr. feksofenadina, aliskirena, ambrisentana, dabigatran eteksilata, digoksina, kolhicina, maraviroka, posakonazola, ranolazina, saksagliptina, sitagliptina, talinolola, tolvaptana) sočasno s kabozantinibom. **NEŽELENI UČINKI** Za popolno informacijo o neželenih učinkih, prosimo, preberite celoten povzetek glavnih značilnosti zdravila Cabometyx. Najpogostejši resni neželeni učinki zdravila v populaciji bolnikov s KLC so bili driska, hipertenzija, dehidracija, hiponatremija, navzea, zmanjšanje apetita, embolija, utrujenost, hipomagnezija in PPES. Najpogostejši neželeni učinki katere koli stopnje (ki so se pojavili pri vsaj 25 % bolnikov) v populaciji bolnikov s KLC so bili driska, hipertenzija, utrujenost, zvišanje vrednosti AST, zvišanje vrednosti ALT, navzea, zmanjšanje apetita, PPES, paragevzja, zmanjšanje števila trombocitov, stomatitis, anemija, bruhanje, zmanjšanje telesne mase, dispneja in konstipacija. Najpogostejši resni neželeni učinki zdravila v populaciji bolnikov s HCK so bili jetrna encelofalopatija, PPES, astenija in driska. Najpogostejši neželeni učinki katere koli stopnje (ki so se pojavili pri vsaj 25 % bolnikov) v populaciji bolnikov s HCK so bili driska, PPES, utrujenost, zmanjšanje apetita, hipertenzija in navzea. Zelo pogosti (≥ 1/10): anemija, hipotroidizem, zmanjšani apetit, hipomagnezija, hipokaliemija, paragevzja, glavobol, omotica, hipertenzija, krvavitve, dispepsija, kašelj, driska, navzea, bruhanje, stomatitis, konstipacija, bolečine v trebuhu, dispneja, bolečina v zgornjem predelu trebuha, PPES, izpuščaji, bolečine v okončinah, utrujenost, vnetje sluznice, astenija, periferni edem, zmanjšanje telesne mase, zvišanje vrednosti ALT v serumu, zvišanje vrednosti AST. Pogosti (≥ 1/100, < 1/10): absces, trombotična/petehijalna, nevropatija, dehidracija, hipalbuminemija, hipofosfatemija, hiponatremija, hipokalcemija, hiperkaliemija, hiperbilirubinemija, hiperglikemija, hipoglikemija, periferna senzorična nevropatija, tinitus, venska tromboza, arterijska tromboza, pljučna embolija, gastrointestinalna perforacija, fistula, gastroezofagealna refluksna bolezen, hemoroidi, bolečina v ustni votlini, suha usta, jetrna encelofalopatija, pruritus, alopecija, suha koža, akneliformni dermatitis, sprememba barve las oz. dlak, mišični krči, artralgija, proteinurija, zvišanje vrednosti ALP v krvi, GGt, kreatinina v krvi, amilaze, lipaze, holesterola v krvi, zmanjšanje števila belih krvnih celic. Občasni (≥ 1/1000, < 1/100): limfopenija, konvulzije, pankreatitis, glosidija, holestatični hepatitis, osteonekroza čeljusti, zvišanje vrednosti trigliceridov v krvi, zapleti z ranami. **Neznana ogradnost (ni mogoče oceniti iz razpoložljivih podatkov):** možganska kap, miokardni infarkt. **Vesta ovojnine in vsebina:** Plastenka vsebuje 30 filmsko obloženih tablet. **Režim izdaje:** Ro/Spec **Imetnik dovoljenja za promet z zdravilom:** Ipsen Pharma, 65 quai Georges Gorse, 92100 Boulogne-Billancourt, Francija. **Pred predpisovanjem, prosimo, preberite celoten povzetek glavnih značilnosti zdravila!** CAB-121118

 **PharmaSwiss**  
Choose More Life

 **IPSEN**  
Innovation for patient care

SAMO ZA STROKOVNO JAVNOST  
CABO219-01, februar 2019

Odgovoren za trženje v Sloveniji:  
PharmaSwiss d.o.o., Brodišče 32, 1236 Trzin  
telefon: +386 1 236 47 00, faks: +386 1 283 38 10



## Publisher

Association of Radiology and Oncology

## Affiliated with

Slovenian Medical Association – Slovenian Association of Radiology, Nuclear Medicine Society,

Slovenian Society for Radiotherapy and Oncology, and Slovenian Cancer Society

Croatian Medical Association – Croatian Society of Radiology

Societas Radiologorum Hungarorum

Friuli-Venezia Giulia regional groups of S.I.R.M.

Italian Society of Medical Radiology

## Aims and scope

*Radiology and Oncology is a journal devoted to publication of original contributions in diagnostic and interventional radiology, computerized tomography, ultrasound, magnetic resonance, nuclear medicine, radiotherapy, clinical and experimental oncology, radiobiology, radiophysics and radiation protection.*

## Editor-in-Chief

**Gregor Serša**, Institute of Oncology Ljubljana, Department of Experimental Oncology, Ljubljana, Slovenia (Subject Area: Experimental Oncology)

## Executive Editor

**Viljem Kovač**, Institute of Oncology Ljubljana, Department of Radiation Oncology, Ljubljana, Slovenia (Subject Areas: Clinical Oncology, Radiotherapy)

## Editorial Board

**Subject Areas:**  
Radiology and Nuclear Medicine

**Sotirios Bisdas**, National Hospital for Neurology and Neurosurgery, Department of Neuroradiology, London, UK

**Karl H. Bohuslavizki**, Nuklearmedizin Spitalerhof, Hamburg, Germany

**Boris Brkljačić**, University Hospital “Dubrava”, Department of Diagnostic and Interventional Radiology, Zagreb, Croatia

**Maria Gódeny**, National Institute of Oncology, Budapest, Hungary

**Gordana Ivanac**, University Hospital Dubrava, Department of Diagnostic and Interventional Radiology, Zagreb, Croatia

**Damir Miletić**, Clinical Hospital Centre Rijeka, Department of Radiology, Rijeka, Croatia

**Katarina Šurlan Popovič**, University Medical Center Ljubljana, Clinical Institute of Radiology, Ljubljana, Slovenia

**Jernej Vidmar**, University Medical Center Ljubljana, Clinical Institute of Radiology, Ljubljana, Slovenia

## Advisory Committee

**Tullio Giraldi**, University of Trieste, Faculty of Medicine and Psychology, Department of Life Sciences, Trieste, Italy

**Vassil Hadjidekov**, Medical University, Department of Diagnostic Imaging, Sofia, Bulgaria

**Marko Hočevar**, Institute of Oncology Ljubljana, Department of Surgical Oncology, Ljubljana, Slovenia

**Miklós Kásler**, National Institute of Oncology, Budapest, Hungary

## Deputy Editors

**Andrej Cör**, University of Primorska, Faculty of Health Science, Izola, Slovenia (Subject Areas: Clinical Oncology, Experimental Oncology)

**Maja Čemažar**, Institute of Oncology Ljubljana, Department of Experimental Oncology, Ljubljana, Slovenia (Subject Area: Experimental Oncology)

**Igor Kocijančič**, University Medical Center Ljubljana, Institute of Radiology, Ljubljana, Slovenia (Subject Areas: Radiology, Nuclear Medicine)

**Subject Areas:**  
Clinical Oncology and Radiotherapy

**Luca Campana**, Veneto Institute of Oncology (IOV-IRCCS), Padova, Italy

**Christian Dittrich**, Kaiser Franz Josef - Spital, Vienna, Austria

**Dirk Rades**, University of Lubeck, Department of Radiation Oncology, Lubeck, Germany

**Luka Milas**, UT M. D. Anderson Cancer Center, Houston, USA

**Csaba Polgar**, National Institute of Oncology, Budapest, Hungary

**Mirjana Rajer**, University Clinic of Pulmonary and Allergic Diseases Golnik, Golnik, Slovenia

**Luis Souhami**, McGill University, Montreal, Canada

**Borut Štabuc**, University Medical Center Ljubljana, Division of Internal Medicine, Department of Gastroenterology, Ljubljana, Slovenia

**Andrea Veronesi**, Centro di Riferimento Oncologico- Aviano, Division of Medical Oncology, Aviano, Italy

**Branko Zakotnik**, Institute of Oncology Ljubljana, Department of Medical Oncology, Ljubljana, Slovenia

**Serena Bonin**, University of Trieste, Department of Medical Sciences, Cattinara Hospital, Surgical Pathology Blg, Molecular Biology Lab, Trieste, Italy

**Maja Osmak**, Ruder Bošković Institute, Department of Molecular Biology, Zagreb, Croatia

**Dušan Pavčnik**, Dotter Interventional Institute, Oregon Health Science University, Oregon, Portland, USA

**Stojan Plesničar**, Institute of Oncology Ljubljana, Department of Radiation Oncology, Ljubljana, Slovenia

**Tomaž Benulič**, Institute of Oncology Ljubljana, Department of Radiation Oncology, Ljubljana, Slovenia

**Karmen Stanič**, Institute of Oncology Ljubljana, Department of Radiation Oncology, Ljubljana, Slovenia (Subject Areas: Radiotherapy; Clinical Oncology)

**Primož Strojjan**, Institute of Oncology Ljubljana, Department of Radiation Oncology, Ljubljana, Slovenia (Subject Areas: Radiotherapy, Clinical Oncology)

**Subject Area:**  
Experimental Oncology

**Metka Filipič**, National Institute of Biology, Department of Genetic Toxicology and Cancer Biology, Ljubljana, Slovenia

**Janko Kos**, University of Ljubljana, Faculty of Pharmacy, Ljubljana, Slovenia

**Tamara Lah Turnšek**, National Institute of Biology, Ljubljana, Slovenia

**Damijan Miklavčič**, University of Ljubljana, Faculty of Electrical Engineering, Ljubljana, Slovenia

**Geoffrey J. Pilkington**, University of Portsmouth, Institute of Biomedical and Biomolecular Sciences, School of Pharmacy and Biomedical Sciences, Portsmouth, UK

**Justin Teissié**, CNRS, IPBS, Toulouse, France  
**Gillian M. Tozer**, University of Sheffield, Academic Unit of Surgical Oncology, Royal Hallamshire Hospital, Sheffield, UK

**Subject Area: Radiophysics**

**Robert Jeraj**, University of Wisconsin, Carbone Cancer Center, Madison, Wisconsin, USA

**Håkan Nyström**, Skandionkliniken, Uppsala, Sweden

**Ervin B. Podgoršak**, McGill University, Medical Physics Unit, Montreal, Canada

**Matthew Podgorsak**, Roswell Park Cancer Institute, Departments of Biophysics and Radiation Medicine, Buffalo, NY, USA

Editorial office

**Radiology and Oncology**

Zaloška cesta 2

P. O. Box 2217

SI-1000 Ljubljana

Slovenia

Phone: +386 1 5879 369

Phone/Fax: +386 1 5879 434

E-mail: gsera@onko-i.si

Copyright © Radiology and Oncology. All rights reserved.

Reader for English

**Vida Kološa**

Secretary

**Mira Klemenčič**

**Zvezdana Vukmirović**

Design

**Monika Fink-Serša, Samo Rován, Ivana Ljubanović**

Layout

**Matjaž Lužar**

Printed by

**Tiskarna Ozimek, Slovenia**

Published quarterly in 400 copies

*Beneficiary name: DRUŠTVO RADIOLOGIJE IN ONKOLOGIJE*

*Zaloška cesta 2*

*1000 Ljubljana*

*Slovenia*

*Beneficiary bank account number: SI56 02010-0090006751*

*IBAN: SI56 0201 0009 0006 751*

*Our bank name: Nova Ljubljanska banka, d.d.,*

*Ljubljana, Trg republike 2,*

*1520 Ljubljana; Slovenia*

SWIFT: LJBASIX

*Subscription fee for institutions EUR 100, individuals EUR 50*

*The publication of this journal is subsidized by the Slovenian Research Agency.*

Indexed and abstracted by:

- Baidu Scholar
- Case
- Chemical Abstracts Service (CAS) - CApus
- Chemical Abstracts Service (CAS) - SciFinder
- CNKI Scholar (China National Knowledge Infrastructure)
- CNPIEC - cnpLINKer
- Dimensions
- DOAJ (Directory of Open Access Journals)
- EBSCO (relevant databases)
- EBSCO Discovery Service
- Embase
- Genamics JournalSeek
- Google Scholar
- Japan Science and Technology Agency (JST)
- J-Gate
- Journal Citation Reports/Science Edition
- JournalGuide
- JournalTOCs
- KESLI-NDSL (Korean National Discovery for Science Leaders)
- Medline
- Meta
- Microsoft Academic
- Naviga (Softweco)
- Primo Central (ExLibris)
- ProQuest (relevant databases)
- Publons
- PubMed
- PubMed Central
- PubsHub
- QOAM (Quality Open Access Market)
- ReadCube
- Reaxys
- SCImago (SJR)
- SCOPUS
- Sherpa/RoMEO
- Summon (Serials Solutions/ProQuest)
- TDNet
- Ulrich's Periodicals Directory/ulrichsweb
- WanFang Data
- Web of Science - Current Contents/Clinical Medicine
- Web of Science - Science Citation Index Expanded
- WorldCat (OCLC)

*This journal is printed on acid-free paper*

On the web: ISSN 1581-3207

<https://content.sciendo.com/raon>

<http://www.radioloncol.com>

# contents

## *review*

- 1 **Pericardial disease after breast cancer radiotherapy**  
Tanja Marinko
- 6 **A current review of dose-escalated radiotherapy in locally advanced non-small cell lung cancer**  
Li Ma, Yu Men, Lingling Feng, Jingjing Kang, Xin Sun, Meng Yuan, Wei Jiang, Zhouguang Hui

## *radiology*

- 15 **Diffusion kurtosis imaging and conventional diffusion weighted imaging to assess electrochemotherapy response in locally advanced pancreatic cancer**  
Vincenza Granata, Roberta Fusco, Sergio Venanzio Setola, Raffaele Palaia, Vittorio Albino, Mauro Piccirillo, Robert Grimm, Antonella Petrillo, Francesco Izzo
- 25 **Infarct-core CT perfusion parameters in predicting post-thrombolysis hemorrhagic transformation of acute ischemic stroke**  
Crt Langel, Katarina Surlan-Popovic
- 31 **CT findings predict survival of patients with peripheral T cell lymphoma: a preliminary study**  
Wenbin Yang, Sen Jiang, Jianbang Lin, Yangkang Li
- 39 **Prognostic role of diffusion weighted and dynamic contrast-enhanced MRI in locoregionally advanced head and neck cancer treated with concomitant chemoradiotherapy**  
Manca Garbajs, Primoz Strojjan, Katarina Surlan-Popovic
- 49 **MRI prognostic factors of tongue cancer: potential predictors of cervical lymph nodes metastases**  
Mohamed A.F. Mourad, Mahmoud M. Higazi

## *experimental oncology*

- 57 **Increased cystatin F levels correlate with decreased cytotoxicity of cytotoxic T cells**  
Mateja Prunk, Milica Perisic Nanut, Jerica Sabotic, Urban Svajger, Janko Kos
- 69 **NADPH oxidase inhibitor VAS2870 prevents staurosporine-induced cell death in rat astrocytes**  
Janez Simenc, Damijana Mojca Juric, Metoda Lipnik-Stangelj

## *clinical oncology*

- 77 **Ultralow anterior resection with implantation of gentamicin-collagen sponge and no defunctioning stoma: anastomotic leakage and local cancer relapse**  
Tomasz Michalik, Rafał Matkowski, Przemysław Biecek, Jozef Forgacz, Bartłomiej Szynglarewicz
- 85 **Molecular biomarkers and histological parameters impact on survival and response to first-line systemic therapy of metastatic colorectal cancer patients**  
Martina Rebersek, Tanja Mesti, Marko Boc, Janja Ocvirk
- 96 **Genetic polymorphisms in aquaporin 1 as risk factors for malignant mesothelioma and biomarkers of response to cisplatin treatment**  
Barbara Senk, Katja Goricar, Viljem Kovac, Vita Dolzan, Alenka Franko
- 105 **Potential of osteopontin in the management of epithelial ovarian cancer**  
Katarina Cerne, Benjamin Hadzialjevic, Erik Skof, Ivan Verdenik, Borut Kobal
- 116 **Similar complication rates for irreversible electroporation and thermal ablation in patients with hepatocellular tumors**  
Niklas Verloh, Isabel Jensch, Lukas Lürken, Michael Haimerl, Marco Dollinger, Philipp Renner, Philipp Wiggermann, Jens Martin Werner, Florian Zeman, Christian Stroszczynski, Lukas Philipp Beyer

## *radiophysics*

- 123 **External beam accelerated partial breast irradiation: dosimetric assessment of conformal and three different intensity modulated techniques**  
Gábor Stelczer, Tibor Major, Norbert Mészáros, Csaba Polgár, Csilla Pesznyák

## I *slovenian abstracts*

# Pericardial disease after breast cancer radiotherapy

Tanja Marinko

Institute of Oncology Ljubljana, Department of Radiotherapy, Ljubljana, Slovenia

Radiol Oncol 2019; 53(1): 1-5.

Received 5 May 2018

Accepted 12 May 2018

Correspondence to: Tanja Marinko, M.D., Ph.D., Institute of Oncology Ljubljana, Zaloška cesta 2, SI-1000 Ljubljana, Slovenia. Phone: +386 1 5879 515; Fax: +386 1 5879 400; E-mail: tmarinko@onko-i.si

Disclosure: No potential conflicts of interest were disclosed.

**Background.** Breast cancer is the second most common cancer worldwide. Thanks to the modern oncological treatments, disease specific survival has improved throughout the last decades. The number of breast cancer survivors has been increasing, and more and more attention has been paid to the breast cancer treatment side effects. Whereas there are many data regarding ischemic heart disease after radiotherapy for breast cancer, there is not much data in the literature about the incidence and clinical meaning of pericardial disease after breast cancer radiotherapy.

**Conclusions.** Although radiation-induced pericarditis is the earliest form of radiation-induced cardiovascular disease after irradiation of the heart, it seems that in clinical practice, especially by using modern radiotherapy treatment techniques, it is underdiagnosed because patients are mostly asymptomatic. In some cases, especially in its late form and after multimodal systemic oncological treatment in combination with radiotherapy, it could be presented in severe form and life threatening. Treatment modalities for radiation-induced pericardial diseases are the same as in the non-irradiated population, but in the irradiated patients, surgery may be difficult.

Key words: pericardial disease; cardiotoxicity; cardio- oncology; breast cancer; radiotherapy

## Introduction

Nowadays, breast cancer is a highly curable disease. Thanks to the modern oncological treatments, patients with early breast cancer live many years, decades after the treatment. For many of them life expectancy some years post treatment is the same as for the general population.<sup>1</sup> Consequences of the oncological treatment may have a very important influence on the quality of the subsequent life. Therefore, all the efforts must be oriented towards treatment benefits as well as in minimizing treatment's side effects.

Radiation therapy is an important part of treatment for early breast cancer with a significant impact on survival of breast cancer patients.<sup>2</sup> Besides its treatment effect, it also has side effects. Among them, one of the most important is cardiotoxicity. This is of special concern, because in its severe form it is life-threatening, instead of breast cancer itself.

Radiotherapy of the breast cancer, especially of the left breast, almost always involves some incidental irradiation of the heart. It can result in a range of cardiotoxic effects including coronary artery disease, cardiomyopathy, pericardial disease, valvular dysfunction and conduction abnormalities.<sup>3</sup> Radiation induced heart disease generally occurs with a latent period of 10 to 15 or even more years.<sup>4</sup> It can be intensified with chemotherapy and other systemic oncological treatments, but its occurrence also depends on patient's habits (smoking, diet) and simultaneous, especially cardiovascular diseases.<sup>3,5,6</sup> In addition to radiotherapy, breast cancer therapy may include anthracyclines and therapies targeting human epidermal growth factor receptor 2 (HER2) that may have important cardiotoxic effects (Khoury 2012, Taskforce).<sup>3,7</sup> Radiation-induced heart disease is of special concern, especially in younger patients as they survive longer.<sup>8</sup>

Radiation-induced pericardial disease is one of the most common and also the earliest manifesta-

tion of radiation-induced heart disease to occur following irradiation of the heart.<sup>9</sup> It could be presented as acute pericarditis, pericardial effusion, delayed thickening and constrictive pericarditis. It is classically associated with mediastinal irradiation.<sup>10</sup>

There is not much data in the literature about the incidence of pericardial disease after breast cancer radiotherapy. In 2011, McGale *et al.* published a large study about the incidence of heart disease in 35,000 women treated with radiotherapy for breast cancer between 1976 and 2006 in Denmark and Sweden.<sup>5</sup> In this, clinical and national registers based study, they reported that incidence for pericarditis was 1.61 (95% CI 1.06–2.43) higher if the patient had been irradiated for left breast cancer compared to the patient irradiated for right breast cancer. Altogether, among 35,000 breast cancer patients, they found 96 patients with subsequent, clinically or on autopsy proven pericardial disease. Interestingly, the incidence of pericarditis for left breast cancer patients comparing to the right breast cancer patients was changing through the years passed from the treatment: in the first four years after the treatment it was 1.68 (0.96–2.96), from 5–9 years 1.92 (0.89–4.13), and after 10 years it was 0.95 (0.33–2.73). The weakness of these data is a small number of cases and a broad 95% confidence intervals, but nevertheless, these data are in accordance with the fact that most radiation-induced pericarditis resolve over the years post radiotherapy.

In a recently published study, analyzing early cardiotoxicity after adjuvant concomitant treatment with radiotherapy and trastuzumab in breast cancer patients, treated between 2005 and 2010 and evaluated with transthoracic echocardiography, 10 (5.7%) out of 175 patients had pericardial effusion after a median observation time of 4.7 years.<sup>11</sup> In this study, left breast cancer patients had significant more pericardial effusions than right breast cancer patients (9 [11%] *vs.* 1 [1%];  $p = 0.007$ ). The thickness of pericardial effusion, measured at transthoracic echocardiography, was >1 cm in 1 patient with left breast cancer, all the rest were <1cm wide.

The recently published study, with retrospective analysis of 63 patients who underwent pericardiectomy for constrictive pericarditis, which is the most severe form of radiation induced pericardial disease, between 1997 and 2012, showed a significant decrease in overall survival associated with post-radiation etiology ( $p = 0.05$ ). The number of irradiated patients in this study was very small ( $n = 3$ ; 8.3%), but also other studies report similar data.<sup>12</sup>

A golden standard in the evaluation of cardiotoxicity in cancer patients is standard transthoracic

two-dimensional echocardiography.<sup>13</sup> It provides useful morphologic and hemodynamic information. A standard part of the echocardiographic exam are measurements of heart chambers and great vessels dimensions, estimation of ventricular systolic and diastolic function, assessment of ventricular wall contraction abnormalities, valvular anatomy and function and diagnosis of pericardial disease. In obese patients or in patients after chest irradiation, the quality of measurements can be poor due to suboptimal chest echotranslucency. In these settings tissue Doppler imaging (TDI) offers additional information.<sup>13</sup> Computed tomography is particularly helpful in identifying calcification.<sup>3</sup> In the evaluation of constrictive pericarditis, also magnetic resonance imaging and right-sided catheterization is used.<sup>14</sup>

## Pathophysiology

The pathophysiologic pathway responsible for most manifestations of cardiotoxicity appears to involve damage to blood vessels. The generation of reactive oxygen species, caused by radiation, disrupt DNA strands. Secondary inflammatory changes then lead to fibrosis.<sup>15</sup>

Acute pericarditis is caused by radiation-induced inflammation of the pericard. Pericard becomes porous, resulting in a neutrophilic infiltrate and collection of a high-protein exudate (exudative pericarditis).<sup>16</sup> Changes of pericard in acute stage may later lead to fibrosis of the pericard, impairing the venous drainage of extracellular fluid.<sup>17</sup> Inefficient drainage results in the accumulation and formation of pericardial effusions, which are mostly fibrinous exudates.<sup>18</sup> Pericardial fat is replaced by collagen. Early and acute or delayed and chronic pericarditis should be regarded from a histopathological standpoint as two distinct disease entities.<sup>9</sup>

The histopathologic picture of the radiation-induced pericardial disease, the dose-independent latency time, and the reversibility indicate that radiation-induced pericarditis is an acute radiation response of an actively proliferating cell population. Mesothelial cells are the most likely candidates for target cells, but systematic cell kinetic studies have not been performed.<sup>6</sup>

## Clinical meaning and therapy

Acute pericarditis is a rare short-term complication of radiotherapy and develops during or days

to weeks after irradiation.<sup>14,15</sup> It can be revealed by asymptomatic pericardial effusion or symptomatic pericarditis. Patients may present with chest pain, they may have a fever, pericardial rub, electrocardiogram abnormalities (ST-T changes) and mild elevations in cardiac markers within days to weeks of therapy, near the timing of radiotherapy.<sup>18</sup> Acute pericarditis usually resolves by itself, spontaneous clearance of effusion may occur. Half of the patients do not require any active intervention.<sup>15</sup> Nevertheless, if treatment of pericarditis is needed, it is usually supportive with non-steroidal anti-inflammatory drugs (NSAID) and colchicine.<sup>3,14,19</sup> As a second-line agent, steroids may be prescribed. In resistant cases, interleukin 1 $\beta$  receptor antagonist is also an option.<sup>15,20,21</sup> In the case of large pericardial effusion, especially if the patient is hemodynamically compromised, pericardiocentesis is indicated. According to the literature, 20% of patients may proceed to have chronic pericarditis.<sup>15</sup>

Pericardial effusions may appear weeks, months or even years after irradiation with the mean latency for development of approximately one year.<sup>8,14</sup> Patients may be asymptomatic or develop progressive shortness of breath. Effusions that are hemodynamically insignificant require close monitoring, but those, who are symptomatic or in the case of tamponade, require urgent drainage of fluid.<sup>20</sup>

Constrictive pericarditis is usually the most severe form of pericarditis and commonly occurs with a latent period of 10 or more years post-radiation exposure as congestive heart failure.<sup>18</sup> It can lead to disabling symptoms and severe heart failure with the poor quality of life. Surgical pericardiectomy is the cornerstone of management.<sup>12</sup> In a recently published case report, in a 57-year-old breast cancer patient with late onset radiation-induced constrictive pericarditis and cardiomyopathy 22 years after radiotherapy for left breast cancer, even heart transplant operation was necessary and successfully done.<sup>22</sup>

## Effect of radiation dose and techniques of treatment planning and delivery

Radiation-induced cardiotoxicity is related to both the irradiated volume of the heart and the radiation dose delivered to that volume. It seems that there is no safe dose that could be delivered to the heart with no increased risk of cardiovascular disease.<sup>23</sup>

The so-called »tolerance dose« of the pericard is described in the literature as a mean heart dose of

greater than 36 or 40 Gy, or a > 50 Gy dose administered to > 30% of the heart.<sup>6,8,24</sup> The radiation effect on the pericard is highly dose-dependent, with the incidence of pericarditis increasing from < 5% to > 50% as the total dose to the heart is increased from 40 to 50 Gy.<sup>25</sup>

According to the data from the Quantitative Analysis of Normal Tissue Effects in the Clinic (QUANTEC) review, published in 2010, which based on the previous report from Emami and colleagues published in 1991, the relations between the irradiated volume of the critical structure, threshold and outcome for pericarditis are as follows<sup>25,26</sup>:

- Mean heart dose < 26 Gy ..... < 15% probability for pericarditis
- Heart V30 < 46% ..... < 15% probability for pericarditis

Currently, all predictions for pericarditis probability are based on dose delivered to the heart. In the literature, there is no specific recommendations for dose restrictions that would base on the dose delivered to the pericard, as seems to be more accurate. Namely, in classical left breast irradiation with tangential fields, the pericard is the closest cardiac substructure that lies behind the irradiated target and, because of the steep gradient fall of the dose behind the targets, it probably receives a higher dose than the rest of the heart. In the current breast contouring recommendations and atlases, the whole heart is included, but it is likely that also cardiac substructures are important as we begin to understand the impact of radiotherapy on cardiac function.<sup>27-29</sup> At the moment, in the literature, there are at least two heart atlases, with instructions for countouring heart substructures. No one has detailed instructions for contouring of the pericard, although the second one, published in 2017, enables contouring of 15 cardiac segments.<sup>29,30</sup>

However, do we need to pay special attention on the contouring of the pericard as a specific structure, similarly as we contour coronary artery? According to the incidence of the treatment required, radiation-induced pericardial disease, it seems, that there is maybe no reason for that. But for the definite answer, it needs to be evaluated in a clinical study.

Dose, delivered to the heart during radiotherapy for breast cancer, largely depends on the treatment technique used. With the modern radiotherapy techniques, it is possible to spare the heart much more from radiation, than it was possible in the past by using older techniques.<sup>31</sup> Unlike 2D radiotherapy, 3D radiotherapy allows defining

the dose delivered to any point to the heart. If radiotherapy is delivered in a breath hold, which allows the heart to move down and posterior to the treatment volume, the sparing effect to the heart is even greater.<sup>32</sup> In a study comparing free breathing (FB) with voluntary deep inspiration breath hold (V-DIBH) resulted in a significant reduction of mean cardiac dose from 6.1 +/- 2.5 to 3.2 +/- 1.4 Gy ( $p < 0.001$ ), maximum cardiac dose from 51.1 +/- 1.4 to 48.5 +/- 6.8 Gy ( $p = 0.005$ ) and cardiac V25Gy from 8.5 +/- 4.2 to 3.2 +/- 2.5% ( $p < 0.001$ ). There is no specific data for the dose to the pericard.

With an increasing awareness of potential cardiotoxicity of radiotherapy, new studies with proton therapy have emerged. Stick *et al.* in their study did an estimation of cardiac toxicity after comprehensive nodal photon versus proton therapy for breast cancer. In their report, they concluded that modern photon therapy yields a limited risk of cardiac toxicity in most patients, but proton therapy could reduce the predicted risk of cardiac toxicity by up to 2.9%.<sup>33</sup> A systematic review of the literature with the aim to evaluate proton therapy in locally advanced breast cancer, done by Kammerer *et al.*, showed that proton therapy often decreased mean heart dose by a factor of 2 or 3. As an example for mean heart dose, they listed 1 Gy with proton therapy versus 3 Gy with conventional 3D, and 6 Gy for intensity-modulated radiotherapy (IMRT).<sup>34</sup> There is again no specific data for pericard.

## Future directions

Good news is that the very recently published, registry-based study, reporting long-term heart-specific mortality among 347,476 breast cancer patients treated with radiotherapy or chemotherapy between 2000 and 2011, found that heart-specific mortality among breast cancer survivors was not increased compared with the general population.<sup>35</sup> According to the available literature, the absolute risk for pericardial disease associated with breast cancer radiotherapy is small and appears to be outweighed by the benefits of the treatment.

Nowadays, awareness about potential harm to the heart during radiotherapy is much higher than in the past, and efforts to deliver the prescribed radiation dose to the treatment target with the minimum possible dose delivered to the heart, are a part of a daily treatment planning routine in the majority of radiotherapy departments. But there is still a lot of room for improvement. The challenge for the future is in answering the question of the tolerance

dose and the roll of each heart substructure in the etiology of radiation-induced heart disease.

## References

1. Arrington A, Goldstein L, Kruper L, Vito C, Yim J, Chen SL. Life expectancy after curative-intent treatment of breast cancer: impact on long-term follow-up care. *Am Surg* 2014; **80**: 604-9.
2. Clarke M, Collins R, Darby S, Davies C, Elphinstone P, Evans V, et al; Early Breast Cancer Trialists' Collaborative Group (EBCTCG). Effects of radiotherapy and of differences in the extent of surgery for early breast cancer on local recurrence and 15-year survival: an overview of the randomised trials. *Lancet* 2005; **366**: 2087-106. doi: 10.1016/S0140-6736(14)60488-8
3. Zamorano JL, Lancellotti P, Rodriguez Muñoz D, Aboyans V, Asteggiano R, Galderisi M et al; ESC Scientific Document Group. 2016 ESC Position Paper on cancer treatments and cardiovascular toxicity developed under the auspices of the ESC Committee for Practice Guidelines: The Task Force for cancer treatments and cardiovascular toxicity of the European Society of Cardiology (ESC). *Eur Heart J* 2016; **37**: 2768-801. doi: 10.1093/eurheartj/ehw211
4. Darby SC, McGale P, Taylor CW, Peto R. Long-term mortality from heart disease and lung cancer after radiotherapy for early breast cancer: prospective cohort study of about 300,000 women in US SEER cancer registries. *Lancet Oncol* 2005; **6**: 557-65. doi: 10.1016/S1470-2045(05)70251-5
5. McGale P, Darby SC, Hall P, Adolphsson J, Bengtsson NO, Bennet AM, et al. Incidence of heart disease in 35,000 women treated with radiotherapy for breast cancer in Denmark and Sweden. *Radiother Oncol* 2011; **100**: 167-75. doi: 10.1016/j.radonc.2011.06.016
6. Schultz-Hector S, Trott KR. Radiation-induced cardiovascular diseases: is the epidemiologic evidence compatible with the radiobiologic data? *Int J Radiat Oncol Biol Phys* 2007; **67**: 10-8. doi: 10.1016/j.ijrobp.2006.08.071
7. Khouri MG, Douglas PS, Mackey JR, Martin M, Scott JM, Scherrer-Crosbie M, et al. Cancer therapy-induced cardiac toxicity in early breast cancer: addressing the unresolved issues. *Circulation* 2012; **126**: 2749-63. doi: 10.1161/CIRCULATIONAHA.112.100560
8. Andratschke N, Maurer J, Molls M, Trott KR. Late radiation-induced heart disease after radiotherapy. Clinical importance, radiobiological mechanisms and strategies of prevention. *Radiother Oncol* 2011; **100**: 160-6. doi: 10.1016/j.radonc.2010.08.010
9. Cuomo JR, Sharma GK, Conger PD, Weintraub NL. Novel concepts in radiation-induced cardiovascular disease. *World J Cardiol* 2016 ; **8**: 504-19. doi: 10.4330/wjcv.8.9.504
10. Veinot JP, Edwards WD. Pathology of radiation-induced heart disease: a surgical and autopsy study of 27 cases. *Hum Pathol* 1996; **27**: 766-73. doi: 10.1016/S0046-8177(96)90447-5
11. Marinko T, Borstnar S, Blagus R, Dolenc J, Bilban-Jakopin C. Early cardiotoxicity after adjuvant concomitant treatment with radiotherapy and trastuzumab in patients with breast cancer. *Radiol Oncol* 2019; **53**(1): 1-5.; doi: 10.2478/raon-2018-0011
12. Avgerinos D, Rabinokov Y, Worku B, Neragi-Miandoab S, Girardi LN. Fifteen-year experience and outcomes of pericardiectomy for constrictive pericarditis. *J Card Surg* 2014; **29**: 434-8. doi: 10.1111/jocs.12344
13. Marinko T, Dolenc J, Bilban-Jakopin C. Cardiotoxicity of concomitant radiotherapy and trastuzumab for early breast cancer. *Radiol Oncol* 2014; **48**: 105-12. doi: 10.2478/raon-2013-0040
14. Nielsen KM, Offersen BV, Nielsen HM, Vaage-Nilsen M, Yusuf SW. Short and long term radiation induced cardiovascular disease in patients with cancer. *Clin Cardiol* 2017; **40**: 255-61. doi: 10.1002/clc.22634
15. Madan R, Benson R, Sharma DN, Julka PK, Rath GK. Radiation induced heart disease: Pathogenesis, management and review literature. *J Egypt Natl Canc Inst* 2015; **27**: 187-93. doi: 10.1016/j.jnci.2015.07.005
16. Fajardo LF, Stewart JR, Cohn KE. Morphology of radiation-induced heart disease. *Arch Pathol* 1968; **86**: 512-9.
17. Fajardo LF, Stewart JR. Pathogenesis of radiation-induced myocardial fibrosis. *Lab Invest* 1973; **29**: 244-57.

18. Raghunathan D, Khilji MI, Hassan SA, Yusuf SW. Radiation-induced cardiovascular disease. *Curr Atheroscler Rep* 2017; **19**: 22. doi: 10.1007/s11883-017-0658-x
19. Imazio M, Brucato A, Cemin R, Ferrua S, Maggolini S, Beqaraj F, et al; ICAP Investigators. A randomized trial of colchicine for acute pericarditis. *N Engl J Med* 2013; **369**: 1522-8. doi: 10.1056/NEJMoa1208536
20. Yusuf SW, Hassan SA, Mouhayar E, Negi SI, Banchs J, O'Gara PT, et al. Pericardial disease: a clinical review. *Expert Rev Cardiovasc Ther* 2016; **14**: 525-39. doi: 10.1586/14779072.2016.1134317
21. Nathan PC, Amir E, Abdel-Qadir H. Cardiac outcomes in survivors of pediatric and adult cancers. *Can J Cardiol* 2016; **37**: 871-80. doi: 10.1016/j.cjca.2016.02.065
22. Zhuang XF, Yang YM, Sun XL, Liao ZK, Huang J. Late onset radiation-induced constrictive pericarditis and cardiomyopathy after radiotherapy: a case report. *Medicine (Baltimore)* 2017; **96**: e5932. doi: 10.1097/MD.0000000000005932
23. Darby SC, Ewertz M, McGale P, Bennet AM, Blom-Goldman U, Brønnum D, et al. Risk of ischemic heart disease in women after radiotherapy for breast cancer. *N Engl J Med* 2013; **368**: 987-98. doi: 10.1056/NEJMoa1209825
24. Stewart FA, Seemann I, Hoving S, Russell NS. Understanding radiation-induced cardiovascular damage and strategies for intervention. *Clin Oncol (R Coll Radiol)* 2013; **25**: 617-24. doi: 10.1016/j.clon.2013.06.012
25. Emami B, Lyman J, Brown A, Coia L, Goitein M, Munzenrider JE, et al. Tolerance of normal tissue to therapeutic irradiation. *Int J Radiat Oncol Biol Phys* 1991; **21**: 109-22. doi: 10.1016/0360-3016(91)90171-Y
26. Marks LB, Yorke ED, Jackson A, Ten Haken RK, Constone LS, Eisbruch A, et al. Use of normal tissue complication probability models in the clinic. *Int J Radiat Oncol Biol Phys* 2010; **76(3 Suppl)**: S10-9. doi: 10.1016/j.ijrobp.2009.07.1754
27. RTOG (Radiation therapy oncology group) Breast cancer atlas for radiation therapy planning. [cited 2018 May 5] Available at: <https://www.rtog.org/CoreLab/ContouringAtlases.aspx>
28. Offersen BV, Boersma LJ, Kirkove C, Hol S, Aznar MC, Biete Sola A, et al. ESTRO consensus guideline on target volume delineation for elective radiation therapy of early stage breast cancer. *Radiother Oncol* 2015; **114**: 3-10. doi: 10.1016/j.radonc.2014.11.030
29. Feng M, Moran JM, Koelling T, Chughtai A, Chan JL, Freedman L, et al. Development and validation of a heart atlas to study cardiac exposure to radiation following treatment for breast cancer. *Int J Radiat Oncol Biol Phys* 2011; **79**: 10-8. doi: 10.1016/j.ijrobp.2009.10.058
30. Duane F, Aznar MC, Bartlett F, Cutter DJ, Darby SC, Jaggi R, et al. A cardiac contouring atlas for radiotherapy. *Radiother Oncol* 2017; **122**: 416-22. doi: 10.1016/j.radonc.2017.01.008
31. Shah C, Badiyan S, Berry S, Khan AJ, Goyal S, Schulte K, et al. Cardiac dose sparing and avoidance techniques in breast cancer radiotherapy. *Radiother Oncol* 2014; **112**: 9-16. doi: 10.1016/j.radonc.2014.04.009
32. Al-Hammadi N, Caparrotti P, Naim C, Hayes J, Rebecca Benson K, Vasic A, et al. Voluntary deep inspiration breath-hold reduces the heart dose without compromising the target volume coverage during radiotherapy for left-sided breast cancer. *Radiol Oncol* 2019; **53(1)**: 1-5. doi: 10.1515/raon-2018-0008
33. Stick LB, Yu J, Maraldo MV, Aznar MC, Pedersen AN, Bentzen SM, et al. Joint estimation of cardiac toxicity and recurrence risks after comprehensive nodal photon versus proton therapy for breast cancer. *Int J Radiat Oncol Biol Phys* 2017; **97**: 754-61. doi: 10.1016/j.ijrobp.2016.12.008
34. Kammerer E, Guevelou J, Chaikh A, Danhier S, Geffrelot, Levy C, et al. Proton therapy for locally advanced breast cancer: a systematic review of the literature. *Cancer Treat Rev* 2018; **63**: 19-27. doi: 10.1016/j.ctrv.2017.11.006
35. Weberpals J, Jansen L, Müller OJ, Brenner H. Long-term heart-specific mortality among 347 476 breast cancer patients treated with radiotherapy or chemotherapy: a registry-based cohort study. *Eur Heart J* 2018. doi: 10.1093/eurheartj/ehy167

# A current review of dose-escalated radiotherapy in locally advanced non-small cell lung cancer

Li Ma<sup>1</sup>, Yu Men<sup>2</sup>, Lingling Feng<sup>1</sup>, Jingjing Kang<sup>3</sup>, Xin Sun<sup>3</sup>, Meng Yuan<sup>3</sup>, Wei Jiang<sup>1</sup>, Zhouguang Hui<sup>2,3</sup>

<sup>1</sup> Department of Radiation Oncology, National Cancer Center/Cancer Hospital & Shenzhen Hospital, Chinese Academy of Medical Sciences and Peking Union Medical College, Shenzhen, 518116, China

<sup>2</sup> Department of VIP Medical Services, National Cancer Center/Cancer Hospital, Chinese Academy of Medical Sciences & Peking Union Medical College, Beijing 100021, China

<sup>3</sup> Department of Radiation Oncology, National Cancer Center/Cancer Hospital, Chinese Academy of Medical Sciences & Peking Union Medical College, Beijing 100021, China

Radiol Oncol 2019; 53(1): 6-14.

Received 31 August 2018

Accepted 5 January 2019

Correspondence to: Zhouguang Hui, M.D., Department of VIP Medical Services & Department of Radiation Oncology, National Cancer Center/Cancer Hospital, Chinese Academy of Medical Sciences & Peking Union Medical College, Panjiayuan Nanli 17, Chaoyang District, Beijing 100021, China. Phone: + 861087787656; E-mail: huizg@cicams.ac.cn

Disclosure: No potential conflicts of interest were disclosure

**Background.** The mainstay therapy for locally advanced non-small cell lung cancer is concurrent chemoradiotherapy. Loco-regional recurrence constitutes the predominant failure patterns. Previous studies confirmed the relationship between increased biological equivalent doses and improved overall survival. However, the large randomized phase III study, RTOG 0617, failed to demonstrate the benefit of dose-escalation to 74 Gy compared with 60 Gy by simply increasing fraction numbers.

**Conclusions.** Though effective dose-escalation methods have been explored, including altered fractionation, adapting individualized increments for different patients, and adopting new technologies and new equipment such as new radiation therapy, no consensus has been achieved yet.

**Key words:** non-small cell lung cancer; dose escalation; hyperfractionation; hypofractionation; adaptive radiotherapy; proton radiotherapy; carbon ion radiotherapy

## Introduction

Conventionally fractionated (1.8–2.0 Gy/day) radiotherapy to a dose of 60–70 Gy with concurrent chemotherapy has long been established as the standard care for locally advanced non-small cell lung cancer (LANSCLC). However, the outcomes remain poor with a 5-year overall survival (OS) less than 20%.<sup>1</sup> Local-regional recurrence is the main challenge for long-term survival. Efforts have been made to explore the safe and effective methods to improve loco-regional control (LRC). Of them, dose escalation shows promising prospects.

## Materials and methods

PubMed and EMBASE were searched using the following keywords: locally advanced non-small cell lung cancer, unresectable non-small cell lung cancer, radiotherapy, radiation therapy, dose escalation, hyperfractionation, hypofractionation, adaptive radiotherapy, proton radiotherapy, carbon ion radiotherapy. Clinical studies, clinical trials, meta-analysis, reviews and references from the articles were selected and further classified into altered radiotherapy delivery regimens, personalized radiotherapy regimen and new techniques: proton and heavy ion radiotherapy.

## Results and discussion

### Current status and problems of traditional dose escalation

Machtay *et al.* conducted a retrospective analysis of 1356 LANSCLC patients from seven prospective clinical trials of the Radiation Therapy Oncology Group (RTOG).<sup>2</sup> Biologically equivalent dose (BED) and time-adjusted BED were calculated for each patient. The study revealed that BED was highly correlated with OS and loco-regional relapse-free survival ( $p < 0.0001$ ). Increase of 1 Gy in BED was related with a 3% (HR = 0.97) improvement in local control and a 4% (HR = 0.96) relative improvement in survival. It is noteworthy that accompanied with escalated dose, treatment related-toxicity may be increased. In several randomized trials, a median survival of 15–20.6 months was observed in LANSCLC patients treated with a radiation dose of 60–66 Gy and concurrent chemotherapy.<sup>3–8</sup> A serial phase I and II trials explored the efficacy of dose escalation to 74 Gy radiotherapy concurrent with chemotherapy and showed an improved median OS of 21.6–37 months with acceptable toxicity.<sup>9–12</sup> Motivated by these results, RTOG launched a large randomized phase III study 0617, trying to find out whether a 74 Gy radiotherapy was superior to a 60 Gy radiotherapy administered with concurrent chemotherapy followed by consolidative chemotherapy. The result suggested that compared with 60 Gy radiotherapy, neither overall survival nor local control improved in high-dose radiotherapy arm (median OS time: 28.7 *vs.* 20.3 months,  $p = 0.004$ ; 2-year local failure rate: 30.7% *vs.* 38.6%,  $p = 0.13$ ).<sup>13</sup> The prolongation of overall treatment time (7.5 weeks) and the associated tumor repopulation may be the contributing factors to this unsatisfactory outcome.<sup>14</sup> Radiobiology and clinical trials have confirmed that the doubling time of most tumors is less than one week.<sup>15,16</sup> Dose escalation by simply increasing fraction numbers results in lengthened overall treatment, which has proven to have a negative impact on tumor control. Worse overall survival was observed when the treatment course exceeded 6 weeks.<sup>17,18</sup> In addition, results of RTOG 0617 showed that the exposure of lung, esophagus, and heart were significantly higher in high-dose radiotherapy arm; greater toxicity may be another possible explanation.<sup>13,14</sup> Brower *et al.* analyzed 33566 patients with stage III NSCLC who underwent concurrent chemoradiation and found that dose escalation above 60 Gy was associated with improved OS.<sup>19</sup> But an OS plateau was also found when radiation dose prescribed was greater than

70 Gy. It is suggested that dose escalation should be limited in a specified range.

Recent meta-analysis demonstrated a survival benefit of dose escalation in patients treated with sequential chemoradiotherapy. However, in concurrent chemoradiotherapy group, increased dose was related to poorer survival.<sup>20,21</sup> One possible explanation is that the underlying toxicity accompanied with concurrent chemoradiotherapy compromises the survival benefits of dose escalation in tumor control.

Therefore, in the era of concurrent chemotherapy, applying traditional approaches of dose escalation in unselected patients could lead to extra toxicity and impaired survival. There is a need to explore safe, efficacious and feasible dose escalation methods for LANSCLC.

### Recent progress in dose escalation

#### Altered radiotherapy delivery regimens

Two feasible approaches enable the delivery of an increased BED without prolonging treatment time, hyperfractionation (reduced fraction size, two times or more per day) and hypofractionation (fewer fractions, larger dose-per-fraction).<sup>22</sup>

#### Hyperfractionated radiotherapy

Hyperfractionated radiotherapy demonstrated to have a survival benefit over conventional radiotherapy in NSCLC patients. In the continuous hyperfractionated accelerated radiotherapy (CHART) trial, 563 NSCLC patients were randomized at a 3:2 ratio into CHART and conventional group. Compared with conventional regimen (once daily fraction of 2 Gy to a total of 60 Gy/30 d), CHART (three times per day fraction of 1.5 Gy to a total of 54 Gy/12 d) group appeared to have a significant survival benefit with a 2-year OS rate increased by 9% (20% *vs.* 29%,  $p = 0.004$ ).<sup>23</sup> However, CHART regimen is hard to implement for institutions due to its additional weekend treatment. Therefore, Baumann *et al.* proposed a modified CHARTWEL (CHART weekend less) trial in which the same schedule as CHART was applied except that it omitted the weekend treatment.<sup>24</sup> CHARTWEL group was treated with three times per day fraction of 1.5 Gy to a total dose of 54 Gy in 36 fractions. The conventional group escalated to 66 Gy (2 Gy per fraction). CHARTWEL group showed no significant survival benefit (2-year OS rate: 32% *vs.* 31% at 2 years,  $p = 0.43$ ). One reasonable explanation was that escalated dose in conventional

TABLE 1. Researches on altered fractionation in NSCLC

Author	Regimen	No.	Stage	Treatment outcome	p value	RE	p value	RP	p value
Saunders <sup>23</sup>	Conventional radiotherapy: 60Gy/2Gy/30f	225	-	20%(2-year OS)	0.004	acute: 7%; late: 5%	-	acute: 19%; late: 4%(symptomatic)	-
	CHART: 1.5Gy tid, 7 days/week, a total of 54Gy	339	-	29%(2-year OS)		acute: 9%; late: 7%	-	acute: 10%; late: 16%(symptomatic)	-
Baumann <sup>24</sup>	conventional radiotherapy: 66Gy/2Gy/33f	203	inoperable	31%(2-year OS)	0.43	acute: 2.2%; late: 0.7%(≥G2)	acute: 0.17; late: 0.62	acute: 9.5%; late: 11%(≥G2 symptomatic)	acute: 0.32; late: 0.59
	CHART: 1.5Gy tid, 5 days/week, a total of 54Gy	203	-	32%(2-year OS)		acute: 5%; late: 1.9%(≥G2)		acute: 6.6%; late: 9.2%(≥G2 symptomatic)	
Mauguen <sup>25</sup>	Conventional radiotherapy	2000	-	15.9%(3-year OS), 8.3%(5-year OS)	<0.04	9%	<0.001	-	-
	CHART		-	19.7%(3-year OS), 10.8%(5-year OS)		19%			
Din <sup>26</sup>	55Gy/2.67Gy/20f	609	III	50%(2-year OS)	-	-	-	15.1%(G1-2 symptomatic)	-
Sun <sup>27</sup>	conventional radiotherapy: 70.8Gy/1.86Gy/38f	54	inoperable stage III	48.1%(RR)	0.032	33.3%(G2)	-	42.6% (≥G2)	-
	hypofractionated radiotherapy: 65Gy/2.5Gy/26f	43	-	69.8%(RR)		25.6%(G2)		34.9%(≥G2)	
Cannon <sup>29</sup>	57-85.5Gy/2.28-3.42Gy/25f	79	LANSCLC	29%(3-year OS)	-	acute: 48%(G2); late: 28%(G2)	-	16%(G2)7.6%(G4-5)	-
Feddock <sup>32</sup>	A month after standard radiotherapy to 60Gy with concurrent chemotherapy, an SBRT boost was given in ≤5cm residual primary tumors: 10Gy×2f for peripheral lesions, 6.5Gy×3f for central lesions	61	II/III	82.9%(primary tumor control with a median follow-up of 13 months)	-	1.6%(G2)	-	acute: 17.1%; late: 9.4%(≥G2)	-
Karam <sup>33</sup>	An SBRT boost with 20-30Gy over 5 fractions was prescribed after conventional CCRT to a median dose of 50.4Gy	16	LANSCLC	78%(1-year OS), 76%(1-year LRC)	-	18% (G2)	-	25% (G2)	-
Higgins <sup>34</sup>	Standard radiotherapy to 44Gy with concurrent chemotherapy, followed by an SBRT boost in the lung and nodal residuals in four groups: 9Gy×2f, 10Gy×2f, 6Gy×5f and 7Gy×5f	19	stage III (N1/N2) with primary tumors ≤8cm and lymph nodes ≤5cm	39%(3-year OS), 59%(3-year LRC)	-	-	-	-	-
Hepel <sup>35</sup>	Standard radiotherapy to 50.4Gy with concurrent chemotherapy, followed by an SBRT boost in the lung and nodal residuals in four groups: 8Gy×2f, 10Gy×2f, 12Gy×2f and 14Gy×2f	12	Stage II/III with primary tumor ≤120cc and lymph node volume ≤ 60cc	78%(1-year LRC)	-	0(≥G3)	-	acute: 0(≥G3); late: 8.33%(G5)	-

f = fraction(s); LANSCLC = locally advanced non-small cell lung cancer; LRC = loco-regional control; OS = overall survival; RE = radiation esophagitis; RP = radiation pneumonitis; SBRT = stereotactic body radiation therapy; tid = three-fractions-per-day

treatment group compensated for the adverse effect of longer treatment time. A meta-analysis by Mauguen *et al.* identified 10 clinical trials describing 2000 NSCLC patients treated with hyperfractionated radiotherapy.<sup>25</sup> An increased risk of acute radiation esophagitis (19% *vs.* 9%,  $p < 0.001$ ) was found in the hyperfractionation group. However, the compliablensness was good, over 90% of patients completed the prescribed radiotherapy. The result showed that hyperfractionation significantly improved survival with a 12% reduction in the risk of death (HR = 0.88,  $p = 0.009$ ). The 3-year and 5-year OS rates were improved by 3.8% (19.7% *vs.* 15.9%) and 2.5% (10.8% *vs.* 8.3%), respectively.

### Hypofractionated radiotherapy

It has been well established that the delivery of larger dose-per-fraction in fewer fractions could significantly improve BED, represented by stereotactic body radiation therapy (SBRT). However, SBRT is treatment of choice only for early lung cancer without affected lymph nodes. The delivery of SBRT is limited by the large tumor size and the proximity of normal tissues such as major vessels, esophagus, heart and other important organs. Some studies explored a moderate hypofractionated escalation schedule of 2–4 Gy per fraction dose radiotherapy. With this delivery, treatment time has been significantly shortened without provid-

TABLE 2. Researches on personalized dose escalation radiotherapy in NSCLC

Author	Regimen	No.	Stage	Treatment outcome	p value	RE	p value	RP	p value
Van Baardwijk <sup>26</sup>	Initially 1.5Gy bid to 45Gy, then 2Gy per fraction daily increments until reaching the limit dose of normal tissue	137	III	52.4% (2-year OS)	-	acute: 25.5% (G3); late: 4.6% (G3)	-	late: 3% (≥G3)	-
Van Elmp <sup>38</sup>	Initially 2.75Gy to 66Gy, then boost to the entire primary tumor Initially 2.75Gy to 66Gy, then boost in the high FDG uptake area	15 15	I-III	-	-	-	-	-	-
Vera <sup>40</sup>	<sup>18</sup> F-FMISO PET-CT (-); 66Gy CCRT	20	LANSCLC	95% (1-year OS) 85% (1-year DFS)	p=0.10 (1-year OS)	acute: 75% (G1-3)	-	acute: 15% (G1-2) late: 5% (G1-2)	-
	<sup>18</sup> F-FMISO PET-CT (-); 68-86Gy CCRT	24		81% (1-year OS) 50% (1-year DFS)	p=0.01 (1-year DFS)	acute: 75% (G1-3)		acute: 12.5% (≥G3)	
	<sup>18</sup> F-FMISO PET-CT (+); 66GyCCRT	10		50% (1-year DFS)		acute: 100% (G1-5)		acute: 0	
Kong <sup>41</sup>	Initially 50Gy, then adapt target basing on midtreatment PET-CT and escalate dose to the constraints of normal tissue concurrent with chemotherapy	42	Inoperable stage I-III	2-year LRC: 62%; median OS: 25 months	-	12% (G3)	-	7% (G3)	-

CCRT = concurrent chemoradiotherapy; DFS = disease free survival; LANSCLC = locally advanced non-small cell lung cancer; LRC = loco-regional control; RE = radiation esophagitis; RP = radiation pneumonitis; OS = overall survival

TABLE 3. Researches on proton and heavy ion radiotherapy in NSCLC

Author	Regimen	No.	Stage	Treatment outcome	p value	RE	p value	RP	p value
Higgins <sup>47</sup>	Median dose of photon radiotherapy: 59.4Gy	243474	I-IV	13.5% (5-year OS)	0.01	-	-	-	-
	Median dose of PSPT: 60Gy (RBE)	348		23.1% (5-year OS)					
Chung <sup>48</sup>	74Gy (RBE) PSPT concurrent with chemotherapy	64	III	26.5 months (median OS)	-	8% (G3)	-	14% (G3-4)	-
Liao <sup>49</sup>	IMRT: 66-74Gy	92	LANSCLC	10.9% (LRF)	0.86	-	-	6.5%	0.40
	PSPT: 74Gy (RBE)	57		10.5% (LRF)				10.5%	
Takahashi <sup>50</sup>	68-76Gy (RBE) carbon ion radiotherapy	72	LANSCLC	93.1% (2-year LRC), 51.9% (2-year OS)	-	1.4% (G3)	-	1.4% (G3)	-
Karube <sup>51</sup>	52.8-72Gy (RBE) carbon ion radiotherapy	64	II-III	81.8% (2-year LRC), 62.2% (2-year OS)	-	0 (≥G2)	-	0 (≥G2)	-
Shirai <sup>52</sup>	52.8-70.4Gy (RBE)/4-16f carbon ion radiotherapy	23	T2b-4N0M0	81% (2-year LRC), 70% (2-year OS)	-	0 (≥G3)	-	0 (≥G3)	-

CCRT = concurrent chemoradiotherapy; DFS = disease free survival; IMRT = intensity modulated radiation therapy; LANSCLC = locally advanced non-small cell lung cancer; LRC = loco-regional control; OS = overall survival; PSPT = passive scattered proton therapy; RBE = relative biologic equivalent; RE = radiation esophagitis; RP = radiation pneumonitis

ing additive toxicity. Also, a positive relationship between OS and BED was found.

A retrospective study of four UK centers evaluated 609 NSCLC patients treated with accelerated hypofractionated radiotherapy. Ninety-eight percent of them received the radiotherapy scheme of 2.67 Gy per fraction to a total dose of 55 Gy in 20 fractions. The 2-year OS of stage III NSCLC patients approximates 50% with comparable side effects to previous data.<sup>26</sup> Sun *et al.* conducted a prospective clinical study comparing hypofractionated schedule (2.5 Gy per fraction to 65 Gy) with conventional radiotherapy (1.86 Gy per fraction to 70.8 Gy) in patients with stage III inoperable NSCLC.<sup>27</sup> Hypofractionated schedule had significantly better response rate ( $p = 0.032$ ) over conventional regimen with comparable treatment-related toxicity.

A systematic review by Tyler *et al.* gathered data from 33 articles identifying LANSCLC patients treated with radical hypofractionated radiotherapy between 1990 and 2014, of which, 15 studies included concurrent chemotherapy.<sup>28</sup> A fractionation schedule of 45-85.5 Gy at 2.3-3.5 Gy/fraction daily was administered. The study reported an OS benefit of increased BED ( $p = 0.001$ ): every 1 Gy increase in BED resulted in an absolute OS benefit ranging from 0.36% to 0.7%. Acute radiation esophagitis was the most obvious toxicity with an incidence of 14.9%. However, the incidence of late toxicity had no relationship with BED.

Inconsistent with the above study, the prospective single-center phase I trial of dose-escalated hypofractionated radiotherapy without concurrent chemotherapy still showed that severe toxicity was

related to the total dose. Escalation of per dose fraction ranging from 2.28 Gy to 3.42 Gy to a total dose of 57–85.5 Gy in 25 fractions was prescribed to 79 NSCLC patients. They reported a maximum tolerable dose (MTD) of 2.53 Gy in 25 fractions (63.25 Gy total). Grade 4 to 5 pneumonitis occurred in 6 patients, which was strongly correlated with the total dose ( $p = 0.004$ ).<sup>29</sup> These data confirmed that dose escalation in either hypofractionated or conventional radiotherapy warrants caution and should be in a certain range. The benefit of hypofractionation requires further validation.

### SBRT boost for residual disease

An excellent control rate in NSCLC could be achieved when BED exceeds 100 Gy demonstrated by several studies.<sup>30, 31</sup> Recently, a novel technique has been proposed to improve BED. SBRT boost for residual disease after concurrent chemoradiotherapy in NSCLC patients have effectively escalated BED and showed an encouraging loco regional control (LRC) without increased toxicity.

The study of Feddock *et al.* enrolled 61 patients with stage II/III NSCLC. After conventional radiotherapy to a dose of 60 Gy combined with concurrent chemotherapy, remaining lesions were evaluated.<sup>32</sup> Patients who had no evidence of mediastinum progression and  $\leq 5$  cm residual primary tumors identified by positron emission tomography/computed tomography (PET-CT), were further treated with a SBRT boost. Two different prescriptions were delivered based on tumor locations: 10 Gy  $\times$  2 fractions (cumulative BED: 110 Gy) for peripheral lesions, and 6.5 Gy  $\times$  3 fractions (cumulative BED: 102 Gy) for central lesions. After a median follow-up of 13 months, a favorable outcome was reached with a primary tumor control rate of 82.9%. The incidence of radiation pneumonitis was comparable to standard radiotherapy. Similar findings were achieved in Karam's study, in which 16 LANSCLC patients were included.<sup>33</sup> SBRT boost with 20–30 Gy over 5 fractions was boosted after conventional concurrent chemotherapy to a median dose of 50.4 Gy. The result showed that the 1-year OS and LRC rates were 78% and 76%, respectively. Three patients (18%) underwent grade 2 esophagitis and 4 (25%) developed grade 2 pneumonitis. Dose escalation studies for SBRT boost technique to define the MTD were also explored. Nineteen stage III (N1/N2) NSCLC patients with primary tumors  $\leq 8$  cm and lymph nodes  $\leq 5$  cm were analyzed by Higgins *et al.*<sup>34</sup> In this study, patients were treated with standard radiotherapy to

44 Gy with concurrent chemotherapy, followed by a SBRT boost to the lung and nodal residuals. Four SBRT boost regimens were tested: 9 Gy  $\times$  2 fractions (cumulative BED: 87 Gy), 10 Gy  $\times$  2 fractions (cumulative BED: 92.8 Gy), 6 Gy  $\times$  5 fractions (cumulative BED: 100.8 Gy) and 7 Gy  $\times$  5 fractions (cumulative BED: 112.3 Gy). The study confirmed a maximum tolerable boost dose of 6 Gy  $\times$  5 fractions, and a safe dose prescription of 10 Gy  $\times$  2 fractions with no grade 3 or more toxicity. Hepel *et al.* came to a similar conclusion.<sup>35</sup> The trial included 12 stage II/III NSCLC patients with primary tumor and lymph node volume limited within 120 cc and 60 cc, respectively. The SBRT boost to both primary and nodal disease was delivered after 28 fractions of radiotherapy (50.4 Gy) with concurrent chemotherapy. Patients were assigned to four boost dose arms escalating from 16 Gy to 28 Gy: 8 Gy  $\times$  2 fractions (accumulated BED: 88.3 Gy), 10 Gy  $\times$  2 fractions (accumulated BED: 99.5 Gy), 12 Gy  $\times$  2 fractions (accumulated BED: 112.3 Gy) and 14 Gy  $\times$  2 fractions (accumulated BED: 126.7 Gy). The results revealed that the utilization of SBRT boost technique was well tolerated. There was only one patient that experienced grade 5 adverse effect (fatal bleeding). Also, a favorable outcome with a 1-year LRC of 78% was reported; LRC was 100% in patients with a boost dose over 24 Gy.

It should be noted that patients included in these studies were all required to have tumors with limited size/volume. The prescription of dose should also take into account the location. Furthermore, all these data were from studies with small sample size, the potential benefits should be validated in a larger randomized controlled study.<sup>32, 34, 35</sup>

### Personalized radiotherapy

Fixed dose radiotherapy has been long used in dose dose-escalation studies. However, with varied tumor volumes, the tolerance of normal tissue would be different and dose delivery could be personalized accordingly. Several recent studies explored the feasibility of personalized radiotherapy. The phase II trial of van Baardwijk *et al.* evaluated dose intensification based on normal tissues concurrent with chemotherapy for patients with LANSCLC.<sup>36</sup> After completing concurrent chemoradiotherapy to 45 Gy in 1.5 Gy bid fractions, boost dose was escalated 2 Gy per fraction in daily increments until reaching the limit dose of organ at risk (OARs). A total of 137 patients were included, 27% of them received a maximal allowed dose of 69 Gy. The median radiotherapy dose was 65 Gy. They reported a

2-year OS rate of 52.4% and an acceptable adverse effects (G3 esophagitis: 30.1%,  $\geq$  G3 pneumonitis: 3%).

Selective dose escalation according to tumor activity and radiosensitivity has also been tested. High fludeoxyglucose (FDG) uptake prior to treatment has been demonstrated as a negative indicator for local recurrence.<sup>37</sup> Based on this, a phase II randomized clinical trial evaluated the role of dose escalation in high FDG uptake area. Patients who completed an initial radiotherapy of 66 Gy in 24 fractions were then assigned either to receive a boost in the entire primary tumor (group A) or in the high FDG uptake area ( $> 50\%$  maximum standardized uptake values (SUVmax) (group B). Similar with the previous study, maximal boost dose was delivered within the constraints of normal tissue. The results showed that average doses of primary tumors in groups A and B were  $77.3 \pm 7.9$  Gy and  $77.5 \pm 10.1$  Gy, respectively. For group B, the average dose in boost area reached  $86.9 \pm 14.9$  Gy. Organs in the mediastinum were thought to be the major dose-limiting organs, such as great vessels, trachea etc. However, the local control and survival data was not provided.<sup>38</sup> The existence of hypoxia is strongly associated with radioresistance and unfavorable prognosis.<sup>39</sup> Vera *et al.* carried out a prospective phase II clinical trial to investigate the efficacy of selectively dose increase in hypoxic zones.<sup>40</sup> <sup>18</sup>F-misonidazole (<sup>18</sup>F-FMISO) PET-CT was used to detect hypoxic areas and to guide the delineation of boost volumes. Boost dose was prescribed as high as possible within the tolerated dose of lung and spinal cord. A total of 54 LANSCLC patients treated with concurrent chemoradiotherapy were enrolled and 34 patients were <sup>18</sup>F-FMISO positive, of whom, 24 had a dose escalation up to 86 Gy, 10 received a standard radiotherapy of 66 Gy. In <sup>18</sup>F-FMISO positive patients, dose escalation showed no improvement in progression-free survival and OS. It suggests that with dose of hypoxic region escalated up to 86 Gy, the survival still cannot be improved.

Dynamic changes in tumor volume during radiotherapy lead to the idea of adaptive radiotherapy. Kong *et al.*<sup>41</sup> found that tumor volume was significantly shrunk when radiation dose reached 45 Gy, which offers opportunity to adapt target area in the middle of treatment. The reduction in target volume allows delivering higher radiotherapy dose. They then conducted a Phase II clinical trial to test the efficiency of adapting target volume based on midtreatment PET-CT. Forty-two inoperable patients with stage I–III NSCLC were ana-

lyzed. Patients had their target volume re-planned according to midtreatment PET-CT and received a maximally escalated dose without increasing radiation induced lung toxicity. The median dose was 83 Gy. They provided a promising 2-year LRC approximately 62%.<sup>42</sup> The randomized RTOG 1106 trial (NCT01507428) is currently ongoing attempting to verify this finding. The control group was designed to give 60 Gy in 30 fractions. In the adaptive group, the target was redefined on the midtreatment PET-CT after an initial 46.2 Gy in 21 fractions delivered. An individualized escalated dose ranged from 19.8–34.2 Gy/9 fractions with a total dose up to 80.4 Gy. This result would offer us more information.

Furthermore, individualized radiotherapy based on molecular biological information (sensitivity and risk of injury) has also been investigated. Recently, Scott *et al.* proposed a genome-based model to identify tumor radiosensitivity, genomic-adjusted radiotherapy dose (GARD), which was calculated by gene-expression-based radiosensitivity index and the linear quadratic model.<sup>34</sup> Lower tumor GARD score predicts radiation resistance, thus higher radiation doses could be administered. The analysis confirmed that GARD was highest in head and neck cancers and cervical cancers, while the lowest in gliomas, which could be used to guide individualized escalated dose prescription. Another novel idea proposed by MD Anderson Cancer Center is that escalated tumor dose could be delivered according to the risk of radiation pneumonitis estimated by dose-volume histograms and single-nucleotide polymorphism information.<sup>44</sup> Although the above studies are not yet mature enough to guide clinical practice, it may be a development trend in the future.

### New techniques: proton and heavy ion radiotherapy

A lesson from RTOG 0617 is that normal tissue exposure should be fully considered while escalating doses. Previous studies have shown that protons and heavy ions have unique characteristic known as Bragg peak, which offers the possibility to increase tumor dose while sparing normal tissues.<sup>45, 46</sup>

Higgins *et al.* retrospectively analyzed 243,822 patients with stage I–IV NSCLC in the National Cancer Database; 243,474 of them were treated with photon radiotherapy and 348 were treated with proton radiotherapy.<sup>47</sup> The analysis indicates that low-income groups tend to choose non-pro-

ton therapy ( $p < 0.011$ ). After propensity matching analysis, a significant superior 5-year survival rate of stage II–III patients was found in the proton therapy group (23.1% vs. 13.5%;  $p < 0.01$ ). The prospective single-arm phase II clinical trial conducted by Chung *et al.* also confirmed the safety and efficacy of proton radiotherapy.<sup>48</sup> A total of 64 patients with stage III NSCLC were enrolled in the trial; all patients received 74 Gy (relative biologic equivalent, RBE) proton radiotherapy combined with concurrent chemotherapy. They reported a median OS of 26.5 months. The incidence of grade 3 or greater toxicity including esophagitis and radiation pneumonitis was 8% and 14%, respectively. Contradicts to these findings, the more recent results of phase II randomized trials published by Liao *et al.* failed to show the superiority of proton radiotherapy.<sup>49</sup> This trial compared the local control and toxicity of intensity modulated radiation therapy (IMRT) and proton radiotherapy of 66–74 Gy (RBE) combined with concurrent chemotherapy in NSCLC patients. Although there was no significant difference in the incidence of radiation pneumonitis ( $p = 0.40$ ) and local control ( $p = 0.86$ ) in both groups, proton radiotherapy significantly reduced heart exposure ( $p = 0.002$ ). However, OS was not the endpoint for this study, the effect of reduced heart dose on OS is still unknown. The ongoing Phase III prospective clinical trial RTOG 1308 (NCT01993810) which compares the OS between proton radiotherapy and IMRT may bring some insight into this issue. Patients with inoperable stage II–III NSCLC were randomized to proton radiotherapy versus IMRT photon arm. Patients in the proton radiotherapy arm received 2 Gy (RBE) daily to 70 Gy (RBE) course, whereas, those patients on the IMRT arm received 2 Gy to 60 Gy course, concurrent with weekly platinum-based chemotherapy followed by 2 cycles of consolidation chemotherapy.

Heavy ion beams possess the physical advantages of proton beams, also better biological effects, which seemed to be more suitable for dose escalation studies. Takahashi *et al.* performed phase I/II non-randomized prospective clinical study to test carbon ion radiotherapy in LANSCLC.<sup>50</sup> Phase I trial included a total of 36 patients with escalated dose from 68 Gy (RBE) to 76 Gy (RBE) in 16 fractions. The MTD was 76 Gy (RBE) with 2 patients developed G3 toxicity including pneumonitis and tracheo-esophageal fistula. In the phase II trial, 22 patients were analyzed; all of them received a regimen of 72 Gy (RBE) in 16 fractions. No grade 3 or higher toxicity was found. The 2-year LRC and OS

of 72 patients were 93.1% and 51.9%, respectively. This outcome data are in keeping with the multicenter retrospective analysis reported by Karube *et al.*<sup>51</sup> The median dose prescribed for 64 stage II–III NSCLC patients was 72 Gy (RBE) in 16 fractions. The 2-year LRC and OS rate were 81.8% and 62.2%, respectively. No grade 2 or greater toxicity occurred. Shirai *et al.* conducted a retrospective analysis of 23 patients with T2b–4N0M0 stage NSCLC treated with carbon ion radiotherapy.<sup>52</sup> Sixty-five percent of patients received a total dose of 52.8–60 Gy (RBE) in 4 fractions and 35% of patients were treated with 64–70.5 Gy (RBE) in 16 fractions. The 2-year LRC and OS rates were 81% and 70%, respectively, and no person experienced  $\geq 2$  degree radiation pneumonitis. The above studies showed that hypofractionation carbon ion radiotherapy could be safely and efficiently used in LANSCLC. However, the conclusion still needs to be validated by larger prospective studies. Combined modality such as chemotherapy and immunotherapy could be further explored. In addition, cost-effectiveness of proton and heavy ion radiotherapy should also be considered.

## Conclusions

Local recurrence remains the major failure pattern after concurrent chemoradiotherapy of LANSCLC. Although increasing doses can theoretically improve outcome, the negative results of RTOG 0617 suggested that the traditional one dose fits all modes could not improve survival. Though effective dose-escalation methods have been explored, including altered fractionation, adapting individualized increments for different patients, and adopting new technologies and new equipment such as new radiation therapy, no consensus has been achieved yet. It is expected that the ongoing clinical trials and explorations for increasing doses of radiotherapy can further improve control rate survival in LANSCLC.

## Acknowledgements

This study was supported by National key research and development program (2017YFC1311000), BeijingHopeRunSpecialFundofCancerFoundation of China (No.LC2016L03), CAMS Innovation Fund (No.2016-I2M-1-011), Clinical Application Project of Beijing Municipal Commission of Science and Technology (Z171100001017114).

## References

- Auperin A, Le Pechoux C, Rolland E, Curran WJ, Furuse K, Fournel P, et al. Meta-analysis of concomitant versus sequential radiochemotherapy in locally advanced non-small-cell lung cancer. *J Clin Oncol* 2010; **28**: 2181-90. doi: 10.1200/JCO.2009.26.2543
- Machtay M, Bae K, Movsas B, Paulus R, Gore EM, Komaki R, et al. Higher biologically effective dose of radiotherapy is associated with improved outcomes for locally advanced non-small cell lung carcinoma treated with chemoradiation: an analysis of the Radiation Therapy Oncology Group. *Int J Radiat Oncol Biol Phys* 2012; **82**: 425-44. doi: 10.1016/j.ijrobp.2010.09.004
- Schild SE, Stella PJ, Geyer SM, Bonner JA, Marks RS, McGinnis WL, et al. Phase III trial comparing chemotherapy plus once-daily or twice-daily radiotherapy in Stage III non-small-cell lung cancer. *Int J Radiat Oncol Biol Phys* 2002; **54**: 370-8. doi: 10.1016/S0360-3016(02)02930-9
- Furuse K, Fukuoka M, Kawahara M, Nishikawa H, Takada Y, Kudoh S, et al. Phase III study of concurrent versus sequential thoracic radiotherapy in combination with mitomycin, vindesine, and cisplatin in unresectable stage III non-small-cell lung cancer. *J Clin Oncol* 1999; **17**: 2692-99. doi: 10.1200/JCO.1999.17.9.2692
- Fournel P, Robinet G, Thomas P, Souquet PJ, Lena H, Vergnenegre A, et al. Randomized phase III trial of sequential chemoradiotherapy compared with concurrent chemoradiotherapy in locally advanced non-small-cell lung cancer: Groupe Lyon-Saint-Etienne d'Oncologie Thoracique-Groupe Français de Pneumo-Cancerologie NPC 95-01 Study. *J Clin Oncol* 2005; **23**: 5910-7. doi: 10.1200/JCO.2005.03.070
- Zatloukal P, Petruzella L, Zemanova M, Havel L, Janku F, Judas L, et al. Concurrent versus sequential chemoradiotherapy with cisplatin and vinorelbine in locally advanced non-small cell lung cancer: a randomized study. *Lung Cancer* 2004; **46**: 87-98. doi: 10.1016/j.lungcan.2004.03.004
- Belani CP, Choy H, Bonomi P, Scott C, Travis P, Haluschak J, et al. Combined chemoradiotherapy regimens of paclitaxel and carboplatin for locally advanced non-small-cell lung cancer: a randomized phase II locally advanced multi-modality protocol. *J Clin Oncol* 2005; **23**: 5883-91. doi: 10.1200/JCO.2005.55.405
- Curran WJ Jr, Paulus R, Langer CJ, Komaki R, Lee JS, Hauser S, et al. Sequential vs. concurrent chemoradiation for stage III non-small cell lung cancer: randomized phase III trial RTOG 9410. *J Natl Cancer Inst* 2011; **103**: 1452-60. doi: 10.1093/jnci/djr325
- Bradley JD, Bae K, Graham MV, Byhardt R, Govindan R, Fowler J, et al. Primary analysis of the phase II component of a phase I/II dose intensification study using three-dimensional conformal radiation therapy and concurrent chemotherapy for patients with inoperable non-small-cell lung cancer: RTOG 0117. *J Clin Oncol* 2010; **28**: 2475-80. doi: 10.1200/JCO.2009.27.1205
- Schild SE, McGinnis WL, Graham D, Hillman S, Fitch TR, Northfelt D, et al. Results of a Phase I trial of concurrent chemotherapy and escalating doses of radiation for unresectable non-small-cell lung cancer. *Int J Radiat Oncol Biol Phys* 2006; **65**: 1106-11. doi: 10.1016/j.ijrobp.2006.02.046
- Lee CB, Stinchcombe TE, Moore DT, Morris DE, Hayes DN, Halle J, et al. Late complications of high-dose (>=66 Gy) thoracic conformal radiation therapy in combined modality trials in unresectable stage III non-small cell lung cancer. *J Thorac Oncol* 2009; **4**: 74-9. doi: 10.1097/JTO.0b013e3181915028
- Blackstock AW, Ho C, Butler J, Fletcher-Steede J, Case LD, Hinson W, et al. Phase Ia/Ib chemo-radiation trial of gemcitabine and dose-escalated thoracic radiation in patients with stage III A/B non-small cell lung cancer. *J Thorac Oncol* 2006; **1**: 434-40. doi: 10.1016/S1556-0864(15)31608-7
- Bradley JD, Paulus R, Komaki R, Masters G, Blumenschein G, Schild S, et al. Standard-dose versus high-dose conformal radiotherapy with concurrent and consolidation carboplatin plus paclitaxel with or without cetuximab for patients with stage IIIA or IIIB non-small-cell lung cancer (RTOG 0617): a randomised, two-by-two factorial phase 3 study. *Lancet Oncol* 2015; **16**: 187-99. doi: 10.1016/S1470-2045(14)71207-0
- Belderbos J, Walraven I, van Diessen J, Verheij M, de Ruyscher D. Radiotherapy dose and fractionation for stage III NSCLC. *Lancet Oncol* 2015; **16**: e156-7. doi: 10.1016/S1470-2045(15)70121-X
- Kerr KM, Lamb D. Actual growth rate and tumour cell proliferation in human pulmonary neoplasms. *Br J Cancer* 1984; **50**: 343-9. PMID: 6087867
- Trott KR. Cell repopulation and overall treatment time. *Int J Radiat Oncol Biol Phys* 1990; **19**: 1071-5. doi: 10.1016/0360-3016(90)90036-J
- Machtay M, Hsu C, Komaki R, Sause WT, Swann RS, Langer CJ, et al. Effect of overall treatment time on outcomes after concurrent chemoradiation for locally advanced non-small-cell lung carcinoma: analysis of the Radiation Therapy Oncology Group (RTOG) experience. *Int J Radiat Oncol Biol Phys* 2005; **63**: 667-71. doi: 10.1016/j.ijrobp.2005.03.037
- Fowler JF, Chappell R. Non-small cell lung tumors repopulate rapidly during radiation therapy. *Int J Radiat Oncol Biol Phys* 2000; **46**: 516-7. doi: 10.1016/S0360-3016(99)00364-8
- Brower JV, Amini A, Chen S, Hullett CR, Kimple RJ, Wojcieszynski AP, et al. Improved survival with dose-escalated radiotherapy in stage III non-small-cell lung cancer: analysis of the National Cancer Database. *Ann Oncol* 2016; **27**: 1887-94. doi: 10.1093/annonc/mdw276
- Yamoah K, Showalter TN, Ohri N. Radiation therapy intensification for solid tumors: a systematic review of randomized trials. *Int J Radiat Oncol Biol Phys* 2015; **93**: 737-45. doi: 10.1016/j.ijrobp.2015.07.2284
- Ramroth J, Cutter DJ, Darby SC, Higgins GS, McGale P, Partridge M, et al. Dose and fractionation in radiation therapy of curative intent for non-small cell lung cancer: meta-analysis of randomized trials. *Int J Radiat Oncol Biol Phys* 2016; **96**: 736-47. doi: 10.1016/j.ijrobp.2016.07.022
- Mehta M, Scrimger R, Mackie R, Paliwal B, Chappell R, Fowler J. A new approach to dose escalation in non-small-cell lung cancer. *Int J Radiat Oncol Biol Phys* 2001; **49**: 23-33. doi: 10.1016/S0360-3016(00)01374-2
- Saunders M, Dische S, Barrett A, Harvey A, Gibson D, Parmar M. Continuous hyperfractionated accelerated radiotherapy (CHART) versus conventional radiotherapy in non-small-cell lung cancer: a randomised multicentre trial. CHART Steering Committee. *Lancet* 1997; **350**: 161-5. doi: 10.1016/S0140-6736(97)06305-8
- Baumann M, Herrmann T, Koch R, Matthiessen W, Appold S, Wahlers B, et al. Final results of the randomized phase III CHARTWEL-trial (ARO 97-1) comparing hyperfractionated-accelerated versus conventionally fractionated radiotherapy in non-small cell lung cancer (NSCLC). *Radiother Oncol* 2011; **100**: 76-85. doi: 10.1016/j.radonc.2011.06.031
- Mauguen A, Le Pechoux C, Saunders MI, Schild SE, Turrisi AT, Baumann M, et al. Hyperfractionated or accelerated radiotherapy in lung cancer: an individual patient data meta-analysis. *J Clin Oncol* 2012; **30**: 2788-97. doi: 10.1200/JCO.2012.41.6677
- Din OS, Harden SV, Hudson E, Mohammed N, Pemberton LS, Lester JF, et al. Accelerated hypo-fractionated radiotherapy for non small cell lung cancer: results from 4 UK centres. *Radiother Oncol* 2013; **109**: 8-12. doi: 10.1016/j.radonc.2013.07.014
- Sun LM, Leung SW, Wang CJ, Chen HC, Fang FM, Huang EY, et al. Concomitant boost radiation therapy for inoperable non-small-cell lung cancer: preliminary report of a prospective randomized study. *Int J Radiat Oncol Biol Phys* 2000; **47**: 413-8. doi: 10.1016/S0360-3016(00)00429-6
- Kaster TS, Yaremko B, Palma DA, Rodrigues GB. Radical-intent hypofractionated radiotherapy for locally advanced non-small-cell lung cancer: a systematic review of the literature. *Clin Lung Cancer* 2015; **16**: 71-9. doi: 10.1016/j.clc.2014.08.002
- Cannon DM, Mehta MP, Adkison JB, Khuntia D, Traynor AM, Tome WA, et al. Dose-limiting toxicity after hypofractionated dose-escalated radiotherapy in non-small-cell lung cancer. *J Clin Oncol* 2013; **31**: 4343-8. doi: 10.1200/JCO.2013.51.5353
- Grills IS, Hope AJ, Guckenberger M, Kestin LL, Werner-Wasik M, Yan D, et al. A collaborative analysis of stereotactic lung radiotherapy outcomes for early-stage non-small-cell lung cancer using daily online cone-beam computed tomography image-guided radiotherapy. *J Thorac Oncol* 2012; **7**: 1382-93. doi: 10.1097/JTO.0b013e318260e00d
- Onishi H, Shirato H, Nagata Y, Hiraoka M, Fujino M, Gomi K, et al. Hypofractionated stereotactic radiotherapy (HypoFXSRT) for stage I non-small cell lung cancer: updated results of 257 patients in a Japanese multi-institutional study. *J Thorac Oncol* 2007; **2**: 594-100. doi: 10.1097/JTO.0b013e318074de34
- Feddock J, Arnold SM, Shelton BJ, Sinha P, Conrad G, Chen L, et al. Stereotactic body radiation therapy can be used safely to boost residual disease in locally advanced non-small cell lung cancer: a prospective study. *Int J Radiat Oncol Biol Phys* 2013; **85**: 1325-31. doi: 10.1016/j.ijrobp.2012.11.011
- Karam SD, Horne ZD, Hong RL, McRae D, Duhamel D, Nasr NM. Dose escalation with stereotactic body radiation therapy boost for locally advanced non small cell lung cancer. *Radiat Oncol* 2013; **8**: 179. doi: 10.1186/1748-717X-8-179

34. Higgins KA, Pillai RN, Chen Z, Tian S, Zhang C, Patel P, et al. Concomitant chemotherapy and radiotherapy with SBRT boost for unresectable stage III non-small cell lung cancer: a phase I study. *J Thorac Oncol* 2017; **12**: 1687-95. doi: 10.1016/j.jtho.2017.07.036
35. Hepel JT, Leonard KL, Safran H, Ng T, Taber A, Khurshid H, et al. Stereotactic body radiation therapy boost after concurrent chemoradiation for locally advanced non-small cell lung cancer: a phase 1 dose escalation study. *Int J Radiat Oncol Biol Phys* 2016; **96**: 1021-7. doi: 10.1016/j.ijrobp.2016.08.032
36. van Baardwijk A, Reymen B, Wanders S, Borger J, Ollers M, Dingemans AM, et al. Mature results of a phase II trial on individualised accelerated radiotherapy based on normal tissue constraints in concurrent chemo-radiation for stage III non-small cell lung cancer. *Eur J Cancer* 2012; **48**: 2339-46. doi: 10.1016/j.ejca.2012.04.014
37. Abramuk A, Tokalov S, Zophel K, Koch A, Szluha Lazanyi K, Gillham C, et al. Is pre-therapeutic FDG-PET/CT capable to detect high risk tumor subvolumes responsible for local failure in non-small cell lung cancer? *Radiother Oncol* 2009; **91**: 399-404. doi: 10.1016/j.radonc.2009.01.003
38. van Elmpt W, De Ruysscher D, van der Salm A, Lakeman A, van der Stoep J, Emans D, et al. The PET-boost randomised phase II dose-escalation trial in non-small cell lung cancer. *Radiother Oncol* 2012; **104**: 67-71. doi: 10.1016/j.radonc.2012.03.005
39. Salem A, Asselin MC, Reymen B, Jackson A, Lambin P, West CML, et al. Targeting hypoxia to improve non-small cell lung cancer outcome. *J Natl Cancer Inst* 2018; **110**: 14-30. doi: 10.1093/jnci/djx160
40. Vera P, Thureau S, Chaumet-Riffaud P, Modzelewski R, Bohn P, Vermandel M, et al. Phase II study of a radiotherapy total dose increase in hypoxic lesions identified by (18)F-misonidazole PET/CT in patients with non-small cell lung carcinoma (RTEP5 Study). *J Nucl Med* 2017; **58**: 1045-53. doi: 10.2967/jnumed.116.188367
41. Kong FM, Frey KA, Quint LE, Ten Haken RK, Hayman JA, Kessler M, et al. A pilot study of [18F]fluorodeoxyglucose positron emission tomography scans during and after radiation-based therapy in patients with non small-cell lung cancer. *J Clin Oncol* 2007; **25**: 3116-23. doi: 10.1200/JCO.2006.10.3747
42. Kong FM, Ten Haken RK, Schipper M, Frey KA, Hayman J, Gross M, et al. Effect of midtreatment PET/CT-adapted radiation therapy with concurrent chemotherapy in patients with locally advanced non-small-cell lung cancer: a phase 2 clinical trial. *JAMA Oncol* 2017; **3**: 1358-65. doi: 10.1001/jamaoncol.2017.0982
43. Scott JG, Berglund A, Schell MJ, Mihaylov I, Fulp WJ, Yue B, et al. A genome-based model for adjusting radiotherapy dose (GARD): a retrospective, cohort-based study. *Lancet Oncol* 2017; **18**: 202-11. doi: 10.1016/S1473-2045(16)30648-9
44. Vinogradskiy Y, Tucker SL, Bluett JB, Wages CA, Liao Z, Martel MK. Prescribing radiation dose to lung cancer patients based on personalized toxicity estimates. *J Thorac Oncol* 2012; **7**: 1676-82. doi: 10.1097/JTO.0b013e318269410a
45. Chang JY, Zhang X, Wang X, Kang Y, Riley B, Bilton S, et al. Significant reduction of normal tissue dose by proton radiotherapy compared with three-dimensional conformal or intensity-modulated radiation therapy in Stage I or Stage III non-small-cell lung cancer. *Int J Radiat Oncol Biol Phys* 2006; **65**: 1087-96. doi: 10.1016/j.ijrobp.2006.01.052
46. Kanai T, Endo M, Minohara S, Miyahara N, Koyama-ito H, Tomura H, et al. Biophysical characteristics of HIMAC clinical irradiation system for heavy-ion radiation therapy. *Int J Radiat Oncol Biol Phys* 1999; **44**: 201-10. doi: 10.1016/S0360-3016(98)00544-6
47. Higgins KA, O'Connell K, Liu Y, Gillespie TW, McDonald MW, Pillai RN, et al. National Cancer Database analysis of proton versus photon radiation therapy in non-small cell lung cancer. *Int J Radiat Oncol Biol Phys* 2017; **97**: 128-37. doi: 10.1016/j.ijrobp.2016.10.001
48. Chang JY, Verma V, Li M, Zhang W, Komaki R, Lu C, et al. Proton beam radiotherapy and concurrent chemotherapy for unresectable stage III non-small cell lung cancer: final results of a phase 2 study. *JAMA Oncol* 2017; **3**: e172032. doi: 10.1001/jamaoncol.2017.2032
49. Liao Z, Lee JJ, Komaki R, Gomez DR, O'Reilly MS, Fossella FV, et al. Bayesian adaptive randomization trial of passive scattering proton therapy and intensity-modulated photon radiotherapy for locally advanced non-small-cell lung cancer. *J Clin Oncol* 2018; **36**: 1813-22. doi: 10.1200/JCO.2017.74.0720
50. Takahashi W, Nakajima M, Yamamoto N, Yamashita H, Nakagawa K, Miyamoto T, et al. A prospective nonrandomized phase I/II study of carbon ion radiotherapy in a favorable subset of locally advanced non-small cell lung cancer (NSCLC). *Cancer* 2015; **121**: 1321-7. doi: 10.1002/cncr.29195
51. Karube M, Yamamoto N, Shioyama Y, Saito J, Matsunobu A, Okimoto T, et al. Carbon-ion radiotherapy for patients with advanced stage non-small-cell lung cancer at multicenters. *J Radiat Res* 2017; **58**: 761-4. doi: 10.1093/jrr/rrx037
52. Shirai K, Kawashima M, Saitoh JI, Abe T, Fukata K, Shigeta Y, et al. Clinical outcomes using carbon-ion radiotherapy and dose-volume histogram comparison between carbon-ion radiotherapy and photon therapy for T2b-4N0M0 non-small cell lung cancer - a pilot study. *PLoS One*. 2017; **12**: e0175589. doi: 10.1371/journal.pone.0175589

# Diffusion kurtosis imaging and conventional diffusion weighted imaging to assess electrochemotherapy response in locally advanced pancreatic cancer

Vincenza Granata<sup>1</sup>, Roberta Fusco<sup>1</sup>, Sergio Venanzio Setola<sup>1</sup>, Raffaele Palaia<sup>3</sup>, Vittorio Albino<sup>3</sup>, Mauro Piccirillo<sup>3</sup>, Robert Grimm<sup>4</sup>, Antonella Petrillo<sup>1</sup>, Francesco Izzo<sup>3</sup>

<sup>1</sup> Division of Radiology, Istituto Nazionale Tumori - IRCCS - Fondazione G. Pascale, Napoli, Italia

<sup>2</sup> IGEA SpA

<sup>3</sup> Division of Hepatobiliary Surgical Oncology, Unit, Istituto Nazionale Tumori, IRCCS, Fondazione G. Pascale, Napoli, Italia

<sup>4</sup> Siemens Healthcare GmbH, Erlangen, Germany

Radiol Oncol 2019; 53(1): 15-24.

Received 24 September 2018

Accepted 18 November 2018

Correspondence to: Vincenza Granata, Division of Radiology, Istituto Nazionale Tumori - IRCCS - Fondazione G. Pascale, Napoli, Italia. Phone: +39 081 5903 714; Fax: +39 0815903825; E-mail: v.granata@istitutotumori.na.it

Disclosure: The authors declare that have no conflict of interest. Roberta Fusco is an employee of IGEA S.p.A and she contributes to bio-medical images processing and statistical analysis. Robert Grimm is an employee of Siemens Healthcare and develops the MR Body Diffusion Toolbox, a post-processing software to calculate IVIM and Kurtosis maps.

**Background.** The aim of the study was to evaluate diagnostic performance of functional parameters derived by conventional mono-exponential approach of diffusion weighted imaging (DWI) and by diffusion kurtosis imaging (DKI) in the assessment of pancreatic tumours treated with electrochemotherapy (ECT).

**Patients and methods.** Twenty-one consecutive patients with locally advanced pancreatic adenocarcinoma subjected to ECT were enrolled in a clinical approved trial. Among twenty-one enrolled patients, 13/21 (61.9%) patients were subjected to MRI before and after ECT. DWI was performed with a 1.5 T scanner; a free breathing axial single shot echo planar DWI pulse sequence parameters were acquired using seven b value = 0, 50, 100, 150, 400, 800, 1000 s/mm<sup>2</sup>. Apparent diffusion coefficient by conventional mono-exponential approach and mean of diffusion coefficient (MD) and mean of diffusional kurtosis (MK) by DKI approach were derived from DWI. Receiver operating characteristic (ROC) analysis was performed and sensitivity, specificity, positive and negative predictive value were calculated.

**Results.** Among investigated diffusion parameters, only the MD derived by DKI showed a significant variation of values between pre and post treatment ( $p = 0.02$  at Wilcoxon test) and a significant statistically difference for percentage change between responders and not responders ( $p = 0.01$  at Kruskal Wallis test). MD had a good diagnostic performance with a sensitivity of 80%, a specificity of 100% and area under ROC of 0.933.

**Conclusions.** MD derived by DKI allows identifying responders and not responders patients subject to ECT treatment. MD had higher diagnostic performance to assess ECT response compared to conventional DWI derived parameters.

Key words: pancreatic cancer; electrochemotherapy; magnetic resonance imaging; diffusion weighted imaging; diffusion kurtosis imaging

## Introduction

Electrochemotherapy (ECT) is a promising tool for treatment of deep tumours.<sup>1-6</sup> This ablative technique combines the administration of chemotherapeutic drugs with electric pulses for cell mem-

brane electroporation.<sup>7</sup> In our previous studies<sup>6-9</sup>, we demonstrated the safety and efficacy of the treatment in locally advanced pancreatic cancer. However, the correct assessment of the efficacy of ECT is a challenge for a radiologist since tumour necrosis is not always correlated with a dimension-

al change so that the response evaluation criteria in solid tumour (RECIST) are not adequate to assess the ECT treatment.<sup>9</sup> In this scenario, we evaluated functional parameters extracted by diffusion weighted imaging (DWI).<sup>10</sup> The practice of DWI into a standard magnetic resonance (MR) protocol is increasing, thanks to its ability to detect and characterize a lesion so as its capability in the assessment of treatment response.<sup>11-12</sup> Promising results for improved detection and monitoring of therapeutic effects, in terms of prediction and early response assessment, have been reported, amongst others, for the liver<sup>13</sup>, pancreas<sup>14</sup>, kidneys<sup>15</sup> and prostate.<sup>16</sup> Several authors have reported that DWI sequence have a potential in the evaluation of patients with locally advanced pancreatic cancer, especially improving the staging; nevertheless, it is still unclear whether and how DWI could be helpful for identification, characterization, prognostic stratification and follow-up during treatment. DWI assessment may be done qualitatively or quantitatively, with a mono-exponential (apparent diffusion coefficient map, ADC) or bi-exponential analysis (intravoxel incoherent motion model or diffusion kurtosis imaging, DKI) of data.<sup>17-19</sup> DWI signal is due to the water mobility that reproduces indirectly tissue structures.<sup>14-18</sup> Traditionally DWI approach is based on the hypothesis that water molecules diffuse within a voxel following a single component direction according to a Gaussian behavior, without any restriction.<sup>18-19</sup> However, according to the presence of microstructures, random motion or diffusion of thermally agitated water molecules within biologic tissues exhibits non-Gaussian phenomena due to the presence of microstructures.<sup>19</sup> This model, proposed by Jensen *et al.* in 2005, considers a non-Gaussian diffusion model called DKI.<sup>19</sup> This approach evaluates the kurtosis coefficient (K) that shows the deviation of tissue diffusion from a Gaussian model, and the diffusion coefficient (D) with the correction of non-Gaussian bias. Several researches have shown that DKI is more performing than conventional ADC in tumour detecting and grading assessment.<sup>19-23</sup> Kartalis *et al.*<sup>24</sup> reported that the correction for kurtosis effects has the potential to increase the diagnostic accuracy of DWI in patients with pancreatic ductal adenocarcinoma. To the best of our knowledge, no studies that evaluated the diagnostic performance of DKI parameters to assess ECT response have been published.

The purpose of this retrospective study is to evaluate the diagnostic performance of ADC by conventional mono-exponential approach and MD and MK by DKI to assess ECT response.

## Patients and methods

### Study population

The patients were enrolled in a clinical phase I/II study approved by the Ethical Committee of the National Cancer Institute "G. Pascale Foundation - IRCCS" of Naples (deliberation n. 482 of 02/07/2014). The study endpoints were the feasibility and safety of ECT in the multimodal treatment of pancreatic cancer in patients with locally advanced disease and not suitable for radical surgery.

Twenty-one consecutive patients (11 female and 10 male) were enrolled in a clinical approved trial. Inclusion criteria were: age between 18–80 years; good mental health; life expectancy  $\geq 3$  months; histologically confirmed diagnosis of pancreatic adenocarcinoma; locally advanced disease (stage III) confirmed with preoperative radiological assessment, unfit for curative surgery. Exclusion criteria were: pregnant women, significant heart disease, coagulation disturbances, allergy to bleomycin, lung and kidney dysfunction, implanted defibrillator or pacemaker, concomitant presence of distant metastases. All patient enrolled signed the informed consent. All patients enrolled with diagnosis of locally advanced pancreatic adenocarcinoma received systemic chemotherapy before ECT treatment. Two chemotherapy regimens were adopted: gemcitabine + oxaliplatin (GEMOX) or 5-FU/leucovorin, irinotecan, and oxaliplatin (FOLFIRINOX). GEMOX regime consisted of 100-minute infusion of gemcitabine at a dose 1.000 mg/m<sup>2</sup> administered on day 1 and a 2-hour infusion of oxaliplatin at a dose of 100 mg/m<sup>2</sup> administered on day 2. Treatment was repeated every 2 weeks for 3 months. FOLFIRINOX regime consisted of 2-hour intravenous infusion of oxaliplatin at a dose of 85 mg/m<sup>2</sup> immediately followed 2-hour intravenous infusion of leucovorin at a dose of 400 mg/m<sup>2</sup> with the addition, after 30 minutes, of 90-minute intravenous infusion of irinotecan at a dose of 180 mg/m<sup>2</sup>. This treatment was immediately followed by intravenous bolus of fluorouracil at a dose of 400 mg/m<sup>2</sup>, followed by a continuous intravenous infusion of 2400 mg/m<sup>2</sup> over a 46-hour period every 2 weeks. Fourteen (14/21, 66.7%) patients were subjected to GEMOX and seven patients (7/21, 33.3%) were injected with FOLFIRINOX before ECT treatment (median time between start of chemotherapy treatment and ECT was 124 days, range 118–139).

Among 21 enrolled patients, 13 were subjected to MRI before and after ECT. Median time between basal MR imaging assessment and ECT was 15 days (range 7–19). Median time between ECT

TABLE 1. Patients' characteristics

Patients (n = 21)	
Histotype, %	
Adenocarcinoma	100 (21/21)
Location, %	
Head	52.4 (11/21)
Body/tail	47.6 (10/21)
Largest diameter lesion, cm (range)	5.2 (2.2–9.9)
Venous involvement (superior mesenteric vein [SMV] or portal vein [PV]), %	
Yes	81.0 (17/21)
No	19.0 (4/21)
Arterial encasement, %	
Yes	57.1 (12/21)
No	42.9 (9/21)

and first MR in the follow-up assessment was 38 days (range 27–72). Patient characteristics are summarized in the Table 1.

### ECT protocol

ECT was performed on pancreas tumour intra-operatively, bleomycin was administrated intravenously (15.000 IU/m<sup>2</sup>) before the application of electrical pulses to the target area. Electric pulses were applied by needle electrodes with linear, hexagonal configuration or variable geometry using multiple single needles (IGEA S.p.A., Carpi, Italy) depending on the size and location of the tumours. Cliniporator™ (IGEA S.p.A., Italy) was used to deliver electric voltage with the following parameters using linear or hexagonal geometry: 8–96 pulses of 400–730V and 1000 V/cm, of 100µs duration, at 5000 Hz repetition frequency. When a variable geometry was used, a single pulse of 100µs duration

at 1000 V/cm was delivered with a single relieved R-wave (ECG synchronization). Electric impulses were synchronized with the ECG for a safe delivery of the electric impulses to pancreas. ECG synchronization was done with Accusync 42 (AccuSync Medical Research Corporation, Milford, USA). Treatment was completed within the window from 8 to 40 minutes after the end of the bleomycin bolus. This time window ensures the highest concentration of drug within the lesion.

The standard used to assess treatment outcome has been the consensus between two radiological modalities (computed tomography [CT] assessed using Choi criteria<sup>25</sup>, position emission tomography-CT [PET-CT]) assessed using PERCIST criteria<sup>26</sup> and dynamic contrast enhanced-MRI [DCE-MRI] assessed by variation in wash-in and wash-out slope [WIS and WOS]). Details of these criteria were reported in Granata *et al.* including also the specifications about the two dynamic parameters WIS and WOS extracted by DCE-MRI.<sup>9</sup>

### MR protocol and images analysis

DWI was performed with a 1.5 T scanner (Magnetom Symphony, Siemens Medical System, Erlangen, Germany) equipped with a phased-array body coil. Patients were placed in a supine, head-first position. A free breathing axial single shot echo planar DWI pulse sequence parameters were: repetition time (TR) / echo time (TE) = 7500/91 ms; slice thickness = 3 mm; flip angle = 90 degrees, Matrix = 192x192 and field of view (FOV) = 340 x 340 mm<sup>2</sup>; b value = 0, 50, 100, 150, 400, 800, 1000 s/mm<sup>2</sup>. Other sequences of MRI protocol were provided in the Table 2.

Regions of interest (ROIs) were manually segmented by two expert radiologists in consensus, simultaneously avoiding encircling any distortion artefacts. One radiologist with over 20 years of clinical

TABLE 2. MRI protocol parameters

Sequence	Orientation	TR/TE/FA (ms/ms/deg.)	FOV (mm <sup>2</sup> )	Acquisition matrix	Slice thickness/gap (mm)
HASTE T2-W	Axial	1500/90/180	380 x 380	320 x 320	5/0
FLASH T1-W, In-out phase	Axial	160/4.87/70	285 x 380	192 x 256	5/0
FLASH T1-W, out phase	Axial	178/2.3/80	325 x 400	416 x 412	3/0
DWI	Axial	7500/91/90	340 x 340	192 x 192	3/0
VIBE T1-W	Axial	4.89/2.38/10	325 x 400	320 x 260	3/0
TWIST T1-W, Pre and post contrast agent injection	Axial	3.01/1.09/25	300 x 300	256 x 256	2/0

AT = acquisition time; DWI = diffusion-weighted imaging; FA = flip angle; FLASH = fast low angle shot; FOV = field of view; HASTE = half-Fourier acquisition single-shot turbo spin-echo; TE = echo time; TR = repetition time; TWIST = time-resolved angiography with stochastic trajectories; VIBE = volumetric interpolated breath hold examination; W = weighted

experience, and one with 10 years of clinical experience in interpreting abdominal MR imaging studies drew ROIs on DWI image at the highest b value both on pre-treatment images and on post treatment images. The tumour was contoured slice by slice to obtain the neoplastic volume of interest (VOI). Size of VOI was variable depending by tumour size (maximum diameter range was reported in Table 1).

Features from DWI data have been computed pixel by pixel to obtain the median value of ROIs.

### DWI features

Per each voxel, 3 features were extracted from DWI data using the mono-exponential approach and the DKI model.

DWI signal decay is most commonly analysed using the monoexponential model.<sup>17-18</sup>

$$ADC = \frac{\ln\left(\frac{S_0}{S_b}\right)}{b} \quad [1]$$

where  $S_b$  is the MRI signal intensity with diffusion weighting  $b$ ,  $S_0$  is the non-diffusion-weighted signal intensity and ADC is the apparent diffusion coefficient.

Multi-b DW images were obtained by fitting of voxel-by-voxel using the diffusion kurtosis signal decay equation [2] by a two-variable linear least squares algorithm as used in previous study.<sup>19</sup>

$$S(b) = S_0 \exp\left(-b \cdot D + \frac{1}{6} b^2 \cdot D^2 \cdot K\right) \quad [2]$$

In this equation,  $D$  is a corrected diffusion coefficient; and  $K$  is the excess diffusion kurtosis coefficient.  $K$  describes the degree that molecular motion deviates from the perfect Gaussian distribution. When  $K$  is equal to 0, equation [2] evolves into a conventional monoexponential equation [1]:

The difference between  $D$  and ADC is that  $D$  is a corrected form of ADC for use in non-Gaussian circumstances.

The parameters of conventional DWI (ADC) and DKI (Mean of Diffusion Coefficient (MD) and mean of Diffusional Kurtosis (MK)) were obtained from the multi-b DWI data with all measured  $b$  values using the prototype post-processing software Body Diffusion Toolbox (Siemens Healthcare, Erlangen, Germany).

### CT acquisition protocol and images analysis

Non contrast-enhanced phase and triple-phase contrast-enhanced CT was performed with a 64-de-

tor row scanner (Optima 660, GE Healthcare, USA). CT scanning parameters were 120 kVp, 100–470 mAs (NI 16.36), 2.5-mm slice thickness and table speed 0.984/1 mm/rotation. Scans were carried out including a region encompassing the liver from diaphragm to iliac crests. Phases were as follows; hepatic arterial phase 30–40 s after injection of 120 mL of a nonionic contrast medium (Iomeprol, Iomeron 400, Bracco, Milan, Italy) with a bolus-triggered technique (120 kVp; 40–60 mA; trigger threshold, 180 HUs in descending aorta), portal and equilibrium phase 90 s and 120 s after contrast injection. The contrast medium was administered at a rate of 4 mL/s through antecubital vein with an automated injector system (Empower CTA, E-Z-EM Inc., New York, United States). For CT images, the response to ECT was evaluated according the Choi criteria.<sup>25</sup> CR is disappearance of target lesion; PR is a decrease in tumour size  $\geq 10\%$  or decrease in tumour density  $\geq 15\%$  on CT; SD is neither PR nor PD; and PD is an increase in tumour size  $\geq 10\%$  and does not meet PR criteria by tumour density.

### PET/CT acquisition protocol and images analysis

18F-FDG PET/CT studies were acquired 60 min after the administration of 300–385 MBq of FDG either with a Siemens ECAT EXACT 47 or a General Electric DST 600 PET-CT scanner. Patients fasted for at least 6 h, and blood glucose level was  $< 150$  mg/dl. Each patient underwent the baseline and the pre-operative study on the same scanner. Irregular volumes of interest (VOIs) were semi-automatically drawn by the expert investigator on orthogonal planes using a dedicated workstation and software. For each patient both studies were analysed at the same time in order to minimize discrepancies in VOI positioning. For each study, maximum standardized uptake value (SUVmax) values of the pancreas lesion were recorded. The analysis of 18F-FDG PET/CT results was performed by comparing measurements obtained in the pancreatic lesion at baseline (SUV1) and after treatment (SUV2). This change was expressed as the percentage of SUV reduction ( $\Delta SUV = (SUV1 - SUV2) / SUV1 \times 100$ ). Objective therapeutic response was defined according to PERCIST 1.0.<sup>26</sup> complete metabolic response (CMR) is complete resolution of 18F-FDG uptake within the measurable target lesion and indistinguishable from surrounding background blood-pool levels with no new 18F-FDG-avid lesions; partial metabolic response

(PMR) is reduction of a minimum of 30% in the target tumour 18F-FDG SUVmax; stable metabolic disease (SMD) is disease other than CMR, PMR, or progressive metabolic disease; and progressive metabolic disease is a 30% increase in 18F-FDG PET/CT SUVmax or advent of new 18F-FDG-avid lesions that are typical of cancer.

**Statistical analysis**

Continuous variables were presented as the median ± standard deviation (SD). Wilcoxon test and the Kruskal Wallis test were performed to assess significant statistically differences between pre and post parameters value and between responders and not responders, respectively. As well, Receiver operating characteristic (ROC) curves were calculated to characterize each parameter value for evaluating the capability to differentiate responders versus non responders. The optimal cut-off values (obtained according to the maximal Youden index = sensitivity + specificity-1), the corresponding sensitivity, specificity, positive predictive value (PPV), negative predictive value (NPV) and accuracy were calculated.

A p value < 0.05 was considered statistically significant. The Statistics Toolbox of Matlab R2007a (The Math-Works Inc., Natick, MA) was used to perform statistical analysis.

**TABLE 3.** Electrochemotherapy (ECT) response classification for each patient

No.	CT response according Choi	DCE-MRI response according ΔWIS and ΔWOS	PET response according PERCIST	Consensus among two modalities
1	PR	PR	PD	PR
2	PR	PR		PR
3	PR	PR	PR	PR
4	PR	PR		PR
10	PR		CR	PR
11	PR	SD	PR	SD
12	SD	PR	SD	SD
13	PR	SD	PR	PR
14	PR	PR	PR	PR
17	PR	PR	SD	PR
18	PR	PR	SD	PR
19	PR	PR/SD	PR	PR
20	PR	PR		PR
21	SD	SD		SD

Choi = Choi criteria; CT = computed tomography; DCE-MRI = dynamic contrast enhanced magnetic resonance imaging; PERCIST = positron emission tomography response criteria in solid tumours; PR = partial response; SD = stable disease; WIS = wash-in slope; WOS = wash-out slope; Δ = percentage change between pre and post treatment

**Results**

According to the results reported by our previous study<sup>9</sup>, among 13 patients subjected to MRI, 10 showed a significant response while 3 patients were classified in a stable disease (Table 3).

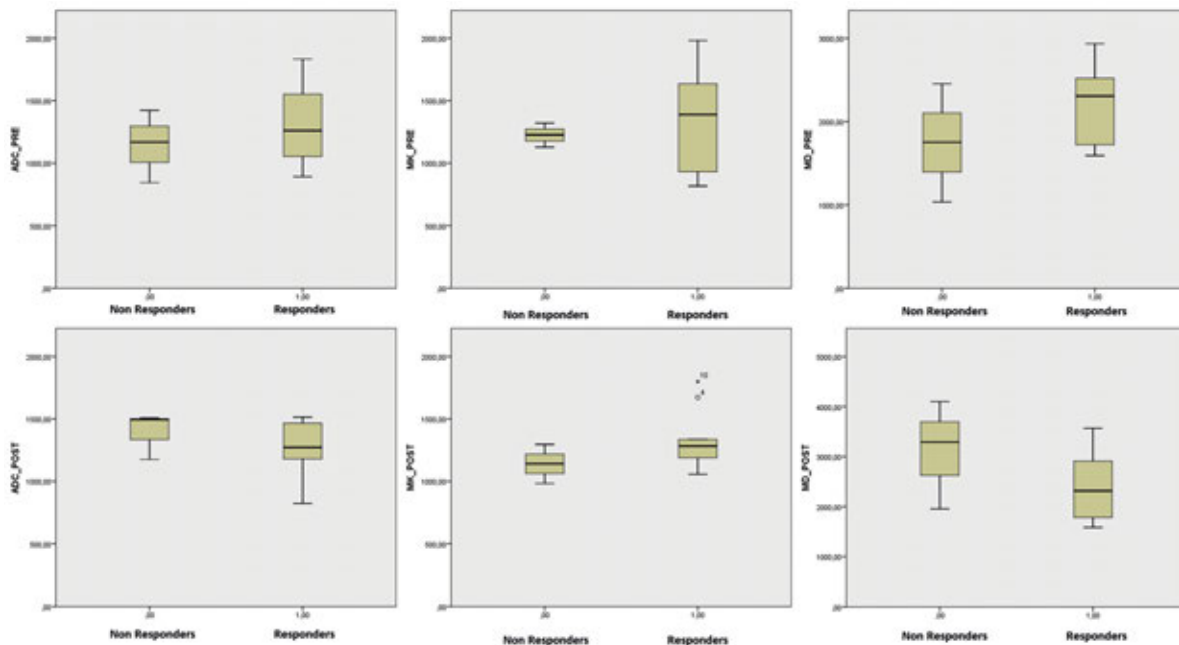


**FIGURE 1.** Boxplot of apparent diffusion coefficient (ADC) and diffusion kurtosis imaging (DKI) parameters pre and post treatment values between responders and not responders.

MD = mean of diffusion coefficient; MK = mean of diffusional kurtosis

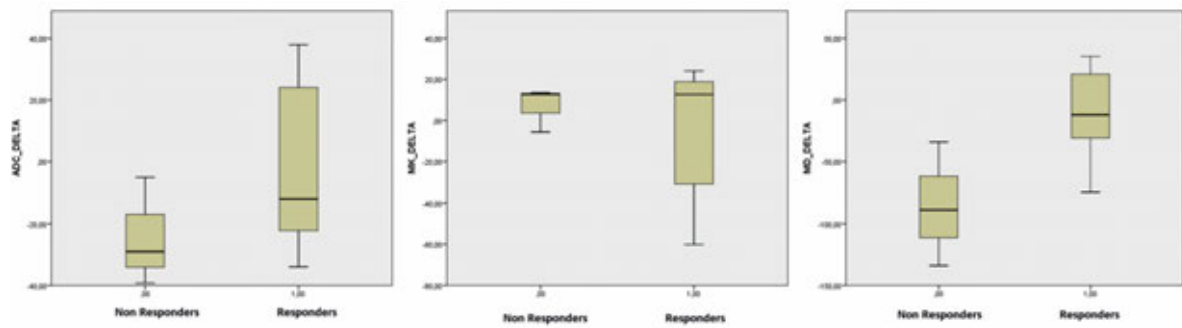


**FIGURE 2.** Boxplot of apparent diffusion coefficient (ADC) and diffusion kurtosis imaging (DKI) parameters percentage change values between responders and not responders.

Delta ( $\Delta$ ) = percentage change between pre and post treatment; MD = mean of diffusion coefficient; MK = mean of diffusional kurtosis

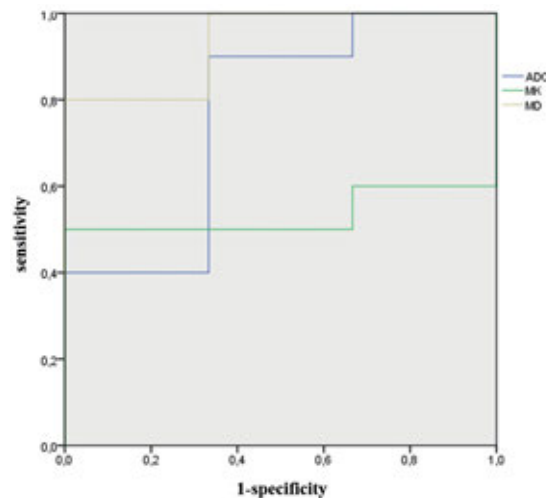


**FIGURE 3.** ROC curve of apparent diffusion coefficient (ADC) and diffusion kurtosis imaging (DKI) features to assess electrochemotherapy (ECT) response.

MD = mean of diffusion coefficient; MK = mean of diffusional kurtosis

**TABLE 4.** Diagnostic accuracy of MRI extracted parameters in discrimination of responders and not responders.

	AUC	95% CI	p value	Sensitivity	Specificity	Cut-off
$\Delta$ ADC	0,767	0,429–1,00	0,176	0,900	0,667	-25,775
$\Delta$ MK	0,533	0,229–0,837	0,866	0,500	1,000	14,555
<b><math>\Delta</math>MD</b>	<b>0,933</b>	<b>0,782–1,000</b>	<b>0,028</b>	<b>0,800</b>	<b>1,000</b>	<b>-32,570</b>
ADC PRE	0,667	0,292–1,000	0,398	0,700	0,667	1182,550
MK PRE	0,667	0,380–1,953	0,398	0,600	1,000	1348,700
MD PRE	0,700	0,360–1,000	0,310	0,400	1,000	2477,500
ADC POST	0,367	0,000–0,766	0,499	0,800	0,333	1177,825
MK POST	0,800	0,505–1,000	0,128	0,500	1,000	1299,075
MD POST	0,267	0,000–0,602	0,237	0,600	0,333	2020,725

ADC = apparent diffusion coefficient; CI = confidence interval; MD = mean of diffusion coefficient; MK = mean of diffusional kurtosis

ADC and MK did not show differences statistically significant between the values pre and post treatment (p value = 0.02 at Wilcoxon test) and between the percentage changes of responder and not responder patients (p value > 0.05 at Wilcoxon test). Only MD showed a significant variation of values between pre and post treatment (p value = 0.02 at Wilcoxon test) and a significant statistically difference for percentage changes between responders and not responders (p value = 0.01 at Kruskal Wallis test).

Figure 1 reports boxplot for each parameter pre and post treatment between responder and not responder patients. Figure 2 shows boxplot for percentage change (delta) between pre and post treatment for each parameters.

Table 4 reports the diagnostic performance of ADC and DKI derived parameters to assess ECT response.

Exclusively MD, among investigated parameters, had a good diagnostic performance with a sensitivity of 80%, a specificity of 100% (Table 1) and area under ROC of 0.933 (Figure 3).

Figure 4 shows a case of significant response on conventional MR images, ADC map and DKI derived parameters maps.

## Discussion

ECT treatment is a very promising tool in oncological patients. The establishment and expansion of ECT in deep-seated tumours (e.g., liver, bone metastases, pancreas) has opened new opportunities for minimally invasive treatment of metastases and carcinomas.<sup>7</sup> ECT is usually applied as palliative treatment for patients with not resectable lesion, causing an improvement of quality

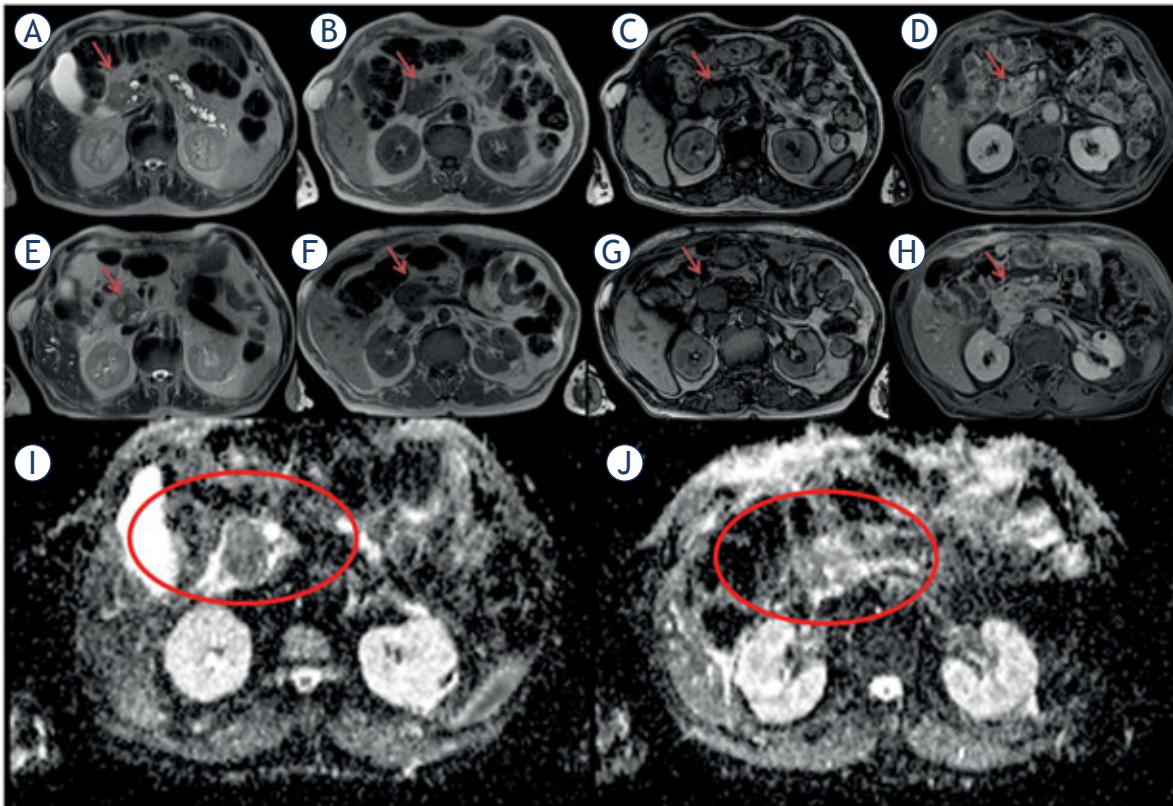


**FIGURE 4.** Adenocarcinoma of the pancreatic head. Before treatment in (A) (half-Fourier acquisition single-shot turbo spin-echo [HASTE] T2-Weighted [W] sequence), the lesion (arrow) appears hyperintense, in (B) (in-phase T1-W sequence) and (C) (out-phase T1-W sequence) appears hypointense and hypovascular in (D) (volumetric interpolated breath hold examination [VIBE] T1-W in equilibrium phase). After the treatment the lesion in (E) (HASTE T2-W sequence), (F) (in-phase T1-W sequence), (G) (out-phase T1-W sequence) and (H) (VIBE T1-W in equilibrium phase): there were not significant differences in size and signal compared to baseline. Apparent diffusion coefficient (ADC) map before and after treatment (I, J).

of life. Several researchers have evaluated it as a treatment of advanced neoplastic lesions in which radical surgery is not possible (e.g., due to lesion location, size, and/or number). ECT allows treatment of lesions in proximity of vital structures like vessels and nerves. The safety profile of ECT is favourable, with local and transient adverse events.<sup>7</sup> Safety and efficacy of ECT have been showed in a prospective series of patients with unresectable Perihilar-Cholangiocarcinoma (PHCCA).<sup>5</sup> A prospective study conducted in 10 patients suffering from hepatocellular carcinomas (HCC) proved that ECT is a feasible and safe treatment. At average of 20.5 months after ECT 15 out of 17 lesions showed a complete response.<sup>27</sup> Recently, Boc *et al.* characterized ultra-sonographic (US) findings during and after electrochemotherapy of liver. US provides a tool for assessment of appropriate electrode insertion for intraoperative electrochemotherapy of liv-

er tumours and assessment of the appropriate coverage of a tumour with a sufficiently strong electric field and can serve as predictor of the response of tumours.<sup>28</sup> As we reported in our previous studies, ECT can be used in locally advanced pancreatic cancer with no side effects or major complications to surrounding viscera that required medical or surgical treatment.<sup>6-8</sup> The major limit of our study is due to how we should assess the ablated area. In fact, we demonstrated in<sup>9</sup> that morphological assessment based on RECIST criteria is not sufficient to stratify the patients as responders or not responders.<sup>9</sup> Conversely, a functional assessment, based on the evaluation of parameters extracted by DCE-MRI and DWI, could be used to identify responders and not responders patients.<sup>9</sup> In the current study, we evaluated conventional DWI parameters (ADC) and the parameters extracted by DKI (MD and MK) in the assessment of ECT

treatment. Only MD by DKI showed a significant variation of value between pre and post treatment and a significant statistically difference for percentage change between responders and not. When we evaluated the diagnostic accuracy of ADC and DKI parameters, MD had a good accuracy with an area under ROC of 0.933. To the best of our knowledge, the few reports on Kurtosis in the assessment of pancreatic tumours, investigate the role of these functional parameters during the characterization of the lesions<sup>29</sup>, other reports on the post treatment assessment by DKI, are not related to pancreas tumours.<sup>30-33</sup>

Diffusion is related to the random Brownian motion of water molecules. In a homogenous medium, diffusion is described by a Gaussian model, while in living tissues is related also by interactions with other molecules and cell membranes and is therefore thought to follow a non-Gaussian model. Also, ADC, in conventional DWI, is influenced by b-values acquired.<sup>10</sup> DKI is an extension of diffusion tensor imaging that evaluates the microstructure features of tissues in a non-Gaussian model.<sup>19</sup> Two quantitative parameters can be extracted by DKI model, including kurtosis values (K, representing deviation from a Gaussian distribution) and diffusion coefficient (D, defining as a corrected ADC for non-Gaussian bias).<sup>19</sup> According to Jensen *et al.* DKI should exhibit a higher sensitivity than conventional DWI for cancer detection.<sup>19</sup> Shen *et al.* assessed the accuracy of DKI parameters in evaluating malignant from benign lesions, performing a systematic meta-analysis.<sup>34</sup> They evaluated 14 studies from 2012 to 2018, for a total of 1847 lesions (895 benign and 952 malignant) in 1107 patients; only two studies were performed with a 1.5 Tesla MR system. The diagnostic performance of three quantitative data, K, D and ADC obtained from MRI with DKI and DWI, for differentiating malignant from benign lesions was evaluated. Pooled results indicated both K and D had a good or excellent diagnostic performance in separating malignant cancer from benign lesions, but D may be more superior because it had the higher AUC.<sup>30</sup> No study on pancreatic cancer was included in this meta-analysis.

Hu *et al.* evaluated DKI in assessing response in rectal cancer compared to conventional DWI.<sup>33</sup> They evaluated ADC, MD (mean diffusion), and MK (mean kurtosis) showing that the  $MK_{pre}$  and  $MK_{post}$  were much lower for the responder than for not responder patients. Also, the  $MD_{post}$  and the

change ratio of MD increased, whereas there are no significant differences for  $ADC_{pre}$ ,  $MD_{pre}$  and the change of MK ratio between responder and not responder patients. The  $MK_{post}$  had higher sensitivity and specificity compared to other data.<sup>33</sup>

DWI has demonstrated to be a great promise as an imaging biomarker. However, it still suffers from inconsistencies in imaging acquisition parameters and DWI analysis that lead to substantial issues with reproducibility. Newer imaging techniques such as DKI may extend the potential of DWI by better characterizing and assessing the lesions pre and after treatment. Therefore, DKI should be added to the routine protocol. Several limitations in our study must be mentioned. First, since this was a retrospective study, there may have been potential selection bias. It will be necessary to perform larger studies to validate our findings. Second our data were acquired with a maximum b value of 1000 s/mm<sup>2</sup>. In general, very high b-values are recommended for the evaluation of non-Gaussian kurtosis in brain applications.<sup>19</sup> However, for abdominal studies, taking into account the lower signal to noise ratio (SNR) and the lower T2 relaxation times of the various organs compared to the brain, very high b-values are not usually applied. Recently, various authors have shown that kurtosis effects could be detectable in abdominal and whole-body applications even when using maximum b-values of 800 s/mm<sup>2</sup> or less at 3T.<sup>35-37</sup> We applied multiple b-values with a maximum of 1000 s/mm<sup>2</sup> that, coupled with the use of a parallel imaging factor, resulted in images with acceptable SNR at 1.5T. Third, the size of our population is very small. In fact, this study had the only objective to report preliminary findings that should be validated in a larger series of patients. At the end, we did not assess the quality of DWI images; this could be considered a future endpoint.

## Conclusions

Our results support the hypothesis that Mean of Diffusion Coefficient derived by DKI allows to identify responders and not responder patients subject to ECT treatment. MD had high diagnostic performance to assess ECT response, showing a significant variation of value between pre and post treatment and a significant statistically difference for percentage change between responders and not responders patients.

## Acknowledgements

The authors are grateful to Alessandra Trocino, librarian at the National Cancer Institute of Naples, Italy. Additionally, authors are grateful to Rita Guarino and Assunta Zazzaro for their collaboration.

## References

- Tarantino L, Busto G, Nasto A, Fristachi R, Cacace L, Talamo M, et al. Percutaneous electrochemotherapy in the treatment of portal vein tumor thrombosis at hepatic hilum in patients with hepatocellular carcinoma in cirrhosis: a feasibility study. *World J Gastroenterol* 2017; **23**: 906-18. doi: 10.3748/wjg.v23.i5.906
- Ethemovic I, Gadzjev E, Breclj E, Miklavcic D, Kos B, Zupanic A, et al. Electrochemotherapy: a new technological approach in treatment of metastases in the liver. *Technol Cancer Res Treat* 2011; **10**: 475-85. doi: 10.7785/tcr.2012.500224
- Miklavcic D, Snoj M, Zupanic A, Kos B, Cemazar M, Kropivnik M, et al. Towards treatment planning and treatment of deep-seated solid tumors by electrochemotherapy. *Biomed Eng Online* 2010; **9**: 10. doi: 10.1186/1475-925X-9-10
- Tafuto S, von Arx C, De Divitiis C, Maura CT, Palaia R, Albino V, et al.; ENETS Center of Excellence Multidisciplinary Group for Neuroendocrine Tumors in Naples (Italy). Electrochemotherapy as a new approach on pancreatic cancer and on liver metastases. *Int J Surg* 2015; **21**(Suppl 1): S78-82. doi: 10.1016/j.ijso.2015.04.095
- Tarantino L, Busto G, Nasto A, Nasto RA, Tarantino P, Fristachi R, et al. Electrochemotherapy of cholangiocellular carcinoma at hepatic hilum: a feasibility study. *Eur J Surg Oncol* 2018; pii: S0748-7983(18) 31169-7. doi: 10.1016/j.ejso.2018.06.025
- Granata V, Fusco R, Piccirillo M, Palaia R, Lastoria S, Petrillo A, et al. Feasibility and safety of intraoperative electrochemotherapy in locally advanced pancreatic tumor: a preliminary experience. *Eur J Inflamm* 2014; **12**: 467-77. doi: 10.1177/1721727X1401200308
- Probst U, Fuhrmann I, Beyer L, Wiggermann P. Electrochemotherapy as a new modality in interventional oncology: a review. *Technol Cancer Res Treat* 2018; **17**: 1533033818785329. doi: 10.1177/1533033818785329
- Granata V, Fusco R, Piccirillo M, Palaia R, Petrillo A, Lastoria S, et al. Electrochemotherapy in locally advanced pancreatic cancer: preliminary results. *Int J Surg* 2015; **18**: 230-6. doi: 10.1016/j.ijso.2015.04.055
- Granata V, Fusco R, Setola S, Piccirillo M, Leongito M, Palaia R, et al. Early radiological assessment of locally advanced pancreatic cancer treated with electrochemotherapy. *World J Gastroenterol* 2017; **23**: 4767-78. doi: 10.3748/wjg.v23.i26.4767
- García-Figueiras R, Padhani AR, Baleato-González S. Therapy monitoring with functional and molecular MR imaging. *Magn Reson Imaging Clin N Am* 2016; **24**: 261-288. doi: 10.1016/j.mric.2015.08.003
- Fusco R, Sansone M, Petrillo A. A comparison of fitting algorithms for diffusion-weighted MRI data analysis using an intravoxel incoherent motion model. *MAGMA* 2017; **30**: 113-120. doi: 10.1007/s10334-016-0591-y
- Petrillo M, Fusco R, Catalano O, Sansone M, Avallone A, Delrio P, et al. MRI for assessing response to neoadjuvant therapy in locally advanced rectal cancer using DCE-MR and DW-MR data sets: a preliminary report. *Biomed Res Int* 2015; **2015**: 514740. doi: 10.1155/2015/514740
- Doblas S, Wagner M, Leitao HS, Daire JL, Sinkus R, Vilgrain V, et al. Determination of malignancy and characterization of hepatic tumor type with diffusion-weighted magnetic resonance imaging: comparison of apparent diffusion coefficient and intravoxel incoherent motion-derived measurements. *Invest Radiol* 2013; **48**: 722-8. doi: 10.1097/RLI.0b013e3182915912
- Concia M, Sprinkart AM, Penner AH, Brossart P, Gieseke J, Schild HH, et al. Diffusion-weighted magnetic resonance imaging of the pancreas: diagnostic benefit from an intravoxel incoherent motion model-based 3 b-value analysis. *Invest Radiol* 2014; **49**: 93-100. doi: 10.1097/RLI.0b013e3182a71cc3
- Chandarana H, Kang SK, Wong S, Rusinek H, Zhang JL, Arizono S, et al. Diffusion-weighted Intravoxel incoherent motion imaging of renal tumors with histopathologic correlation. *Invest Radiol* 2012; **47**: 688-96. doi: 10.1097/RLI.0b013e31826a0a49
- Kobus T, Vos PC, Hambrock T, De Rooij M, Hulsbergen-Van de Kaa CA, Barentsz JO, et al. Prostate cancer aggressiveness: in vivo assessment of MR spectroscopy and diffusion-weighted imaging at 3 T. *Radiology* 2012; **265**: 457-67. doi: 10.1148/radiol.12111744
- Le Bihan D, Breton E, Lallemand D, Aubin ML, Vignaud J, Laval-Jeantet M. Separation of diffusion and perfusion in intravoxel incoherent motion MR imaging. *Radiology* 1988; **168**: 497-505. doi: 10.1148/radiology.168.2.3393671
- Le Bihan D, Breton E, Lallemand D, Grenier P, Cabanis E, Laval-Jeantet M. MR imaging of intravoxel incoherent motions: application to diffusion and perfusion in neurologic disorders. *Radiology* 1986; **161**: 401-7. doi: 10.1148/radiology.161.2.3763909
- Jensen JH, Helpert JA. MRI quantification of non-Gaussian water diffusion by kurtosis analysis. *NMR Biomed* 2010; **23**: 698-710. doi: 10.1002/nbm.1518
- Sun K, Chen X, Chai W, Fei X, Fu C, Yan X, et al. Breast cancer: diffusion kurtosis MR imaging-diagnostic accuracy and correlation with clinical-pathologic factors. *Radiology* 2015; **277**: 46-55. doi: 10.1148/radiol.15141625
- Suo S, Chen X, Wu L, Zhang X, Yao Q, Fan Y, et al. Non-Gaussian water diffusion kurtosis imaging of prostate cancer. *Magn Reson Imaging* 2014; **32**: 421-27. doi: 10.1016/j.mri.2014.01.015
- Nogueira L, Brandão S, Matos E, Nunes RG, Loureiro J, Ramos I, et al. Application of the diffusion kurtosis model for the study of breast lesions. *Eur Radiol* 2014; **24**: 1197-203. doi: 10.1007/s00330-014-3146-5
- Rosenkrantz AB, Sigmund EE, Winnick A, Niver BE, Spieler B, Morgan GR, et al. Assessment of hepatocellular carcinoma using apparent diffusion coefficient and diffusion kurtosis indices: preliminary experience in fresh liver explants. *Magn Reson Imaging* 2012; **30**: 1534-40. doi: 10.1016/j.mri.2012.04.020
- Kartal N, Manikis GC, Loizou L, Albiin N, Zöllner FG, Del Chiaro M, et al. Diffusion-weighted MR imaging of pancreatic cancer: a comparison of mono-exponential, bi-exponential and non-Gaussian kurtosis models. *Eur J Radiol Open* 2016; **3**: 79-85. doi: 10.1016/j.ejro.2016.04.002
- Weng Z, Ertle J, Zheng S, Lauenstein T, Mueller S, Bockisch A, et al. Choi criteria are superior in evaluating tumor response in patients treated with transarterial radioembolization for hepatocellular carcinoma. *Oncol Lett* 2013; **6**: 1707-12. doi: 10.3892/ol.2013.1612
- Wahl RL, Jacene H, Kasamon Y, Lodge MA. From RECIST to PERCIST: evolving considerations for PET response criteria in solid tumors. *J Nucl Med* 2009; **50** (Suppl 1): 122S-150S. doi: 10.2967/jnumed.108.057307
- Djokic M, Cemazar M, Popovic P, Kos B, Dezman R, Bosnjak M, et al. Electrochemotherapy as treatment option for hepatocellular carcinoma, a prospective pilot study. *Eur J Surg Oncol* 2018; **44**: 651-57. doi:10.1016/j.ejso.2018.01.090
- Boc N, Ethemovic I, Kos B, Music MM, Breclj E, Trovtovsek B, et al. Ultrasonographic changes in the liver tumors as indicators of adequate tumor coverage with electric field for effective electrochemotherapy. *Radiol Oncol* 2019; **53**(1): 15-24.; **53**(1): 15-24.; **52**: 383-91. doi: 10.2478/raon-2018-0041
- Tang MY, Zhang XM, Chen TW, Huang XH. Various diffusion magnetic resonance imaging techniques for pancreatic cancer. *World J Radiol* 2015; **7**: 424-37. doi:10.4329/wjrv.7.i12.424
- Chen Y, Ren W, Zheng D, Zhong J, Liu X, Yue Q, et al. Diffusion kurtosis imaging predicts neoadjuvant chemotherapy responses within 4 days in advanced nasopharyngeal carcinoma patients. *J Magn Reson Imaging* 2015; **42**: 1354-61. doi: 10.1002/jmri.24910.
- Yu J, Xu Q, Song JC, Li Y, Dai X, Huang DY, et al. The value of diffusion kurtosis magnetic resonance imaging for assessing treatment response of neoadjuvant chemoradiotherapy in locally advanced rectal cancer. *Eur Radiol* 2017; **27**: 1848-57. doi: 10.1007/s00330-016-4529-6
- Goshima S, Kanematsu M, Noda Y, Kondo H, Watanabe H, Bae KT. Diffusion kurtosis imaging to assess response to treatment in hypervascular hepatocellular carcinoma. *AJR Am J Roentgenol* 2015; **204**: W543-9. doi: 10.2214/AJR.14.13235

33. Hu F, Tang W, Sun Y, Wan D, Cai S, Zhang Z, et al. The value of diffusion kurtosis imaging in assessing pathological complete response to neoadjuvant chemoradiation therapy in rectal cancer: a comparison with conventional diffusion-weighted imaging. *Oncotarget* 2017; **8**: 75597-606. doi: 10.18632/oncotarget.17491
34. Shen L, Zhou G, Tang F, Lin Y, Zhou J, Lv P, et al. MR diffusion kurtosis imaging for cancer diagnosis: a meta-analysis of the diagnostic accuracy of quantitative kurtosis value and diffusion coefficient. *Clin Imaging* 2018; **52**: 44-56. doi: 10.1016/j.clinimag.2018.06.005
35. Kartalis N, Lindholm TL, Aspelin P, Permert J, Albiin N. Diffusion-weighted magnetic resonance imaging of pancreas tumors. *Eur Radiol* 2009; **19**: 1981-90. doi: 10.1007/s00330-009-1384-8
36. Fusco R, Sansone M, Granata V, Grimm R, Pace U, Delrio P, et al. Diffusion and perfusion MR parameters to assess preoperative short-course radiotherapy response in locally advanced rectal cancer: a comparative explorative study among Standardized Index of Shape by DCE-MRI, intravoxel incoherent motion- and diffusion kurtosis imaging-derived parameters. *Abdom Radiol (NY)*. 2018 Oct 25.
37. Rosenkrantz AB, Sigmund EE, Johnson G, Babb JS, Mussi TC, Melamed J, et al. Prostate cancer: feasibility and preliminary experience of a diffusional kurtosis model for detection and assessment of aggressiveness of peripheral zone cancer. *Radiology* 2012; **264**: 126-35. doi: 10.1148/radiol.12112290

# Infarct-core CT perfusion parameters in predicting post-thrombolysis hemorrhagic transformation of acute ischemic stroke

Crt Langel<sup>1</sup>, Katarina Surlan Popovic<sup>2</sup>

<sup>1</sup> Novo Mesto General Hospital, Slovenia

<sup>2</sup> Institute of Radiology, University Medical Centre Ljubljana, Slovenia

Radiol Oncol 2019; 53(1): 25-30.

Received 26 August 2018

Accepted 11 November 2018

Correspondence to: Assoc. Prof. Šurlan Popović Katarina, M.D., Ph.D., Institute of Radiology, University Medical Centre Ljubljana, Zaloška cesta 7, SI-1000 Ljubljana, Slovenia. Phone: +386 1 522 85 30; E-mail: katarina.surlan@gmail.com

Disclosure: No potential conflicts of interest were disclosed.

**Background.** Intravenous thrombolysis (IVT) is the method of choice in reperfusion treatment of patients with signs and symptoms of acute ischemic stroke (AIS) lasting less than 4.5 hours. Hemorrhagic transformation (HT) of acute ischemic stroke is a serious complication of IVT and occurs in 4.5–68.0% of clinical cases. The aim of our study was to determine the infarct core CT perfusion parameter (CTPP) most predictive of HT.

**Patients and methods.** Seventy-five patients with AIS who had undergone CT perfusion (CTP) imaging and were treated with IVT were enrolled in this retrospective study. Patients with and without HT after IVT were defined as cases and controls, respectively. Controls were found by matching for time from AIS symptom onset to IVT  $\pm$  0.5 h. The following CTPPs were measured: cerebral blood flow (CBF), cerebral blood volume (CBV), mean transit time (MTT), relative CBF (rCBF) and relative CBV (rCBV). Receiver operating characteristic analysis curves of significant CTPPs determined cut-off values that best predict HT.

**Results.** There was a significant difference between cases and controls for CBF ( $p = 0.004$ ), CBV ( $p = 0.009$ ), rCBF ( $p < 0.001$ ) and rCBV ( $p = 0.001$ ). Receiver operating characteristic analysis revealed that rCBF  $< 4.5\%$  of the contralateral mean (area under the curve = 0.736) allowed prediction of HT with a sensitivity of 71.0% and specificity of 52.5%.

**Conclusions.** CTP imaging has a considerable role in HT prediction, assisting in selection of patients that are likely to benefit from IVT. rCBF proved to have the highest HT predictive value.

Key words: acute ischemic stroke; computed tomography perfusion; infarct core; hemorrhagic transformation

## Introduction

Ischemic stroke is defined as an episode of neurological dysfunction caused by focal cerebral, spinal or retinal infarction accompanied by overt symptoms.<sup>1</sup> About 90% of all strokes are ischemic, while roughly 10% are hemorrhagic (including intracerebral and subarachnoid hemorrhage).<sup>2</sup>

Patients presenting signs and symptoms of acute ischemic stroke (AIS) undergo a series of CT imaging procedures, including non-contrast CT to exclude pre-treatment intracranial hemorrhage, CT angiography (CTA) to determine the precise location of vessel occlusion, CT perfusion (CTP) to

differentiate between potentially salvageable and irreversibly damaged brain tissue, and post-treatment non-contrast CT to exclude thrombolysis-related hemorrhage.<sup>3-6</sup>

The standard AIS treatment method within 4.5 hours of symptom onset is intravenous thrombolysis (IVT) with tissue plasminogen activator (tPA) injection.<sup>7,8</sup> Patients with IVT-therapy contraindications or ineffectiveness may be eligible for endovascular mechanical thrombectomy (MT).<sup>8,9</sup>

Hemorrhagic transformation (HT) is a conversion of ischemic brain tissue into a hemorrhagic lesion due to blood-brain barrier disruption. It may occur spontaneously in ischemic brain tissue but

may also be triggered by reperfusion.<sup>10, 11</sup> HT occurs in 4.5 - 68.0% of AIS clinical cases and has a higher incidence in patients treated with IVT than in patients without such treatment.<sup>12-14</sup> While mild to moderate HT may not seriously impact the clinical outcome, severe HT is a significant predictor of neurological deterioration and higher mortality.<sup>14, 15</sup>

CTP is an imaging technique that measures brain tissue blood perfusion by analyzing time-attenuation curves of contrast agent in input artery and parenchyma, generating maps of CT perfusion parameters (CTPPs). CTPPs are cerebral blood volume (CBV), mean transit time (MTT) and cerebral blood flow (CBF). CBV is defined as the total volume of flowing blood in a given volume of brain. MTT is defined as the average transit time of blood through a given brain region. CBF is defined as the volume of flowing blood moving through a given volume of brain in a specific amount of time. The three CTPPs are associated by the equation:  $CBF = CBV / MTT$ .<sup>16</sup>

Absolute CTPPs are values of a certain brain region while relative CTPPs are values of a certain brain region divided by values of the contralateral brain region. In the context of AIS, relative CTPPs are values measured in the pathological hemisphere expressed as a percentage of the values measured in the contralateral normal hemisphere.<sup>17</sup>

Previous studies have shown that CTPPs of the whole infarct area (penumbra and infarct core as a single region) could be used to predict HT, finding relative CBV ( $rCBV$ )  $\leq 1.09$  and  $T_{max} > 14$  s, respectively, to be the most predictive of HT, with relative CBF ( $rCBF$ )  $< 30\%$  also being of considerable utility in predicting HT.<sup>18, 19</sup> One study found neither CBF nor CBV to be significantly different between cases and controls, while not examining relative CTPPs.<sup>20</sup> Another study examined infarct-core CTPPs, finding  $CBV \leq 0.5$  mL/100 g to be predictive of symptomatic intra-cerebral hemorrhage, while also not investigating relative CTPPs.<sup>21</sup> One study initially proposed separate analysis of infarct-core CTPPs but eventually dismissed the idea due to insufficient sample size.<sup>18</sup>

The rationale for separate analysis of the infarct core subregion is that it may provide a different insight into HT prediction than a whole-infarct approach, due to the elimination of the "average-out" effect.<sup>21</sup> The reasoning behind the use of relative rather than absolute CTPPs is to account for potential interpatient variability, while also avoiding the inter-vendor variability of postprocessing software.<sup>18, 22</sup> Our study thus aimed to investigate

CTPPs of the infarct core in predicting HT, with an emphasis on relative CTPPs

## Patients and methods

### Patients

This single-centre retrospective study enrolled 75 patients (47 males, 37 females, mean age  $\pm$  SD  $72.63 \pm 11.7$  years) who had been admitted to neurological emergency, with AIS symptoms lasting less than 4.5 hours. Patients underwent admission non-contrast CT, CTA and CTP imaging, and were treated with IVT according to guidelines, in the period from January 2012 – April 2015. The study was performed in accordance with the Declaration of Helsinki and was approved by the National Medical Ethics Committee (Trial registration number: 0120-453/2017-3).

### Methods

CT, CTA and CTP imaging were performed with a Siemens Sensation Open 40 (Siemens Medical Systems, Erlangen, Germany). CTP was performed using 40 mL of iodinated contrast medium at a flow rate of 6 mL/s, followed by 40 mL of saline flush at the same rate, injected into the cubital vein. Four s after initiation of the injection, a continuous (cine) scan was initiated using the following parameters: 80 kVp, 209 mAs,  $4 \times 5$  mm sections, 1-second per rotation for a duration of 40 s.

The images were loaded onto a workstation (Syngo MultiModality Workplace; Siemens Healthcare, Erlangen, Germany). CTPPs - cerebral blood flow (CBF), cerebral blood volume (CBV) and mean transit time (MTT) - were automatically calculated from CTP data using commercial software (Neuro PCT; Siemens Healthcare, Erlangen, Germany). A single circular region of interest (ROI) measuring 15–20 mm in diameter was placed in the region of the infarct core. Mirror ROI was automatically placed by the software in the contralateral (i.e., asymptomatic) hemisphere. Region-specific CTPPs of both ROIs were measured. Relative CTPPs were calculated by dividing the CTPP values of infarct core ROI by asymptomatic hemisphere ROI.

The development of HT was documented by follow-up non-contrast CT 24 h after initial imaging. Patients who developed HT were assigned to the cases group ( $n=35$ ), while patients that did not develop HT were assigned to the controls group ( $n=40$ ), matching the cases based on time from AIS symptom onset to IVT  $\pm 0.5$  h. The matching was

carried out by first obtaining the data regarding the time period from AIS symptom onset to the start of the IVT procedure for each patient, then selecting those patients from the pool of controls group candidates that most closely matched each cases group patient's time period,  $\pm 0.5$  h being the cut-off point beyond which a controls group candidate would not be considered for matching. Adhering to these conditions 40 cases were assigned controls, however due to technical inadequacies of some of the imaging studies (e.g. patient movement) cases group was later reduced to 35 patients.

### Statistical analysis

All numerical data were reported as means  $\pm$  standard deviation. The normality of data distribution was evaluated by the Shapiro-Wilk test. The Mann-Whitney U-test was used to determine the existence of a statistically significant difference in CTPPs between cases and controls. A  $p$  value  $< 0.05$  was regarded as statistically significant. The area of the receiver operating characteristic (ROC) curve under the curve (AUC) determined the ability of CTPPs to differentiate between the occurrence and non-occurrence of HT. ROC curve analysis identified optimal cut-off values of CTPPs that predict the onset of HT with the highest sensitivity and specificity. IBM SPSS Statistics (version 20.0, SPSS Inc., Chicago, IL, USA) was used to perform statistical analyses.

### Results

Seventy-five patients with AIS who had undergone CTP imaging and had been treated with IVT were included in the study. Significant differences in mean values between cases and controls were observed ( $p = < 0.000-0.009$ ) for CBF, CBV, rCBF and rCBV.

The area under the curve (AUC) of the receiver operating characteristic (ROC) of rCBF (0.736) showed a satisfactory ability to differentiate between the occurrence and non-occurrence of HT, while AUCs of CBF, CBV and rCBV showed comparatively inferior differentiation abilities (0.704-0.676).

### Discussion

HT is a potentially grave complication of IVT, occurring in 4.5-68.0% of clinical AIS cases. Severe

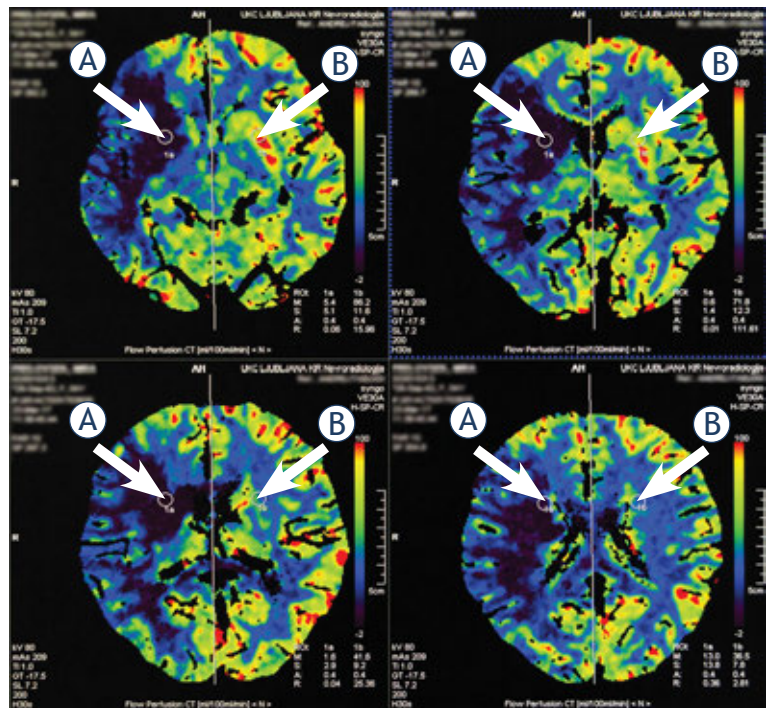


**FIGURE 1.** CT perfusion (CTP) in a 64-year old patient with acute ischemic stroke (AIS) in the territory supplied by the right middle cerebral artery (MCA). Four radiological slices correspond to different anatomical levels of image acquisition. (A) Hand-drawn region of interest (ROI) in the region of infarct core. (B) Automatically generated ROI of the asymptomatic contralateral hemisphere.

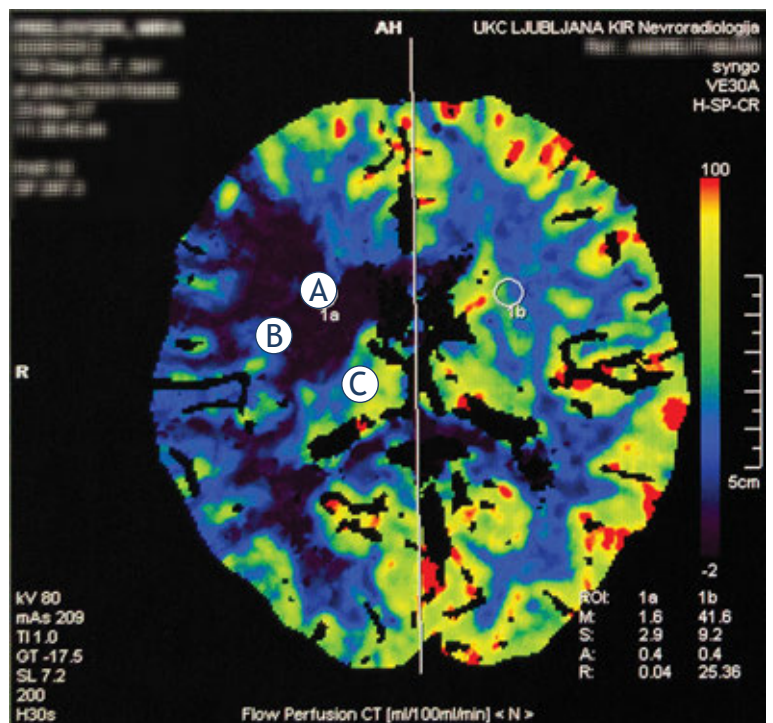


**FIGURE 2.** CT perfusion (CTP) in a 64-year old patient with acute ischemic stroke (AIS) in the territory supplied by the right middle cerebral artery (MCA). (A) Infarct core. (B) Penumbra. (C) Intact brain parenchyma.

TABLE 1. Characteristics of study cohort

Parameter	Cases	Controls	p value
CBF (mean (SD)) [mL/100 g/min]	0.38 (0.47)	0.98 (1.37)	0.004
CBV (mean (SD)) [mL/100 g]	1.45 (1.7)	3.06 (2.99)	0.009
MTT (mean (SD)) [s]	4.27 (4.00)	4.22 (3.26)	0.718
rCBF (mean (SD))	0.03 (0.05)	0.10 (0.12)	< 0.000
rCBV (mean (SD))	0.07 (0.09)	0.10 (0.12)	0.001
rMTT (mean (SD))	2.47 (2.05)	2.36 (1.65)	0.948

CBF = cerebral blood flow; CBV = cerebral blood volume; MTT = mean transit time; rCBF = relative cerebral blood flow; rCBV = relative cerebral blood volume; rMTT = relative mean transit time

TABLE 2. Region of interest (ROI) curve analysis results

	AUC	cut-off value	sensitivity	specificity
CBF [mL/100 g/min]	0.691	0.35	62.0%	35.0%
CBV [mL/100g]	0.676	1.65	68.6%	40.0%
rCBF	0.736	4.5%	71.0%	52.5%
rCBV	0.704	8.5%	71.4%	42.5%

CBF = cerebral blood flow; CBV = cerebral blood volume; rCBF = relative cerebral blood flow; rCBV = relative cerebral blood volume

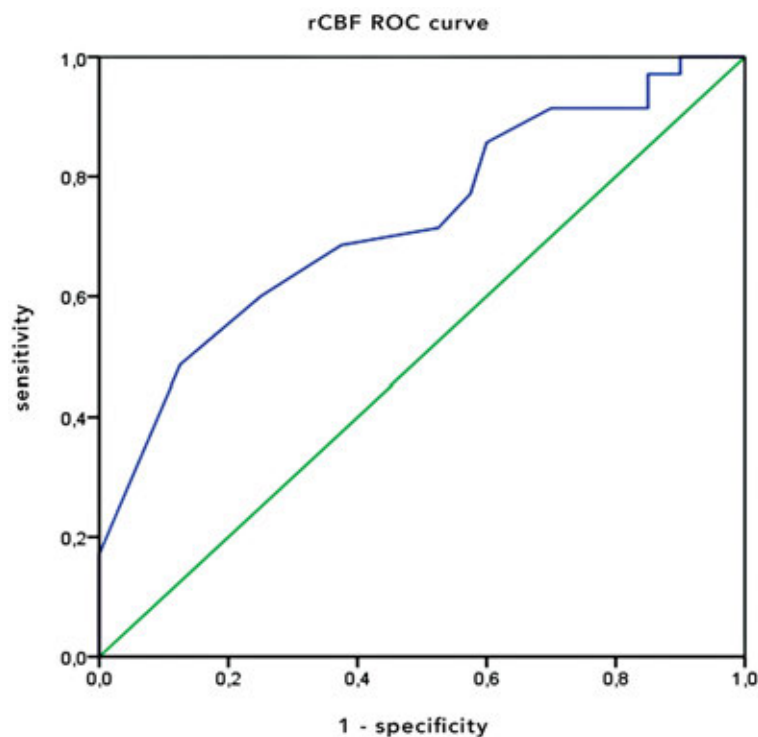


FIGURE 3. Region of interest (ROI) curve of relative cerebral blood flow (rCBF) in patients with and without hemorrhagic transformation (HT). rCBF represents the CBF of the infarct core region normalized to the intact contralateral side. The cut-off point marks the threshold at which relative cerebral blood volume (rCBV) can predict HT with optimal sensitivity and specificity. Diagonal segments are produced by ties.

HT is a significant predictor of neurological deterioration and higher mortality.<sup>15</sup> Various HT prediction methods have been investigated, including CT, CTP, SPECT and diffusion- and perfusion-weighted MR imaging.<sup>21-26</sup> According to previously published data, CTPPs of the whole infarct area effectively predict HT. Jain *et al.* and Yassi *et al.* found relative CTPPs – rCBV and rCBF, respectively, – to be the most predictive of HT.<sup>18,19</sup>

To the best of our knowledge, this study is the first to analyze relative CTPPs of infarct core in predicting HT. On the one hand, the infarct core itself seems not to have been the main focal point of investigations so far, due to various circumstances, including limited sample size, as was the case with Jain *et al.*<sup>18</sup> On the other hand, the sole study that did analyze infarct core, carried out by Lin *et al.*, investigated absolute CTPPs only. The findings of Zussman *et al.* cautioned against using absolute CTPPs due to inter-vendor variability of post-processing software, while Jain *et al.* also warned of possible interpatient variability of absolute CTPPs, encouraging the use of relative CTPPs instead.<sup>21,22</sup>

The above arguments prompted us to focus on analyzing relative CTPPs of the infarct core, with the full knowledge that there might currently be no point of reference to compare our results directly. We found additional reasoning for an infarct-core approach in the fact that our attempts at free-hand whole-infarct designation with image segmentation to eliminate structures that were irrelevant for CTP (*e.g.*, large vessels and sulci) proved futile in many cases; eliminating a large vessel completely often required such a large Hounsfield units (HU) exclusion interval that it inadvertently also deselected the majority of tissue viable for CTP analysis. Additionally, we found the non-segmentation single-ROI infarct-core approach to be fast and straightforward – a potential advantage when using CTPPs in an emergency clinical setting.

Our study of infarct-core CTPPs demonstrates that rCBF < 4.5% of the contralateral mean best predicts the occurrence of HT (sensitivity 71.0%, specificity 52.5%). Considering studies that opted for whole-infarct measurement of relative CTPPs, it should be noted that our approach offered considerably inferior sensitivity but better specificity than whole-infarct rCBF < 30% (sensitivity 100%, specificity 39.0%) studied by Yassi *et al.*, while whole-infarct rCBV < 1.09 (sensitivity 100%, specificity 58.3%) researched by Jain *et al.* proved to be superior to both infarct-core rCBF and whole-infarct rCBF. Infarct-core rCBV < 8.5% (sensitivity 71.4%, specificity 42.5%) examined by our study

proved to be inferior in HT prediction to the aforementioned CTPPs but might be considered as an additional parameter to rCBF when evaluating the infarct core due to similar sensitivity.

A possible reason for the extremely low infarct-core rCBF examined in our study being less sensitive in prediction of HT than the moderately low whole-infarct rCBF examined by Yassi *et al.* might be that the severe hypo-perfused stroke region contains very low levels of contrast, which in certain cases could be undetectable by CTP.<sup>19</sup> Additionally, our ROI placement protocol limited the maximum diameter of circular ROI to 20 mm, and while smaller ROIs help eliminate the “average-out” effect that is associated with large, whole-infarct freehand ROIs, they may also be more susceptible to the effect of random pixel noise.<sup>21</sup> Another possible source of the comparatively higher data heterogeneity in our study may be the potential temporal truncation of the contrast bolus in the infarct region.<sup>27, 28</sup>

Our study has several limitations. It was a retrospective study. The effects of stroke severity and anatomical location were not controlled by matching, nor was the anatomical location of HT. HT was not stratified into subtypes. The time to treatment was controlled by matching; this, however, decreased the final cohort size. ROI placement was performed by a single experienced operator but no estimation of the intra-observer reproducibility of this procedure was made. Our results represent only a single-institution experience.

In conclusion, our analysis indicates that infarct-core CTPPs - low rCBF in particular - can predict HT in patients with AIS. Should this be further verified by larger multi-centre studies, CTP imaging could become the method of choice for identification of patients at low risk of HT, thus helping decide on IVT treatment.

## References

- Sacco RL, Kasner SE, Broderick JP, Caplan LR, Connors JJ, Culebras A, et al. An updated definition of stroke for the 21st century: a statement for healthcare professionals from the American Heart Association/American Stroke Association. *Stroke* 2013; **44**: 2064-89. doi: 10.1161/STR.0b013e318296aeca
- Mozaffarian D, Benjamin EJ, Go AS, Arnett DK, Blaha MJ, Cushman M, et al. Heart Disease and Stroke Statistics-2016 Update: A Report From the American Heart Association. *Circulation* 2016; **133**: e38-360. doi: 10.1161/CIR.0000000000000350
- Rathore SS, Hinn AR, Cooper LS, Tyroler HA, Rosamond WD. Characterization of incident stroke signs and symptoms: findings from the atherosclerosis risk in communities study. *Stroke* 2002; **33**: 2718-21. PMID: 12411667
- Shetty SK, Lev MH. CT perfusion in acute stroke. *Neuroimaging Clin N Am* 2005; **15**: 481-501. doi: 10.1016/j.nic.2005.08.004
- Phan TG, Donnan GA, Koga M, Mitchell LA, Molan M, Fitt G, et al. Assessment of suitability of thrombolysis in middle cerebral artery infarction: a proof of concept study of a stereologically-based technique. *Cerebrovasc Dis* 2007; **24**: 321-7. doi: 10.1159/000106977
- Hoeffner EG, Case I, Jain R, Gujar SK, Shah GV, Deveikis JP, et al. Cerebral perfusion CT: technique and clinical applications. *Radiology* 2004; **231**: 632-44. doi: 10.1148/radiol.2313021488
- Demaerschalk BM, Kleindorfer DO, Adeoye OM, Demchuk AM, Fugate JE, Grotta JC, et al. Scientific rationale for the inclusion and exclusion criteria for intravenous alteplase in acute ischemic stroke: a statement for healthcare professionals from the American Heart Association/American Stroke Association. *Stroke* 2016; **47**: 581-641. doi: 10.1161/STR.0000000000000086
- Powers WJ, Rabinstein AA, Ackerson T, Adeoye OM, Bambakidis NC, Becker K, et al. 2018 guidelines for the early management of patients with acute ischemic stroke: a guideline for healthcare professionals from the American Heart Association/American Stroke Association. *Stroke* 2018; **49**: e46-e110. doi: 10.1161/STR.0000000000000158
- Powers WJ, Derdeyn CP, Biller J, Coffey CS, Hoh BL, Jauch EC, et al. 2015 American Heart Association/American Stroke Association focused update of the 2013 guidelines for the early management of patients with acute ischemic stroke regarding endovascular treatment: a guideline for healthcare professionals from the American Heart Association/American Stroke Association. *Stroke* 2015; **46**: 3020-35. doi: 10.1161/STR.0000000000000074
- Wang X, Lo EH. Triggers and mediators of hemorrhagic transformation in cerebral ischemia. *Mol Neurobiol* 2003; **28**: 229-44. doi: 10.1385/MN:28:3:229
- Nour M, Scalzo F, Liebeskind DS. Ischemia-reperfusion injury in stroke. *Interv Neurol* 2013; **1**: 185-99. doi: 10.1159/000353125
- Sussman ES, Connolly ES Jr. Hemorrhagic transformation: a review of the rate of hemorrhage in the major clinical trials of acute ischemic stroke. *Front Neurol* 2013; **4**: 69. doi: 10.3389/fneur.2013.00069
- Larrue V, von Kummer R R, Müller A, Bluhmki E. Risk factors for severe hemorrhagic transformation in ischemic stroke patients treated with recombinant tissue plasminogen activator: a secondary analysis of the European-Australasian Acute Stroke Study (ECASS II). *Stroke* 2001; **32**: 438-41. PMID: 11157179
- Kablau M, Kreisel SH, Sauer T, Binder J, Szabo K, Hennerici MG, et al. Predictors and early outcome of hemorrhagic transformation after acute ischemic stroke. *Cerebrovasc Dis* 2011; **32**: 334-41. doi: 10.1159/000331702
- D'Amelio M, Terruso V, Famoso G, Di Benedetto N, Realmuto S, Valentini F, et al. Early and late mortality of spontaneous hemorrhagic transformation of ischemic stroke. *J Stroke Cerebrovasc Dis* 2014; **23**: 649-54. doi: 10.1016/j.jstrokecerebrovasdis.2013.06.005
- Konstas AA, Goldmakher GV, Lee TY, Lev MH. Theoretic basis and technical implementations of CT perfusion in acute ischemic stroke. Part 1. Theoretic basis. *AJNR Am J Neuroradiol* 2009; **30**: 662-68. doi: 10.3174/ajnr.A1492
- Wintermark M, Flanders AE, Velthuis B, Meuli R, van Leeuwen M, Goldsher D, et al. Perfusion-CT assessment of infarct core and penumbra: receiver operating characteristic curve analysis in 130 patients suspected of acute hemispheric stroke. *Stroke* 2006; **37**: 979-85. doi: 10.1161/01.STR.0000209238.61459.39
- Jain AR, Jain M, Kanthala AR, Damania D, Stead LG, Wang HZ, et al. Association of CT perfusion parameters with hemorrhagic transformation in acute ischemic stroke. *AJNR Am J Neuroradiol* 2013; **34**: 1895-900. doi: 10.3174/ajnr.A3502
- Yassi N, Parsons MW, Christensen S, Sharma G, Bivard A, Donnan GA, et al. Prediction of poststroke hemorrhagic transformation using computed tomography perfusion. *Stroke* 2013; **44**: 3039-43. doi: 10.1161/STROKEAHA.113.002396
- Aviv RI, d'Este CD, Murphy BD, Hopyan JJ, Buck B, Mallia G, et al. Hemorrhagic transformation of ischemic stroke: prediction with CT perfusion. *Radiology* 2009; **250**: 867-77. doi: 10.1148/radiol.2503080257
- Lin K, Zink WE, Tsiouris AJ, John M, Tekchandani L, Sanelli PC. Risk assessment of hemorrhagic transformation of acute middle cerebral artery stroke using multimodal CT. *J Neuroimaging* 2012; **22**: 160-6. doi: 10.1111/j.1552-6569.2010.00562.x

22. Zussman BM, Boghosian G, Gorniak RJ, Olszewski ME, Read KM, Siddiqui KM, et al. The relative effect of vendor variability in CT perfusion results: a method comparison study. *AJR Am J Roentgenol* 2011; **197**: 468-73. doi: 10.2214/AJR.10.6058
23. Toni D, Fiorelli M, Bastianello S, Sacchetti ML, Sette G, Argentino C, et al. Hemorrhagic transformation of brain infarct: predictability in the first 5 hours from stroke onset and influence on clinical outcome. *Neurology* 1996; **46**: 341-5. PMID: 8614491
24. Hom J, Dankbaar JW, Soares BP, Schneider T, Cheng SC, Bredno J, et al. Blood-brain barrier permeability assessed by perfusion CT predicts symptomatic hemorrhagic transformation and malignant edema in acute ischemic stroke. *AJNR Am J Neuroradiol* 2011; **32**: 41-8. doi: 10.3174/ajnr.A2244
25. Alexandrov AV, Black SE, Ehrlich LE, Caldwell CB, Norris JW. Predictors of hemorrhagic transformation occurring spontaneously and on anticoagulants in patients with acute ischemic stroke. *Stroke* 1997; **28**: 1198-202. PMID: 9183351
26. Tong DC, Adami A, Moseley ME, Marks MP. Prediction of hemorrhagic transformation following acute stroke: role of diffusion- and perfusion-weighted magnetic resonance imaging. *Arch Neurol* 2001; **58**: 587-93. doi: 10.1001/archneur.58.4.587
27. Campbell BC, Christensen S, Levi CR, Desmond PM, Donnan GA, Davis SM. Cerebral blood flow is the optimal CT perfusion parameter for assessing infarct core. *Stroke* 2011; **42**: 3435-40. doi: 10.1161/STROKEAHA.111.618355.
28. Borst J, Marquering HA, Beenen LF, Berkhemer OA, Dankbaar JW, Riordan AJ. Effect of extended CT perfusion acquisition time on ischemic core and penumbra volume estimation in patients with acute ischemic stroke due to a large vessel occlusion. *PLoS One* 2015; **10**: e0119409. doi: 10.1371/journal.pone.0119409

# CT findings predict survival of patients with peripheral T cell lymphoma: a preliminary study

Wenbin Yang, Sen Jiang, Jianbang Lin, Yangkang Li

Department of Radiology, Cancer Hospital, Shantou University Medical College, Guangdong, China

Radiol Oncol 2019; 53(1): 31-38.

Received 28 October 2018

Accepted 19 December 2018

Correspondence to: Yangkang Li, Department of Radiology, Cancer Hospital, Shantou University Medical College, No7, Raoping Rd, Shantou, Guangdong Province 515041, P. R. China. Phone: +86 0754 8855 5844; Fax: +86 0754 8856 0352; E-mail: liyangkang@yahoo.com

Disclosure: No potential conflicts of interest were disclosed.

**Background.** Peripheral T-cell lymphoma (PTCL) is an uncommon disease with poor clinical outcomes. Radiological reports on the survival of patients with PTCL are scarce. The purpose of this study is to investigate the prognostic value of CT findings to predict clinical outcomes in fifty-one patients with histologically proven PTCL.

**Patients and methods.** The clinical data and CT images of all patients were retrospectively reviewed. CT features including number of involvement sites, lesion size, shape, margin, density, peritumoral invasion, intratumoral necrosis, lymph node involvement, and degree of contrast enhancement were evaluated. Univariate and multiple logistic regression analysis were used to determine the association between the clinical outcome and radiologic factors.

**Results.** Multiple site involvement, an ill-defined margin with peritumoral invasion, inhomogeneous density, and intratumoral necrosis were found to be associated with poor outcomes in univariate analysis ( $P < 0.05$ ). An ill-defined margin with peritumoral invasion, was identified as an independent risk sign by further multivariate logistic regression analysis ( $P < 0.05$ ). The area under the ROC curve of this CT feature was 0.745 ( $P < 0.05$ ).

**Conclusions.** An ill-defined margin with peritumoral invasion was a valuable prognostic factor to predict the worse clinical outcomes in patients with PTCL.

Key words: lymphoma; peripheral T cell lymphoma; computed tomography; prognosis

## Introduction

Peripheral T-cell lymphoma (PTCL) is an uncommon disease entity more prevalent in Asia than in Western countries and accounts for 5% to 30% of all non-Hodgkin lymphomas (NHL).<sup>1-3</sup> It is a heterogeneous group of clinically aggressive lymphomas including PTCL-not otherwise specified (PTCL-NOS), anaplastic large cell lymphoma (ALCL) and angioimmunoblastic T-cell lymphoma (AITL). PTCL is usually associated with poor outcome compared with B-cell lymphomas.<sup>4-7</sup> Thus, PTCL requires prompt diagnosis and vigilant monitoring of progression since it is a life-threatening disease.

The International Prognostic Index (IPI), which was developed for predicting the clinical course

of aggressive lymphomas, is commonly used in PTCL. This system is based on age, performance status, lactate dehydrogenase, stage, and extranodal involvement. Establishing the correct diagnosis and accurately evaluating the extent of tumor involvement are important for patients with PTCL because they directly impact the staging and treatment of the tumor. Therefore, accurately describing the characteristics of PTCL (for example, the tumor size and local extension, lymph node metastases, or extranodal involvement, *etc.*) is fundamental in clinical imaging practice.

Computed tomography (CT) is usually used for evaluation of the patient who has lymphoma, because it offers the advantage of obtaining information about both the nodal and extranodal

components of the disease. Hence, it allows for accurate staging of the disease and follow-up of the therapeutic response. Radiologic manifestations about lymphoma have been described in many studies; however, most of them have focused on B-cell lymphoma. Although several reports concerning the imaging characteristics of PTCL have been published<sup>8-10</sup>, these studies usually focused on nodal diseases or conducted on this entity only targeting one extranodal site, for example, the head and neck. Furthermore, the prognostic value of the imaging findings was absent in these studies. The purpose of this study was to evaluate the prognostic value of CT findings to predict clinical outcomes in patients with PTCL involving both nodal and extranodal sites.

## Patients and methods

### Study population and clinical data

This study was conducted in accordance with the declaration of Helsinki and was approved by the Medical Ethics Committee of Cancer Hospital of Shantou University Medical College. The requirement of informed consent was waived, due to the retrospective nature of the study.

Fifty-one patients with pathologically confirmed PTCL were included in our study through a computerized search of the pathology database between October 2005 and July 2015. The histological diagnosis of PTCL was made by pathologists according to the World Health Organization classification, and all of the biopsy specimens were reviewed through immunohistochemical examination. The patient inclusion criteria were as follows: (a) no patient received any treatment; (b) each patient had complete CT data (unenhanced scan and contrast-enhanced scan of head and neck, chest, and abdominopelvic area); (c) visible tumor on CT. Clinical data collected included the patient's age, gender, tumor location, tumor stage, treatment and outcome.

### Image analysis

CT examinations of 10 patients were performed on a PQ5000 spiral CT scanner (Picker, New York, NY, USA), 41 patients were examined using a GE Brightspeed Elite 16-detector-row scanner (GE Healthcare, Milwaukee, WI, USA). After a series of unenhanced sections, all patients received intravenous bolus injection of contrast medium (Ultravist 300; Bayer Schering Pharma, Berlin-Wedding,

Germany) at a rate of 2.5–3 mL/sec and a volume of 75–90 mL. The section thickness of all images of the single spiral CT was 10 mm. For multidetector CT, contiguous axial images and multiplanar reconstructions (MPR) were performed routinely. The section thickness was 5 mm and reconstruction interval was 1.25 mm.

The qualitative CT findings were reviewed by a consensus between two experienced radiologists (W.B.Y., with 8 years of experience in diagnostic imaging, and S.J., with 12 years of experience in diagnostic imaging). They were aware that the study population had lymphoma, but they were blinded to the pathological type, tumor stage and survival outcome. They evaluated the tumor location, tumor size, margin, shape, density, intratumoral necrosis, peritumoral invasiveness, contrast enhancement pattern, degree of enhancement, and lymph node enlargements. For patients with multiple tumors, the largest tumor was selected as the patient's representative tumor. Tumor size was measured in maximal dimension on the transverse plane. Tumor shape was categorized as round/oval or irregular. Tumor density was categorized as homogenous or heterogeneous on unenhanced CT images with normal muscle as the standard for comparison. The tumor margin was categorized as well-defined or ill-defined. Areas with reduced or missing contrast enhancement were considered to represent intratumoral necrosis. Peritumoral invasiveness was defined as infiltration of surrounding fat, bony invasion or invasion of the skin. The criteria for vascular invasion were vessel occlusion, focal narrowing, or contour deformity, and more than half of the perimeter in contact with the tumor.<sup>11</sup> The degree of enhancement was subjectively assessed and categorized as follows: mild, when the enhancement was similar to that of adjacent muscle; moderate, when the enhancement was higher than that of muscle, but lower than that of blood vessels; and marked, when the enhancement was approaching that of blood vessels. Lymph node enlargements were defined as short axis > 1cm, abnormal round morphology, or central necrosis.

### Statistical analysis

To determine the prognostic value of the CT features, the clinical outcomes of patients were simplified into two categories: poor outcome if lesion progression during therapy or recurrence occurred within 24 months after therapy; good outcome if patients survived for more than 24 months with

no evidence of recurrence. Recurrence was defined as local (limited to the primary lesion site), distant (disseminates to distant tissues and organs), or both local and distant.

The radiologic variables included for analysis were categorized as follows: involvement site (single or multiple sites), tumor size ( $\geq 6.0$  cm or  $< 6.0$  cm), shape, lesion margin, density, intratumoral necrosis, peritumoral invasion, lymph node involvement, and degree of contrast enhancement.

The  $\chi^2$  test was applied to compare the frequency of the imaging findings between the poor and good outcome groups in patients. When the radiological signs appeared to be significant in the univariate analysis, multivariate analysis was developed to determine the association between clinical outcomes and individual radiologic variables using logistic regression model.

In the multivariate logistic regression model, variables with a *P* value less than 0.05 as determined by each univariate analysis were chosen as the independent variables. Odds ratios (OR) as estimates of relative risk with 95% confidence intervals (CI) were obtained for each risk factor.

The diagnostic performance of each risk factor was established using the area under the receiver operating characteristic (ROC) curve. A two-sided *P* value of less than 0.05 was considered statistically significant. All statistical tests were performed by using SPSS version 18.0 software (SPSS Inc., Chicago, IL, USA).

## Results

### Clinical findings

As shown in Table 1, the median age of the patients at diagnosis was 47.8 years (ranged 9 to 83 years), and 35 of 51 patients (68.6%) were below 60 years old. The male to female ratio was 1.7:1. Thirty (58.8%) patients presented with advanced Ann Arbor stage. According to the histology, there were 27 PTCL-NOS, 15 ALCL (8 anaplastic lymphoma kinase [ALK] positive and 7 ALK negative), and 9 AITL. All the patients received cyclophosphamide, doxorubicin, vincristine, and prednisone (CHOP)-based chemotherapy. 11 patients also accepted radiotherapy. Follow-up period ranged from 10 to 115 months (mean,  $45.9 \pm 24.6$  months). The lesion showed progression during therapy in 8 patients. Lesion relapse within 24 months after therapy was found in 19 patients, including local relapse in 7, systemic dissemination in 10, and local relapse with dissemination in 2. These 27 patients were

TABLE 1. Clinical characteristics of 51 patients with PTCL

Characteristics	Number of cases	Percentage(%)
Gender		
Male	32	62.7
Female	19	37.3
Age(y)	47.8 $\pm$ 19.1 (range, 9–83)	
Histology		
PTCL-NOS	27	52.9
ALCL ALK+	8	13.7
ALCL ALK-	7	15.7
AITL	9	17.6
Ann Arbor stage		
I-II	21	41.2
III-IV	30	58.8
Clinical outcome		
Progression or relapse within 24 months	27	52.9
No evidence of relapse within 24 months	24	47.1

ALCL ALK+ = anaplastic large cell lymphoma anaplastic lymphoma kinase positive; ALCL ALK- = ALCL anaplastic lymphoma kinase negative; AITL = angioimmunoblastic T-cell lymphoma; PTCL-NOS = PTCL-not otherwise specified

categorized as the poor outcome group. 24 patients survived without any evidence of relapse at least 24 months after therapy, and were classified as the good outcome group.

### CT characteristics

Nodal disease was found in 32 cases (62.7%). Extranodal involvement was found in 39 cases (76.5%). The extranodal involvement sites included nasal cavity, paranasal sinus, periorbital area, Waldeyer's ring, parotid gland, lung, liver, spleen, adrenal gland, gastrointestinal tract, breast and musculoskeletal tissue. The size of the tumors ranged from 1.5 to 14.0 cm (mean, 6.0 cm). The shape was depicted as oval ( $n = 17$ ) or irregular ( $n = 34$ ). The density was described as homogeneous ( $n = 28$ ) and heterogeneous ( $n = 23$ ). A well-defined margin was seen in 29 cases. An ill-defined margin with peritumoral invasion was seen in 22 cases. Intratumoral necrosis was seen in 14 cases. On unenhanced CT images, the density of the solid component of all tumors was 31–58 HU (mean, 45 HU) which was similar to that of muscle. After contrast medium administration, mild or moderate enhancement was detected in 21 and 30 cases, re-

TABLE 2. CT findings of 51 patients with PTCL

Characteristics	Number of cases	Percentage(%)
Involvement site		
Single	27	52.9
Multiple	24	47.1
Tumor size(cm)	6.0 ± 2.4 (range, 1.5–14.0)	
Tumor margin		
Well-defined	29	56.9
Ill-defined with peritumoral invasion	22	43.1
Tumor shape		
Round/oval	17	33.3
Irregular	34	66.7
Tumor density		
Homogenous	28	54.9
Heterogeneous	23	45.1
Intratumoral necrosis		
Present	14	27.5
Absent	37	72.5
Enhancement degree		
Mild	21	41.2
Moderate	30	58.8
Lymph node involvement		
Present	32	62.7
Absent	19	37.3

spectively. CT findings of all cases are summarized in Table 2. CT findings of one patient with good clinical outcomes are depicted in Figure 1. CT findings of three patients with poor clinical outcomes are depicted in Figures 2–4.

## Prognostic analysis

The statistical results of univariate analysis are summarized in Table 3. In univariate analysis, four CT features, including multiple site involvement, an ill-defined margin with peritumoral invasion, intratumoral necrosis, and inhomogeneous density were associated with poor clinical outcomes ( $P < 0.05$ ). Multivariate analysis showed that only one feature, an ill-defined margin with peritumoral invasion, remained a significantly independent predictor of poor clinical outcomes ( $P < 0.05$ ). Further ROC curve analysis showed that the area under the curve of this significant CT feature was 0.745 ( $P < 0.05$ ), which suggests that the multivariate logistic regression model is a reasonable predictor of clinical outcome (Table 4).

## Discussion

In the present study, an ill-defined margin with peripheral tissue invasion was identified to be an independent risk factor for clinical outcome of patients with PTCL. This CT sign is considered more indicative of squamous cell carcinomas than of NHL, if there is no history of previous treatment or recent infection. For squamous cell carcinoma, an ill-defined margin with peripheral tissue invasion increases the risk of local failure, distant metastases, and decreased survival.<sup>10,12</sup> To our knowledge, there are only a few reports on the prognostic significance of ill-defined margin and local tumor invasion in NHL, perhaps because they have been considered uncommon findings in malignant lymphoma. Zhou *et al.*<sup>13</sup> reported that the lesion margin was an independent risk factor for clinical outcome

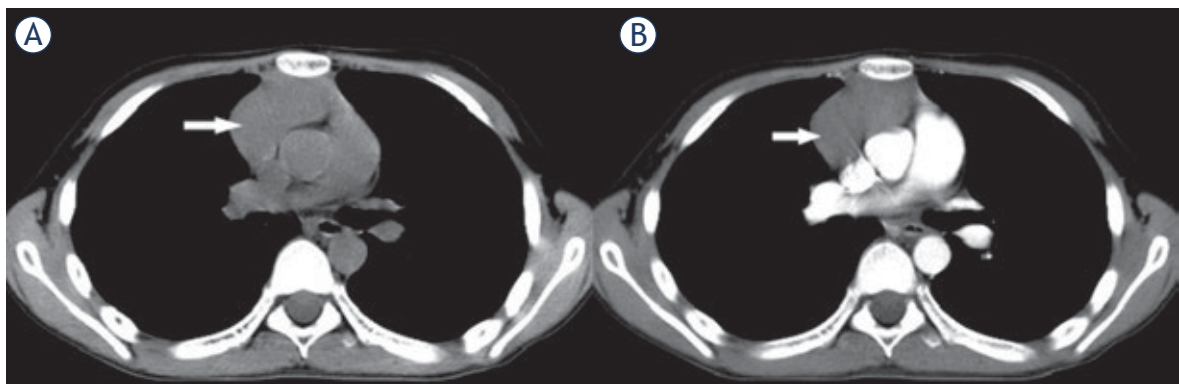


FIGURE 1. A 13-year-old boy with PTCL in the anterior mediastinum. (A) Axial non-contrast CT image shows an oval, well-defined mass with homogeneous density in the anterior mediastinum (white arrow). (B) Contrast-enhanced CT image shows the tumor with homogeneously mild enhancement (white arrow). Tumor recurrence was not noted during the 36-month follow-up period.

in 59 patients with head and neck NHL. Kim *et al.*<sup>14</sup> also reported that local tumor invasion as assessed by CT or MR imaging was a more important prognostic factor than IPI in predicting a low probability of complete remission and lower overall and disease-free survival in extranodal lymphoma. The result of our study was in agreement with previous literatures.

For malignant solid tumors, direct invasion may result in the infiltration of tumor cells to surrounding tissues and neighboring organs. Although a lymphoma is not really considered as a solid tumor, it does form a mass. For aggressive lymphoma subtypes, peritumoral/extracapsular infiltration often occurs. In the present study, the local invasion of PTCL, affected the fat, bone, skin or vessel nearby the tumor and gave the tumor an ill-defined margin on CT images. Of primary importance in the prognosis of patients with PTCL is the sequence of events leading to the development of tumor cell invasion. In previous studies, extensive deregulation of genes that control functions typically damaged in malignant cells, such as matrix remodeling, cell adhesion, transcription regulation, proliferation, and apoptosis, was found in T-cell or B-cell lymphomas.<sup>15-19</sup> The complexity of these tumors is represented by 25 to 30 up-regulated cancer genes and several down-regulated tumor suppressors that provide a growth advantage and enhance the ability to invade and disseminate. This might explain the mechanisms of local invasion and distant dissemination of PTCL in our study. The course of tumor invasion entails a series of stages that lead to dissemination and the formation of secondary tumors in distant organs and is, largely, responsible for the mortality and morbidity of PTCL.

TABLE 3. Univariate analyses of CT findings

Factor	Category	Number of good vs poor outcomes	P value
Involvement site	Single	17:10	0.016*
	Multiple	7:17	
Tumor size	< 6.0cm	14:13	0.328
	≥ 6.0cm	10:14	
Ill-defined margin with peritumoral invasion	Present	4:18	< 0.001*
	Absent	20:9	
Tumor shape	Round/oval	8:9	0.617
	Irregular	16:18	
Inhomogenous density	Present	5:18	0.001*
	Absent	19:9	
Intratumoral necrosis	Present	3:11	0.025*
	Absent	21:16	
Enhancement degree	Mild	10:11	0.586
	Moderate	14:16	
Lymph node involvement	Present	12:20	0.069
	Absent	12:7	

\*P < 0.05

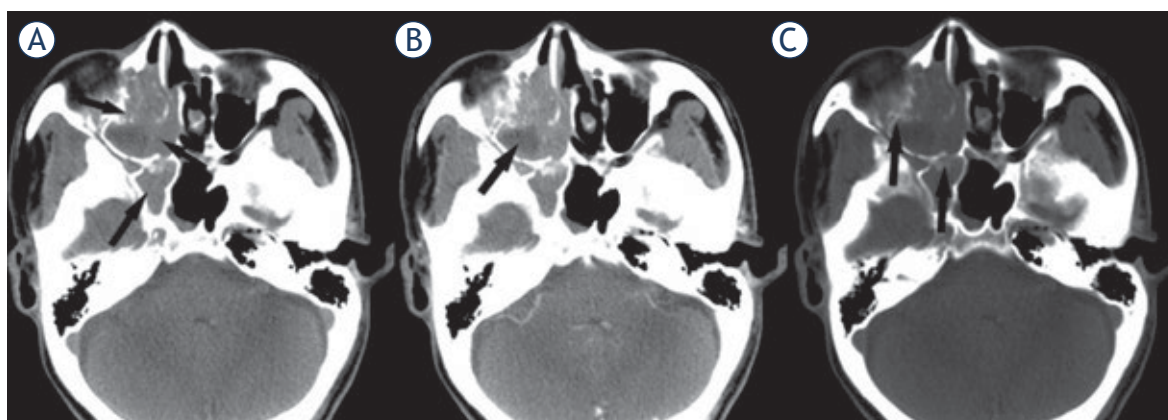
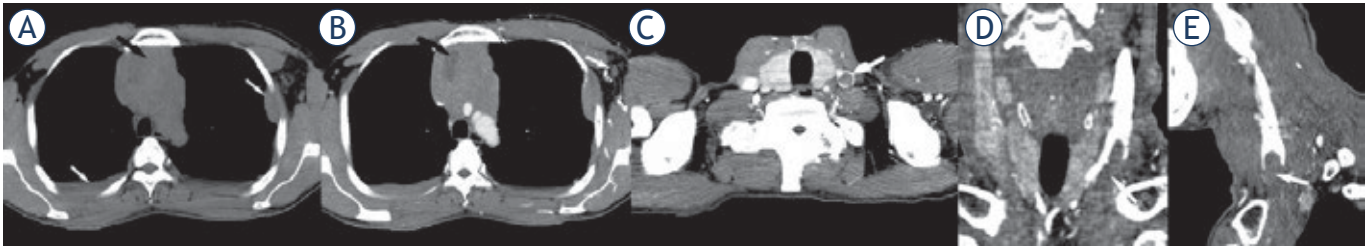


FIGURE 2. A 54-year-old man with PTCL in the sinonasal cavity. (A) Axial non-contrast CT image shows an ill-defined, irregular mass with inhomogeneous density in the right nasal cavity, maxillary and sphenoid sinus (black arrows). (B) Contrast-enhanced CT image shows the tumor with heterogeneously moderate enhancement. Intratumoral necrosis is seen in the mass (black arrow). (C) Bony destruction is detected on non-contrast CT image. The tumor relapsed 11 months after therapy.



**FIGURE 3.** A 47-year-old man with PTCL in the anterior mediastinum. **(A)** Axial non-contrast CT image shows an ill-defined, irregular mass with inhomogeneous density in the anterior mediastinum (black arrow). Multiple pleural metastases are detected (white arrows). **(B)** Contrast-enhanced CT image shows the tumor with heterogeneously mild enhancement. Intratumoral necrosis is seen in the mass (black arrow). Lymphadenopathy is seen in the left axillary fossa (white arrows). **(C, D, E)** The left internal jugular vein is invaded by the tumor and vessel occlusion is detected on contrast-enhanced CT image and MPR images (white arrows). Tumor progression was found during therapy. This patient deceased at 3 months after therapy.

**TABLE 4.** Multivariate analyses of CT findings

Factor	Odd ratio	95% CI	P value
Involvement site	3.499	0.766–15.987	0.106
Ill-defined margin with peritumoral invasion	7.749	1.567–38.315	0.012*
Inhomogenous density	2.356	0.324–17.116	0.397
Intratumoral necrosis	3.157	0.253–39.370	0.372

\*P < 0.05

Concentrating research efforts on identifying and understanding the mechanisms concerned in peritumoral invasion may lead to limiting tumor progression and, as a result, to a reduction in mortality for PTCL patients. In our opinion, when PTCL manifests as an ill-defined margin and peritumoral invasion, no matter the nodal disease or the extranodal lesion, patients are significantly more likely to experience poor outcomes than those with a well-defined lesion without local tumor invasion. And

it may suggest the high aggressiveness of the disease, and more aggressive therapy is warranted for such circumstances.

A severely inhomogeneous tumor pattern on CT images was found to be associated with a high malignancy grade in NHL. This CT pattern was also compatible with a poor prognosis in patients treated with chemotherapy.<sup>10,20</sup> In this study, inhomogeneous density was another radiological sign that was associated with poor survival outcome in univariate analysis. This result was similar to those of previous studies. Although inhomogeneous density can be noted in other diseases, such as epithelial tumor, soft tissue neoplasia or infection, nearly a half of the patients (about 45%) with PTCL in our study showed this radiological characteristic. Inhomogeneous density may correspond to asymmetric tumor cell density, intralesional hemorrhage, necrosis or cystic change. This heterogeneity of tumor parenchyma always leads to heterogeneous density on CT images. Intratumoral hemorrhage and cystic change are seldom seen in

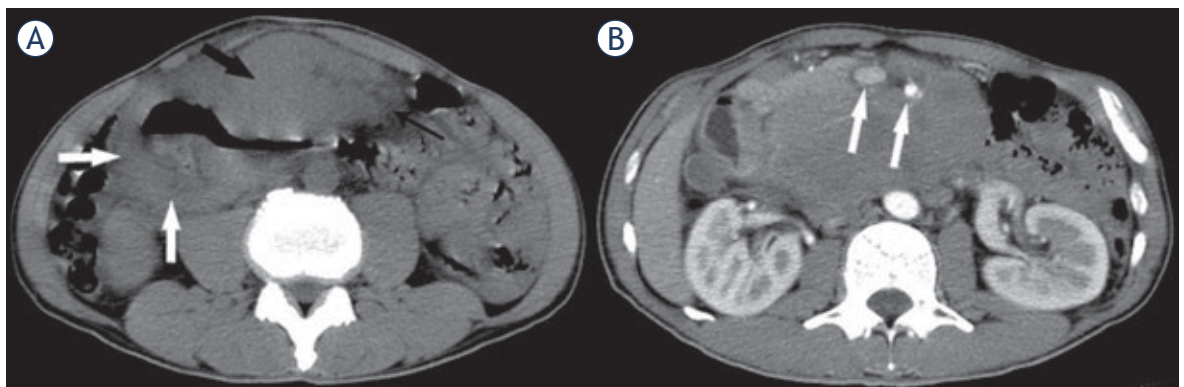


**FIGURE 4.** A 61-year-old man with PTCL in the duodenum. **(A)** Axial non-contrast CT image shows the thickening of the duodenal wall (white arrows). The lesion grows in an expansive centripetal fashion (black arrow) with an ill-defined margin and invasion of adjacent fatty tissue (thin black arrow). **(B)** Contrast-enhanced CT image shows the tumor with heterogeneously mild enhancement. Superior mesenteric artery and vein are encased by the tumor (white arrows). Tumor progression was found during therapy. This patient deceased at 5 months after therapy.

untreated lymphoma. In our opinion, asymmetric tumor cell density and uneven distribution of blood vessel density in PTCL may contribute to inhomogeneous density on CT images, though the corresponding radiological-pathological studies are absent in our study. A previous study showed that tumor cells of T-cell lymphoma grown under an inhomogeneous cell density, especially under a high cell density environment, become better adapted to survival. They are not only superior in their tumorigenic potential, but are also resistant to the antitumor action of multiple anticancer drugs.<sup>21</sup> Increased intratumoral vascularity has also been described as a negative prognostic factor in diffuse large B-cell lymphoma (DLBCL) treated with rituximab plus chemotherapy.<sup>22</sup>

Although intratumoral necrosis was not a common feature of NHL, it was found in nearly 27.5% of patients (14/51) in our study. Three previous studies have investigated the prognostic implications of tumor necrosis at CT or MRI in lymphoma.<sup>23-25</sup> Hopper *et al.*<sup>23</sup> investigated chest CT scans of 76 patients with newly diagnosed Hodgkin lymphoma with mediastinal involvement. Their results showed that the presence of mediastinal necrotic lymph nodes appears to have little prognostic significance in patients with Hodgkin lymphoma. Saito *et al.*<sup>24</sup> evaluated CT and MRI scans of 60 patients with different non-Hodgkin lymphoma subtypes for the presence of necrosis in lymph nodes. They found that lymph node necrosis had no significant influence on patients' disease-free survival, but may have a prognostic significance in patients with non-Hodgkin lymphomas. Adams *et al.*<sup>25</sup> studied CT scans of 51 patients with DLBCL for the tumor necrosis in lymph nodes as well as extranodal sites. The findings of their study also indicate the prognostic potential of tumor necrosis at CT in newly diagnosed DLBCL. The result of our study was similar to those of Saito *et al.* and Adams *et al.* Univariate analysis showed that intratumoral necrosis was associated with poor clinical outcomes. This may indicate that the underlying PTCL has an aggressive tumor growth. Although intratumoral necrosis was not an independent risk factor by multivariate analysis, it may have a prognostic significance in patients with PTCL.

The results of our study showed that PTCL is likely to involve multiple regions and manifest as a generalized disease. Lee *et al.*<sup>8</sup> also found that the most common radiologic feature of PTCL was systemic dissemination, including various organ involvement and generalized lymphadenopathy. In addition, in their series of 581 patients with in-

testinal non-Hodgkin lymphoma, Kim *et al.*<sup>26</sup> identified that B-cell lymphoma mainly presented as localized disease while T-cell lymphoma involved multiple sites. Three subtypes of T-cell lymphoma including PTCL-NOS, EATL and NK/T lymphoma had a relatively lower response rate and a higher recurrence rate. Although multiple site involvement was not an independent risk factor to predict patients' prognosis in our study, it was associated with poor clinical outcome in univariate analysis. Again, this may suggest that this characteristic is an indicative sign of the aggressive clinical course of PTCL.

In diagnosis, staging, monitoring of treatment and prediction of prognosis in patients with lymphoma, <sup>18</sup>F-fluorodeoxyglucose positron emission tomography-computed tomography (<sup>18</sup>F-FDG PET/CT) has proved to be a more effective modality than diagnostic CT.<sup>27-30</sup> Jung *et al.*<sup>31</sup> investigated the prognostic accuracy of interim PET/CT in PTCL and derived cutoffs for standardized uptake value (SUV) and metabolic tumor volume (MTV) assessments that were significantly predictive for survival. Cottreau *et al.*<sup>32</sup> also reported that higher MTV predicted a poor survival in patients with PTCL. However, in China the limited number of hybrid PET/CT scanners and major financial restrictions also prevent widespread use of this expensive modality. Furthermore, intravenous contrast material administration is usually absent in FDG PET/CT studies and blood vessel invasion by lymphoma may not be clearly depicted. Small disease missed by PET/CT because of the absence of FDG uptake and non-pathological FDG accumulation can also be properly identified by contrast-enhanced CT.

Our study has several limitations, the first of which is its retrospective nature. Second, a detailed pathological study was absent to be correlated to the imaging findings. Therefore, further investigation on large cases with a detailed radiological-pathological correlation study is needed. Third, different CT equipment and techniques were used. CT examinations of 10 patients were performed on a single spiral CT with a section thickness of 10 mm. Compared with the smaller section thickness, it may affect the quality of the CT images and decrease the probability that more tissue of a given lesion will be captured. Fourth, different histological subtypes of PTCL were involved, and each subtype may have different clinical features and treatment response. However, this problem is simply unavoidable due to the limitations of a retrospective study and the rarity of PTCL, and should not have significantly affected the imaging characteristics studied.

In conclusion, multiple site involvement, an ill-defined margin with peritumoral invasion, inhomogeneous density, and intratumoral necrosis are relatively significant CT features of PTCL. An ill-defined margin with peritumoral invasion indicates a high risk of unfavorable survival outcome for PTCL. Nevertheless, the interaction between the different clinical and radiologic parameters is complex, and the imaging-based criteria for the assessment of treatment success and outcome is still the subject of ongoing investigations. To reliably evaluate the survival of patients with PTCL, it is important that the imaging examinations be performed according to unified technology and are interpreted according to standardized rules.

## References

- Anderson JR, Armitage JO, Weisenburger DD. Epidemiology of the non-Hodgkin's lymphomas: distributions of the major subtypes differ by geographic locations. Non-Hodgkin's Lymphoma Classification Project. *Ann Oncol* 1998; **9**: 717-20. PMID: 9739436
- Shea L, Liu J, Cashen A. Prognostic significance of [18F]fluorodeoxyglucose-positron emission tomography in peripheral T-cell lymphoma treated with stem cell transplantation: a retrospective analysis. *Leuk Lymphoma* 2015; **56**: 256-9. doi: 10.3109/10428194.2014.914194
- Park S, Ko YH. Peripheral T cell lymphoma in Asia. *Int J Hematol* 2014; **99**: 227-39. doi: 10.1007/s12185-014-1520-3
- Yi S, An G, Qi J, Zou D, Zhao Y, Zhang P, et al. The significance of bone marrow involvement in aggressive lymphomas: A retrospective comparison of clinical outcomes between peripheral T cell lymphoma and diffuse large B cell lymphoma in China. *Acta Haematol* 2010; **124**: 239-44. doi: 10.1159/000321544
- Gisselbrecht C, Gaulard P, Lepage E, Coiffier B, Briere J, Haioun C, et al. Prognostic significance of T-cell phenotype in aggressive non-Hodgkin's lymphomas. Groupe d'Etudes des Lymphomes de l'Adulte (GELA). *Blood* 1998; **92**: 76-82. PMID: 9639502
- Adams SV, Newcomb PA, Shustov AR. Racial patterns of peripheral T-cell lymphoma incidence and survival in the United States. *J Clin Oncol* 2016; **34**: 963-71. doi: 10.1200/JCO
- Lim ST, Hee SW, Quek R, Lim LC, Yap SP, Loong EL, et al. Comparative analysis of extra-nodal NK/T-cell lymphoma and peripheral T-cell lymphoma: significant differences in clinical characteristics and prognosis. *Eur J Haematol* 2008; **80**: 55-60. doi: 10.1111/j.1600-0609.2007.00978.x
- Lee HJ, Im JG, Goo JM, Kim KW, Choi BI, Chang KH, et al. Peripheral T-cell lymphoma: spectrum of imaging findings with clinical and pathologic features. *Radiographics* 2003; **23**: 7-26. doi: 10.1148/rg.231025018
- Otero HJ, Jagannathan JP, Prevedello LM, Johnston CJ, Ramaia NH, Van den Abbeele AD, et al. CT and PET/CT findings of T-cell lymphoma. *Am J Roentgenol* 2009; **193**: 349-58. doi: 10.2214/AJR.08.1398
- Choi JW, Kim SS, Kim EY, Heran M. Peripheral T-cell lymphoma in the neck: CT findings of lymph node involvement. *Am J Neuroradiol* 2006; **27**: 1079-82. PMID: 16687547
- Lu DS, Reber HA, Krasny RM, Kadell BM, Sayre J. Local staging of pancreatic cancer: criteria for unresectability of major vessels as revealed by pancreatic-phase, thin-section helical CT. *Am J Roentgenol* 1997; **168**: 1439-43. doi: 10.2214/ajr.168.6.9168704
- Weber AL, Rahemtullah A, Ferry JA. Hodgkin and non-Hodgkin lymphoma of the head and neck: clinical, pathologic, and imaging evaluation. *Neuroimaging Clin N Am* 2003; **13**: 371-92. doi: 10.1016/S1052-5149(03)00039-X
- Zhou C, Duan X, Lan B, Liao J, Shen J. Prognostic CT and MR imaging features in patients with untreated extranodal non-Hodgkin lymphoma of the head and neck region. *Eur Radiol* 2015; **25**: 3035-42. doi: 10.1007/s00330-015-3708-1
- Kim TM, Park YH, Lee SY, Kim JH, Kim DW, Im SA, et al. Local tumor invasiveness is more predictive of survival than International Prognostic Index in stage I(E)/II(E) extranodal NK/T-cell lymphoma, nasal type. *Blood* 2005; **106**: 3785-90. doi: 10.1182/blood-2005-05-2056
- Opdam FJ, Kamp M, de Bruijn R, Roos E. Jak kinase activity is required for lymphoma invasion and metastasis. *Oncogene* 2004; **23**: 6647-53. doi: 10.1038/sj.onc.1207887
- Mahadevan D, Spier C, Della Croce K, Miller S, George B, Riley C, et al. Transcript profiling in peripheral T-cell lymphoma, not otherwise specified, and diffuse large B-cell lymphoma identifies distinct tumor profile signatures. *Mol Cancer Ther* 2005; **4**: 1867-79. doi: 10.1158/1535-7163.MCT-05-0146
- Pileri SA, Piccaluga PP. New molecular insights into peripheral T cell lymphomas. *J Clin Invest* 2012; **122**: 3448-55. doi: 10.1172/JCI61205
- Ruddell A, Mezquita P, Brandvold KA, Farr A, Iritani BM. B lymphocyte-specific c-Myc expression stimulates early and functional expansion of the vasculature and lymphatics during lymphomagenesis. *Am J Pathol* 2003; **163**: 2233-45. doi: 10.1016/S0002-9440(10)63581-X
- Ruddell A, Harrell MI, Furuya M, Kirschbaum SB, Iritani BM. B lymphocytes promote lymphogenous metastasis of lymphoma and melanoma. *Neoplasia* 2011; **13**: 748-57. PMID: 21847366
- Rodriguez M, Rehn SM, Nyman RS, Sundström JC, Ahlström H, Glimelius BL. CT in malignancy grading and prognostic prediction of non-Hodgkin's lymphoma. *Acta Radiol* 1999; **40**: 191-7. PMID: 10080733
- Singh V, Singh MP, Singh SM. Cell density-dependent alterations in tumorigenic potential of a murine T-cell lymphoma: implication in the evolution of multidrug resistance in tumor cells. *Anticancer Drugs* 2008; **19**: 793-804. doi: 10.1097/CAD.0b013e32830ce4f5
- Cardesa-Salzmann TM, Colomo L, Gutierrez G, Chan WC, Weisenburger D, Climent F, et al. High microvessel density determines a poor outcome in patients with diffuse large B-cell lymphoma treated with rituximab plus chemotherapy. *Haematologica* 2011; **96**: 996-1001. doi: 10.3324/haematol.2010.037408
- Hopper KD, Diehl LF, Cole BA, Lynch JC, Meilstrup JW, McCauslin MA. The significance of necrotic mediastinal lymph nodes on CT in patients with newly diagnosed Hodgkin disease. *Am J Roentgenol* 1990; **155**: 267-70. doi: 10.2214/ajr.155.2.2115249
- Saito A, Takashima S, Takayama F, Kawakami S, Momose M, Matsushita T. Spontaneous extensive necrosis in non-Hodgkin lymphoma: prevalence and clinical significance. *J Comput Assist Tomogr* 2001; **25**: 482-6. PMID: 11351202
- Adams HJ, de Klerk JM, Fijnheer R, Dubois SV, Nievelstein RA, Kwee TC. Prognostic value of tumor necrosis at CT in diffuse large B-cell lymphoma. *Eur J Radiol* 2015; **84**: 372-7. doi: 10.1016/j.ejrad.2014.12.009
- Kim SJ, Choi CW, Mun YC, Oh SY, Kang HJ, Lee SJ, et al. Multicenter retrospective analysis of 581 patients with primary intestinal non-hodgkin lymphoma from the Consortium for Improving Survival of Lymphoma (CISL). *BMC Cancer* 2011; **11**: 321-32. doi: 10.1186/1471-2407-11-321
- Raanani P, Shasha Y, Perry C, Metsker U, Naparstek E, Apter S, et al. Is CT scan still necessary for staging in Hodgkin and non-Hodgkin lymphoma patients in the PET/CT era? *Ann Oncol* 2006; **17**: 117-22. doi: 10.1093/annonc/mdj024
- la Fougère C, Hundt W, Bröckel N, Pfluger T, Haug A, Scher B, et al. Value of PET/CT versus PET and CT performed as separate investigations in patients with Hodgkin's disease and non-Hodgkin's lymphoma. *Eur J Nucl Med Mol Imaging* 2006; **33**: 1417-25. doi: 10.1007/s00259-006-0171-x
- Fueger BJ, Yeom K, Czernin J, Sayre JW, Phelps ME, Allen-Auerbach MS. Comparison of CT, PET, and PET/CT for staging of patients with indolent non-Hodgkin's lymphoma. *Mol Imaging Biol* 2009; **11**: 269-74. doi: 10.1007/s11307-009-0200-9
- Ricard F, Giammarile F, Tychyj-Pinel C, Houzard C, Decullier E, Chateau F, et al. PET-CT and diagnostic CT: the synergy of metabolic and morphological data in onco-haematology. *Diagn Interv Imaging*. 2014; **95**: 55-62. doi: 10.1016/j.diii.2013.07.008
- Jung SH, Ahn JS, Kim YK, Kweon SS, Min JJ, Bom HS, et al. Prognostic significance of interim PET/CT based on visual, SUV-based, and MTV-based assessment in the treatment of peripheral T-cell lymphoma. *BMC Cancer* 2015; **15**: 198. doi: 10.1186/s12885-015-1193-1
- Cottreau AS, Becker S, Broussais F, Casasnovas O, Kanoun S, Roques M, et al. Prognostic value of baseline total metabolic tumor volume (TMTV0) measured on FDG-PET/CT in patients with peripheral T-cell lymphoma (PTCL). *Ann Oncol* 2016; **27**: 719-24. doi: 10.1093/annonc/mdw011

# Prognostic role of diffusion weighted and dynamic contrast-enhanced MRI in loco-regionally advanced head and neck cancer treated with concomitant chemoradiotherapy

Manca Garbajs<sup>1</sup>, Primoz Strojan<sup>2</sup>, Katarina Surlan-Popovic<sup>1</sup>

<sup>1</sup> Institute of Clinical Radiology, University Medical Centre Ljubljana, Slovenia

<sup>2</sup> Division of Radiation Oncology, Institute of Oncology, Ljubljana, Slovenia

Radiol Oncol 2019; 53(1): 39-48.

Received 23 January 2019  
Accepted 04 February 2019

Correspondence to: Manca Garbajs, M.D., Institute of Clinical Radiology, University Medical Centre, Zaloška c. 7, SI-1000 Ljubljana, Slovenia. Phone: + 386 40 212 226; E-mail: manca.garbajs@kclj.si

Disclosure: No potential conflicts of interest were disclosed.

**Background.** In the study, the value of pre-treatment dynamic contrast-enhanced (DCE) and diffusion weighted (DW) MRI-derived parameters as well as their changes early during treatment was evaluated for predicting disease-free survival (DFS) and overall survival (OS) in patients with locoregionally advanced head and neck squamous carcinoma (HNSCC) treated with concomitant chemoradiotherapy (cCRT) with cisplatin.

**Patients and methods.** MRI scans were performed in 20 patients with locoregionally advanced HNSCC at baseline and after 10 Grays (Gy) of cCRT. Tumour apparent diffusion coefficient (ADC) and DCE parameters (volume transfer constant [ $K_{trans}$ ], extracellular extravascular volume fraction [ $v_e$ ], and plasma volume fraction [ $V_p$ ]) were measured. Relative changes in parameters from baseline to 10 Gy were calculated. Univariate and multivariate Cox regression analysis were conducted. Receiver operating characteristic (ROC) curve analysis was employed to identify parameters with the best diagnostic performance.

**Results.** None of the parameters was identified to predict for DFS. On univariate analysis of OS, lower pre-treatment ADC ( $p = 0.012$ ), higher pre-treatment  $K_{trans}$  ( $p = 0.026$ ), and higher reduction in  $K_{trans}$  ( $p = 0.014$ ) from baseline to 10 Gy were identified as significant predictors. Multivariate analysis identified only higher pre-treatment  $K_{trans}$  ( $p = 0.026$ ; 95% CI: 0.000–0.132) as an independent predictor of OS. At ROC curve analysis, pre-treatment  $K_{trans}$  yielded an excellent diagnostic accuracy (area under curve [AUC] = 0.95, sensitivity 93.3%; specificity 80 %).

**Conclusions.** In our group of HNSCC patients treated with cisplatin-based cCRT, pre-treatment  $K_{trans}$  was found to be a good predictor of OS.

Key words: dynamic contrast-enhanced MRI; diffusion-weighted imaging; overall survival; squamous cell head and neck cancer; concomitant chemoradiotherapy

## Introduction

Head and neck squamous carcinoma (HNSCC) is the seventh most commonly diagnosed cancer and the sixth most common cause of cancer death worldwide.<sup>1</sup> In a significant portion of patients with loco-regionally advanced disease, platin-based concomitant chemo-radiotherapy (cCRT) is the mainstay of treatment.<sup>2,3</sup> However, current

treatment options remain suboptimal, since around 50% of patient experience tumour recurrence<sup>4,5</sup> with the pathohistological evidence of residual regional lymph node metastases in up to 26% of patients with clinically determined complete response after cCRT.<sup>6</sup> In addition, the reported 5-year overall survival (OS) rates are still well below 50%.<sup>7</sup> In this scenario, improving prognostic stratification either before or early during cCRT would allow for pos-

sible modification of treatment regime in order to improve clinical outcomes and survival rates.

Multi-parametric imaging with functional imaging techniques has recently been used to evaluate biological properties of malignant tumours as changes at a cellular level typically occur prior to morphological changes. CT perfusion (CTP) has already been reported to provide a valuable information on tumour vascularity.<sup>8-10</sup> In recent years, diffusion-weighted (DW) MR imaging (MRI) and dynamic contrast-enhanced MRI (DCE) have been used for assessing tumour biology and to predict tumour response and survival rates in patients with HNSCC. DWI is a widely used technique that allows for non-invasive measurement of the Brownian motion of water molecules by calculating the apparent diffusion coefficient (ADC) which reflects tumour cellularity and tissue microstructure.<sup>11</sup>

Dynamic contrast-enhanced MRI (DCE-MRI) can assess the flow of blood through vessels in scanned tissues and therefore enables non-invasive characterization of tumour vascularity and perfusion.<sup>12</sup> Due to lack of standardization of data acquisition and analysis<sup>12</sup>, the results of studies assessing the value of DCE-MRI derived parameters are still scarce and contradictory.<sup>13-15</sup> In addition, studies addressing prognostic values of DCE-MRI parameters acquired early during treatment are lacking.

To the best of our knowledge, there is no data in the literature that would address the utility of combined DWI and DCE-MRI derived parameters before and early during treatment as prognostic factors for survival in HNSCC. Therefore, the objective of current study was to evaluate the prognostic value of imaging parameters from DWI and DCE MRI at baseline and early during treatment in loco-regionally advanced HNSCC patients treated with cisplatin-based cCRT.

## Patients and methods

### Patients and treatment

The study was approved by the National Medical Ethics Committee of the Republic of Slovenia (No. 22k/03/13) and written informed consent was obtained from all patients. Twenty patients with locally and/or regionally advanced (stages III-IVB) and histologically proven p16/HPV-negative SCC of the oro- or hypopharynx were enrolled in the study. p16/HPV status was assessed as described elsewhere.<sup>16</sup> All patients were treated with cisplatin-based cCRT as recommended by the institutional multidisciplinary tumour board.

Patients were irradiated with a 6-MV linear accelerator photon beam using a concomitant boost intensity-modulated radiation technique. The dose to the primary tumour and enlarged lymph nodes was 70 Gy (gross tumour volume with a margin to compensate microscopic tumour extensions), whereas elective doses of 63 Gy (intermediate-risk volume - around larger nodes and non-palpable but radiologically suspicious nodes) and 56 Gy (low-risk volume) were applied for neck regions of probable microscopic disease in daily fractions of 2.0, 1.8 and 1.6 Gy, respectively, over 7 weeks. During radiotherapy, cisplatin in a dose of 40 mg/m<sup>2</sup>/week was concurrently administered. No antiangiogenic therapy was added to the protocol.

During therapy, toxicity was monitored on a weekly basis. After treatment completion, patients were examined for toxicity and tumour response every 2 to 3 months in the first and second year and every six months thereafter.

### MR imaging protocol

All patients underwent three MR examinations with DWI and DCE-MRI: (1) 0–7 days before the treatment; (2) after 1 week (i.e., after the fifth fraction of radiotherapy, i.e. 10 Gy) and (3) 2.5–3 months after the completion of cCRT to assess radiological response to treatment.

MR imaging was performed on 3T MAGNETOM Trio, A Tim System (Siemens Medical Systems®, Erlangen, Germany) with a neck array coil. The diagnostic imaging protocol included axial T2-weighted sequences with short tau inversion recovery (STIR) from the base of the skull to aortic arch (TR/TE 5010/71 ms, TI 170 ms, flip angle (FA) 70°, receiver bandwidth 287 Hz/pixel, matrix size 256 × 256, slice thickness 3 mm, gap 0.3 mm and field of view (FOV) 18 × 18 cm). Axial slices that covered the entire primary tumour were selected for DWI and DCE-MR imaging.

DWI images were acquired in axial plane using pulsed spin-echo echo-planar image sequence (TR/TE 3600/86 ms, receiver bandwidth 1302 Hz/pixel, matrix size 180 × 192, slice thickness 5 mm, gap 1.5 mm, FOV 230 cm<sup>2</sup> and total acquisition time 5.04 min). Five different b-values (b = 0, 100, 200, 500 and 1000 s/mm<sup>2</sup>) were used with all diffusion-sensitizing gradients applied in three orthogonal directions to obtain trace-weighted images.

DCE-MRI was performed using 3D fast low angle shot (FLASH) sequence optimised for spatial and temporal resolution (TR/TE 5/1.16 ms, FA 15°, receiver bandwidth 490 Hz/pixel, matrix size 220

cm<sup>2</sup>, slice thickness 4 mm, temporal resolution 4 s, total acquisition time 5 min. T1 mapping was used to convert signal intensities into gadolinium concentration. The T1 map was calculated from pre-contrast multiple flip angle images (6°, 10° in 15°). A k-space weighted image contrast algorithm was used to generate images with full spatial resolution of 128 x 128. Baseline images were acquired for 28 s. While the imaging continued, the gadobutrol (Gadovist®, Bayer HealthCare Pharmaceuticals) was administered intravenously in a dose of 0.1 mmol/kg body weight with a flow-rate of 3.5 ml/s followed by a 20 ml of saline flush with power injector.

Finally, post-contrast axial T1 weighted volumetric interpolated breath-hold examination (VIBE) sequences were acquired from skull base to aortic arch (TR/TE 3,26/1,26 ms, voxel size 1,1 x 0,9 x 1,5 mm with 4 mm averages, receiver bandwidth 640 Hz/pixel, matrix size 218 x 288 and FOV 250 cm<sup>2</sup>).

### Imaging parameters analysis

Post-processing of all the images was performed at a workstation running commercially available software Olea Sphere® 3.0 MR Head & Neck expanded applications (Olea Medical®, La Ciotat, France). Before data analysis, motion correction algorithm was applied that allowed for pairwise in-plane (acquisition plane) rigid co-registration of all raw perfusion images of a given slice location with well-chosen reference image over time.

Quantitative DCE-MRI parameters were volume transfer constant ( $K_{trans}$ ), extracellular extravascular volume fraction ( $v_e$ ) and plasma volume fraction ( $V_p$ ). The pharmacokinetic modelling was done on a pixel-by-pixel basis using the extended Tofts model - a two compartment model, which is suitable for any freely diffusible tracer. The equation modelling the contrast agent's concentration was the following<sup>17</sup>:

$$C(t) = v_p c_p(t) + K_{trans} c_p(t) \exp(-K_{ep} t)$$

where  $C(t)$  is the tissue contrast agent concentration time course,  $V_p$  is plasma volume fraction,  $c_p$  is plasma contrast agent concentration,  $K_{trans}$  is the volume transfer constant and  $K_{ep}$  is the transfer function from extracellular extravascular space to the plasma space. The Arterial Input Function (AIF) for the pharmacokinetic analysis was derived from automatic selection of perfusion weighted image pixels selected in suitable arteries using a dedicated algorithm. The following multi-parametric

maps with  $K_{trans}$ ,  $V_e$  and  $V_p$  were then obtained automatically.

Apparent diffusion coefficient (ADC) maps were computed by a single exponential fit using the DW signal intensity-b value curves.

ADC and DCE-MRI derived parameters as well as tumour volumes were measured at baseline and after 10 Gy. A radiologist (three years of experience in head and neck imaging) placed three regions of interest (ROIs) and analysed the multi-parametric ADC and DCE maps independently, with the T1 post-contrast images serving as the reference images. The ROIs were drawn manually on all imaging sections encircling solid-appearing portions of primary tumours and metastatic lymph node or nodal masses. Special attention was paid not to include necrotic and cystic areas (hyper-intense areas on STIR images), large feeding vessels and surrounding normal tissue.

Tumour volumes were calculated by manually encircling tumour borders on each T1 post-contrast sequence on all axial slices. Soft wear algorithm then calculated the volume by using the equation:

$$V = \text{encircled area} \times \text{section thickness}$$

Mean value of the selected ROIs from primary tumour was calculated for each parameter at each time point. Relative changes of the ADC and DCE-MRI parametric values as well as tumour volumes were calculated by dividing the mathematical difference of the corresponding parametric and tumour volume values after 10Gy and at pre-treatment by the pre-treatment parameter value for individual patient using the formula:

$$\Delta P_{10Gy} = \left[ \frac{P_{10Gy} - P_0}{P_0} \right] * 100$$

where  $P$  represents any given parameter (ADC,  $K_{trans}$ ,  $V_e$ ,  $V_p$  or tumour volume),  $P_{10Gy}$  represents absolute value of the parameter after 10Gy, and  $P_0$  absolute value of the pre-treatment parameter.

### Outcome determination and statistical analysis

All data analysis and graphs were performed using statistical software SPSS 19.0 (IBM SPSS Statistics for Windows, Version 19.0. Armonk, NY: IBM Corp.). Shapiro-Wilk test and Levene test were used for normality testing and homogeneity-of-variance testing, respectively. The continuous variables are presented by median value and range. The relative changes in parameters between pre-treatment values and at 10 Gy are expressed in percentage (%). OS (event: death from any cause)

TABLE 1. The baseline clinical characteristics of all the patients

Patient	Sex	Age (yrs)	Tumour location	TNM	Stage
1	M	53	Oropharynx	T4aN1	IVA
2	M	67	Hypopharynx	T3N1	III
3	M	66	Hypopharynx	T3N2b	IVA
4	M	56	Oropharynx	T3N2b	IVA
5	M	49	Oropharynx	T2N2b	IVA
6	M	57	Oropharynx	T4aN2c	IVA
7	M	59	Hypopharynx	T4aN2b	IVA
8	M	60	Oropharynx	T3N2b	IVA
9	M	58	Oropharynx	T4aN2b	IVA
10	M	53	Oropharynx	T4aN2c	IVA
11	M	64	Oropharynx	T3N2c	IVA
12	M	56	Hypopharynx	T3N2b	IVA
13	M	65	Oropharynx	T2N2b	IVA
14	M	53	Hypopharynx	T4aN2c	IVA
15	M	66	Oropharynx	T3N2b	IVA
16	M	65	Oropharynx	T3N2a	IVA
17	M	46	Oropharynx	T3N3	IVB
18	M	67	Hypopharynx	T3N1	III
19	F	58	Oropharynx	T3N1	III
20	M	48	Hypopharynx	T3N1	III

Yrs = years

and DFS (event: persistent tumour after cCRT, loco/regional recurrence, systemic dissemination) was calculated from the first day of therapy using Kaplan-Meier curves. For assessment of prognostic value of MRI-derived parameters, patients were divided into two groups, according to treatment effect (DFS: without *vs.* with persistent tumour after cCRT or local/regional recurrence or systemic metastasis) or survival status at the end of observation period (OS: alive *vs.* death).

Non-parametric tests (Wilcoxon Signed Rank test, Mann-Whitney U test) were employed for comparative analysis of MRI-derived parameters under study. DFS and OS were plotted using the Kaplan-Meier method and significant predictors for survival outcomes were identified by univariate Cox regression analysis. All variables that reached the level of statistical significance in univariate analyses were entered into the multivariate Cox regression model, and stepwise forward selection was used to identify the independent predictors of DFS and OS. Receiver operating characteristic (ROC) curve analysis was applied to determine the discriminatory power of the ADC and DCE-MRI

parameters as well as tumour volume and clinical parameters for predicting survival rates. Area under curve (AUC) was computed and the optimal cut-off values were calculated by maximizing sensitivity and specificity. Two-tailed p values less than 0.05 were considered statistically significant.

## Results

### Patient data

All of the 20 consecutive patients (19 men, 1 woman; median age 58 years, range 46–67 years) with loco-regionally advanced HNSCC (oropharynx 13, hypopharynx 7) were free of systemic disease at presentation. The baseline clinical characteristics of the patients are listed in Table 1.

The median follow-up times of the entire study cohort and of the surviving patients were 27.2 months (range, 2.6–51.4 months) and 30.2 months (range, 18.2–51.4 months), respectively. In all patients, radiological complete tumour response to cCRT was determined 2.5–3 months post-therapy. Disease reappearance was diagnosed in 5 patients: 3 (15%) patients had recurrence at primary site, and 2 patients (10%) developed distant metastases (lungs). At the time of analysis, five patients (25%) were dead. Locoregional disease was the cause of death in three patients (with survival rates of 5.2, 10.6, and 22.9 months post-therapy), distant metastasis in one patient (14.1 months) and acute lower respiratory tract infection in the remaining patient (2.6 months, considered as treatment failure). A mean DFS was 38.9 months (2.6–51.4 months, 95% Confidence Interval [CI] 30.7–47.1). A mean OS time was 40.6 months (2.6–51.4 months, 95% CI 32.4–48.8). The 1- and 2- year DFS survival rates were 88.8% and 88.2% and for OS they were 84.4% and 73.8%.

### Descriptive analysis of ADC and DCE-MRI derived parameters before and during treatment

For all the included patients, the pre-treatment values of ADC and DCE-MRI derived parameters  $K_{trans}$ ,  $V_e$  and  $V_p$  were 0.81 (0.62–1.07)  $\times 10^{-3}$  mm<sup>2</sup>/s, 0.48 (0.13–0.79) min<sup>-1</sup>, 0.32 (0.15–0.64) and 0.17 (0.06–0.43), respectively. A statistically significant change from pre-treatment to 10 Gy was seen in all parameters: an increase of 22.5% (1.7 to 52.4%) in ADC ( $p < 0.001$ ) and of 70% (73.2 to 357.14%) in  $V_p$  ( $p = 0.015$ ) and a reduction of 50.3% (-93.4 to 179.2%) in  $K_{trans}$  ( $p = 0.003$ ) and of 35.2% (-88.9

**TABLE 2.** Absolute values of DWI and DCE-MRI derived parameters and tumour volumes before treatment and their relative changes after 10 Gy (expressed as median and range) for the entire cohort of the patients and separately for alive and deceased patients at the end of follow-up

Parameters	The entire cohort of patients (n = 20, 100%)	Patients still alive at the end of follow-up (n = 15; 75%)	Deceased patients at the end of follow-up (n = 5; 25%)
<b>Pre-treatment values</b>			
ADC ( $\times 10^{-3}$ mm <sup>2</sup> /s)	0.81 (0.62–1.07)	0.76 (0.62–0.91)	0.96 (0.76–1.07)
K <sub>trans</sub> (min <sup>-1</sup> )	0.48 (0.13–0.79)	0.57 (0.23–0.79)	0.22 (0.13–0.35)
V <sub>e</sub>	0.32 (0.15–0.64)	0.32 (0.17–0.64)	0.22 (0.15–0.37)
V <sub>p</sub>	0.17 (0.06–0.43)	0.15 (0.07–0.43)	0.35 (0.06–0.41)
Tumour volume (ml)	10.5 (2.6–54.9)	8.8 (2.6–44.55)	18.21 (6.6–54.9)
<b>Relative changes after 10 Gy</b>			
$\Delta$ ADC	22.5% (1.7 to 52.4%)	25.0 (4.7 to 51.4)	9.2 (1.7 to 52.4)
$\Delta$ K <sub>trans</sub>	-50.3% (-93.4 to 179.2%)	-60.0 (-93.0 to -43.2)	4.2 (-37.1 to 179.2)
$\Delta$ V <sub>e</sub>	-35.2% (-88.9 to 126.8%)	-40.0 (-88.9 to 65.4)	-14.7 (-40. to 126.8)
$\Delta$ V <sub>p</sub>	70% (73.2 to 357.14%)	92.9 (-18.6 to 357.2)	10.0 (-73.2 to 100)
$\Delta$ Tumour volume	(-15.0%; -76.3 to 254.6%);	-14.0 (-76.3 to 254.6)	-19.6 (-37.7 to 114.72)

ADC = apparent diffusion coefficient; DCE-MRI = dynamic contrast-enhanced MRI; DWI = diffusion weighted imaging; Gy = gray; K<sub>trans</sub> = volume transfer constant; V<sub>e</sub> = extracellular extravascular volume fraction; V<sub>p</sub> = plasma volume fraction;  $\Delta$  = relative change in the parameter

to 126.8%) in V<sub>e</sub> (p = 0.024). Pre-treatment tumour volume was 10.5 ml (2.6–54.9 ml). However, the change after 10 Gy from pre-treatment was not statistically different (-15.0%; -76.3 to 254.6%; p = 0.823) (Table 2).

The values of ADC and DCE-MRI derived parameters before treatment and the relative change of parameters after 10 Gy from baseline were com-

pared between patients alive at the end of follow-up and those who died (Table 2). Pre-treatment ADC ( $0.76 \times 10^{-3}$  mm<sup>2</sup>/s;  $0.62\text{--}0.91 \times 10^{-3}$  mm<sup>2</sup>/s) was significantly lower (p = 0.042) in patients which were still alive at the end of follow-up versus the patients who died ( $0.96 \times 10^{-3}$  mm<sup>2</sup>/s;  $0.76\text{--}1.07 \times 10^{-3}$  mm<sup>2</sup>/s). Alive patients also showed a significantly higher (p = 0.002) pre-treatment DCE-MRI

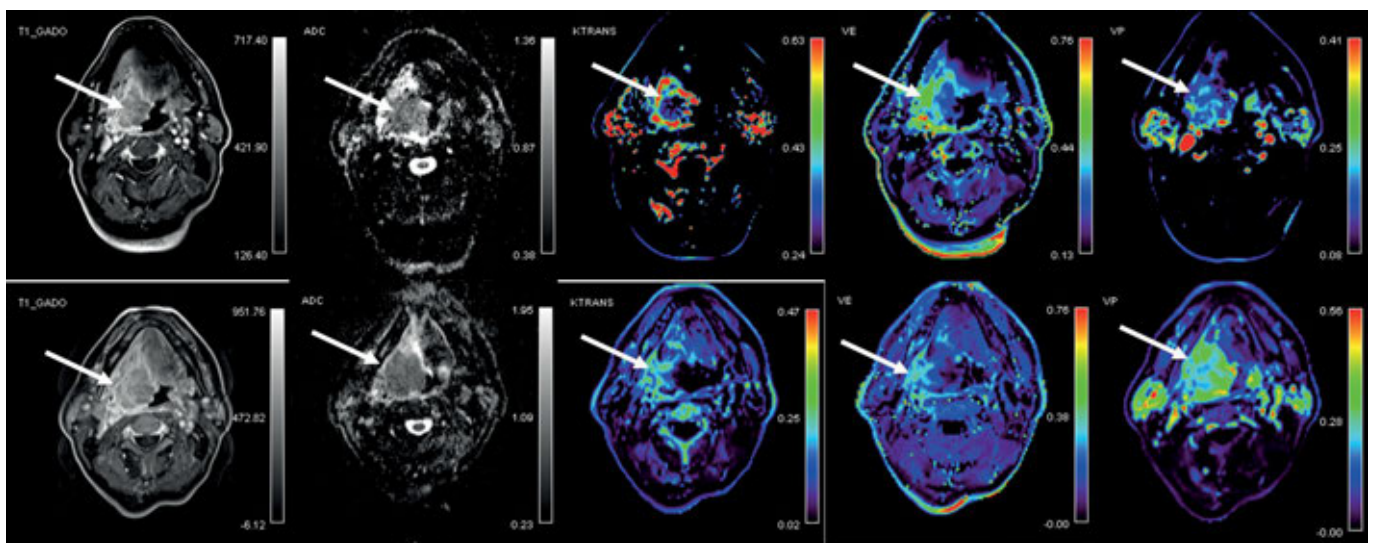


**FIGURE 1.** 58 year old patient with oropharyngeal squamous cell carcinoma (T4a N2b) who was alive at the end of follow up with overall survival of 41.1 months. Axial post-contrast T1 images, co-registered and corresponding apparent diffusion coefficient (ADC) maps and color-coded dynamic contrast-enhanced MRI derived volume transfer constant (Ktrans), extracellular extravascular fraction (Ve) and plasma volume fraction (Vp) maps in the area of the tumour (arrows) are shown. Top: before treatment; bottom: after 10 Gray of chemo-radiotherapy.

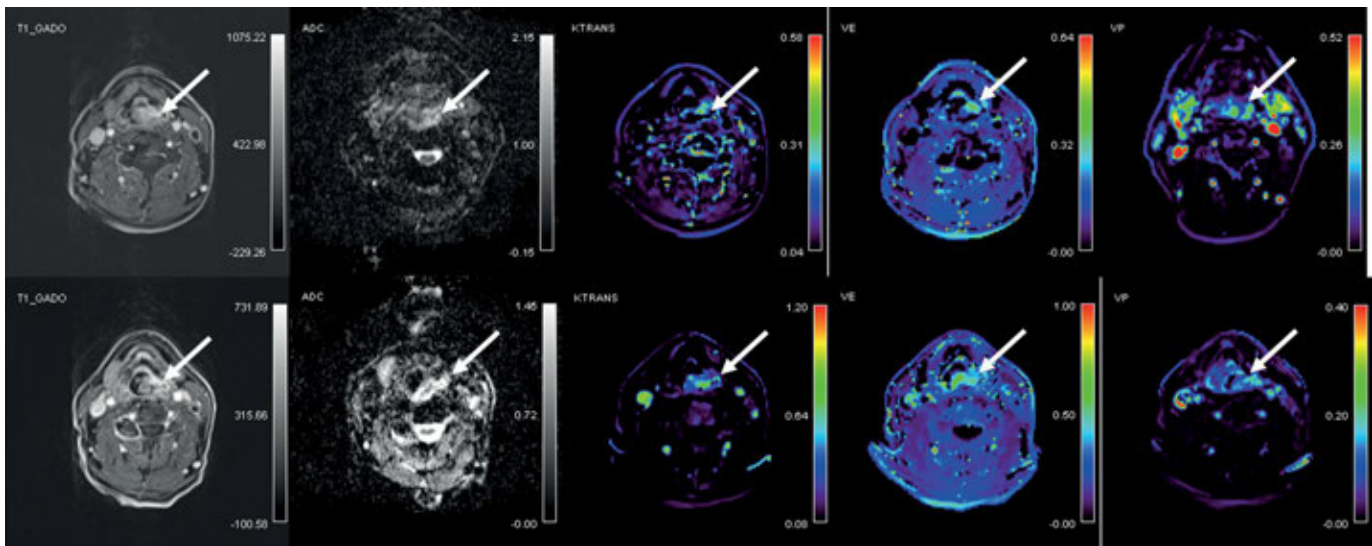


**FIGURE 2.** 65 year old patient with hypopharyngeal squamous cell carcinoma (T2 N2) who died 14 months of starting of chemo-radiotherapy due to disease relaps into the lungs. Axial post-contrast T1 images, co-registered and corresponding apparent diffusion coefficient (ADC) maps and color-coded dynamic contrast-enhanced MRI derived volume transfer constant (Ktrans), extracellular extravascular fraction (Ve) and plasma volume fraction (Vp) maps in the area of the tumour (arrows) are shown. Top: before treatment; bottom: after 10 Gray of chemo-radiotherapy.

derived parameter  $K_{trans}$  ( $0.57 \text{ min}^{-1}$ ;  $0.23\text{--}0.79 \text{ min}^{-1}$ ) compared with patients that died during follow-up ( $0.22 \text{ min}^{-1}$ ;  $0.13\text{--}0.35 \text{ min}^{-1}$ ). In addition, alive patients demonstrated a reduction in  $K_{trans}$  after 10

Gy from baseline ( $-60.0\%$ ;  $-93.0$  to  $-43.2\%$ ) whereas the patients who died showed no change or an increase in  $K_{trans}$  ( $4.2\%$ ;  $-37.1$  to  $179.2\%$ ) ( $p < 0.001$ ). There was no difference in the pre-treatment values of other perfusion parameters and tumour volumes ( $p > 0.05$ ) nor in the relative changes from 10 Gy to baseline of ADC,  $V_e$ ,  $V_p$  and tumour volume ( $p > 0.05$ ). Illustrative examples of DW and DCE MRI images of alive and deceased patient at the end of follow up are shown in Figure 1 and 2, respectively.

On contrary, no significant difference was observed when values of all the functional parameters and tumour volumes were compared between patients that showed disease progression during follow-up and patients without disease progression ( $p > 0.05$ ). However, in patients with noted disease progression there was a trend of larger pre-treatment tumour volume ( $14.0 \text{ ml}$ ;  $8.9\text{--}55.0 \text{ ml}$ ) compared to the group with disease controlled ( $6.6 \text{ ml}$ ;  $2.6\text{--}50.8 \text{ ml}$ ) ( $p = 0.054$ ).

**TABLE 3.** Univariate analysis of risk factors associated with disease-free survival and overall survival rates ( $n = 20$ )

Parameters	Disease-free survival (p value)	Overall survival (p value)
<b>Clinical parameters</b>		
Age	0.338	0.556
Tumour location	0.396	0.752
Stage	1.000	0.198
<b>Pre-treatment values of functional parameters and tumour volume</b>		
ADC ( $\times 10^{-3} \text{ mm}^2/\text{s}$ )	0.856	0.012*
$K_{trans}$ ( $\text{min}^{-1}$ )	0.116	0.026*
$V_e$	0.754	0.293
$V_p$	0.165	0.342
Tumour volume	0.959	0.048*
<b>Relative changes after 10 Gy of functional parameters and tumour volume</b>		
$\Delta\text{ADC}$ (%)	0.740	0.061
$\Delta K_{trans}$	0.688	0.014*
$\Delta V_e$	0.957	0.405
$\Delta V_p$	0.672	0.077
$\Delta\text{Tumour volume}$ (ml)	0.495	0.486

\* = significant predictor at univariate analysis; ADC = Apparent diffusion coefficient;  $K_{trans}$  = volume transfer constant;  $V_e$  = extracellular extravascular volume fraction;  $V_p$  = plasma volume fraction;  $\Delta$  = relative change in the parameter

### Univariate and multivariate Cox regression analysis

When assessing potential prognostic factors for DFS, none of them reached the level of statistical significance on univariate analysis (Table 3). Pre-treatment parameters that significantly influenced OS on univariate analysis were ADC ( $p = 0.012$ ),  $K_{trans}$  ( $p = 0.026$ ), and tumour volume ( $p = 0.048$ )

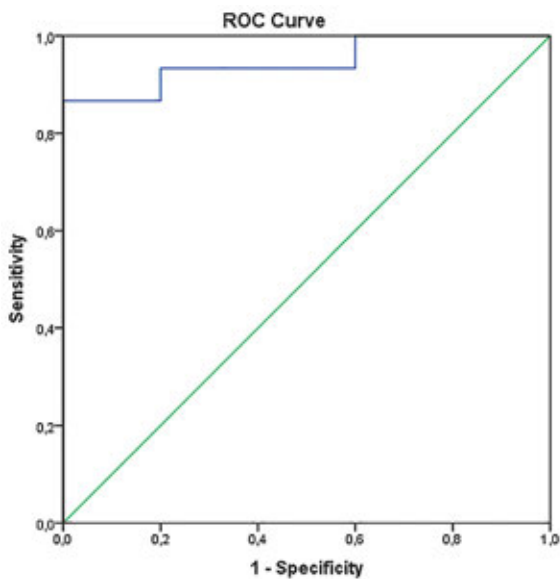


**FIGURE 3.** Receiver operating characteristic (ROC) curves for dynamic contrast-enhanced MRI (DCE-MRI) derived parameter  $K_{trans}$  (volume transfer constant) exhibiting area under ROC curve (AUC) of 0.95 with sensitivity 93.3% and specificity 80%. ( $p = 0.003$ ).

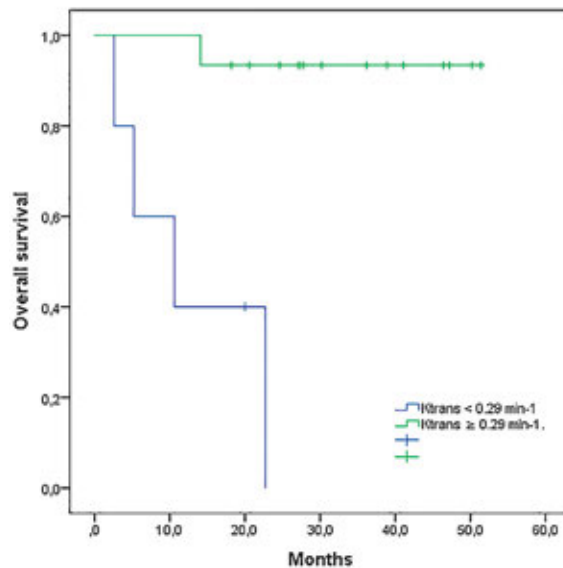


**FIGURE 4.** Kaplan-Meier estimates of overall survival in HNSCC patients (20) stratified according to pre-treatment DCE-MRI derived parameter  $K_{trans}$  (cut-off value of  $\geq 0.29 \text{ min}^{-1}$ , determined at ROC curve analysis).

DCE-MRI = dynamic contrast-enhanced MRI;  $K_{trans}$  = volume transfer constant; ROC = receiver operating curve

(higher  $K_{trans}$  and lower ADC and tumour volume were associated with longer survival). In addition, higher reduction in  $K_{trans}$  ( $p = 0.014$ ) from baseline to 10 Gy was also identified as a significant prognosticator for OS but not also any of the clinical parameters (age, tumour location, TNM stage). Multivariate Cox regression analysis identified only higher pre-treatment  $K_{trans}$  ( $p = 0.026$ ; 95% CI: 0.000–0.132) as an independent predictor of OS.

### ROC curve analysis

When ROC curve analysis was performed, pre-treatment  $K_{trans}$  provided an excellent diagnostic accuracy with an area under curve (AUC) of 0.95 ( $p = 0.003$ ; 95% CI: 0.85–1.00) and a sensitivity and specificity of 93.3% and 80.0%, respectively (Figure 1). The cut-off value for longer survival was set at  $\geq 0.29 \text{ min}^{-1}$ . In addition, a reduction in  $v_e$  after 10 Gy (survivors: median -40.0%, range -88.9% to 65.4%; deceased patients: median -14.7%, range -40.0 to 126.8%) yielded a good diagnostic accuracy with AUC 0.80 ( $p = 0.055$ ; 95% CI: 0.569–1.000), sensitivity 73.3% and specificity 80.0%. Pre-treatment  $v_e$  showed only poor diagnostic usefulness accuracy (AUC 0.63), whereas other parameters failed to show any diagnostic accuracy (AUC < 0.6). When patients were grouped according to the  $K_{trans}$  cut-off value of  $0.29 \text{ min}^{-1}$ , the log rank test confirmed

a statistically significant difference in the length of OS between the two groups with mean survival of 48.9 months (95% CI: 44.2–53.6) in patients with pre-treatment  $K_{trans} \geq 0.29 \text{ min}^{-1}$  and 12.8 months (95%CI: 4.1–21.4) in patients with pre-treatment  $K_{trans} < 0.29 \text{ min}^{-1}$  ( $p < 0.001$ ) (Figure 3).

### Discussion

Our study showed that pre-treatment DCE-MRI derived parameter  $K_{trans}$  could serve as an independent prognosticator of OS. Thus, DCE-MRI may be used before and early during treatment to get insight into tumour vascularity and perfusion, which conditioned, among other biological factors, the response of the HNSCC to platin-based cCRT. The ability to identify specific pre-treatment parameters as well as their changes early during treatment could assist in identification of patients at higher recurrence and mortality risk. Therefore, re-consideration of existing treatment scenario might be indicated in such patients in order to maximize the chance of favourable outcome and to avoid unnecessary toxicity.<sup>18,19</sup> In addition, more intensive surveillance could be performed in those individuals to detect eventual treatment failure in a timely manner.<sup>19</sup>

In present study, pre-treatment  $K_{trans}$  was found to be an independent prognostic factor for OS in both univariate and multivariate analysis with an excellent diagnostic accuracy in ROC analysis. DCE-MRI allows the analysis of vascular-related parameters in tumours and has primarily been used to predict treatment response and loco-regional control in HNSCC patients.<sup>20-25</sup> Very few studies evaluated the role of pre-treatment DCE-MRI on the survival of HNSCC patients treated with cCRT. Chan and Chawla with co-workers found that lower pre-treatment  $K_{trans}$  is associated with poorer DFS and OS.<sup>21,26</sup> On the contrary, two studies by Ng *et al.* failed to show the prognostic role of  $K_{trans}$  for survival in oropharyngeal HNC treated with CRT. Previous studies have already shown that higher pre-treatment  $K_{trans}$  values indicate better tumour response<sup>20,22</sup> and loco-regional control to CRT.<sup>24</sup>  $K_{trans}$  is the volume transfer constant between the blood plasma and extracellular extravascular space and is a measure of both tumour blood flow and vascular permeability. Studies on different tumours found that  $K_{trans}$  correlates with the proliferating cell density and micro-vessel density (MVD).<sup>13,27,28</sup> Both are used as markers of angiogenesis which is supposed to be the leading process for tumour growth, metastasis and radio-sensitivity.<sup>29</sup> The leading factor for stimulating angiogenesis is hypoxia, caused by structurally and functionally abnormal vessels and higher oxygen consumption by fast proliferating cells within the tumour micro-environment.<sup>30</sup> It is well-known that hypoxia enhances radio-chemoresistance through several mechanisms.<sup>31</sup> Higher pre-treatment  $K_{trans}$  may therefore reflect greater tumour blood flow and vessels permeability, indicating enriched oxygenation that resulted in favourable radio-chemo-sensitivity status of the tumour.

Although the multivariate analysis failed to confirm an independent prognostic value of relative changes of  $K_{trans}$ , a higher reduction of  $K_{trans}$  after 10 Gy from baseline was found to be important for better OS in univariate analysis. Studies addressing the prognostic values on survival rates of DCE-MRI early during treatment are lacking. Kim *et al.* reported a reduction of  $K_{trans}$  in human head and neck tumour xenografts after only three days of RT or chemotherapy.<sup>13</sup> Conversely, Baer *et al.* reported that patients with large-volume HNSCC with decreased  $K_{trans}$  after two weeks of therapy may have a shorter survival period.<sup>15</sup> Aforementioned study by Kim *et al.* showed that reduction of  $K_{trans}$  correlates with the changes of both proliferating cell density and MVD and the authors postulated that

repopulation of RT-resistant endothelial cells after first days of CRT may be faster in more radio-sensitive tumours leading to lower permeability.<sup>13</sup> Therefore, successful treatment leads to lower tumour perfusion and permeability, thus reflecting as a reduction of  $K_{trans}$ .

In addition, lower pre-treatment ADC was found to be a significant factor for longer survival at univariate analysis, but was not significant when multivariate analysis was applied. This is in agreement with Chan *et al.*<sup>26</sup> and Ng *et al.*<sup>32</sup> who also found no significant prognostic value of pre-treatment ADC for 3-year OS in HNSCC treated with CRT. On the contrary, lower pre-treatment ADC was shown to be a consistent predictor of higher DFS of head and neck cancer to CRT.<sup>33,34</sup> DW MRI is a quantitative imaging technique that measures diffusion of water molecules. Thus, in tissues with high cellularity (e.g. tumours), diffusion of water molecules is limited, showing as low ADC. Driessen *et al.* demonstrated that tumours with higher pre-treatment ADC had poorer prognosis due to lower cellularity and higher proportion of stroma that is a known independent poor prognostic factor.<sup>35,36</sup> However, ADC value is probably affected by various physiologic parameters other than tumour cellularity and that needs to be explored further.<sup>37</sup>

Our study has several limitations which have to be addressed. The main one is the small sample size and high number of parameters to analyse. However, our series is relatively homogeneous concerning primary tumour site and histological characteristics when compared to other studies conducted in HNSCC. This could explain why ADC or majority of DCE-MRI parameters failed to show any prognostic role when assessing OS and why none of the parameters was predictive for DFS. Larger prospective studies with higher number of patients and longer follow-up are needed in order to address the true prognostic role of DW and DCE-MRI derived parameters. Second, the DWI- and DCE-MRI-derived parameters were calculated as a mean value from the three most representative ROIs, delineated by only one radiologist. Therefore, no interobserver variability could be analysed, and appropriateness of ROIs marking procedure can also be questioned. Another limitation was that the DCE-MRI derived parameters and ADC were not compared to well-established histological biomarkers of angiogenesis (e.g. CD31 and Ki67 expressing cells). The last drawback can be attributed to the patient-specific AIF measurement as was used in our study: according to relevant studies, the use of a population-based AIF is

recommended due to most favourable repeatability.<sup>38</sup>

In conclusion, the results of our study show that pre-treatment  $K_{trans}$  may serve as a biomarker of tumour angiogenesis. Therefore, DCE-MRI could play a role in determining prognosis of HNSCC patient treated with platin-based cCRT.

## Acknowledgments

The authors thank Ass. Prof. Sotirios Bisdas, M.D., Ph.D., of University College London Hospitals NHS for help with establishing the DCE- and DWI-MR protocols.

## References

1. Ferlay J, Soerjomataram I, Dikshit R, Parkin DM, Forman D, Bray F. Cancer incidence and mortality worldwide: sources, methods and major patterns in GLOBOCAN 2012. *Int J Cancer* 2015; **136**: E359-86. doi: 10.1002/ijc.29210
2. Strojanc P. [New approaches to radiotherapy of head and neck tumors]. [Slovenian]. *Zdr Vestn* 2010; **79**: 339-53.
3. Winquist E, Agbassi C, Meyers BM, Yoo J, Chan KKW. Systemic therapy in the curative treatment of head and neck squamous cell cancer: a systematic review. *J Otolaryngol Head Neck Surg* 2017; **46**: 29. doi: 10.1186/s40463-017-0199-x
4. Leeman JE, Li J, Pei X, Venigalla P, Zumsteg ZS, Katsoulakis E, et al. Patterns of treatment failure and postrecurrence outcomes among patients with locally advanced head and neck squamous cell carcinoma after chemoradiotherapy using modern radiation techniques. *JAMA Oncol* 2017; **3**: 1487-94. doi: 10.1001/jamaoncol.2017.0973
5. Pignon J-P, Maître A le, Maillard E, Bourhis J. Meta-analysis of chemotherapy in head and neck cancer (MACH-NC): an update on 93 randomised trials and 17,346 patients. *Radiother Oncol* 2009; **92**: 4-14. doi: 10.1016/j.radonc.2009.04.014
6. Brizel DM, Prosnitz RG, Hunter S, Fisher SR, Clough RL, Downey MA, et al. Necessity for adjuvant neck dissection in setting of concurrent chemoradiation for advanced head-and-neck cancer. *Int J Radiat Oncol* 2004; **58**: 1418-23. doi: 10.1016/j.ijrobp.2003.09.004
7. Blanchard P, Baujat B, Holostenco V, Bourredjem A, Baey C, Bourhis J, et al; MACH-CH Collaborative group. Meta-analysis of chemotherapy in head and neck cancer (MACH-NC): a comprehensive analysis by tumour site. *Radiother Oncol* 2011; **100**: 33-40. doi: 10.1016/j.radonc.2011.05.036
8. Bisdas S, Rumboldt Z, Surlan-Popovic K, Baghi M, Koh TS, Vogl TJ, et al. Perfusion CT in squamous cell carcinoma of the upper aerodigestive tract: long-term predictive value of baseline perfusion CT measurements. *AJNR Am J Neuroradiol* 2010; **31**: 576-81. doi: 10.3174/ajnr.A1852
9. Surlan-Popovic K, Bisdas S, Rumboldt Z, Koh TS, Strojanc P. Changes in perfusion CT of advanced squamous cell carcinoma of the head and neck treated during the course of concomitant chemoradiotherapy. *Am J Neuroradiol* 2010; **31**: 570-5. doi: 10.3174/ajnr.A1859
10. Pietsch C, de Galiza Barbosa F, Hullner MW, Schmid DT, Haerle SK, Huber GF, et al. Combined PET/CT-perfusion in patients with head and neck cancers might predict failure after radio-chemotherapy: a proof of concept study. *BMC Med Imaging* 2015; **15**: 60. doi: 10.1186/s12880-015-0102-z
11. Koh D-M, Lee J-M, Bittencourt LK, Blackledge M, Collins DJ. Body diffusion-weighted MR imaging in oncology. *Magn Reson Imaging Clin N Am* 2016; **24**: 31-44. doi: 10.1016/j.mric.2015.08.007
12. Gaddikeri S, Gaddikeri RS, Tailor T, Anzai Y. Dynamic contrast-enhanced MR imaging in head and neck cancer: techniques and clinical applications. *AJNR Am J Neuroradiol* 2016; **37**: 588-95. doi: 10.3174/ajnr.A4458
13. Kim H, Hartman YE, Zhai G, Chung TK, Korb ML, Beasley TM, et al. Dynamic contrast-enhanced MRI evaluates the early response of human head and neck tumor xenografts following anti-EMMPRIN therapy with cisplatin or irradiation. *J Magn Reson Imaging* 2015; **42**: 936-45. doi: 10.1002/jmri.24871
14. Cao Y, Popovtzer A, Li D, Chepeha DB, Moyer JS, Prince ME, et al. Early prediction of outcome in advanced head-and-neck cancer based on tumor blood volume alterations during therapy: a prospective study. *Int J Radiat Oncol Biol Phys* 2008; **72**: 1287-90. doi: 10.1016/j.ijrobp.2008.08.024.EARLY
15. Baer AH, Hoff BA, Srinivasan A, Galbán CJ, and Mukherji SK. Feasibility analysis of the parametric response map as an early predictor of treatment efficacy in head and neck cancer. *AJNR Am J Neuroradiol* 2015; **36**: 757-62. doi: 10.3174/ajnr.A4296
16. Strojanc P, Zadnik V, Šifrer R, Lanišnik B, Didanović V, Jereb S, et al. Incidence trends in head and neck squamous cell carcinoma in Slovenia, 1983–2009: role of human papillomavirus infection. *Eur Arch Otorhinolaryngol* 2015; **272**: 3805-14. doi: 10.1007/s00405-014-3459-7
17. Tofts PS, Brix G, Buckley DL, Evelhoch JL, Henderson E, Knopp MV, et al. Estimating kinetic parameters from dynamic contrast-enhanced T(1)-weighted MRI of a diffusible tracer: standardized quantities and symbols. *J Magn Reson Imaging* 1999; **10**: 223-32. doi: 10.1002/(SICI)1522-2586(199909)10:3<223::AID-JMRI2>3.0.CO;2-S
18. Schwartz DL, Garden AS, Thomas J, Chen Y, Zhang Y, Lewin J, et al. Adaptive radiotherapy for head-and-neck cancer: initial clinical outcomes from a prospective trial. *Int J Radiat Oncol Biol Phys* 2012; **83**: 986-93. doi: 10.1016/j.ijrobp.2011.08.017
19. Yuan J, Lo G, King AD. Functional magnetic resonance imaging techniques and their development for radiation therapy planning and monitoring in the head and neck cancers. *Quant Imaging Med Surg* 2016; **6**: 430-48. doi: 10.21037/qims.2016.06.11
20. Kim S, Loevner LA, Quon H, Kilger A, Sherman E, Weinstein G, et al. Prediction of response to chemoradiation therapy in squamous cell carcinomas of the head and neck using dynamic contrast-enhanced MR imaging. *AJNR Am J Neuroradiol* 2010; **31**: 262-8. doi: 10.3174/ajnr.A1817
21. Chawla S, Kim S, Loevner LA, Hwang WT, Weinstein G, Chalian A, et al. Prediction of disease-free survival in patients with squamous cell carcinomas of the head and neck using dynamic contrast-enhanced MR imaging. *AJNR Am J Neuroradiol* 2011; **32**: 778-84. doi: 10.3174/ajnr.A2376
22. Chawla S, Kim S, Dougherty L, Wang S, Loevner LA, Quon H, et al. Pretreatment diffusion-weighted and dynamic contrast-enhanced MRI for prediction of local treatment response in squamous cell carcinomas of the head and neck. *Am J Roentgenol* 2013; **200**: 35-43. doi: 10.2214/AJR.12.9432
23. Chikui T, Kitamoto E, Kawano S, Sugiura T, Obara M, Simonetti AW, et al. Pharmacokinetic analysis based on dynamic contrast-enhanced MRI for evaluating tumor response to preoperative therapy for oral cancer. *J Magn Reson Imaging* 2012; **36**: 589-97. doi: 10.1002/jmri.23704
24. Ng SH, Lin CY, Chan SC, Yen TC, Liao CT, Chang JT, et al. Dynamic contrast-enhanced MR imaging predicts local control in oropharyngeal or hypopharyngeal squamous cell carcinoma treated with chemoradiotherapy. *PLoS One* 2013; **8**: 1-11. doi: 10.1371/journal.pone.0072230
25. Ng SH, Lin CY, Chan SC, Lin YC, Yen TC, Liao CT, et al. Clinical utility of multi-modality imaging with dynamic contrast-enhanced MRI, diffusion-weighted MRI, and 18F-FDG PET/CT for the prediction of neck control in oropharyngeal or hypopharyngeal squamous cell carcinoma treated with chemoradiation. *PLoS One* 2014; **9**: 1-19. doi: 10.1371/journal.pone.0115933
26. Chan SC, Cheng NM, Hsieh CH, et al. Multiparametric imaging using 18F-FDG PET/CT heterogeneity parameters and functional MRI techniques: prognostic significance in patients with primary advanced oropharyngeal or hypopharyngeal squamous cell carcinoma treated with chemoradiotherapy. *Oncotarget* 2017; **8**: 62606-21. doi: 10.18632/oncotarget.15904
27. Surov A, Meyer HJ, Leifels L, Höhn A-K, Richter C, Winter K. Histogram analysis parameters of dynamic contrast-enhanced magnetic resonance imaging can predict histopathological findings including proliferation potential, cellularity, and nucleic areas in head and neck squamous cell carcinoma. *Oncotarget* 2018; **9**: 21070-7. doi: 10.18632/oncotarget.24920
28. Kim SH, Lee HS, Kang BJ, Song BJ, Kim HB, Lee H, et al. Dynamic contrast-enhanced MRI perfusion parameters as imaging biomarkers of angiogenesis. *PLoS One* 2016; **11**: 1-12. doi: 10.1371/journal.pone.0168632

29. Choi YJ, Lee JH, Kim HO, Kim DY, Yoon RG, Cho SH, et al. Histogram analysis of apparent diffusion coefficients for occult tonsil cancer in patients with cervical nodal metastasis from an unknown primary site at presentation. *Radiology* 2016; **278**: 146-55. doi: 10.1148/radiol.2015141727
30. García-Figueiras R, Padhani AR, Beer AJ, Baleato-González S, Vilanova JC, Luna A, et al. Imaging of tumor angiogenesis for radiologists - part 1: biological and technical basis. *Curr Probl Diagn Radiol* 2015; **44**: 407-24. doi: 10.1067/j.cpradiol.2015.02.010
31. Manoochehri Khoshinani H, Afshar S, Najafi R. Hypoxia: a double-edged sword in cancer therapy. *Cancer Invest* 2016; **34**: 536-45. doi: 10.1080/07357907.2016.1245317
32. Ng SH, Liao CT, Lin CY, Chan SC, Lin YC, Yen TC, et al. Dynamic contrast-enhanced MRI, diffusion-weighted MRI and <sup>18</sup>F-FDG PET/CT for the prediction of survival in oropharyngeal or hypopharyngeal squamous cell carcinoma treated with chemoradiation. *Eur Radiol* 2016; **26**: 4162-72. doi: 10.1007/s00330-016-4276-8
33. Preda L, Conte G, Bonello L, Giannitto C, Travaini LL, Raimondi S, et al. Combining standardized uptake value of FDG-PET and apparent diffusion coefficient of DW-MRI improves risk stratification in head and neck squamous cell carcinoma. *Eur Radiol* 2016; **26**: 4432-41. doi: 10.1007/s00330-016-4284-8
34. Noij DP, de Jong MC, Mulders LG, Marcus JT, de Bree R, Lavini C, et al. Contrast-enhanced perfusion magnetic resonance imaging for head and neck squamous cell carcinoma: a systematic review. *Oral Oncol* 2015; **51**: 124-38. doi: 10.1016/j.oraloncology.2014.10.016
35. Driessen JP, Caldas-Magalhaes J, Janssen LM, et al. Diffusion-weighted MR imaging in laryngeal and hypopharyngeal carcinoma: association between apparent diffusion coefficient and histologic findings. *Radiology* 2014; **272**: 456-63. doi: 10.1148/radiol.14131173
36. Kolenda T, Przybyła W, Kapalczyńska M, Teresiak A, Zajączkowska M, Bliźniak R, et al. Tumor microenvironment - unknown niche with powerful therapeutic potential. *Rep Pract Oncol Radiother* 2018; **23**: 143-53. doi: 10.1016/j.rpor.2018.01.004
37. Choi HS, Kim AH, Ahn SS, Shin NY, Kim J, Lee SK. Glioma grading capability: comparisons among parameters from dynamic contrast-enhanced MRI and ADC value on DWI. *Korean J Radiol* 2013; **14**: 487-92. doi: 10.3348/kjr.2013.14.3.487
38. Rata M, Collins DJ, Darcy J, Messiou C, Tunariu N, Desouza N, et al. Assessment of repeatability and treatment response in early phase clinical trials using DCE-MRI: comparison of parametric analysis using MR- and CT-derived arterial input functions. *Eur Radiol* 2016; **26**: 1991-1998. doi: 10.1007/s00330-015-4012-9

# MRI prognostic factors of tongue cancer: potential predictors of cervical lymph nodes metastases

Mohamed A.F. Mourad, Mahmoud M. Higazi

Department of Radiology, Minia University, Egypt

Radiol Oncol 2019; 53(1): 49-56.

Received 20 October 2018

Accepted 15 January 2019

Correspondence to: Mahmoud M. Higazi, M.D., Lecturer of Radiology, Minia University Egypt. E-mail: mahmoud.higazi@minia.edu.eg

Disclosure: No potential conflicts of interest were disclosed.

**Background.** This study aimed to evaluate the efficacy of three MR imaging parameters, which are tumour thickness, para-lingual distance and apparent diffusion coefficient (ADC) value for prediction of cervical lymph nodes metastasis in cancer tongue patients.

**Patients and methods.** Fifty patients with proved cancer tongue by histopathological examination underwent MRI examination. T1 and T2-weighted MRI, diffusion-weighted images and post-contrast T1 fat suppression sequences were used.

**Results.** The patients were classified according to lymph nodes involvement as seen by MRI into two groups. Significant differences between positive and negative nodes groups were observed regarding tumour thickness and para-lingual distance ( $p$ -values = 0.008 and 0.003 respectively). ROC curve analyses revealed cut-off values  $>13.8$  mm and  $\leq 3.3$  mm for tumour thickness and para-lingual distance respectively for prediction of nodes involvement. No significant differences between patients with and without cervical lymph nodes metastasis were found regarding corresponding ADC value of the tumour ( $p$ -value = 0.518).

**Conclusions.** Para-lingual distance and tumour thickness are factors that could influence pre-operative judgment and prognosis of tongue cancer patients. ADC value of the tumour itself seem not to be a reliable index of cancer progression to regional lymph nodes.

Key words: tongue cancer; tumour thickness; para-lingual distance; apparent diffusion coefficient; cervical lymph nodes metastases

## Introduction

Squamous cell carcinoma is the commonest pathology of head and neck cancers and represents at least 90% of oral malignancies.<sup>1</sup> The World Health Organization expects a worldwide rising oral squamous cell carcinomas incidence in the next decades.<sup>2</sup> Most important risk factors including tobacco smoking, alcohol consumption and Human papilloma virus infection (HPV).<sup>1,3</sup> Squamous cell carcinoma of the tongue is one of the most critical issue due to rich vascular and lymphatic supply of the tongue.<sup>4</sup> High morbidity is associated regard-

ing speech, swallowing and mastication with subsequent life upset.<sup>5,6</sup>

Multiple parameters are responsible for patient survival including tumour thickness, para-lingual distance and metastatic cervical lymph nodes that should be well assessed as an informative prognostic parameters for local recurrence and survival.<sup>7-10</sup> Tongue carcinoma is strongly associated with regional lymph nodes metastases. Therefore, it is crucial to improve cervical lymph nodes management as much as possible.<sup>11-13</sup>

Imaging is superior to clinical neck examination for detection of clinically occult subclinical meta-

static lymph nodes. The incidence of occult metastases varies from 20% to 50% and represents a big unsolved issue as a clinically negative patient.<sup>14-18</sup> MRI is considered the widespread imaging modality in assessment of carcinoma of the tongue due to its high soft tissue capability and it can define the true extent, loco-regional involvement and tumour depth. The role of diffusion-weighted imaging (DWI) and apparent diffusion coefficient (ADC) in differentiation of benign from malignant lesions and grading of malignancies is under investigation.<sup>19-22</sup>

In this study, we attempted to detect potential accuracy and cut-off values for MRI tumour thickness and para-lingual distance as well as DWI/ADC values associated with positive cervical lymph nodes spread for better pre-operative evaluation of tongue cancer patients.

## Patients and methods

The study included 50 patients who were diagnosed as squamous cell carcinoma of the tongue by histopathological examination. The hospital's ethics committee approved the protocol of the study and all patients enrolled in this study signed the informed consent. The patients underwent MRI examination prior to surgery. MR examinations were performed using a 1.5-T system (Avanto, Siemens, Germany). Head/Neck 20 coil was used. The patient's head was secured using relaxing cushion; ensuring that the shoulders touch the lower part of the coil. The protocol included axial, sagittal and coronal T1-weighted turbo spin echo (TSE), axial and coronal T2-weighted turbo spin echo (TSE) and gadolinium enhanced axial and coronal T1-weighted sequences with fat suppression (FS) as well as diffusion-weighted (DW) sequences. T1-weighted images were done with the following parameters; TR/TE: 550/18 ms; slice thickness/interslice gap: 5/2 mm; mean field of view: 250 mm; slices number: 23; matrix: 320 X 288. T2-weighted turbo spin-echo (TSE) images were done with the following parameters; TR/TE: 4000/41 ms, slice thickness/interslice gap: 5/2 mm; mean field of view: 250 mm; slices number: 23; matrix: 512 X 460. Gadolinium diethylenetriamine pentaacetic acid (Gd-DTPA, Magnevist, Schering, Berlin, Germany) was administered intravenously at a rate of 2 mL/s (total dose, 0.1 mmole/kg of body weight) using a power injector, followed by a 20-mL saline flush.

DWI was done by using the spin echo single-shot by using the spin echo single-shot echo-planar

sequence. The parameters were as follows: TR/TE of 3200/70 ms, Slice thickness/inter-slice gap: 5/2 mm, mean field of view of 240mm, slices number: 23, matrix of 192X 192. DWI was done with b-values of 500 and 1000  $\text{mm}^2$ . Apparent diffusion coefficient (ADC) maps were then automatically generated. As ADC maps suffer from relatively poor resolution, delineation of the tumour is typically performed on T2 or post-contrast (T1)-weighted images and the region of interest (ROI) is then overlaid on ADC maps.

ROIs were measured from the most representative part of the tumour. The tumour thickness, para-lingual distance and ADC values were measured at coronal MR images separately by the two radiologists shared in the study and inter-observer variability was calculated. The tumour depth and para-lingual distance were measured at post contrast T1 coronal FS. The tumour thickness was defined by the distance from the deepest point of invasion to the tumour surface. At first, a vertical line joining the maximum length between tumour-mucosa junctions was drawn as a reference line. The tumour thickness was determined by summation of two lines drawn perpendicular from the reference line to the point of maximum tumour extension. The para-lingual distance was defined as the distance measured between the para-lingual space and the tumour. The patients in whom tumour invasion extended beyond the midline, the para-lingual distances were expressed as a minus (examples of how the representative lines were drawn are shown on Figures 4 and 5).

## Statistical analysis

Descriptive statistics were shown as mean  $\pm$  SD. The differences between positive and negative nodes metastases groups were detected using two tail Student *t* test. Logistic regression analyses were performed for radiologic predictors of nodes spread. ROC curves were constructed for MRI cut-off values. The inter-observer agreement was assessed using Kappa statistics. The statistical analyses were performed using commercially available software (Medcalc, Version 15 for Windows). P-value ( $< 0.05$ ) was considered statistically significant.

## Results

This study included 50 patients with proved cancer tongue, their mean age was  $61 \pm 10$  years, 34/50

(68%) were males. They all underwent MRI examination for detection of MR tumour thickness and para-lingual distance; including post-contrast study as well as diffusion-weighted imaging with corresponding measurement of ADC values of tumour tissue. According to tumour site, 42/50 (84%) were in oral tongue, while 8/50 (16%) of patients had tongue base tumour. MRI tumour thickness ranged between 5.5 mm and 43.2 mm ( $16.62 \pm 9.45$ ). Para-lingual distances ranged between -15 and 12.4 mm ( $3.8 \pm 5.15$ ). Regression analysis revealed that tumour thickness had a very strong negative association with para-lingual distance ( $p$ -value  $< 0.001$  and  $R^2 = 0.578$ ) (Figure 1). Most of the patients had either T1 stage or T2 stage disease. They were 36/50 (72%) patients who had T1 stage and 12/50 (24%) patients who had T2 stage disease. This is while 2/50 patients (4%) had T3 stage disease. The ADC values for tumour tissue of studied population ranged between 0.724 and 1.310 ( $0.944 \pm 0.124$ ). No significant correlation could be detected between T stage of the tumours and their ADC values ( $p$ -value = 0.744). The Kappa value for inter-observer agreement was 0.80 indicating substantial to perfect agreement. The patients (either clinically positive or occult for lymph nodes) were classified according to lymph nodes spread as detected by MRI into two groups Table 1 shows absolute values of the three parameters (tumour thickness, para-lingual distance and ADC value) for patients with (N1) and those without (N0) lymph nodes spread.

The 1<sup>st</sup> group included those patients with positive MRI nodes metastases (N1); they were 28/50 (56%) patients, of which 23/28 (82%) had unilateral lymph nodes metastases; while 5/28 (18%) had bi-

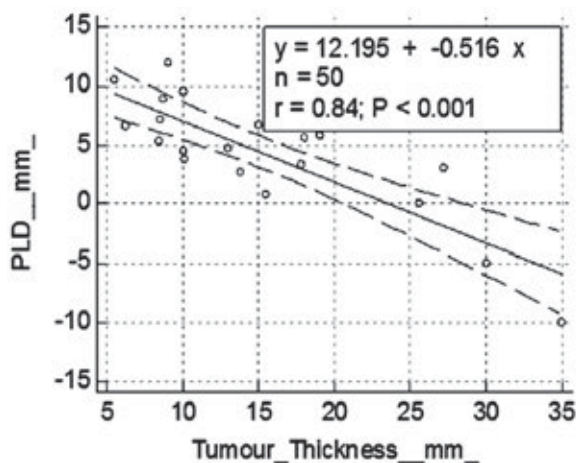


FIGURE 1. Scatter plot showing strong negative correlation between MR tumour thickness and para-lingual distance ( $p$ -value  $< 0.001$  and  $r = 0.84$ ).

TABLE 1. Absolute values for TT, PLD and ADC for (N0) and (N1) LN spread

N0		
TT (mm)	PLD (mm)	ADC
10	9.5	0.899
8.4	5.3	0.937
15	6.7	0.815
8.7	8.9	0.953
10.1	3.8	1.051
5.5	10.5	0.875
6.2	6.6	0.988
9	12	0.836
13	4.7	0.864
8.5	7.2	0.955
9.8	10	0.832
9	7.8	0.968
12.3	6.3	0.843
7.6	9.2	0.915
10.7	4.3	1.31
6.3	10.8	0.864
6.4	6.7	0.978
9.3	12.4	0.834
9.1	7.9	0.869
10	9.5	0.899
8.4	5.3	0.937
8.7	8.9	0.953
N1		
19	5.8	1.18
17.8	3.3	0.928
10	4.5	1.16
15.5	0.8	0.795
13.8	2.7	0.961
18	5.6	0.793
16.9	3.1	0.874
12.3	4.7	1.17
13.7	0.5	0.778
14.8	3.7	0.959
19	5.8	1.18
17.8	3.3	0.928
15	6.7	0.815
13.8	4.4	0.83
35	-10	0.987
27.2	3.1	1.03
30	-5	0.976
25.6	0	0.892
34	-8	0.984
25	7	1.21
23.2	3.2	1.07
29.7	-3	0.938
22.8	0	0.792
21.4	5.8	0.724
27.8	-7	0.852
23.9	0	0.897
42.7	-15	0.893
43.2	-12	1.051

TABLE 2. Summary of descriptive statistics for studied population

	N	N1	N0	P value
Age (mean+/-SD)	61 ± 10	61 ± 11	60 ± 9	0.794
Sex (male, no., %)	34/50 (68%)	20/28 (71%)	14/22 (64%)	–
Tumour Thickness (mean+/-SD)	16.62 ± 9.45	19.8 ± 8.8	9.9 ± 2.6	0.008*
Para-lingual distance (mean+/-SD)	3.8 ± 5.12	0.9 ± 5.5	7.2 ± 2.5	0.003*
ADC (mean+/-SD)	0.944 ± 0.124	0.952 ± 0.112	0.928 ± 0.118	0.518

\* = significant p value

lateral lymph nodes on both sides of the neck. MRI tumour thickness of this group ranged between 10 mm and 43.2 mm ( $19.8 \pm 8.8$ ). The para-lingual distance ranged between -15 mm and 7 mm ( $0.9 \pm 5.5$ ). The ADC values ranged between 0.724 and 1.212 ( $0.952 \pm 0.112$ ). The 2<sup>nd</sup> group included those patients with negative MRI nodes metastases (N0); they were 22/50 (44%) patients. MRI tumour thickness of this group ranged between 6.2 and 15 mm ( $9.9 \pm 2.6$ ). The para-lingual distance ranged be-

tween 3.8 mm and 12 mm ( $7.2 \pm 2.5$ ). The ADC values ranged between 0.793 and 1.161 ( $0.928 \pm 0.118$ ). Table 2 shows summary of descriptive statistics for the two groups of the study.

Significant differences between the two groups were observed regarding tumour thickness and para-lingual distance (p-values 0.008 and 0.003 respectively) (Figure 2); while ADC values were not significantly different between patients with and without lymph nodes metastases (p-value = 0.518). Logistic regression analyses (Table 2) showed that MRI tumour thickness and para-lingual distance were significant strong predictors for positive nodes metastases (p-values < 0.0001, 0.0001 and  $R^2$  0.755, 0.697 respectively). This is while ADC value does not seem to be useful for prediction of lymph nodes metastases (p-value = 0.472). ROC curve analyses (Figure 3) revealed cut-off value > 13.8 mm for tumour thickness for prediction of positive nodes metastases; which achieved 72% sensitivity and 88% specificity (AUC = 0.864, p-value = 0.0001 and 95% confidence interval 0.637 to 0.974). For para-lingual distance, the detected cut-off value for prediction of positive nodes metastases was  $\leq 3.3$  mm, which resulted in best sensitivity (64%) and specificity (89%) (AUC = 0.848, p-value = 0.0002 and 95% confidence interval 0.619 to 0.967). Representative example for T1N0 patient who showed MRI negative lymph nodes spread is shown at (Figure 4) and another T4N1 patient who had MRI positive lymph nodes spread is shown at (Figure 5).

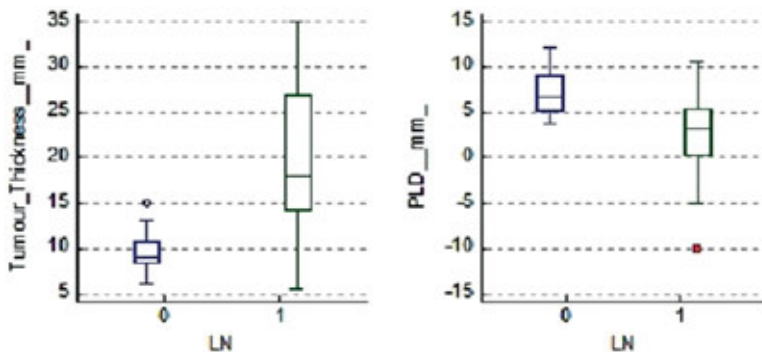


FIGURE 2. Comparison graphs illustrating the significant differences between tumour thickness and para-lingual distance among nodes positive (N1) and negative (N0) patients (p-values 0.008 and 0.003 respectively).

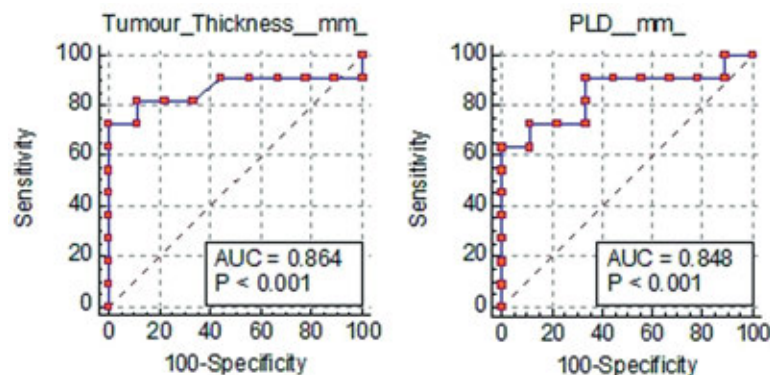


FIGURE 3. Receiver Operator Characteristic (ROC) curve analyses for tumour thickness and para-lingual distance predicting nodes spread (p-values < 0.001 and AUC 0.864 and 0.848 respectively).

## Discussion

Lymph nodes metastasis in many cancers including head and neck cancers is an important clinically accepted prognostic factor; either reflecting tumour aggressiveness or invasiveness or being an indicator for further tumour dissemination.<sup>23</sup>

TABLE 3. Logistic regression analysis for independent variables predicting LN spread

	P value	R2	Odds Ratio	95% CI
Age	0.926	0.0005	1.004	0.917 to 1.099
Tumour Thickness	<0.0001**	0.755	1.756	1.075 to 2.866
Para-lingual distance	0.0001**	0.697	0.325	0.107 to 0.982
ADC	0.472	0.023	1.003	0.995 to 1.015

\*\* = highly significant p value; CI: confidence Interval

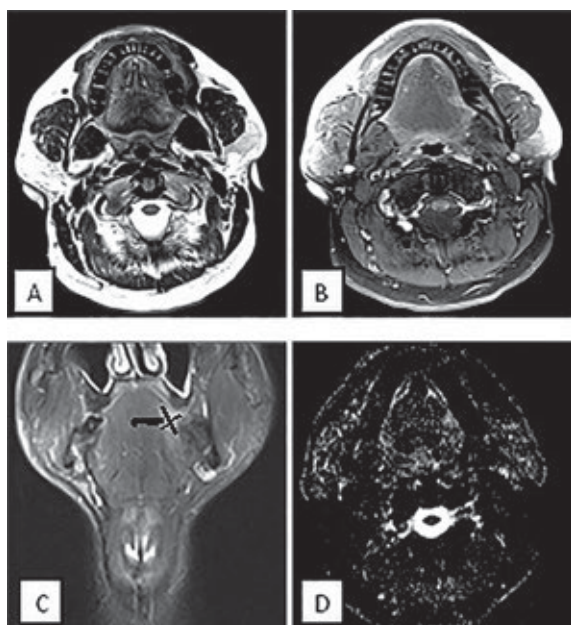


FIGURE 4. MRI of a male patient 65-years-old with small lesion at left hemi-tongue (T1N0) disease. (A) Axial T2 (B) Axial T1 fat suppression post contrast (C) T2 coronal (D) Axial DWI. MRI and elective dissected neck revealed no positive cervical lymph nodes spread. The vertical black line was drawn as a reference line connecting maximum tumour-mucosa junctions. Two horizontal lines were drawn perpendicular to the reference line. Tumour thickness is the sum of both of these horizontal lines and was determined as 5.5 mm. The thick black line between the tumour and the para-lingual space represented the para-lingual distance = 10.5 mm.

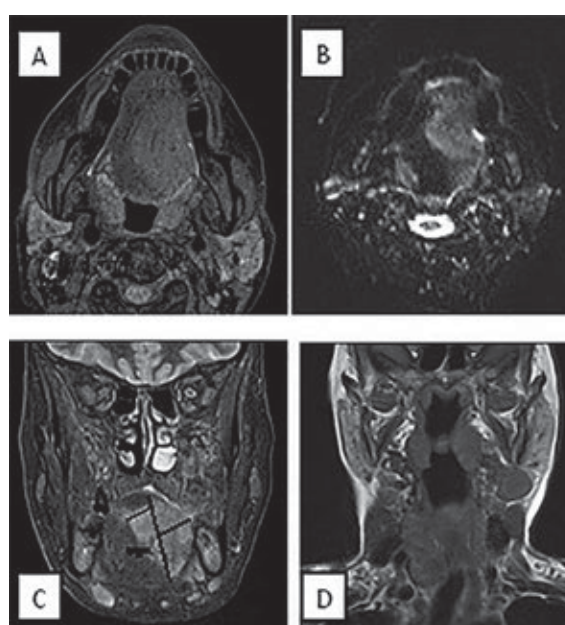


FIGURE 5. MRI of a 75-years-old female with sizable tongue mass crossing the midline (T4N1) disease. (A) Axial T1 post contrast fat suppression (B) Axial DWI (C) Coronal T1 post contrast fat suppression (D) Coronal T1 post contrast shows metastatic cervical lymph nodes. Tumour thickness is the sum of the two horizontal black lines drawn perpendicular to the vertical black line connecting maximum tumour junction distance and was determined as 30 mm. The thick black line representing para-lingual distance between the tumour and the para-lingual space was determined as 10 as the tumour margin extends beyond the midline by 10 mm

Therefore; an accurate preoperative assessment of lymph nodes spread is essential to provide an appropriate management strategy for head and neck cancer patients.<sup>8</sup> The lymphatic system serves as a primary escape route for cancer. Lymphatic capillaries have a thin discontinuous basement membrane, and contain endothelial gaps that can be invaded by cancer cells. In addition, tumour cells secrete factors that stimulate lymphangiogenesis.<sup>24</sup> Cancer cells commonly metastasize through these lymphatic vessels to regional lymph nodes. The

presence of metastatic cells in the sentinel lymph nodes is a prognostic indicator for many types of cancer, and the degree of dissemination determines the therapeutic course of action.<sup>24</sup>

In this study, we found that both tumour thickness and para-lingual distance which measured at pre-treatment MRI were significantly different between patients who had positive versus negative cervical lymph nodes spread. Tumour thickness and para-lingual distance were important predictors for cervical lymph nodes spread in tongue

cancer patients in our study. This may be a logic relation which can be easily explained by that with deeper local invasion, tumour cells may come close to deep blood vessels and lymphatics which would carry tumour emboli to regional lymph nodes.<sup>25</sup> This relation is supported by that therapeutic strategies which target both tumour-associated blood and lymphatic vessels can lead to a decrease in tumour size and decrease incidence of local/distant spread.<sup>24</sup>

There are several studies which tested the reliability of MRI in measuring tongue tumour thickness, and correlated it well with histologic tumour thickness.<sup>26-28</sup> Spiro *et al.*, postulated that disease-related death is apparently unusual when oral tumours are thin, regardless of tumour stage, and that tumour thickness rather than stage may have the best correlation with treatment failure and survival.<sup>29</sup> However; tongue cancer may vary in shape and growth pattern. Therefore, depth of invasion (represented by para-lingual distance), not merely tumour thickness, is another important prognostic factor.<sup>30-32</sup>

Recent research is directed at establishing important prognostic pre-operative cut-off values for cancer tongue. Some investigators have attempted to define a cut-off point for oral cavity cancer thickness that correlates well with positive lymph nodes spread.<sup>30,33</sup> Yuen *et al.* have demonstrated 44% incidence of cervical lymph nodes metastases for tumours having a thickness between 3 mm and 9 mm.<sup>34</sup> Jung *et al.* recommended a cut-off value of 11 mm on contrast-enhanced T1-weighted images and showed a significant correlation with nodes metastasis.<sup>35</sup> In this study; tumour thickness value > 13.8 mm and para-lingual distance value ≤ 3.3 mm were detected as best cut-off values for prediction of MRI detectable positive nodes spread. According to Okura *et al.*, preoperative decision to perform elective neck dissection can be based on tumour thickness of > 9.7 mm and para-lingual distance of < 5.2 mm.<sup>18</sup> This should be kept in mind when planning for prophylactic neck dissection especially in clinically negative nodes.<sup>36</sup> These results are in coincidence with AJCC (8th edition) recommendations of reporting tumour thickness during oral cancer staging.<sup>37</sup>

Multiple pulse sequences had been used in previous works to detect small tongue cancers and accurately identify tumour margins, including T2WI, STIR and T1-weighted fat-suppressed contrast-enhanced sequences. Lam *et al.* reported that particularly contrast-enhanced T1-weighted MRI, provides satisfactory accurate correlation between

MRI tumour thickness and histologic tumour thickness in oral tongue cancer.<sup>28</sup> Background Diffusion-weighted imaging obtained with magnetic resonance (DW-MRI) is a non-invasive imaging tool potentially able to provide information about micro-structure tumour characteristics.<sup>38,39</sup> The inclusion of DWI/ADC values might be helpful for differentiation between true tumour margin and oedema; and also for distinction between benign and malignant head and neck tumours.<sup>20,21,40</sup> Multiple studies reported high diagnostic accuracy of DWI for differentiation of malignant from benign status of metastatic cervical lymph nodes.<sup>21,40,41</sup>

In this study ADC value does not seem to be an important predictor of metastatic cervical lymph nodes spread. We did not find any significant differences between positive and negative nodes groups regarding tumour ADC values. Curvo-Semedo *et al.* found that pre-treatment ADC values were significantly lower for tumours with higher T stages and extra-nodal tumour deposits.<sup>42</sup> This was explained by the fact that ADC values are derived from the diffusive movement of water molecules, which is often influenced by cell density, and other histological components. The lower ADC values of malignant tumours can be attributed to the histopathological characteristics of such tumours *i.e.* presence of a more abundant macromolecular protein contents, an enlarged nuclear: cytoplasmic ratio, hyper-chromatism and hypercellularity which are associated with poorly differentiated SCC with a resultant decrease of ADC values.<sup>43</sup> Thus, ADC values might reflect the aggressiveness of a particular tumour tissue. The earlier mentioned studies demonstrated the potential capability of ADC value for characterization of head and neck cancers, but they suffer from the limited number of studied patients, as well as a certain degree of inevitable overlap between different tumour types. Therefore, care should be taken when translating the results of these published studies in daily routine clinical practice. Multi-centeric studies in a large cohort of patients with identical imaging protocols are required to substantiate these preliminary results.

Whether ADC values of tumours can be helpful for predicting tumour aggressiveness is a matter of debate that may require further justification. Sun *et al.* revealed no statistically significant correlation between ADC value and tumour differentiation grade upon histological examination.<sup>43</sup> Also, our results are supported by Bonello *et al.* as they did not observe any statistically significant correlation between ADC values and clinical-histological

characteristics of SCCA of the oral cavity and oropharynx.<sup>44</sup> The poorly differentiated squamous cell carcinoma (SCC) might have a high degree of small foci of tissue necrosis than well-differentiated SCC, which was confirmed histopathologically. These areas of tumour necrosis will ultimately result in increased membrane permeability through breakdown of cell membrane, with consequently free diffusion.<sup>43</sup> In addition; higher proportion of tumour stroma is acting as stimulator of cancer growth. Tumour associated fibroblasts (TAFs) are the largest stromal cellular components of the tumour microenvironment in head and neck squamous cell carcinomas. Tumour associated fibroblasts enhance cancer proliferation, invasion, and metastasis.<sup>45</sup>

The preoperative decision of the extent of neck dissection based on ADC value measurements alone might be useless in daily clinical practice. Moreover, it may offer false impression to clinicians about the chance of lymph nodes spread. This is unlike the information derived from simple measurements of tumour dimensions and depth of the primary tumour, which can give more reliable data to take an appropriate management plan decisions.

The limitations of our study include the relative small number of cases pertaining to each group and errors caused by manual measurement of tumour thickness and para-lingual distances. Additionally, artifacts due to tongue motion or dental fillings were a limiting factor and the patients had to be well sedated and in most comfortable position during examination. The inevitable individual difference of manual ADC measurements, ROI size and shape is another limitation, which may result in different outcomes.

## Conclusions

Tumour thickness and para-lingual distance are important prognostic factors that motivate the search for metastatic cervical lymph nodes to better tailor pre-operative judgment and management plan of cancer tongue patients. ADC value of the tumour itself is not a reliable index that could be useful in daily clinical practice to pinpoint to the stage of cancer progression. Further long term large scale studies are recommended for assessment of relation between tumour ADC value and anticipated nodes spread in cancers as well as influence upon survival rate.

## References

1. Funk GF, Karnell LH, Robinson RA, Zhen WK, Trask DK, Hoffman HT. Presentation, treatment, and outcome of oral cavity cancer: a National Cancer Data Base report. *Head Neck* 2002; **24**: 165-80.
2. Lubek JE, Clayman L. An update on squamous carcinoma of the oral cavity, oropharynx, and maxillary sinus. *Oral Maxillofac Surg Clin North Am* 2012; **24**: 307-16, x. doi: 10.1016/j.coms.2012.01.003
3. Syrjanen S. Human papillomavirus infections and oral tumors. *Med Microbiol Immunol* 2003; **192**: 123-8. doi: 10.1007/s00430-002-0173-7
4. Tshering Vogel DW, Zbaeren P, Thoency HC. Cancer of the oral cavity and oropharynx. *Cancer Imaging* 2010; **10**: 62-72. doi: 10.1102/1470-7330.2010.0008
5. Stone M, Davis EP, Douglas AS, Aiver MN, Gullapalli R, Levine WS, et al. Modeling tongue surface contours from Cine-MRI images. *J Speech Lang Hear Res* 2001; **44**: 1026-40.
6. Wilhelms-Tricarico R. Physiological modeling of speech production: methods for modeling soft-tissue articulators. *J Acoust Soc Am* 1995; **97**: 3085-98.
7. Kane SV, Gupta M, Kakade AC, D'Cruz A. Depth of invasion is the most significant histological predictor of subclinical cervical lymph node metastasis in early squamous carcinomas of the oral cavity. *Eur J Surg Oncol* 2006; **32**: 795-803. doi: 10.1016/j.ejso.2006.05.004
8. Clark JR, Naranjo N, Franklin JH, Almeida J de, Gullane PJ. Established prognostic variables in NO oral carcinoma. *Otolaryngol Neck Surg* 2006; **135**: 748-53. doi: 10.1016/j.otohns.2006.05.751
9. Yamazaki H, Inoue T, Yoshida K, Tanaka E, Yoshioka Y, Nakamura H, et al. Lymph node metastasis of early oral tongue cancer after interstitial radiotherapy. *Int J Radiat Oncol Biol Phys* 2004; **58**: 139-46. doi: 10.1016/S0360-3016(03)01459-7
10. Mohit-Tabatabai MA, Sobel HJ, Rush BF, Mashberg A. Relation of thickness of floor of mouth stage I and II cancers to regional metastasis. *Am J Surg* 1986; **152**: 351-3.
11. Alsaffar HA, Goldstein DP, King E V, de Almeida JR, Brown DH, Gilbert RW, et al. Correlation between clinical and MRI assessment of depth of invasion in oral tongue squamous cell carcinoma. *J Otolaryngol Head Neck Surg* 2016; **45**: 61. doi: 10.1186/s40463-016-0172-0
12. O-charoenrat P, Pillai G, Patel S, Fisher C, Archer D, Eccles S, et al. Tumour thickness predicts cervical nodal metastases and survival in early oral tongue cancer. *Oral Oncol* 2003; **39**: 386-90. doi: 10.1016/S1368-8375(02)00142-2
13. Huang SH, Hwang D, Lockwood G, Goldstein DP, O'Sullivan B. Predictive value of tumor thickness for cervical lymph-node involvement in squamous cell carcinoma of the oral cavity. *Cancer* 2009; **115**: 1489-97. doi: 10.1002/ncr.24161
14. Franceschi D, Gupta R, Spiro RH, Shah JP. Improved survival in the treatment of squamous carcinoma of the oral tongue. *Am J Surg* 1993; **166**: 360-5. doi: 10.1016/S0002-9610(05)80333-2
15. Byers RM, El-Naggar AK, Lee YY, Rao B, Fornage B, Terry NH, et al. Can we detect or predict the presence of occult nodal metastases in patients with squamous carcinoma of the oral tongue? *Head Neck* 1998; **20**: 138-44.
16. Ferlito A, Rinaldo A, Silver CE, Gourin CG, Shah JP, Clayman GL, et al. Elective and therapeutic selective neck dissection. *Oral Oncol* 2006; **42**: 13-24. doi: 10.1016/j.oraloncology.2005.03.009
17. Takes RP, Righi P, Meeuwis CA, Manni JJ, Knekt P, Marres HA, et al. The value of ultrasound with ultrasound-guided fine-needle aspiration biopsy compared to computed tomography in the detection of regional metastases in the clinically negative neck. *Int J Radiat Oncol Biol Phys* 1998; **40**: 1027-32. doi: 10.1016/S0360-3016(97)00953-X
18. Okura M, Iida S, Aikawa T, Adachi T, Yoshimura N, Yamada T, et al. Tumor thickness and paralingual distance of coronal MR imaging predicts cervical node metastases in oral tongue carcinoma. *Am J Neuroradiol* 2008; **29**: 45-50. doi: 10.3174/ajnr.A0749
19. Sumi M, Sakihama N, Sumi T, Morikawa M, Uetani M, Kabasawa H, et al. Discrimination of metastatic cervical lymph nodes with diffusion-weighted MR imaging in patients with head and neck cancer. *AJNR Am J Neuroradiol* 2003; **24**: 1627-34.

20. Srinivasan A, Dvorak R, Perni K, Rohrer S, Mukherji SK. Differentiation of benign and malignant pathology in the head and neck using 3T apparent diffusion coefficient values: early experience. *Am J Neuroradiol* 2008; **29**: 40-4. doi: 10.3174/ajnr.A0743
21. Vandecaveye V, De Keyzer F, Vander Poorten V, Dirix P, Verbeken E, Nuyts S, et al. Head and neck squamous cell carcinoma: value of diffusion-weighted MR imaging for nodal staging. *Radiology* 2009; **251**: 134-46. doi: 10.1148/radiol.2511080128
22. Park JO, Jung SL, Joo YH, Jung CK, Cho KJ, Kim MS. Diagnostic accuracy of magnetic resonance imaging (MRI) in the assessment of tumor invasion depth in oral/oropharyngeal cancer. *Oral Oncol* 2011; **47**: 381-6. doi: 10.1016/j.oraloncology.2011.03.012
23. Cho JK, Hyun SH, Choi N, Kim MJ, Padera TP, Choi JY, et al. Significance of lymph node metastasis in cancer dissemination of head and neck cancer. *Transl Oncol* 2015; **8**: 119-25. doi: 10.1016/j.tranon.2015.03.001
24. Zwaans BMM, Bielenberg DR. Potential therapeutic strategies for lymphatic metastasis. *Microvasc Res* 2007; **74**: 145-58. doi: 10.1016/j.mvr.2007.08.006
25. Chen SL, Iddings DM, Scheri RP, Bilchik AJ. Lymphatic mapping and sentinel node analysis: current concepts and applications. *CA Cancer J Clin* 2006; **56**: 292-309; quiz 316-7.
26. Goel V, Parihar PS, Parihar A, Goel AK, Waghwanvi K, Gupta R, et al. Accuracy of MRI in prediction of tumour thickness and nodal stage in oral tongue and gingivobuccal cancer with clinical correlation and staging. *J Clin Diagnostic Res* 2016; **10**: TC01-5. doi: 10.7860/JCDR/2016/17411.7905
27. Bashir U, Manzoor MU, Majeed Y, Khan RU, Hassan U, Murtaza A, et al. Reliability of MRI in measuring tongue tumour thickness: a 1.5T study. *J Ayub Med Coll Abbottabad* 2011; **23**: 101-4.
28. Lam P, Au-Yeung KM, Cheng PW, Wei WI, Yuen AP, Trendell-Smith N, et al. Correlating MRI and histologic tumor thickness in the assessment of oral tongue cancer. *Am J Roentgenol* 2004; **182**: 803-8. doi: 10.2214/ajr.182.3.1820803
29. Spiro RH, Huvos AG, Wong GY, Spiro JD, Gnecco CA, Strong EW. Predictive value of tumor thickness in squamous carcinoma confined to the tongue and floor of the mouth. *Am J Surg* 1986; **152**: 345-50.
30. Hegde P, Roy S, Shetty T, Prasad BR, Shetty U. Tumor infiltration depth as a prognostic parameter for nodal metastasis in oral squamous cell carcinoma. *Int J Appl basic Med Res* 2017; **7**: 252-7. doi: 10.4103/ijabmr.IJABMR\_66\_17
31. Almangush A, Bello IO, Keski-Säntti H, Mäkinen LK, Kauppila JH, Pukkila M, et al. Depth of invasion, tumor budding, and worst pattern of invasion: prognostic indicators in early-stage oral tongue cancer. *Head Neck* 2014; **36**: 811-8. doi: 10.1002/hed.23380
32. Pentenero M, Gandolfo S, Carozzo M. Importance of tumor thickness and depth of invasion in nodal involvement and prognosis of oral squamous cell carcinoma: a review of the literature. *Head Neck* 2005; **27**: 1080-91. doi: 10.1002/hed.20275
33. Mücke T, Kanatas A, Ritschl LM, Koerdt S, Tannapfel A, Wolff KD, et al. Tumor thickness and risk of lymph node metastasis in patients with squamous cell carcinoma of the tongue. *Oral Oncol* 2016; **53**: 80-4. doi: 10.1016/j.oraloncology.2015.11.010
34. Yuen AP, Ho CM, Chow TL, Tang LC, Cheung WY, Ng RW, et al. Prospective randomized study of selective neck dissection versus observation for NO neck of early tongue carcinoma. *Head Neck* 2009; **31**: 765-72. doi: 10.1002/hed.21033
35. Jung J, Cho NH, Kim J, Choi EC, Lee SY, Byeon HK, et al. Significant invasion depth of early oral tongue cancer originated from the lateral border to predict regional metastases and prognosis. *Int J Oral Maxillofac Surg* 2009; **38**: 653-60. doi: 10.1016/j.ijom.2009.01.004
36. Jarungroongruangchai W, Charoenpitakchai M, Silpeeyodom T, Pruksapong C, Burusapat C. Size of cervical lymph node and metastasis in squamous cell carcinoma of the oral tongue and floor of mouth. *J Med Assoc Thai* 2014; **97** (Suppl 2): S101-6.
37. Huang SH, O'Sullivan B. Overview of the 8th edition TNM classification for head and neck cancer. *Curr Treat Options Oncol* 2017; **18**: 40. doi: 10.1007/s11864-017-0484-y
38. Charles-Edwards EM, deSouza NM. Diffusion-weighted magnetic resonance imaging and its application to cancer. *Cancer Imaging* 2006; **6**: 135-43. doi: 10.1102/1470-7330.2006.0021
39. Chilla GS, Tan CH, Xu C, Poh CL. Diffusion weighted magnetic resonance imaging and its recent trend-a survey. *Quant Imaging Med Surg* 2015; **5**: 407-22. doi: 10.3978/j.issn.2223-4292.2015.03.01
40. Vandecaveye V, De Keyzer F, Hermans R. Diffusion-weighted magnetic resonance imaging in neck lymph adenopathy. *Cancer Imaging* 2008; **8**: 173-80. doi: 10.1102/1470-7330.2008.0025
41. Holzapfel K, Duetsch S, Fauser C, Eiber M, Rummeny EJ, Gaa J. Value of diffusion-weighted MR imaging in the differentiation between benign and malignant cervical lymph nodes. *Eur J Radiol* 2009; **72**: 381-7. doi: 10.1016/j.ejrad.2008.09.034
42. Curvo-Semedo L, Lambregts DMJ, Maas M, Beets GL, Caseiro-Alves F, Beets-Tan RGH. Diffusion-weighted MRI in rectal cancer: Apparent diffusion coefficient as a potential noninvasive marker of tumor aggressiveness. *J Magn Reson Imaging* 2012; **35**: 1365-71. doi: 10.1002/jmri.23589
43. Sun Y, Tong T, Cai S, Bi R, Xin C, Gu Y. Apparent diffusion coefficient (ADC) value: a potential imaging biomarker that reflects the biological features of rectal cancer. *PLoS One* 2014; **9**: e109371. doi: 10.1371/journal.pone.0109371
44. Bonello L, Preda L, Conte G, Giannitto C, Raimondi S, Ansarin M, et al. Squamous cell carcinoma of the oral cavity and oropharynx: what does the apparent diffusion coefficient tell us about its histology? *Acta Radiol* 2016; **57**: 1344-51. doi: 10.1177/0284185115587734
45. Wheeler SE, Shi H, Lin F, Bednash J, Thorne S, Watkins S, et al. Enhancement of head and neck squamous cell carcinoma proliferation, invasion, and metastasis by tumor-associated fibroblasts in preclinical models. *Head Neck* 2014; **36**: 385-92. doi: 10.1002/hed.23312

# Increased cystatin F levels correlate with decreased cytotoxicity of cytotoxic T cells

Mateja Prunk<sup>1,2</sup>, Milica Perisic Nanut<sup>1</sup>, Jerica Sabotic<sup>1</sup>, Urban Svajger<sup>3</sup>, Janko Kos<sup>1,2</sup>

<sup>1</sup> Jožef Stefan Institute, Department of Biotechnology, Ljubljana, Slovenia

<sup>2</sup> University of Ljubljana, Faculty of Pharmacy, Ljubljana, Slovenia

<sup>3</sup> Blood Transfusion Centre of Slovenia, Ljubljana, Slovenia

Radiol Oncol 2019; 53(1): 57-68.

Received 8 December 2018

Accepted 5 January 2019

Correspondence to: Prof. Janko Kos, Ph.D., Faculty of Pharmacy, University of Ljubljana, Aškerčeva cesta 7, SI-1000 Ljubljana, Slovenia. Phone: +386 1 4769 604; Fax: +386 1 4258 031; E-mail: janko.kos@ffa.uni-lj.si

Disclosure: No potential conflicts of interest were disclosed.

**Background.** Cystatin F is a protein inhibitor of cysteine peptidases, expressed predominantly in immune cells and localised in endosomal/lysosomal compartments. In cytotoxic immune cells cystatin F inhibits both the major pro-granzyme convertases, cathepsins C and H that activate granzymes, and cathepsin L, that acts as perforin activator. Since perforin and granzymes are crucial molecules for target cell killing by cytotoxic lymphocytes, defects in the activation of either granzymes or perforin can affect their cytotoxic potential.

**Materials and methods.** Levels of cystatin F were assessed by western blot and interactions of cystatin F with cathepsins C, H and L were analysed by immunoprecipitation and confocal microscopy. In TALL-104 cells specific activities of the cathepsins and granzyme B were determined using peptide substrates.

**Results.** Two models of reduced T cell cytotoxicity of TALL-104 cell line were established, either by treatment by ionomycin or by immunosuppressive transforming growth factor beta. Reduced cytotoxicity correlated with increased levels of cystatin F and with attenuated activities of cathepsins C, H and L and of granzyme B. Co-localisation of cystatin F and cathepsins C, H and L and interactions between cystatin F and cathepsins C and H were demonstrated.

**Conclusions.** Cystatin F is designated as a possible regulator of T cell cytotoxicity, similar to its role in natural killer cells.

Key words: cystatin F; cysteine cathepsins; TALL-104; TGFβ; ionomycin; anergy

## Introduction

The ability of cancer cells to avoid immune response is one of hallmarks of cancer<sup>1</sup> and thus, several therapeutic approaches are aimed to enhance anticancer immunity. In cancer immunotherapy the activation and maintaining of T cells directed towards tumour antigens provided promising results.<sup>2</sup> In this case the main players are CD8+ cytotoxic T lymphocytes (CTLs), major cell effectors of adaptive immunity, since they possess the ability to kill target cells directly.<sup>3</sup> The key pathway employed by CTLs in target cell killing involves release of perforin and granzymes from cytotoxic granules. Perforin is a pore-forming protein that enables entry of granzymes into the target cell.

Perforin deficiency, or failure to deliver fully functional perforin due to its genetic mutations, leads to the fatal immunoregulatory disorder, familial hemophagocytic lymphohistiocytosis.<sup>4</sup> Granzymes are a family of serine peptidases that, once in the target cell, trigger different cell death signalling pathways. In humans there are five granzymes, A, B, H, K and M, among them granzymes A and B have established cytotoxic roles. Indeed, the cytotoxicity of CTLs in mice lacking granzymes A and B, even if they possess functional perforin and other granzymes, is greatly reduced.<sup>5</sup> Granzyme B has the most potent pro-apoptotic role, since its activity to cleave after aspartate residues mimics the function of caspases. On the other hand, granzyme A cleaves substrates after basic residues and induces

a slower type of cell death. In addition to different substrate specificity, both granzymes differ also in their potency; while nanomolar levels of granzyme B are cytotoxic, micromolar levels of granzyme A are needed for cytotoxicity.<sup>5</sup>

As well as perforin and granzymes, cytotoxic granules contain certain cysteine cathepsins. These comprise a group of 11 cysteine peptidases (cathepsins B, C, F, H, K, L, O, S, V, X and W) exhibiting different tissue distributions, cellular localisations, proteolytic activities and protein levels, all involved in a variety of physiological and pathological processes. In CTLs the most notable is the role of cathepsin C, which is responsible for the activation of pro-granzymes by removing an N-terminal dipeptide.<sup>6</sup> However, cathepsin C null mice, while active granzyme A is completely absent, still possess active granzyme B in functional cytotoxic cells, and it has been shown that cathepsin H can act as an additional pro-granzyme convertase.<sup>7</sup> Furthermore, cysteine cathepsins are implicated in the activation of perforin by cleaving its C-terminus.<sup>8,9</sup> Thus, cathepsin L can cleave perforin, although redundancy with other peptidases has also been demonstrated.<sup>8,10</sup>

The activity of cysteine cathepsins is regulated by their endogenous protein inhibitors, the cystatins. In immune cells a notable role is attributed to cystatin F, a tight-binding inhibitor of cysteine cathepsins and legumain, which has several features distinguishing it from other members of cystatins II family. First, it is synthesised predominantly in immune cells and its expression depends on their activation state or differentiation status.<sup>11-14</sup> Secondly, it presents as a dimer, stabilized by disulphide bonds<sup>15</sup> and as a dimer it does not inhibit cysteine cathepsins.<sup>16,17</sup> Its monomerization can be facilitated by proteolytic cleavage of the 15 N-terminal amino acids, however, this truncation significantly changes the inhibitory profile.<sup>18</sup> While full-length monomeric cystatin F does not inhibit cathepsin C, after N-terminal truncation it becomes its potent inhibitor.<sup>18</sup> Furthermore, cystatin F is, apart from cystatin E/M, the only cystatin that is glycosylated, a feature crucial for its endosomal/lysosomal trafficking and internalisation.<sup>19</sup> Lastly, cystatin F can also function *in trans*, so that secreted cystatin F can be taken up by bystander cells and regulate the activity of cysteine cathepsins in the endosomal/lysosomal pathway.<sup>20,21</sup>

Cystatin F can regulate the cytotoxicity of natural killer (NK) cells by inhibiting the pro-granzyme convertases, cathepsins C and H, and cathepsin L that is implicated in perforin processing.<sup>22,23</sup> The

result is lower activity of granzymes A and B and, consequently, lower cytotoxicity of NK cells.<sup>21</sup> Cystatin F is therefore an upstream regulator of split anergy, an NK cell status in which cells lose their cytotoxicity but increase their expression and secretion of various cytokines.<sup>24,25</sup> A similar anergic state was also described in CTLs, where anergy is defined as a hyporesponsive state that a lymphocyte can acquire after it encounters an antigen.<sup>26</sup> The minimal requirement for a cell to be termed anergic is hypo- or un-responsiveness to at least one of its effector functions.<sup>27</sup> However, even though the regulatory role of cystatin F in NK cells is well established, much less is known about its role in CTLs. Since both cell types share the same molecular machinery for target cell killing, cystatin F could affect CTL cytotoxicity. In fact, it has been shown that overexpression of cystatin F in mouse CTLs leads to lower activity of cathepsin C. In human CD8+ T cell blasts, cystatin F was found co-localised with granzyme A, perforin and LAMP-1.<sup>18</sup> A role for cystatin F in regulating human CTL's cytotoxicity has, however, not yet been demonstrated.

We have investigated both the involvement of endogenous cystatin F in the inhibition of intracellular cathepsins C and H and its impact on the cytotoxicity of CTLs, using primary human CTLs and TALL-104 cells. Treatment with transforming growth factor  $\beta$  (TGF $\beta$ ) and ionomycin were shown to induce anergy of TALL-104 cells, attenuating their cytotoxicity against both NK-sensitive K-562 cells and NK-resistant Raji cells. It was further shown that the attenuated cytotoxicity correlates with increased levels of cystatin F and decreased specific activities of cathepsins C, H and L and granzyme B. Our results thus designate cystatin F as a regulator of the cytotoxicity of CTLs.

## Materials and methods

### Antibodies

Rabbit anti-cystatin F antibody from Davids Biotechnologie GmbH (Regensburg, Germany) was used in all experiments except in western blots, where rabbit anti-cystatin F antibody from Sigma-Aldrich (St. Louis, MO, USA) was used. Mouse anti-cathepsin C was from Santa Cruz Biotechnology (Santa Cruz, CA, USA). Other antibodies against human cathepsins were developed: 1D10 mouse anti-cathepsin H antibody<sup>28</sup>, sheep anti-cathepsin H<sup>28</sup> and sheep anti-cathepsin L.<sup>29</sup> Rabbit and mouse anti- $\beta$ -actin antibodies

were from Sigma-Aldrich, rabbit anti-glyceraldehyde 3-phosphate dehydrogenase (GAPDH) was from Santa Cruz Biotechnology and mouse anti-GAPDH from Proteintech (Rosemont, IL, USA). Secondary anti-rabbit, anti-mouse and anti-sheep antibodies conjugated with horseradish peroxidase (HRP), were from Jackson Immuno Research (West Grove, PA, USA). Secondary anti-rabbit and anti-mouse antibodies conjugated with fluorescent dyes DyLight 650 and DyLight 550, respectively, were from Invitrogen (Carlsbad, CA, USA). For immunofluorescence studies all secondary antibodies were from Thermo Fisher Scientific (Thermo Scientific, Rockford, IL, USA): donkey anti-rabbit Alexa Fluor 488, goat anti-rabbit Alexa Fluor 647, donkey anti-mouse Alexa Fluor 555 and donkey anti-sheep Alexa Fluor 488.

### Cell culture and isolation

TALL-104 cells (CRL-11386) (ATCC, Manassas, VA, USA) were cultured in IMDM medium (ATCC) with 20% foetal bovine serum (Gibco, Carlsbad, CA, USA), 100 IU/ml interleukin-2 (Bachem, Bubendorf, Switzerland), 2.5 µg/ml recombinant human albumin (Sigma-Aldrich) and 0.5 µg/ml D-mannitol (Sigma-Aldrich). TALL-104 cell line was used as a model of cytotoxic T lymphocytes since these cells express markers typical of a T-cell phenotype (CD2+, CD7+, CD3+, CD8+, TCRα/β+)<sup>30</sup>, can kill NK-sensitive as well as NK-resistant target cells and use primarily the perforin/granzyme pathway.<sup>31</sup> K-562 (CCL-243) (ATCC) and Raji cells (CCL-86) (ATCC) were cultured in RPMI-1640 (Lonza) with 10% foetal bovine serum, 100 U/mL penicillin (Lonza) and 100 U/mL streptomycin (Lonza). The same complete medium, but with 30 IU/mL interleukin-2, was used for primary human CD8+ T cells (pCTLs) that were isolated from buffy coats of healthy volunteers at the Blood Transfusion Centre of Slovenia, Republic of Slovenia, according to institutional guidelines. The National Medical Ethics Committee of the Ministry of Health, Republic of Slovenia, approved the study. Cytotoxic CD8+ T cells were isolated by negative selection magnetic beads kit (Miltenyi Biotech, Bergisch Gladbach, Germany), according to the manufacturer's protocol. The purity of pCTLs was determined by flow cytometry using fluorescence labelled antibodies against CD3, CD4, CD8, CD56, CD16, CD19 and TCRα/β (all from Miltenyi Biotech) and was always >95%. All cells were grown in a humidified incubator at 37°C in 5% CO<sub>2</sub>.

### Cell activation, TGFβ and ionomycin treatment

TALL-104 and pCTLs were stimulated with anti-CD3/anti-CD28 antibody coated beads (CD3/CD28 Dynabeads® human T-Activator, Thermo Fischer Scientific), a protocol that mimics the physiological activation of T-cells, since immobilised anti-CD3 antibody triggers signalling through T-cell receptor complex, while anti-CD28 antibody triggers the co-stimulatory signalling.<sup>32</sup> Stimulation was performed according to manufacturer's instructions; beads were added to TALL-104 or pCTLs at a cell density of 10<sup>6</sup>/mL and at a bead to cell ratio of 1:1. Before stimulation, pCTLs were rested in the complete medium with interleukin-2 overnight. TALL-104 cells were treated with 100 pM TGFβ (R&D Systems, Minneapolis, MN, USA) for 24 hours in the presence or absence of anti-CD3/anti-CD28 antibody coated beads in complete medium. For induction of anergy the cells were treated with 0.5 µM Ca<sup>2+</sup> ionophore ionomycin (Santa Cruz) for 16h in complete medium. After ionomycin treatment, cells were washed and either analysed or, to test if anergy is reversed after full activation, resuspended in fresh complete medium and activated. pCTLs were activated with anti-CD3/anti-CD28 antibody coated beads, while TALL-104 cells were activated with 1 µM ionomycin and 10 nM phorbol 12-myristate 13-acetate (PMA; Sigma-Aldrich), a stimulation protocol that similarly to stimulation with anti-CD3/anti-CD28 antibody coated beads mimics activation of the T-cell receptor, since ionomycin triggers signalling pathways of T-cell receptor, while PMA triggers signalling pathways of co-stimulatory molecules.

### Calcein-AM release assay

The calcein-AM release assay<sup>33</sup> was used for measuring TALL-104 cytotoxic activity. TALL-104 cells were used as effector cells and K-562 or Raji as target cells. First, the target cells were resuspended in serum-free RPMI and loaded with 15 µM calcein-AM (Sigma) for 30 minutes and after two washes in complete RPMI medium the cell density was adjusted to 10<sup>5</sup>/ml. Wells of a U-bottom 96-well plate were preloaded with sufficient numbers of TALL-104 cells in 100 µL of complete IMDM to produce the desired effector to target cell ratios (E:T). To measure spontaneous and total release of calcein-AM, wells were preloaded with 100 µL of complete IMDM or 100 µL of lysis buffer (50 mM sodium borate, 0.1% Triton X), respectively. Assays

were started by adding  $5 \times 10^3$  target cells in 50  $\mu\text{L}$  of complete RPMI to each well. The plate was then centrifuged for 2 minutes at  $200 \times g$  to enhance conjugate formation by amassing the cells at the bottom of the plate, then incubated for 4 hours in a humidified incubator at  $37^\circ\text{C}$  with 5%  $\text{CO}_2$ . After incubation the plate was centrifuged for 5 minutes at  $700 \times g$ . 50  $\mu\text{L}$  of supernatant was then transferred to a new microtiter plate. Fluorescence of released calcein-AM was measured with a microplate reader (Tecan M1000) with 496 nm excitation and 516 nm emission filters. Fluorescence of each E:T ratio was measured in at least three replicate wells. Specific lysis (%) was calculated as  $[(\text{test release} - \text{spontaneous release}) / (\text{total release} - \text{spontaneous release}) \times 100]$ . Lytic units (LU30/ $10^6$  cells) were determined by using the inverse of the number of effector cells needed to lyse 30% of target cells  $\times 100$ .<sup>34</sup> To investigate the requirement for extracellular  $\text{Ca}^{2+}$ , the cytotoxicity assay was performed in the presence of 2 mM EGTA and 1 mM  $\text{Mg}^{2+}$ . Excess  $\text{Ca}^{2+}$  was added at 2 mM concentration.

### Cell death analysis by Annexin V-FITC/propidium iodide double-staining

Cell death was assessed using an FITC-conjugated Annexin V/propidium iodide kit (Apoptosis detection kit, Beckton Dickinson, Franklin Lakes, NJ, USA), according to the manufacturer's protocol. Stained cells were examined by flow cytometry (FACS Calibur, Beckton Dickinson) using Cell Quest pro software (Beckton Dickinson). A minimum of twenty thousand cells were analysed per sample.

### Preparation of whole cell lysates

Cells were first washed in PBS then lysed in lysis buffer. For western blot analysis, cell lysis buffer (50 mM Tris-HCl pH 8, 150 mM NaCl, 1% Triton X-100, 0.5% sodium deoxycholate, 0.1% SDS and 1 mM EDTA) with addition of protease inhibitors (Roche) was used. For the activity assay of cathepsins 0.1 M citrate buffer pH 6.2 with 1% Triton X-100 lysis buffer was used, while the lysis buffer for granzyme B activity was 25 mM HEPES, 250 mM NaCl, 2.5 mM EDTA, 0.1% Nonident p-40, pH 7.4. Cell lysates were incubated on ice for 30 minutes then centrifuged at  $16,000 \times g$  for 20 minutes at  $4^\circ\text{C}$ . Supernatants were transferred to fresh tubes and protein concentration determined using the DC-Protein Assay Kit (Bio-Rad Laboratories, Hercules, CA, USA).

### Western blot

Samples containing 30 to 50  $\mu\text{g}$  of cell lysates' total protein were heated for 10 minutes at  $100^\circ\text{C}$  in either non-reducing or reducing (40 mM dithiothreitol) loading buffer, resolved in SDS-PAGE and transferred onto a nitrocellulose membrane (GE Healthcare, Chicago, IL, USA) using wet transfer at 200 mA for 90 minutes. Membranes were blocked in 5% non-fat dry milk in PBS (cystatin F) or 5% non-fat dry milk in tris-buffered saline (TBS) with 0.1% Tween-20 (for cathepsins C, H and L and granzyme B) for 1 hour at room temperature. Primary antibodies were diluted in blocking solution and incubated overnight at  $4^\circ\text{C}$ . After washing with PBS or TBS with 0.1% Tween-20 the membranes were incubated with HRP-conjugated secondary antibodies or in the dark with fluorescently labelled secondary antibodies (anti-rabbit-DyLight 650 or anti-mouse-DyLight 550) in blocking solution. Membranes with HRP-conjugated antibodies were incubated with Lumi-Light western blotting substrate (Roche). Images were acquired using a ChemiDoc MP System (Bio-Rad) and quantification analysis was performed in Image Lab, version 5.1 software (Bio-Rad).

### Confocal immunofluorescence microscopy and proximity ligation assay

Cells were washed in PBS and left to adhere to microscope slides for 30 minutes at  $37^\circ\text{C}$ . The slides were then fixed with 4% paraformaldehyde in PBS for 20 minutes, permeabilized with 0.1% Triton X-100 in PBS for 10 minutes and blocked with 3% BSA (Sigma-Aldrich) in PBS for 30 minutes. Primary antibodies were diluted in 1% BSA in PBS and incubated for 90 minutes. Fluorescence labelled secondary antibodies were diluted in PBS and incubated for 1 hour. Slides were mounted with Prolong Gold Antifade Mountant containing 4',6'-diamidino-2-phenylindole (DAPI) (Thermo Scientific). Control samples were run in the absence of one or both primary antibodies. Images were taken with a Carl Zeiss LSM 710 confocal microscope (Carl Zeiss, Oberkochen, Germany) with ZEN 2011 image software (Carl Zeiss).

For proximity ligation assay (PLA), after incubation with primary antibodies, PLA was performed according to the manufacturer's protocol (Olink Bioscience, Uppsala, Sweden). Briefly, for a single recognition experiment for cystatin F, anti-rabbit PLUS and anti-rabbit MINUS were used as PLA probes, and the PLA probes anti-rabbit PLUS and

anti-mouse MINUS for cystatin F–cathepsin C interaction. PLA probes were diluted in 1% BSA in PBS and incubated for 1 hour at 37°C. Ligation and amplification were performed using Detection Reagents Red. Coverslips were mounted on glass slides using Duolink In Situ Mounting Medium with DAPI. Controls were run in the absence of one or both primary antibodies. A cystatin F single recognition experiment was performed as a positive control. Fluorescence microscopy, using a Carl Zeiss LSM 710 confocal microscope, and high resolution images (63x 1.4NA) of at least 100 cells per condition were acquired. Cell images were exported using ZEN 2012 SP1 (black edition) version 8.1 software (Carl Zeiss) in TIF format for further analysis and signal quantification in Blobfinder 3.2 software (Centre for Image Analysis, Uppsala University, Uppsala, Sweden).

### Immunoprecipitation

TALL-104 cells were washed once in PBS and lysed in ice-cold lysis buffer (50 mM Tris-HCl pH 7.4, 100 mM NaCl, 0.25% Triton X-100, with protease inhibitors (Roche)). After incubation on ice for 30 minutes, lysates were centrifuged at 16,000 x g for 20 minutes and supernatants were transferred into fresh tubes. Dynabeads protein G (Thermo Scientific) were coated with either rabbit anti-cystatin F antibody (Davids Biotechnologie) or an antibody raised against lectin isolated from *Macrolepiota procera* (BioGenes GmbH, Berlin, Germany), as a negative control. Dynabeads protein G with bound antibodies was then added to lysates. After rotation at 4°C overnight, beads were washed three times with lysis buffer and boiled for 10 minutes in 1x SDS loading buffer. Eluted proteins were analysed by western blot.

### Determination of enzyme activities

Enzyme activities were determined using specific fluorogenic substrates: 70 μM H-Gly-Phe-7-amino-4-methylcoumarin (AMC) (Bachem) for cathepsin C, 20 μM H-Arg-AMC (Bachem) for cathepsin H, 50 μM Z-Phe-Arg-AMC for cathepsin L (Bachem) and 50 μM acetyl-Ile-Glu-Pro-Asp-AMC for granzyme B (Bachem). The assay buffers used were 25 mM MES, 100 mM NaCl, 5 mM cysteine, pH 6 for cathepsin C, 100 mM MES, 2mM EDTA, 5 mM cysteine, pH 6.5 for cathepsins H and L and 50 mM Tris-HCl, 100 mM NaCl, pH 7.4 for granzyme B. Whole-cell lysates were first activated in assay buffer for 15 minutes at room temperature

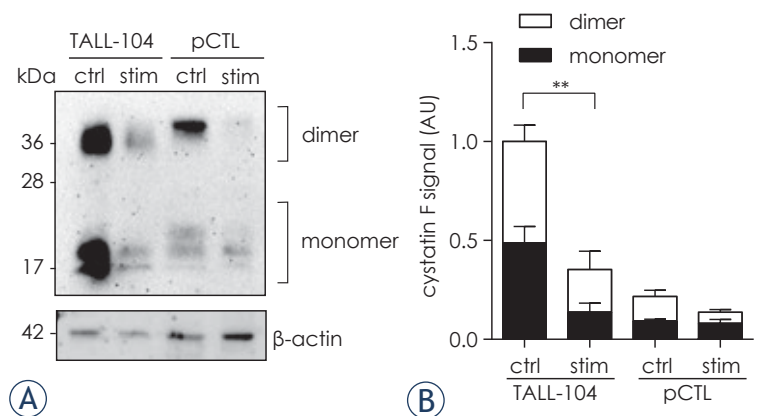


**FIGURE 1.** Expression of cystatin F in TALL-104 cells and human CD8+ T cells. **(A)** Representative western blot experiment showing expression of the monomeric and dimeric form of cystatin F in unstimulated and stimulated TALL-104 cells and human CD8+ T cells. Both, TALL-104 and human CD8+ T cells, were stimulated with anti-CD3/anti-CD28 antibody coated beads. Multiple bands correspond to differently glycosylated forms of cystatin F.<sup>21</sup> **(B)** Quantification of western blot data was performed in Image Lab software. Signals for cystatin F were first normalized to β-actin signal and TALL-104 control sample intensity was set to 1 arbitrary unit (AU). Relative intensities of other bands were calculated accordingly. Error bars represent s.e.m between three separate experiments.

\*\*  $p \leq 0.01$ , statistical analysis was performed for total cystatin F levels.

ctrl = control; pCTL = primary human cytotoxic T cells; stim = stimulated;

for cathepsins or for 30 minutes at 37°C for granzyme B. The substrate was then added and formation of fluorescent degradation products was measured continuously with excitation at 370 nm and emission at 460 nm on a microplate reader Infinite M1000 (Tecan, Männedorf, Switzerland). To determine cathepsin L activity, 5 μM irreversible inhibitor of cathepsin B, CA-074 (Bachem), was added before the addition of substrate. The rate of AMC release was calculated and normalised to the enzyme protein levels determined from western blot. The activity of the control sample was set to 100% and activities of other samples were adjusted accordingly.

### Statistical analyses

Data were analysed using GraphPad Prism 6 (GraphPad Software, San Diego, CA, USA). Differences between groups were analysed with the t test when two groups were compared or with one-way ANOVA followed by Šidák's multiple comparisons test to assess which groups differed significantly when more than two groups were compared. Differences were accepted as significant when  $p \leq 0.05$ .

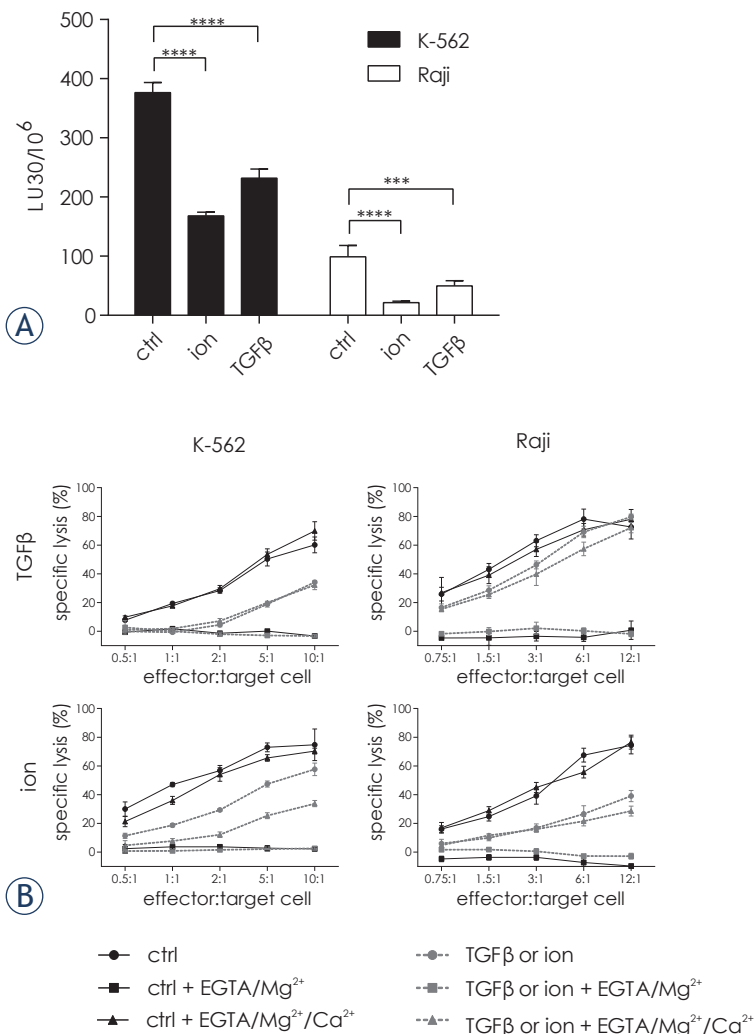


**FIGURE 2.** Cytotoxicity of TALL-104 after TGFβ or ionomycin treatment is reduced. **(A)** TALL-104 cells were treated with 100 pM TGFβ for 24 hours or 0.5 μM ionomycin for 16 hours. Cytotoxicity against NK-sensitive targets K-562 cells and NK-resistant targets Raji cells was measured by a 4 hour calcein-AM release assay at different effector-to-target cell ratios. Lytic units (LU 30/10<sup>6</sup>) were calculated using the inverse number of TALL-104 cells needed to lyse 30% of target cells × 100. Error bars represent SD between triplicates. ANOVA was used for statistical analysis, \*\*\* p ≤ 0.001 and \*\*\*\*p ≤ 0.0001. **(B)** Cytotoxicity of control, TGFβ and ionomycin treated TALL-104 cells against K-562 and Raji target cells was measured by a 4 hour calcein-AM release assay at different effector-to-target cell ratio. During the assay the Ca<sup>2+</sup> chelator EGTA or EGTA with excess Ca<sup>2+</sup> was added. Error bars represent SD between triplicates.

ctrl = control; ion = ionomycin

## Results

### Cystatin F is expressed in TALL-104 and in human primary CD8<sup>+</sup> T cells

Expression of cystatin F in TALL-104 cells and in human primary CD8<sup>+</sup> T cells (pCTLs) isolated from peripheral blood mononuclear cells of healthy donors was examined by western blot. Both cell

types expressed cystatin F but at a higher level in TALL-104. Stimulation of cells with anti-CD3/anti-CD28 antibody coated beads led to a decrease in both monomeric and dimeric forms of cystatin F (Figure 1).

### Cytotoxicity is decreased and cystatin F levels increased in response to TGFβ and ionomycin

Since TGFβ has been reported to target the effector function of CTLs by transcriptional repression of perforin and granzymes<sup>35</sup>, we determined whether TALL-104 cytotoxic function is affected by TGFβ. After TGFβ treatment, the cytotoxicity of TALL-104 cells against NK-sensitive targets, *i.e.* K-562 cells, as well as against NK-resistant Raji cells, tested by calcein-AM release assay, was significantly reduced (Figure 2A). The killing of target cells was completely inhibited by the addition of Ca<sup>2+</sup> chelating agent EGTA to the assay medium, while addition of excess Ca<sup>2+</sup> restored the cytotoxic function (Figure 2B), implying that the loss of cytotoxic function was due to the Ca<sup>2+</sup> chelating action of EGTA. Furthermore, we confirmed, by double staining of cells with annexin V-FITC and propidium iodide, that TGFβ treatment did not induce cell death of TALL-104 cells. More than 97% of both control and TGFβ treated cells were negative for both markers of cell death, excluding cell death as the cause of the lower cytotoxicity.

Further, ionomycin was used to induce the anergy and decrease the cytotoxicity of TALL-104 cells. TALL-104 cells treated with low concentrations of ionomycin displayed a marked decrease in cytotoxicity against K-562 and Raji targets (Figure 2A) and, like that with TGFβ, the addition of EGTA during the calcein-AM release assay completely abrogated the cytotoxicity, while addition of excess Ca<sup>2+</sup> restored the cytotoxic activity, confirming the involvement of the granzyme/perforin pathway in cell cytotoxicity (Figure 2B). Propidium iodide staining confirmed that ionomycin treatment does not trigger cell death in TALL-104 and pCTLs (data not shown).

Levels of cystatin F in cell lysates were further assessed by western blot. In TALL-104 cells, total cystatin F levels increased after treatment with TGFβ (Figure 3A,B) or with ionomycin (Figure 3C,D). In TGFβ treated TALL-104 cells the increase of total cystatin F levels was due to an increase of the active monomeric form, while the dimeric form, that does not inhibit cysteine cathepsins, was decreased. Ionomycin treatment on the other hand triggered an increase of both monomeric and dimeric forms.

Both control and ionomycin treated TALL-104 cells were stimulated with PMA/ionomycin, which decreased cystatin F levels (Figure 3D). Nevertheless, in ionomycin treated cells stimulated with PMA/ionomycin cystatin F levels remained higher compared to the control TALL-104 cells stimulated with PMA/ionomycin (Figure 3D). Similarly, in pCTLs cystatin F levels were increased after ionomycin treatment in both, unstimulated cells and following stimulation with anti-CD3/anti-CD28 beads.

### Cysteine cathepsins C, H and L are expressed in TALL-104 cells and in human CD8+ T cells and co-localise with cystatin F

It has been postulated that, in NK cells, the most prominent targets of cystatin F are cathepsins C and H, that act as pro-granzyme convertases<sup>21</sup>, and cathepsin L, that is implicated in perforin processing.<sup>10,21</sup> In this study, both pCTLs and TALL-104 cells were found to express cathepsins C, H and L (Figure 4A-C). Using confocal microscopy, cystatin F was shown to be co-localised with cathepsins C, H and L in TALL-104 cells (Figure 4D) and pCTLs (Figure 4E). Co-localisation of cystatin F with cathepsins C and H was confirmed by co-immunoprecipitation (Figure 4F) and with cathepsin C by proximity ligation assay (Figure 4G).

### Increased cystatin F levels are correlated with decreased specific activities of cathepsins C, H and L and of granzyme B

We further studied, using specific substrates and whole cell lysates, whether cystatin F can affect enzymatic activities of cathepsins C, H and L in TALL-104 cells (Figure 5). Activities of cathepsins C, H and L were significantly decreased in ionomycin treated TALL-104 cells and, after stimulation with PMA/ionomycin, their activity remained significantly decreased (Figure 5A-C). Similarly, activities of cathepsins C and L were significantly decreased in TGF $\beta$  treated TALL-104 cells both unstimulated and stimulated with anti-CD3/anti-CD28 antibody coated beads (Figure 5E,G). However, cathepsin H activity was decreased in TGF $\beta$  treated TALL-104 cells stimulated with anti-CD3/anti-CD28 antibody coated beads, but not in unstimulated cells (Figure 5F).

It was next determined as to whether lower cathepsins C and H activities result in lower granzyme B activities. Indeed, in ionomycin treated

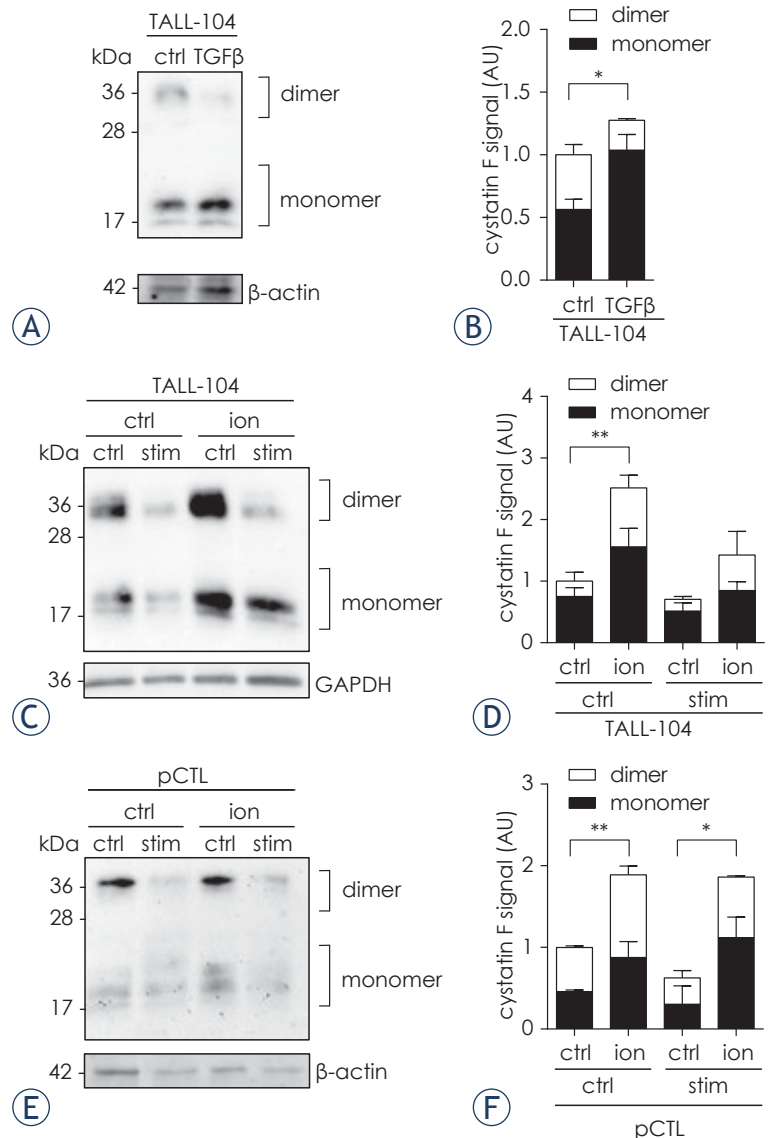


**FIGURE 3.** TGF $\beta$  and ionomycin increase cystatin F protein levels. **(A, B)** TALL-104 cells were stimulated with anti-CD3/anti-CD28 antibody coated beads in the presence or absence of 100 pM TGF $\beta$ . **(C, D)** TALL-104 cells were treated with 0.5  $\mu$ M ionomycin for 16 hours and stimulated with 10 nM PMA and 1  $\mu$ M ionomycin. **(E, F)** Human CD8+ T cells were treated with 0.5  $\mu$ M ionomycin for 16 hours and stimulated with anti-CD3/anti-CD28 antibody coated beads. **(A, C, E)** show representative western blots for cystatin F, while **(B, D, F)** show quantification of 3 **(B, D)** or 2 **(F)** independent experiments. Quantification was performed in Image Lab software. Signals for cystatin F were first normalized to  $\beta$ -actin **(B, F)** or GAPDH **(D)** signal and TALL-104 control sample intensity was set to 1 arbitrary unit (AU). Relative intensities of other bands were calculated accordingly. Data are presented as mean  $\pm$  s.e.m. \*  $p \leq 0.05$ , \*\*  $p \leq 0.01$ , statistical analysis was performed for total cystatin F levels.

ctrl = control; ion = ionomycin; pCTL = primary human cytotoxic T cells; stim = stimulated

TALL-104 cells and in unstimulated TGF $\beta$  treated TALL-104 cells the granzyme B activity was significantly reduced (Figure 5D), while in TGF $\beta$  treated TALL-104 cells stimulated with anti-CD3/anti-

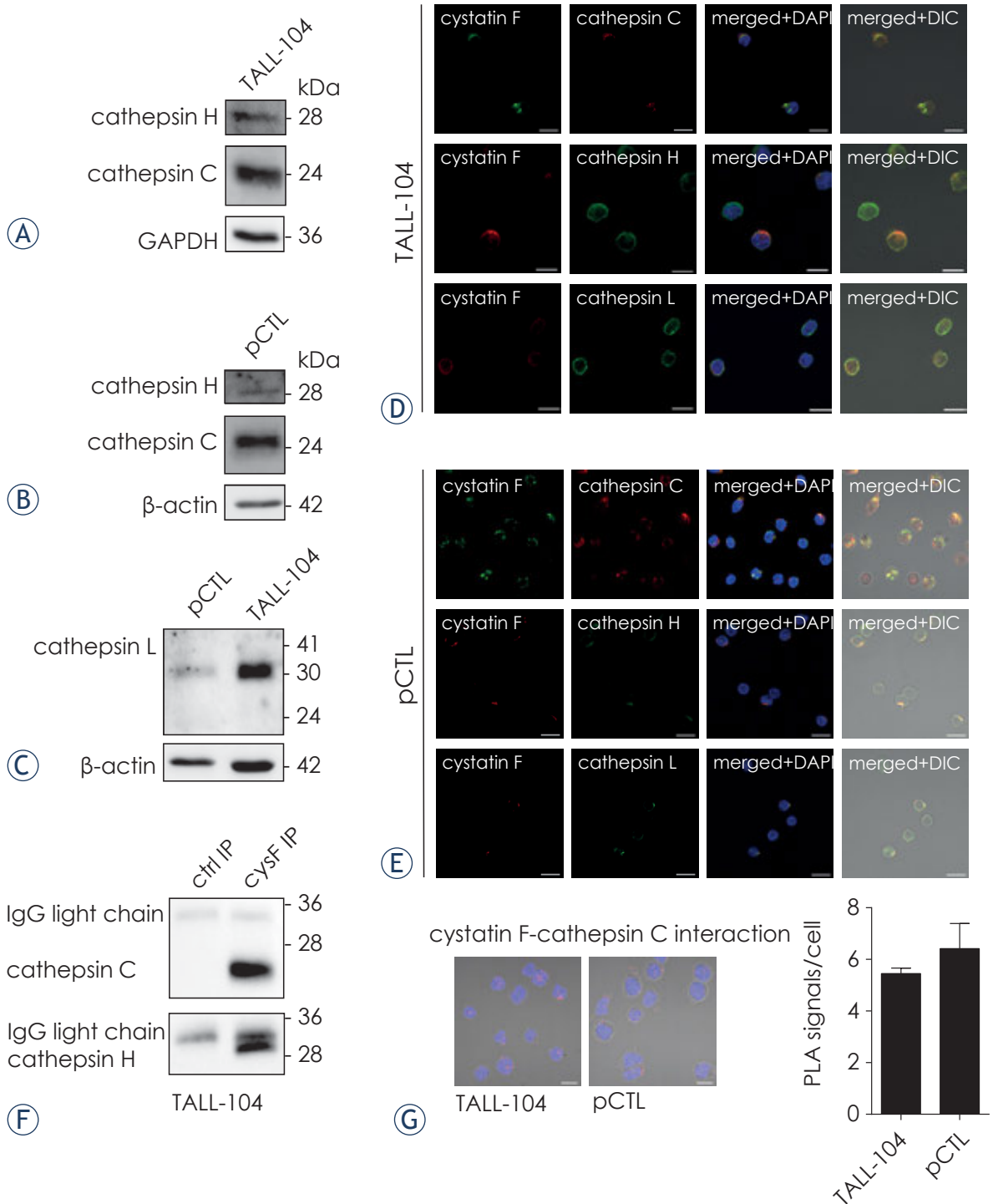


**FIGURE 4.** Expression of cathepsins C, H and L in TALL-104 cells and human CD8+ T cells and their co-localisation with cystatin F. **(A-C)** TALL-104 and pCTLs were analysed for cathepsins C, H and L expression by western blot. GAPDH or β-actin staining was used to show protein loading. **(D, E)** Co-localisation of cystatin F with cathepsins C, H and L was studied by immunofluorescence microscopy in TALL-104 **(D)** and pCTLs **(E)**. Cystatin F (green) and cathepsin C (red) co-localisation is shown in first row, cystatin F (red) and cathepsin H (green) in second row and cystatin F (red) and cathepsin L (green) in third row. Bars represent 10 μm. **(F)** TALL-104 cell lysates were immunoprecipitated with cystatin F antibody and analysed by western blot with anti-cathepsin C and H antibodies. **(G)** Proximity ligation experiment for cystatin F-cathepsin C interaction in TALL-104 cells and pCTLs. Signals were quantified in BlobFinder software. Bars represent 10 μm.

ctrl = control; cysF = cystatin F; IP = immunoprecipitation; pCTL = primary human cytotoxic T cells

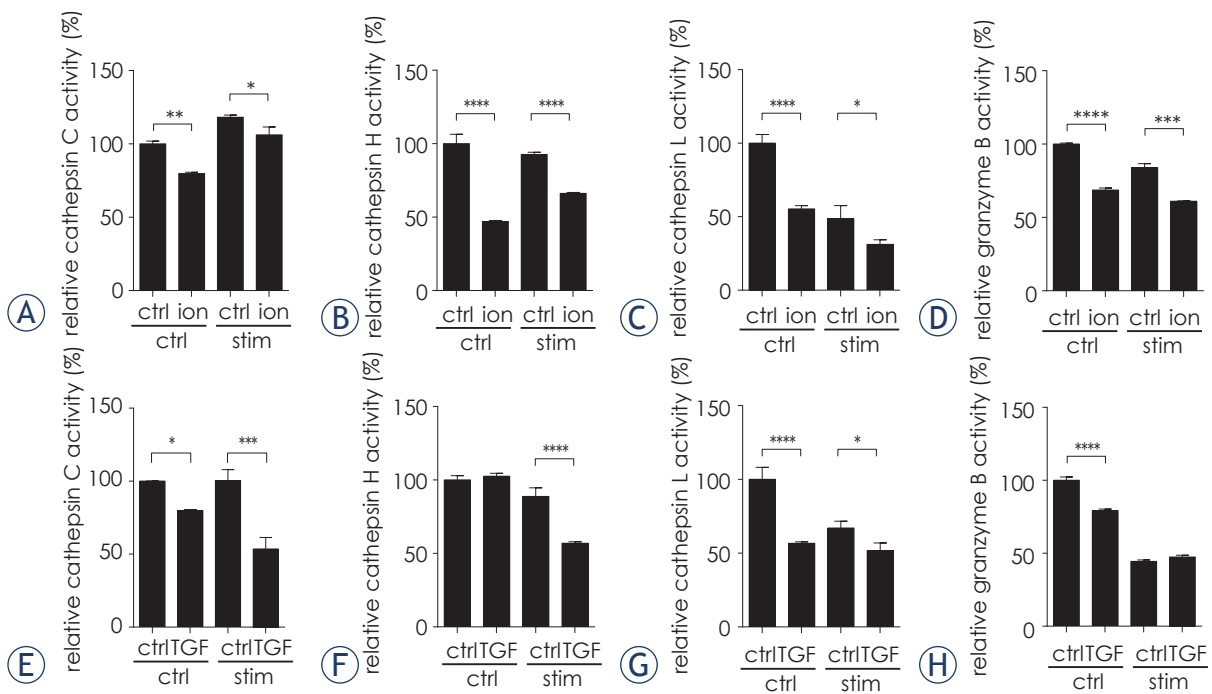


**FIGURE 5.** Activities of cathepsins C, H and L and granzyme B in TALL-104 cells. Activities of cathepsins C (A, E), H (B, F), L (C, G) and granzyme B (D, H) in TALL-104 whole cell lysates after TGF $\beta$  or ionomycin treatment. Error bars represent SD between triplicates. \*  $p \leq 0.05$ , \*\*  $p \leq 0.01$ , \*\*\*  $p \leq 0.001$  and \*\*\*\*  $p \leq 0.0001$ .

ctrl = control; ion = ionomycin; stim = stimulated; TGF = transforming growth factor beta

CD3/anti-CD28 antibody coated beads granzyme B activity was not decreased (Figure 5H).

## Discussion

Cystatin F has recently been shown to be an upstream regulator of split anergy in NK cells, where it inhibits cathepsins C and H, major pro-granzyme convertases, resulting in reduced cytotoxicity of NK cells.<sup>21,34</sup> Even if NK cells and CTLs differ greatly in their mechanisms of target cell recognition and activation, the molecular mechanism, i.e. granule dependent cytotoxicity, that they exploit to trigger cell death is very similar. Therefore, we hypothesised that cystatin F could also be involved in regulating the cytotoxicity of CTLs. It has already been shown that, in mouse CTLs, overexpressed cystatin F decreases cathepsin C activity and that, in human CTLs, it is co-localised with granzyme A and perforin<sup>18</sup> and granzyme B (unpublished observation). The ability of cystatin F to regulate the cytotoxicity of CTLs had not, however, been addressed before. Here we demonstrate that increased levels of cystatin F correlate with lower specific activities of cathepsins C, H and L and

granzyme B and, consequently, with the decreased cytotoxicity of CTLs.

First, the expression of cystatin F in primary human CTLs and the TALL-104 cell line was demonstrated by western blot (Figure 1) and found to be significantly higher in TALL-104 than in CTLs. On stimulation with anti-CD3/anti-CD28 antibody coated beads, cystatin F levels were decreased in both cell types. Changes in cystatin F levels following stimulation have been reported and were dependent on cell type and stimulation agents. Similarly to our findings, the differentiation of U937 and HL-60 cells with PMA caused a decrease in dimeric and monomeric forms of cystatin F.<sup>11,36</sup> On the other hand, in monocyte-derived dendritic cells stimulated with toll-like receptor 3 ligand (polyinosinic:polycytidylic acid) or toll-like receptor 4 ligand (lipopolysaccharide), cystatin F levels were increased.<sup>18</sup> As in primary human NK cells, stimulation with interleukin-2 led to increased levels of the dimeric cystatin F, while those of the monomeric form remained unchanged.<sup>21,34</sup>

Secondly, TALL-104 cells were found to be less cytotoxic after treatment with either TGF $\beta$  or ionomycin (Figure 2). TGF $\beta$  is an immunosuppressive cytokine present in large amounts in tumour mi-

croenvironment, its source being the cancer cells themselves or various cells of stromal and tumour-infiltrating cells.<sup>37</sup> TGF $\beta$  plural: roles in cancer, notably suppressing the anti-cancer immune response by its inhibitory action on T cell proliferation, activation and effector functions.<sup>38</sup> Indeed, it has been demonstrated that TGF $\beta$  directly inhibits the effector function of CTLs by inhibiting expression of perforin, granzymes A and B, interferon-gamma and Fas ligand.<sup>35</sup> In accordance with this, TGF $\beta$  was shown here to decrease TALL-104 cytotoxicity against NK-sensitive as well as NK-resistant target cells (Figure 2). Furthermore, cytotoxicity is completely inhibited by addition of the Ca<sup>2+</sup> chelating agent EGTA, indicating that the Ca<sup>2+</sup>-dependent perforin/granzyme pathway is responsible for cytotoxicity in the setting of the present assay. This finding could be relevant for patient treatment, since TALL-104 cells have already been used in Phase I clinical trials on patients with refractory metastatic breast cancer<sup>39</sup> and peritoneal carcinosis<sup>40</sup> and are currently in Phase II clinical trial in patients with ovarian carcinoma.<sup>41</sup>

The effect of TGF $\beta$  on TALL-104 cells is comparable to that of ionomycin, a compound known to trigger T cell anergy.<sup>26,42</sup> Ionomycin triggers activation of Ca<sup>2+</sup>/calcineurin signalling and activation of transcription factor NFAT. Because co-stimulation is absent, the PKC/IKK/Ras/MAP kinase arm is not activated and, consequently, activation of NFAT co-operating transcription factor AP1 is absent, leading to transcription of anergy associated genes.<sup>42,43</sup> Interestingly, in ionomycin induced anergic CD4+ T cells, cystatin F was shown to be among the genes that were strongly induced.<sup>42</sup> In this study we demonstrated that, in TALL-104 cells, ionomycin triggers a hyporesponsive state characterised by their reduced ability to kill target cells (Figure 2). In both models of reduced cell cytotoxicity we consistently found increased levels of active monomeric cystatin F (Figure 3). This is in accordance with our previous results where active monomeric form of cystatin F was increased in split anergic NK cells.<sup>34</sup> Split anergic NK cells, after interaction with NK-sensitive targets, lose their cytotoxicity but still proliferate and secrete higher levels of cytokines.<sup>25</sup>

Among the possible peptidases that could be inhibited by cystatin F, we focused on cathepsins C, H and L, since these are involved in the activation of effector molecules of the perforin/granzyme pathway. In previous studies it was shown that cystatin F is co-localised with cathepsins C and H in the same vesicles in NK-92 cells<sup>34</sup> and with granzyme A and perforin in human CD8+ T cell

blasts.<sup>18</sup> Here, by immunofluorescence staining, we report the co-localisation of cystatin F with cathepsin C in primary human CTLs and TALL-104 cells and confirm its interaction with proximity ligation assay and co-immunoprecipitation (Figure 4). Furthermore, we have shown that cystatin F co-localizes and co-immunoprecipitates with cathepsin H, confirming that cystatin F interacts with both major pro-granzyme convertases (Figure 4). With regard to cathepsin L, in PMA/ionomycin stimulated CD8+ T cells obtained from NOD mice, cathepsin L activity was observed.<sup>44</sup> In accordance with these results we detected cathepsin L protein in human CTLs and TALL-104 cells. Furthermore, we showed that cathepsin L co-localises with cystatin F in both cell types (Figure 4).

Increased expression of monomeric cystatin F in anergic and TGF $\beta$  treated TALL-104 cells was expected to have an impact on cathepsins' activity. Indeed, after treating TALL-104 cells with ionomycin, a significant drop in the specific activities of cathepsins C, H and L was observed in both unstimulated and stimulated TALL-104 cells (Figure 5). With TGF $\beta$  the effect was similar for cathepsins C and L, but less evident for cathepsin H (Figure 5). Given that cathepsins C and H are pro-granzyme B convertases, decreased levels of cathepsins C and H should affect the processing of granzymes from their precursor forms. In ionomycin treated TALL-104 cells this impact on granzyme B activity was evident, whereas in TGF $\beta$  treated TALL-104 cells this was the case in unstimulated TALL-104 cells. However, in stimulated TALL-104 cells, granzyme B activity was not affected. It is possible that the combination of TGF $\beta$  treatment and stimulation with anti-CD3/anti-CD28 antibody coated beads triggers upregulation of an additional activating peptidase that compensates for the decreased activities of cathepsins C and H. Indeed, in activated lymphocytes from mice lacking either cathepsin C or both cathepsins C and H, granzyme A activity was absent, but there was still granzyme B activity and it was suggested, similarly to our results, that an additional granzyme B convertase is present.<sup>7</sup>

To conclude, it has been demonstrated that induction of a hyporesponsive state in CTLs, either by the immunosuppressive cytokine TGF $\beta$  or by ionomycin, correlates with decreased specific activities of cathepsins C and H and of their substrate, granzyme B. At the same time the expression of cystatin F, an inhibitor of cysteine cathepsins, is increased, suggesting that cystatin F could be a negative regulator of the cytotoxicity of CTLs. Additional stud-

ies, including silencing of cystatin F in CTLs and *in vivo* studies using mice lacking cystatin F, would be needed to demonstrate unequivocally the role of cystatin F in CTLs and its potential as a target to improve the immunotherapy of cancer.

## Acknowledgement

This work was supported by the Slovenian Research Agency [grant numbers P4-0127 and J4-6811 to JK].

Authors thank prof. Roger Pain for critical reading of the manuscript.

## References

- Hanahan D, Weinberg RA. Hallmarks of cancer: the next generation. *Cell* 2011; **144**: 646-74. doi: 10.1016/j.cell.2011.02.013
- Durgeau A, Virk Y, Cornnac S, Mami-Chouaib F. Recent advances in targeting CD8 T-cell immunity for more effective cancer immunotherapy. *Front Immunol* 2018; **9**: 14. doi: 10.3389/fimmu.2018.00014
- Trapani JA, Smyth MJ. Functional significance of the perforin/granzyme cell death pathway. *Nat Rev Immunol* 2002; **2**: 735-47. doi: 10.1038/nri911
- Voskoboinik I, Trapani JA. Perforinopathy: a spectrum of human immune disease caused by defective perforin delivery or function. *Front Immunol* 2013; **4**: 441. doi: 10.3389/fimmu.2013.00441
- Voskoboinik I, Whistock JC, Trapani JA. Perforin and granzymes: function, dysfunction and human pathology. *Nat Rev Immunol* 2015; **15**: 388-400. doi: 10.1038/nri3839
- Sutton VR, Waterhouse NJ, Browne KA, Sedelies K, Ciccone A, Anthony D, et al. Residual active granzyme B in cathepsin C-null lymphocytes is sufficient for perforin-dependent target cell apoptosis. *J Cell Biol* 2007; **176**: 425-33. doi: 10.1083/jcb.200609077
- D'Angelo ME, Bird PI, Peters C, Reinheckel T, Trapani JA, Sutton VR. Cathepsin H is an additional convertase of pro-granzyme B. *J Biol Chem* 2010; **285**: 20514-9. doi: 10.1074/jbc.M109.094573
- House IG, House CM, Brennan AJ, Gilan O, Dawson MA, Whistock JC, et al. Regulation of perforin activation and pre-synaptic toxicity through C-terminal glycosylation. *EMBO Rep* 2017; **18**: 1775-85. doi: 10.15252/embr.201744351
- Uellner R, Zvelebil MJ, Hopkins J, Jones J, MacDougall LK, Morgan BP, et al. Perforin is activated by a proteolytic cleavage during biosynthesis which reveals a phospholipid-binding C2 domain. *EMBO J* 1997; **16**: 7287-96. doi: 10.1093/emboj/16.24.7287
- Konjar S, Sutton VR, Hoves S, Repnik U, Yagita H, Reinheckel T, et al. Human and mouse perforin are processed in part through cleavage by the lysosomal cysteine proteinase cathepsin L. *Immunology* 2010; **131**: 257-67. doi: 10.1111/j.1365-2567.2010.03299.x
- Dautović E, Perišić Nanut M, Softić A, Kos J. The transcription factor C/EBP  $\alpha$  controls the role of cystatin F during the differentiation of monocytes to macrophages. *Eur J Cell Biol* 2018; **97**: 463-73. doi: 10.1016/j.ejcb.2018.07.002
- Halfon S, Ford J, Foster J, Dowling L, Lucian L, Sterling M, et al. Leukocystatin, A New Class II cystatin expressed selectively by hematopoietic cells. *J Biol Chem* 1998; **273**: 16400-8. doi: 10.1074/jbc.273.26.16400
- Magister S, Kos J. Cystatins in immune system. *J Cancer* 2013; **4**: 45-56. doi: 10.7150/jca.5044
- Ni J, Fernandez MA, Danielsson L, Chillakuru RA, Zhang J, Grubb A, et al. Cystatin F is a glycosylated human low molecular weight cysteine proteinase inhibitor. *J Biol Chem* 1998; **273**: 24797-804. doi: 10.1074/jbc.273.38.24797
- Cappello F, Gatti E, Camossetto V, David A, Lelouard H, Pierre P. Cystatin F is secreted, but artificial modification of its C-terminus can induce its endocytic targeting. *Exp Cell Res* 2004; **297**: 607-18. doi: 10.1016/j.yexcr.2004.03.048
- Langerholc T, Zavasnik-Bergant V, Turk B, Turk V, Abrahamson M, Kos J. Inhibitory properties of cystatin F and its localization in U937 promonocyte cells. *FEBS J* 2005; **272**: 1535-45. doi: 10.1111/j.1742-4658.2005.04594.x
- Schüttelkopf AW, Hamilton G, Watts C, van Aalten DMF. Structural basis of reduction-dependent activation of human cystatin F. *J Biol Chem* 2006; **281**: 16570-5. doi: 10.1074/jbc.M601033200
- Hamilton G, Colbert JD, Schüttelkopf AW, Watts C. Cystatin F is a cathepsin C-directed protease inhibitor regulated by proteolysis. *EMBO J* 2008; **27**: 499-508. doi: 10.1038/sj.emboj.7601979
- Colbert JD, Plechanovová A, Watts C. Glycosylation directs targeting and activation of cystatin F from intracellular and extracellular sources. *Traffic* 2009; **10**: 425-37. doi: 10.1111/j.1600-0854.2009.00881.x
- Colbert JD, Matthews SP, Kos J, Watts C. Internalization of exogenous cystatin F suppresses cysteine proteases and induces the accumulation of single-chain cathepsin L by multiple mechanisms. *J Biol Chem* 2011; **286**: 42082-90. doi: 10.1074/jbc.M111.253914
- Perišić Nanut M, Sabotič J, Švajger U, Jewett A, Kos J. Cystatin F affects natural killer cell cytotoxicity. *Front Immunol* 2017; **8**: 1459. doi: 10.3389/fimmu.2017.01459
- Kos J, Nanut MP, Prunk M, Sabotič J, Dautović E, Jewett A. Cystatin F as a regulator of immune cell cytotoxicity. *Cancer Immunol Immunother* 2018; **67**: 1931-8. doi: 10.1007/s00262-018-2165-5
- Perišić Nanut M, Sabotič J, Jewett A, Kos J. Cysteine cathepsins as regulators of the cytotoxicity of NK and T cells. *Front Immunol* 2014; **5**: 616. doi: 10.3389/fimmu.2014.00616
- Jewett A, Bonavida B. Target-induced anergy of natural killer cytotoxic function is restricted to the NK-target conjugate subset. *Cell Immunol* 1995; **160**: 91-7. doi: 10.1016/0008-8749(95)80013-9
- Jewett A, Tseng H-C. Tumor induced inactivation of natural killer cell cytotoxic function; implication in growth, expansion and differentiation of cancer stem cells. *J Cancer* 2011; **2**: 443-57. doi: 10.7150/jca.2.443
- Choi S, Schwartz RH. Molecular mechanisms for adaptive tolerance and other T cell anergy models. *Semin Immunol* 2007; **19**: 140-52. doi: 10.1016/j.smim.2007.02.005
- Schwartz RH. Models of T cell anergy: is there a common molecular mechanism? *J Exp Med* 1996; **184**: 1-8. doi: 10.1084/jem.184.1.1
- Schweiger A, Stabuc B, Popović T, Turk V, Kos J. Enzyme-linked immunosorbent assay for the detection of total cathepsin H in human tissue cytosols and sera. *J Immunol Methods* 1997; **201**: 165-72. doi: 10.1016/S0022-1759(96)00218-9
- Kos J, Stabuc B, Schweiger A, Krasovec M, Cimerman N, Kopitar-Jerala N, et al. Cathepsins B, H, and L and their inhibitors stefin A and cystatin C in sera of melanoma patients. *Clin Cancer Res* 1997; **3**: 1815-22.
- O'Connor R, Cesano A, Lange B, Finan J, Nowell PC, Clark SC, et al. Growth factor requirements of childhood acute T-lymphoblastic leukemia: correlation between presence of chromosomal abnormalities and ability to grow permanently in vitro. *Blood* 1991; **77**: 1534-45.
- Cesano A, Santoli D. Two unique human leukemic T-cell lines endowed with a stable cytotoxic function and a different spectrum of target reactivity analysis and modulation of their lytic mechanisms. *In Vitro Cell Dev Biol* 1992; **28A**: 648-56.
- Li Y, Kurlander RJ. Comparison of anti-CD3 and anti-CD28-coated beads with soluble anti-CD3 for expanding human T cells: differing impact on CD8 T cell phenotype and responsiveness to restimulation. *J Transl Med* 2010; **8**: 104. doi: 10.1186/1479-5876-8-104.
- Lichtenfels R, Biddison WE, Schulz H, Vogt AB, Martin R. CARE-LASS (calcein-release-assay), an improved fluorescence-based test system to measure cytotoxic T lymphocyte activity. *J Immunol Methods* 1994; **172**: 227-39. doi: 10.1016/0022-1759(94)90110-4
- Magister S, Tseng H-C, Bui VT, Kos J, Jewett A. Regulation of split anergy in natural killer cells by inhibition of cathepsins C and H and cystatin F. *Oncotarget* 2015; **6**: 22310-27. doi: 10.18632/oncotarget.4208

35. Thomas DA, Massagué J. TGF-beta directly targets cytotoxic T cell functions during tumor evasion of immune surveillance. *Cancer Cell* 2005; **8**: 369-80. doi: 10.1016/j.ccr.2005.10.012
36. Nathanson C-M, Wassélius J, Wallin H, Abrahamson M. Regulated expression and intracellular localization of cystatin F in human U937 cells. *Eur J Biochem* 2002; **269**: 5502-11. doi: 10.1046/j.1432-1033.2002.03252.x
37. Massagué J. TGFbeta in cancer. *Cell* 2008; **134**: 215-30. doi: 10.1016/j.cell.2008.07.00
38. Dahmani A, Delisle J-S. TGF- $\beta$  in T Cell Biology: Implications for cancer immunotherapy. *Cancers* 2018; **10**. doi: 10.3390/cancers10060194
39. Visonneau S, Cesano A, Porter DL, Luger SL, Schuchter L, Kamoun M, et al. Phase I trial of TALL-104 cells in patients with refractory metastatic breast cancer. *Clin Cancer Res* 2000; **6**: 1744-54.
40. Bengala C, Rasini V, Sternieri R, Dominici M, Andreotti A, Gelmini R, et al. Phase I study of intraperitoneal MHC unrestricted adoptive cell therapy with TALL-104 cells in patients with peritoneal carcinosis. *J Clin Oncol* 2007; **25**: 3054-3054. doi: 10.1200/jco.2007.25.18\_suppl.3054
41. Conte PF, Accoto M, Nannipieri F, Baretta Z, Baldoni A, Bonanno L, et al. Phase II trial of intraperitoneal (IP) MHC unrestricted adoptive cell therapy with TALL-104 cells in patients with ovarian carcinoma (OC) with minimal or microscopic residual disease at second look laparotomy/laparoscopy. *Ann Oncol* 2015; **26**: viii10-viii11. doi: 10.1093/annonc/mdv514.21
42. Macián F, García-Cózar F, Im S-H, Horton HF, Byrne MC, Rao A. Transcriptional mechanisms underlying lymphocyte tolerance. *Cell* 2002; **109**: 719-31. doi: 10.1016/S0092-8674(02)00767-5
43. Martinez GJ, Pereira RM, Äijö T, Kim EY, Marangoni F, Pipkin ME, et al. The transcription factor NFAT promotes exhaustion of activated CD8<sup>+</sup> T cells. *Immunity* 2015; **42**: 265-78. doi: 10.1016/j.immuni.2015.01.006
44. Yamada A, Ishimaru N, Arakaki R, Katunuma N, Hayashi Y. Cathepsin L inhibition prevents murine autoimmune diabetes via suppression of CD8<sup>+</sup> T cell activity. *PLoS ONE* 2010; **5**. doi: 10.1371/journal.pone.0012894

# NADPH oxidase inhibitor VAS2870 prevents staurosporine-induced cell death in rat astrocytes

Janez Simenc, Damijana Mojca Juric, Metoda Lipnik-Stangelj

University of Ljubljana, Faculty of Medicine, Department of Pharmacology and Experimental Toxicology, Ljubljana, Slovenia

Radiol Oncol 2019; 53(1): 69-76.

Received 24 September 2018

Accepted 18 November 2018

Correspondence to: Prof. Metoda Lipnik-Stangelj, M.D., M.Pharm., Ph.D., University of Ljubljana, Faculty of Medicine, Department of Pharmacology and Experimental Toxicology, Korytkova ulica 2, SI-1000 Ljubljana, Slovenia. Phone: +386 1 5437330; E-mail: metoda.lipnik-stangelj@mf.uni-lj.si

Disclosure: No potential conflicts of interest were disclosed.

**Background.** Astrocytes maintain central nerve system homeostasis and are relatively resistant to cell death. Dysfunction of cell death mechanisms may underlie glioblastoma genesis and resistance to cancer therapy; therefore more detailed understanding of astrocytic death modalities is needed in order to design effective therapy. The purpose of this study was to determine the effect of VAS2870, a pan-NADPH oxidase inhibitor, on staurosporine-induced cell death in astrocytes.

**Materials and methods.** Cultured rat astrocytes were treated with staurosporine as activator of cell death. Cell viability, production of reactive oxygen species (ROS), and mitochondrial potential were examined using flow cytometric analysis, while chemiluminescence analysis was performed to assess caspase 3/7 activity and cellular ATP.

**Results.** We show here for the first time, that VAS2870 is able to prevent staurosporine-induced cell death. Staurosporine exerts its toxic effect through increased generation of ROS, while VAS2870 reduces the level of ROS. Further, VAS2870 partially restores mitochondrial inner membrane potential and level of ATP in staurosporine treated cells.

**Conclusions.** Staurosporine induces cell death in cultured rat astrocytes through oxidative stress. Generation of ROS, mitochondrial membrane potential and energy level are sensitive to VAS2870, which suggests NADPH oxidases as an important effector of cell death. Consequently, NADPH oxidases activation pathway could be an important target to modulate astrocytic death.

Key words: astrocytes; VAS2870; mitochondrial potential; ATP; reactive oxygen species; cell death

## Introduction

Astrocytes are the most abundant non-excitatory cell type in the central nervous system (CNS), where they play a key role in brain development and survival of neurons.<sup>1</sup> They maintain CNS homeostasis, modulate neuronal excitation, synaptic transmission and brain plasticity.<sup>2-5</sup> Generally, astrocytes are more robust than neurons and are highly resistant to apoptosis.<sup>6</sup> However, traumatic brain injury, infection, or various neurodegenerative diseases, with subsequent ischemia-hypoxia,

calcium overload or oxidative stress, can induce extensive astrocytic demise.<sup>7-9</sup> On the other hand, it is believed that the dysfunction of cell death in astrocytes underlies glioblastoma genesis, proliferation, and resistance to therapy.<sup>10-13</sup> Therefore, it is of immense importance to better understand cell death mechanisms in astroglial cells, either for the design of more effective therapies to prevent cell death in case of trauma and neurodegenerative disease, or to improve anti-cancer agents and limit the likelihood of resistance development in glioblastoma.

Diverse stimuli may induce cell death with distinctive molecular and cellular characteristics. In this sense, apoptosis is a form of regulated cell removal, mainly mediated by cysteine proteases-caspases and characterized by gradual cell degradation with intact plasma membrane till the late phase of the process.<sup>14</sup> On the contrary, necrosis is a cell death form which is independent of caspases and is characterized by rapid cell collapse due to early loss of plasma membrane integrity and dissipation of the mitochondrial transmembrane potential.<sup>15</sup> The membrane pores can release cytoplasmic components outside the cell, where they can evoke inflammatory response and additional cell loss.<sup>8,16</sup> Necrosis may happen accidental due to overwhelming stress, but may occur as another regulated form of cell death – necroptosis, mediated through receptor-interacting serine-threonine (RIP1 and RIP3) kinases activity.<sup>17</sup>

Degradation of electron transport chain may increase the production of reactive oxygen species (ROS) and hence contribute to apoptosis.<sup>18</sup> On the other hand the execution of necroptosis downstream of RIP kinases activity also depends on ROS overproduction. In addition to damaged mitochondria, another important source of ROS could be the nicotinamide adenine dinucleotide phosphate (NADPH) oxidases activity.<sup>19,20</sup> In the CNS, expression of several NADPH oxidase isoforms has been described in neurons, microglia and astrocytes, with different functions, both in health and disease.<sup>21,22</sup>

Previously we reported that staurosporine, a broad-spectrum protein kinase inhibitor, is able to trigger cell death in cultured rat cortical astrocytes through caspases dependent pathways as well as through RIP1 kinase activity.<sup>23,24</sup> Here we explored whether VAS2870, a pan-NADPH oxidase inhibitor, is able to inhibit staurosporine induced cell death in cultured rat astrocytes. Also, we checked how VAS2870 mechanically operates in preventing cell death, since we determined the effect of VAS2870 on staurosporine-induced ROS production, mitochondrial function and ATP level in cultured rat cortical astrocytes.

## Materials and methods

### Materials

Bovine serum albumin (BSA), Fetal bovine serum (FBS), L-15 Leibowitz medium, Dulbecco's modified Eagle medium and Ham's nutrient mixture F-12 (DMEM/F12), Penicillin (10,000 IU/

ml), Streptomycin (10,000 mg/ml), Dulbecco's phosphate buffered saline (PBS) were supplied from Gibco BRL, Life Technologies (Paisley, Scotland). Staurosporine, 3-benzyl-7-(2-benzoxazolyl) thio-1,2,3-triazolo[4,5-d]pyrimidine (VAS2870), 3,3'-dihexyloxacarbo-cyanide iodide (DiOC6(3)), and 2-7-dichlorodihydrofluorescein diacetate (DCFH-DA) were purchased from Sigma Chemicals (St. Louis, Missouri, USA). The pan-caspase inhibitor (z-vad-fmk) was purchased from R&D Systems (Minneapolis, Minnesota, USA). 7-Aminoactinomycin D (7-AAD) staining dye for flow cytometry was purchased from Beckman-Coulter, Inc. (Brea, California, USA). Bio-Rad protein assay kit was purchased from Bio-Rad Laboratories, München, Germany. 1,2-diaminocyclohexanetetraacetic acid (DCTA), dithiothreitol (DTT), Triton X-100, Tris-phosphate, and glycerol were supplied from Merck KGaA, Darmstadt, Germany. ATPlite 1-step assay system was supplied from Perkin Elmer, Boston, Massachusetts, USA. Caspase-Glo 3/7 Assay was purchased from Promega, Madison, Wisconsin, USA.

### Animals

New-born Wistar rats (1–2 days old) were obtained from our own breeding colony. The animals were kept under constant environmental conditions with an ambient temperature of 22°C, relative humidity 55%, and a natural light-dark cycle. The breeding colony was kept in Ehret type-4 cages (Emmerdingen, Germany). The bedding material was Lignocel 3/4 (Altromin, Lage, Germany). The colony received a standard rodent diet (Altromin, Germany), and had free access to food and water. All animal studies were approved by the Veterinary Authority of the Republic of Slovenia (License number: 34401-7/2012/3), and performed in accordance with the EU Directive 2010/63/EU and the European Convention for the protection of vertebrate animals used for experimental and other scientific purposes (ETS 123).

### Cell cultures

Cultures of rat cortical astrocytes were prepared from the brain of new-born rats in DMEM/F12 (1:1), 10 % FBS, 1 % Penicillin-Streptomycin culture medium as described previously.<sup>24</sup> The cells were grown in tissue culture flasks at 37°C in a humidified environment containing 10% CO<sub>2</sub> until they became confluent (10 to 12 days). In order to reduce microglia contamination, confluent cultures

were shaken at 150 rpm for a day. After shaking, the cells were trypsinized, reseeded onto 35 mm Petri dishes (approx.  $1 \times 10^6$  cells/ml) and grown for the next 5 to 7 days. When the cultures reached confluence, they were used for the treatment. The purity of the cell culture (> 98% of astrocytes) was checked using immuno-cytochemical staining for the glial fibrillary acidic protein, which is the major component of the astrocyte cytoskeleton.

### Induction and inhibition of cell death

After the cultures became confluent, culture medium was replaced with 1 ml of fresh serum-free medium. Then the cells were treated with 1  $\mu$ M staurosporine for 3 hours, to induce cell death. After the treatment, the cells were allowed to regenerate for 22 hours in a staurosporine-free medium. The control cells were not exposed to staurosporine.

For the inhibition experiments, the cells were pre-treated with 5 and 10  $\mu$ M VAS2870 or 20  $\mu$ M z-vad-fmk, 1 hour before 1  $\mu$ M staurosporine was added. Then the cells were incubated for an additional 3 hours. The cells were then regenerated in the staurosporine, VAS2870 and z-vad-fmk free medium for 22 hours. The cells were also exposed to 5 and 10  $\mu$ M VAS2870 or to 20  $\mu$ M z-vad-fmk only for 3 hours and allowed to regenerate in an inhibitor-free medium for 22 hours.

For the testing of viability, ROS and mitochondrial potential, the cells were trypsinized and stained for an analysis in a flow cytometer. For the detection of caspases-3/7 activity and level of cellular ATP, the cells were harvested and solubilized in a cell culture lysis buffer.

### Viability determination

The cells from individual dishes ( $1-5 \times 10^6$  cells/ml) were stained with 7-AAD viability dye, according to the manufacturer's protocol. Briefly, the cells were harvested and washed in the ice cold PBS (500  $\mu$ l). Then the cells were re-suspended in 100 ml PBS buffer with 1% BSA and 0.1%  $\text{NaN}_3$ . The cell suspension was stained with 20 ml of 7-AAD solution and incubated at 4°C for 15 minutes. After the incubation, an additional 400  $\mu$ l PBS buffer with 1% BSA and 0.1%  $\text{NaN}_3$  was added. Aliquots (200  $\mu$ l) of cell suspensions were analysed on the Quanta SC MPL flow cytometer (Beckman Coulter, USA) with 488 nm argon laser. In each sample, approximately 5.000 cells were gated. Gating was done in a hierarchical fashion. First, total cell population was identified by plotting electronic volume (EV) ver-

sus side scatter (SSC). High EV and SSC population was gated. Next, viability (red fluorescence) scatter gate was used to identify dead cells. Three populations were observed: viable, dim and positive. The positive population (high red signal) was considered dead. The dead population was identified and gated by comparison of treated cells to untreated (negative) controls.

### Detection of caspases-3/7 activity and cellular ATP

Harvested cells from individual dishes were solubilized in a 150  $\mu$ l of cell culture lysis buffer (250 mM Tris-phosphate pH 7.8, 2 mM DCTA, 2 mM DTT, 1% Triton X-100, 10% glycerol). Aliquots (5  $\mu$ l) of cell samples were used for determination of protein concentrations by Bio-Rad protein assay kit. Cellular ATP concentration was determined with the ATPlite 1-step assay system as described in the manufacturer's manual. The chemiluminescent signals were measured by a Synergy HT microplate reader (BioTek USA). The amount of ATP in each sample, diluted to contain 1 mg protein/mL, was calculated using a generated standard ATP curve (1 pM - 1 mM). The same samples were used for detection of caspases-3/7 activity by Caspase-Glo 3/7 Assay (Promega, Madison, USA) as described in the manufacturer's manual.

### Detection of ROS and mitochondrial potential

After the treatment, the cells ( $1-5 \times 10^6$  cells/ml) were harvested and washed in the PBS (500  $\mu$ l). For the detection of ROS production, the cells were re-suspended in 500 ml of PBS at room temperature and stained with 2  $\mu$ M DCFH-DA, as proposed by manufacturer's protocol. Similar, for the detection of inner mitochondrial membrane potential, the cells were stained with 100 nM DiOC6(3), as described in the manufacturer's manual. After the staining for either the detection of ROS or mitochondrial potential, the cell suspensions were incubated at 37°C for 30 minutes. Aliquots (200  $\mu$ l) of cell suspensions were analysed on the Quanta SC MPL flow cytometer (Beckman Coulter, USA) with 488 nm argon laser. Gating was done in a hierarchical fashion. First, total cell population (approximately 5.000 cells) was identified by plotting EV versus SSC. High EV and SSC population was gated. Then ROS (green fluorescence) scatter plot was used to identify the level of ROS and untreated (negative) controls were used to set the gate for

high ROS population. Similar strategy was used for the identification of low mitochondrial membrane potential cell population. First, high EV and SSC population was identified. Next, green fluorescent histogram was plotted with marker showing low potential population. As previously, untreated (negative) cells were used to identify low mitochondrial membrane cell population.

### Statistical analyses

All data are presented as a mean  $\pm$  SEM of three to five determinations from five independent experiments. Data analysis was performed using Graph Pad Prism 5.0 (Graph Pad Software, Inc., USA). The statistical significance of differences between various groups was evaluated using one-way ANOVA followed by the Tukey multiple comparison test. A p value of  $< 0.05$  was considered to be statistically significant.

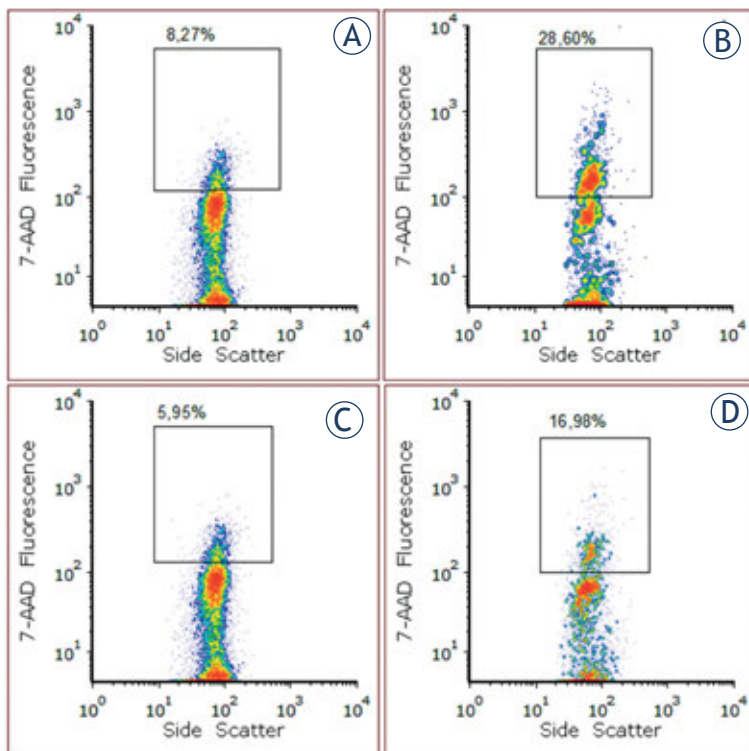


**FIGURE 1.** The effect of staurosporine on viability of rat astrocytes. Representative flow cytometric experiment is showing the uptake of 7-AAD vital dye in rat astrocytes. The percentages of dead cells with high red fluorescence intensity are shown in rectangular regions. (A) The control cells were not treated. (B) The cells were exposed to 1  $\mu$ M staurosporine. (C) The cells were exposed to 10  $\mu$ M VAS2870. (D) The cells were pre-treated with 10  $\mu$ M VAS2870 and exposed to 1  $\mu$ M staurosporine. (E) The percentages of dead cells as determined by 7-AAD uptake. (Con) The control cells were not treated. (STS) The cells were exposed to 1  $\mu$ M staurosporine. (STS+VAS2870) The cells were pre-treated with 5 or 10  $\mu$ M VAS2870 and exposed to 1  $\mu$ M staurosporine. (VAS2870) The cells were exposed to 5 or 10  $\mu$ M VAS2870. Data were analysed using one-way ANOVA and a Tukey multiple comparison test; p  $< 0.05$  indicates significance.

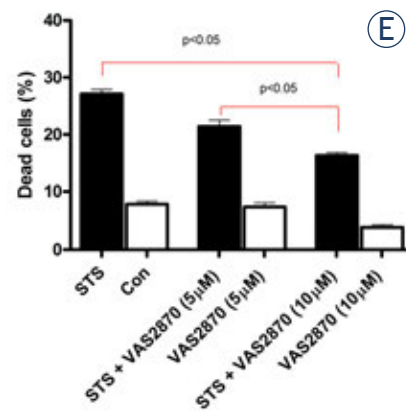
## Results

### VAS2870 inhibits staurosporine-induced cell death in astrocytes

3 h treatment with 1  $\mu$ M staurosporine revealed a significant cytotoxic effect on cultured astrocytes causing 27.1  $\pm$  0.8% decrease of viability as detected by high red fluorescent signal in a flow cytometry (Figure 1). Pre-treatment with 5  $\mu$ M VAS2870 reduced cell death by 1.3-fold, whereas 10  $\mu$ M VAS2870 diminished staurosporine-triggered cell death even more, by 1.7-fold. In untreated control cells, on average 7.8  $\pm$  0.6% of dead cells was detected. The proportions of dead cells in the culture exposed to VAS2870 alone were low and did not differ significantly from the untreated controls (Figure 1).

### Staurosporine induces caspases-3/7 activity and reduces level of ATP in rat astrocytes

1  $\mu$ M staurosporine activated caspases-3/7 (Figure 2A), a key indicator of the execution phase of apoptotic cell death. While pre-incubation of cultured astrocytes with 20  $\mu$ M z-vad-fmk lowered the activity of caspases-3/7 by 13.9-fold in comparison to the cells, treated by staurosporine alone, pre-treatment of the cells with 10  $\mu$ M VAS2870 did not significantly inhibit caspases-3/7 activity. In the untreated controls, VAS2870 or z-vad-fmk caused no caspases-3/7 activation.



Furthermore, staurosporine critically reduced cellular energetic supply in astrocytes, decreasing the level of intracellular ATP by 15.9-fold compared to untreated controls, which represents 0.59 +/- 0.08 nM ATP/mg cell protein. While in the cells, pre-treated with z-vad-fmk, the level of ATP remained low and did not differ significantly from the staurosporine treated cells (Figure 2B), pre-treatment of the cells with VAS2870 partially reversed the level of ATP, which represents 6.51-fold enhancement in comparison to the cells, treated by staurosporine. In the cells, exposed to either VAS2870 or z-vad-fmk only, the level of ATP remained high and did not differ significantly from the untreated cells (9.30 +/- 0.56 nM ATP/mg cell protein) (Figure 2B).

### VAS2870 reduces level of ROS in rat astrocytes

VAS2870 (5 and 10 µM) was applied to staurosporine-treated cells as a putative inhibitor of ROS production. Detection of ROS was performed with DCFH-DA probe by flow cytometry. In each exper-

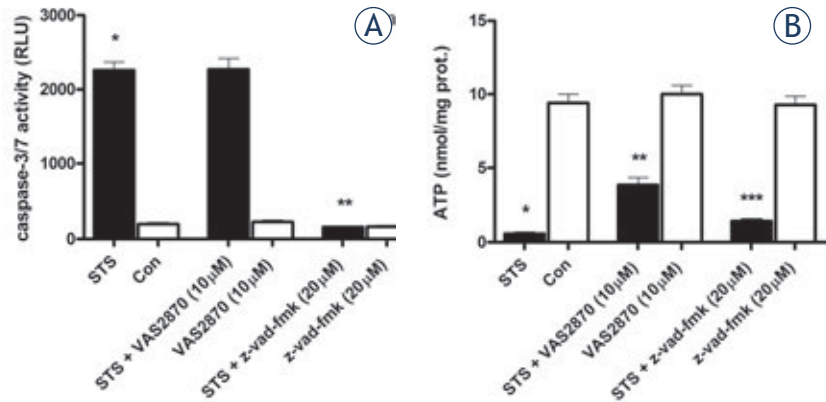


**FIGURE 2.** (A) The effect of staurosporine on caspases-3/7 activation and (B) level of intracellular ATP. (STS) The cells were exposed to 1 µM staurosporine. (Con) The control cells were not treated. (STS+VAS2870) The cells were pre-treated with 10 µM VAS2870 and exposed to 1 µM staurosporine. (VAS2870) The cells were exposed to 10 µM VAS2870. (STS + z-vad-fmk) The cells were pre-treated with 20 µM z-vad-fmk and exposed to 1 µM staurosporine. (z-vad-fmk) The cells were exposed to 20 µM z-vad-fmk. Data were analysed using one-way ANOVA and a Tukey multiple comparison test; \*p < 0.05 vs. Con, \*\*p < 0.05 vs. STS, \*\*\*p < 0.05 vs STS + VAS2870 indicate significance. RLU- relative luminescence units.

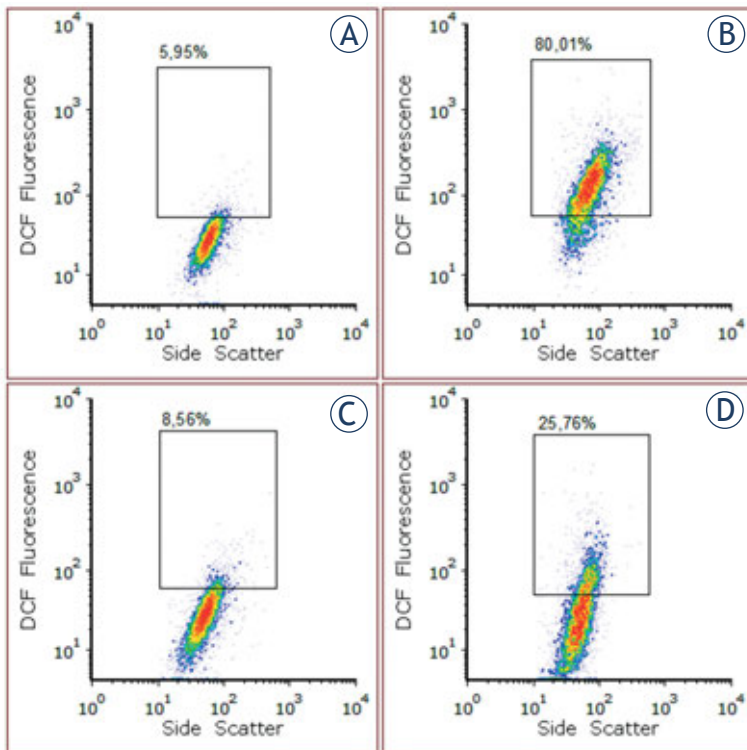


**FIGURE 3.** Representative flow cytometric experiment is showing detection of ROS production in rat astrocytes after staurosporine activation. The percentages of cells with high DCF fluorescence intensity are shown in rectangular regions. (A) Untreated control cells. (B) The cells were exposed to 1 µM staurosporine. (C) The cells were exposed to 10 µM VAS2870. (d) The cells were pre-treated with 10 µM VAS2870 and exposed to 1 µM staurosporine. (E) Production of ROS, detected as the percentage of cells with high DCF fluorescence intensity. (STS) The cells were exposed to 1 µM staurosporine. (Con) Untreated control cells. (STS + VAS2870) The cells were pre-treated with 5 or 10 µM VAS2870 and exposed to 1 µM staurosporine. (VAS2870) The cells were exposed to 5 or 10 µM VAS2870. Data were analysed using one-way ANOVA and a Tukey multiple comparison test; p < 0.05 indicates significance.

iment, fluorescence intensity of dichlorofluorescein (DCF), a product of DCFH-DA degradation and oxidation, was detected (Figure 3A-D). The results showed that 1 µM staurosporine induces ROS production; on average 81.6 +/- 1.8% of DCF fluorescent cells was detected (Figure 3E) and ROS production was increased by 10.2-fold. Pre-treatment with 5 µM VAS2870 reduced the levels of ROS by 1.6-fold, while 10 µM VAS2870 diminished ROS

levels 3.0-fold compared to the cells, treated by staurosporine (Figure 3E). VAS2870 itself showed no influence on ROS production (Figure 3E).

### VAS2870 restores mitochondrial potential in rat astrocytes

The potential of inner mitochondrial membrane ( $\Delta\psi_m$ ) was measured with DiOC6(3) potentiometric dye using flow cytometry. DiOC6(3) is taken up into the healthy cell and distributed across the inner mitochondrial membrane. The collapse of proton gradient across inner mitochondrial membrane of dying cells results in the loss of DiOC6(3) and hence loss of fluorescence intensity. In each experiment, green fluorescent signal of DiOC6(3) was analysed, identifying regions with low fluorescence intensity. As depicted in the representative flow cytometric experiment (Figure 4), 1  $\mu\text{M}$  staurosporine potently reduced mitochondrial potential. The proportion of the cells with low mitochondrial potential was increased by 7.3-fold as compared to untreated controls (Figure 4B, E), while the untreated control cells and VAS2870 treated cells yielded a high fluorescent signal (Figure 4A, C). When astrocytes were pre-incubated with 5  $\mu\text{M}$  VAS2870, the potential was partially restored (Figure 4E), whereas 10  $\mu\text{M}$  VAS2870 restored the potential even more, as evidenced by 2.6-fold decrease of low potential cells compared to staurosporine only treated cells (Figure 4D, E).

## Discussion

Astroglial cells death could be executed through different pathways, where increased production of ROS plays a critical role. In the present work, we triggered cell death in rat cortical astrocytes by staurosporine which is known to induce caspases-dependent and -independent cell death in many cell types,<sup>25,26</sup> including astrocytes.<sup>24,27</sup> Indeed, staurosporine significantly increased proportion of death cells, as indicated by the bright population of 7-AAD positive cells (Figure 1).

Staurosporine increased caspases-3/7 activity, which indicates apoptosis (Figure 2A). Further, the production of ATP in astrocytes was significantly reduced, which surprisingly could not be preserved by pan-caspase inhibitor (Figure 2B). This observation suggests that necroptosis also occurred, which is in accordance with the findings of Leist *et al.*<sup>28</sup>, where depletion of intracellular ATP has been associated with a switch from apoptosis to necroptosis. It seems that in our experimental model, both forms of cell death coexist. This is in line with our previous report, where we showed that staurosporine-induced cell death in rat cortical astrocytes could be partially inhibited by necrostatin-1, an inhibitor of RIP1 kinase activity.<sup>24</sup> Similar observation was described in neurons, where staurosporine at higher concentrations induced necroptosis and not apoptosis.<sup>29</sup> Importantly, as shown in Figure 1, VAS2870 reduced cell death, triggered by staurosporine

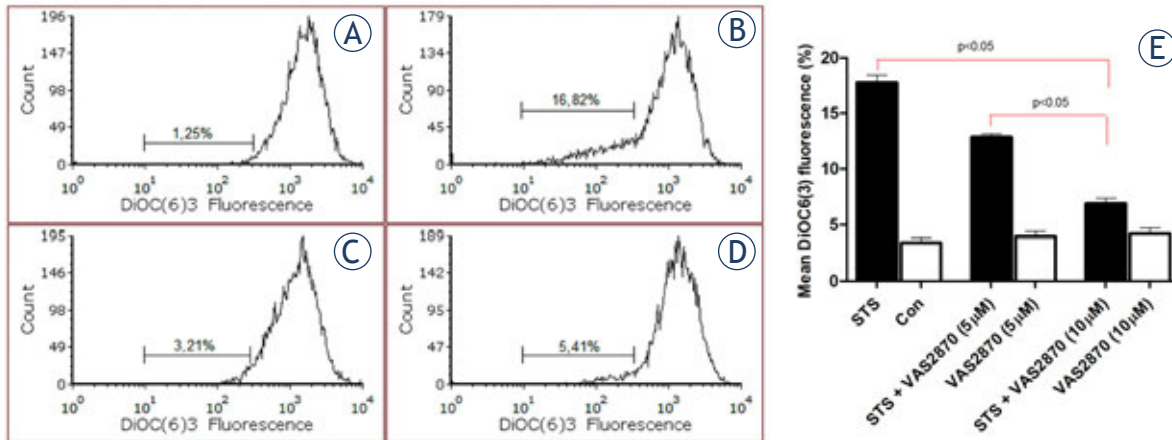


**FIGURE 4.** A representative flow cytometric experiment is showing the DiOC6(3) fluorescence intensity in rat astrocytes. The markers show the percentage of cells with reduced mitochondrial potential. **(A)** Untreated control cells. **(B)** The cells were exposed to 1  $\mu\text{M}$  staurosporine. **(C)** The cells were exposed to 10  $\mu\text{M}$  VAS2870. **(D)** The cells were pre-treated with 10  $\mu\text{M}$  VAS2870 and exposed to 1  $\mu\text{M}$  staurosporine. **(E)** The reduction of mitochondrial potential, detected as the percentage of low DiOC6(3) fluorescence. (STS) The cells were exposed to 1  $\mu\text{M}$  staurosporine. (Con) Untreated control cells. (STS+VAS2870) The cells were pre-treated with 5 or 10  $\mu\text{M}$  VAS2870 and exposed to 1  $\mu\text{M}$  staurosporine. (VAS2870) The cells were exposed to 5 or 10  $\mu\text{M}$  VAS2870. Data were analysed using one-way ANOVA and a Tukey multiple comparison test;  $p < 0.05$  indicates significance.

and, contrary to z-vad-fmk, VAS2870 also significantly preserved the level of ATP (Figure 2B). Since VAS2870 has been shown as a specific pan-NADPH oxidase inhibitor<sup>30</sup>, our observations indicate that necroptosis could be mediated through NADPH oxidases activity. However other anti-necrotic or pro-survival effects of VAS2870 could not be excluded and require further investigation.

The programmed cell death, in particular necroptosis, is executed through increased generation of ROS in several cell types,<sup>19,31</sup> including rat astrocytes.<sup>23</sup> Since VAS2870 operates as a powerful inhibitor of ROS generation, we explored the influence of VAS2870 on ROS production. Indeed, as shown in Figure 3E, VAS2870 significantly reduced ROS production at concentrations where probably does not act as an antioxidant.<sup>30</sup> However, in the untreated control cells, some basic level of ROS still remained which may be due to ROS generation at the mitochondrial respiratory chain, as has been shown by Vanlangenakker *et al.*<sup>32</sup> Functionally, staurosporine generates oxidative stress as underlying mechanisms of cell death in cultured rat astrocytes and this mechanism is sensitive to VAS2870. Similar to our observations, staurosporine-induced cell demise and ROS generation in cultured rat astrocytes was efficiently reduced by broad serine protease inhibitor - AEBSF.<sup>33</sup> Our results are also in agreement with the model of necroptosis, triggered by hemin in mouse astrocytes, where hemin induced necroptosis through increased ROS and rapid depletion of intracellular reduced glutathione, while necroptosis, ROS and glutathione depletion were significantly reduced by apocynin, another pharmacological inhibitor of NADPH oxidases.<sup>34</sup> Overall, these observations indicate that NADPH oxidases are an effector of cell death in astrocytes. If this is the case, it remains to be established, how the NADPH oxidases are activated to mediate cell death. One possibility is that they are activated in the necrosome, as has been shown in L929 and MEF cells during tumour necrosis factor induced necroptosis.<sup>31</sup> Alternatively, the NADPH oxidases may mediate cell death independently of necrosome; however, both signalling pathways are needed. Interestingly, Liu *et al.*<sup>35</sup> reported that activation of NADPH oxidases and increased ROS are necessary for astrocytes to survive when challenged with calcium ionophore or opsonized zymosan. Taken together, these findings suggest a pivotal role of NADPH oxidases both in astrocyte survival and death under chemical stress or pathological conditions.

In astrocytes, mitochondrial function is fundamental for maintaining the energetic balance of the brain and antioxidant production that contributes to neuronal protection.<sup>36</sup> Due to high amounts of redox enzymes with sulphur iron centres in the mitochondria, we reasoned that ROS could have an adverse effect on the mitochondrial potential and thus we analysed the potential of inner mitochondrial membrane. As shown in Figure 4, staurosporine indeed reduced the inner mitochondrial membrane potential, while the potential was almost restored when the cells were pre-treated with VAS2870. This observation is corroborated with partially restored level of ATP in VAS2870 pre-treated cells. Mitochondrial depolarization is a part of cell death execution and it can be limited by VAS2870, hence it may operate downstream of NADPH oxidases activity. At least part of ROS is exogenous, probably derived either from cell-membrane or mitochondrial NADPH oxidases.<sup>37</sup> Therefore mitochondria are also the target and not only the source of ROS. In contrast to our observation, Remijsen *et al.*<sup>38</sup> demonstrated in L929 cells that mitochondrial depolarization does not occur during tumour necrosis factor induced cell death. The mitochondrial depolarization during necroptosis seems to depend on the cell type or the exact stimulus to initiate cell death.

## Conclusions

Our results show that staurosporine-induced cell death in rat astrocytes involves generation of ROS, and is sensitive to VAS2870. Also, mitochondrial depolarization and depletion of ATP are part of cell death process and may be partially reversed by VAS2870. We conclude that NADPH oxidases activation pathway may be useful target to execute cell death. In addition, our observations add to the recognition of astrocytes as an important source of ROS, which may significantly contribute to various pathologies, such as traumatic brain injury, haemorrhagic stroke, neurodegenerative disorders and cancer.

## Acknowledgement

The authors acknowledge the financial support from the Slovenian Research Agency (research core funding No. P3-0067). The authors wish to thank Mojca Kranjec for her excellent technical assistance.

## References

- Wozniak W. Ependymal cells and astrocytes generate neurones. *Folia Morphol (Warsz)* 1999; **58(3 Suppl 2)**: 7-11. PMID: 10959256
- Magistretti PJ, Pellerin L. Astrocytes couple synaptic activity to glucose utilization in the brain. *News Physiol Sci* 1999; **14**: 177-82. PMID: 11390847
- Perea G, Araque A. Astrocytes potentiate transmitter release at single hippocampal synapses. *Science* 2007; **317**: 1083-86. doi: 10.1126/science.1144640
- Stogsdill JA, Ramirez J, Liu D, Kim, YH, Baldwin KT, Enustun E, et al. Astrocytic neurotrophins control astrocyte morphogenesis and synaptogenesis. *Nature* 2017; **551**: 192-97. doi: 10.1038/nature24638
- Papouin T, Dunphy J, Tolman M, Foley JC, Haydon PG. Astrocytic control of synaptic function. *Philos Trans R Soc Lond B Biol Sci* 2017; **5**: 372(1715) pii:20160154. doi: 10.1098/rstb.2016.0154
- Song JH, Bellail A, Tse CLM, Yong Wee V, Hao C. Human astrocytes are resistant to Fas ligand and Tumor necrosis factor related apoptosis inducing ligand induced apoptosis. *J Neurosci* 2006; **26**: 3299-308. doi: 10.1523/JNEUROSCI.5572-05.2006
- Jurič DM, FINDERLE Ž, ŠUPUT D, BRVAR M. The effectiveness of oxygen therapy in carbon monoxide poisoning is pressure- and time-dependent: a study on cultured astrocytes. *Toxicol Lett* 2015; **233**: 16-23. doi: 10.1016/j.toxlet.2015.01.004
- Leyns CEG, Holtzman D. Glial contributions to neurodegeneration in tauopathies. *Mol Neurodegener* 2017; **12**: 50. doi: 10.1186/s13024-017-0192-x
- Dos Santos AA, López-Granero C, Farina M, Rocha JBT, Bowman AB, Aschner M. Oxidative stress, caspase-3 activation and cleavage of ROCK-1 play an essential role in MeHg-induced cell death in primary astroglial cells. *Food Chem Toxicol* 2018; **113**: 328-36. doi: 10.1016/j.fct.2018.01.057
- Jiang YG, Peng Y, Koussougbo KS. Necroptosis: a novel therapeutic target for glioblastoma. *Med Hypotheses* 2011; **76**: 350-52. doi: 10.1016/j.mehy.2010.10.037
- Fulda S. Cell death-based treatment of glioblastoma. *Cell Death Dis* 2018; **9**: 121. doi: 10.1038/s41419-017-0021-8
- Smrđel U, Skoblar-Vidmar M, Smrđel A. Glioblastoma in patients over 70 years of age. *Radiol Oncol* 2018; **52**: 167-72. doi: 10.2478/raon-2018-0010
- Kazda T, Dziacky A, Burkon P, Pospisil P, Slavik M, Rehak Z, et al. Daily clinical radiotherapy of glioblastoma 15 years after the landmark Stupp' trial: more controversies than standards? *Radiol Oncol* 2018; **52**: 121-8. doi: 10.2478/raon-2018-0023
- Taylor RC, Cullen SP, Martin SJ. Apoptosis: controlled demolition at the cellular level. *Nature Rev* 2008; **9**: 231-41. doi: 10.1038/nrm2312
- Degterev A, Huang Z, Boyce M, Li Y, Jagtap P, Mizushima N, et al. Chemical inhibitor of nonapoptotic cell death with therapeutic potential for ischemic brain injury. *Nat Chem Biol* 2005; **2**: 112-9. doi: 10.1038/nchembio711
- Scaffidi P, Misteli T, Bianchi ME. Release of chromatin protein HMGB1 by necrotic cells triggers inflammation. *Nature* 2002; **418**: 191-5. doi: 10.1038/nature00858
- Oberst A, Dillon CP, Weinlich R, McCormick LL, Fitzgerald P, Pop C, et al. Catalytic activity of the caspase-8-FLIP(L) complex inhibits RIPK3 dependent necrosis. *Nature* 2011; **471**: 363-7. doi: 10.1038/nrm3214
- Ricci JE, Muñoz-Pinedo C, Fitzgerald P, Bailly-Maitre B, Perkins GA, Yadava N, et al. Disruption of mitochondrial function during apoptosis is mediated by caspase cleavage of the p75 subunit of complex I of the electron transport chain. *Cell* 2004; **117**: 773-86. doi: 10.1016/j.cell.2004.05.008
- Zhang DW, Shao J, Lin J, Zhang N, Lu BJ, Lin SC, et al. RIP3, an energy metabolism regulator that switches TNF-induced cell death from apoptosis to necrosis. *Science* 2009; **325**: 332-6. doi: 10.1126/science.1172308
- Dong W, Li Z, Chen Y, Zhang L, Ye Z, Liang H, et al. NADPH oxidase inhibitor, diphenyleneiodonium prevents necroptosis in HK-2 cells. *Biomed Rep* 2017; **7**: 226-30. doi: 10.3892/br.2017.948
- Nayernia Z, Jaquet V, Krause KH. New insights on NOX enzymes in the central nervous system. *Antioxid Redox Signal* 2014; **20**: 2815-37. doi: 10.1089/ars.2013.5703
- Haslund-Vinding J, McBean G, Jaquet V, Vilhardt F. NADPH oxidases in oxidant production by microglia: activating receptors, pharmacology and association with disease. *Br J Pharmacol* 2017; **174**: 1733-49. doi: 10.1111/bph.13425
- Simenc J, Lipnik-Stangelj M. Staurosporine induces different cell death forms in cultured rat astrocytes. *Radiol Oncol* 2012; **46**: 312-20. doi: 10.2478/v10019-012-0036-9
- Šimenc J, Lipnik-Štangelj M. Staurosporine induces apoptosis and necroptosis in cultured rat astrocytes. *Drug Chem Toxicol* 2012; **35**: 399-405. doi: 10.3109/01480545.2011.633087
- Belmokhtar AC, Hillion J, Segal-Bendirdjian E. Staurosporine induces apoptosis through both caspase-dependent and caspase-independent mechanisms. *Oncogene* 2001; **20**: 3354-62. doi: 10.1038/sj.onc.1204436
- Zhang XD, Gillespie SK, Hersey P. Staurosporine induces apoptosis of melanoma by both caspase dependent and independent apoptotic pathways. *Mol Cancer Ther* 2004; **3**: 187-97. PMID: 14985459
- D'Alimonte I, Ballerini P, Nargi E, Buccella S, Giuliani P, Di Iorio P, et al. Staurosporine-induced apoptosis in astrocytes is prevented by A1 adenosine receptor activation. *Neurosci Lett* 2007; **418**: 66-71. doi: 10.1016/j.neulet.2007.02.061
- Leist M, Single B, Castoldi AF, Kühnle S, Nicotera P. Intracellular adenosine triphosphate (ATP) concentration: a switch in the decision between apoptosis and necrosis. *J Exp Med* 1997; **8**: 1481-6. doi: 10.1084/jem.185.8.1481
- Jantas D, Krawczyk S, Lason W. The predominant protective effect of tianeptine over other antidepressants in models of neuronal apoptosis: the effect blocked by inhibitors of MAPK/ERK1/2 and PI3-K/Akt pathways. *Neurotox Res* 2014; **25**: 208-25. doi: 10.1007/s12640-013-9430-3
- ten Freyhaus H, Huntgeburth M, Wiegler K, Schitker J, Bäumer AT, Vantler M, et al. Novel Nox inhibitor VAS2870 attenuates PDGF dependent smooth muscle cell chemotaxis, but not proliferation. *Cardiovasc Res* 2006; **71**: 331-41. doi: 10.1016/j.cardiores.2006.01.022
- Kim SY, Morgan MJ, Choksi S, Liu ZG. TNF induced activation of the Nox 1 NADPH oxidase and its role in the induction of necrotic cell death. *Mol Cell* 2007; **26**: 675-87. doi: 10.1016/j.molcel.2007.04.021
- Vanlangenakker N, Vanden Berghe T, Bogaert P, Laukenc B, Zobel K, Deshayes K, et al. cIAP1 and TAK1 protect cells from TNF induced necrosis by preventing RIP1/RIP3 dependent reactive oxygen species production. *Cell Death Differ* 2011; **18**: 656-65. doi: 10.1038/cdd.2010
- Olguin-Albuerna M, Domínguez G, Morán J. Effect of staurosporine in the morphology and viability of cerebellar astrocytes: role of reactive oxygen species and NADPH oxidase. *Oxid Med Cell Longev* 2014; **2014**: 678371. doi: 10.1155/2014/678371
- Laird MD, Wakade C, Alleyne CH, Dhandapani KM. Hemin induced necroptosis involves glutathione depletion in mouse astrocytes. *Free Radic Biol Med* 2008; **45**: 1103-14. doi: 10.1016/j.freeradbiomed.2008.07.003
- Liu Q, Kang JH, Zheng RL. NADPH oxidase produces reactive oxygen species and maintain survival of rat astrocytes. *Cell Biochem Funct* 2005; **2**: 93-100. doi: 10.1002/cbf.1171
- Cabezas R, El-Bachá RS, González J, Barreto GE. Mitochondrial functions in astrocytes: neuroprotective implications from oxidative damage by rotenone. *Neurosci Res* 2012; **74**: 80-90. doi: 10.1016/j.neures.2012.07.008
- Kozielec R, Pircher H, Kratochwil M, Lener B, Hermann M, Dencher NA, et al. Mitochondrial respiratory chain complex I is inactivated by NADPH oxidase Nox 4. *Biochem J* 2013; **452**: 231-9. doi: 10.1042/BJ20121778
- Remijsen Q, Goossens V, Grootjans S, Van de Haute C, Vanlangenakker N, Dondelinger Y, et al. Depletion of RIPK3 or MLKL blocks TNF-driven necroptosis and switches towards a delayed RIPK1 kinase-dependent apoptosis. *Cell Death Dis* 2014; **5**: e1004. doi: 10.1038/cddis.2013.531

# Ultralow anterior resection with implantation of gentamicin-collagen sponge and no defunctioning stoma: anastomotic leakage and local cancer relapse

Tomasz Michalik<sup>1</sup>, Rafał Matkowski<sup>1,2</sup>, Przemysław Biecek<sup>3</sup>, Józef Forgacz<sup>1</sup>, Bartłomiej Szynglarewicz<sup>1,2</sup>

<sup>1</sup> Department of Surgical Oncology, Lower Silesian Oncology Centre - Regional Comprehensive Cancer Centre, Wrocław, Poland

<sup>2</sup> Department of Oncology, Faculty of Postgraduate Medical Training, Wrocław Medical University, Wrocław, Poland

<sup>3</sup> Faculty of Mathematics and Information Science, Warsaw University of Technology, Warsaw, Poland

Radiol Oncol 2019; 53(1): 77-84.

Received 7 November 2018

Accepted 10 January 2019

Correspondence to: Dr. Bartłomiej Szynglarewicz, Assoc. Prof.; Department of Oncology, Wrocław Medical University, and Department of Surgical Oncology, Lower Silesian Oncology Centre - Regional Comprehensive Cancer Centre, Plac Hirszfelda 12, 53413 Wrocław, Poland. Phone: +48 071 3689391; Fax: +48 071 3619111; E-mail: szynglarewicz.b@dco.com.pl

Disclosure: No potential conflicts of interest were disclosed.

**Background.** Anterior resection with total mesorectal excision (TME) of ultralow rectal cancer may result in the increased risk of the anastomotic leakage (AL). The aim of this study was to evaluate the usefulness of the gentamicin-collagen sponge (GCS) for the protection against symptomatic AL and investigate association between AL and local relapse (LR).

**Patients and methods.** A series of 158 patients with ultralow rectal cancer was studied. All the patients underwent R0 sphincter-saving TME with anastomosis wrapping using GCS. In none of the cases a temporary protective stoma was constructed.

**Results.** AL rate was 3.2% (5/158) while median time to AL diagnosis was 5 days following surgery (range 3-15). There was no postoperative and leakage-related mortality. Patient age > 75 years and smoking were independent risk factors related to significantly increased AL rate: 12.5% vs. 0.8% ( $P = 0.0004$ ) and 5.7% vs. 0% ( $P = 0.043$ ), respectively. LR was observed in 12% of cases. It was highly significantly more common and developed earlier in patients who have had AL when compared with non-AL group: 80% vs. 9% ( $P = 0.00001$ ) and 8.5 vs. 17 months ( $P = 0.014$ ), respectively.

**Conclusions.** Anastomosis wrapping with GCS after anterior resection with TME is a safe procedure resulting in the low incidence of anastomotic leakage which may be also associated with decreased risk of local relapse.

Key words: rectal cancer; anterior resection; total mesorectal excision; anastomotic leakage; gentamicin-collagen sponge

## Introduction

Because of effective local control, total mesorectal excision (TME) is nowadays the mainstay of curative treatment in rectal cancer. However, sphincter-saving TME may result in the increased risk of the anastomotic leakage (AL) due to the short rectal remnant and local oxygen tissue deficiency

in anastomosis associated with the reduced distal blood supply. Moreover, this technique produces the large splinted cavity within the pelvis, conducive to the exudate retention and the formation of haematoma, which may become infected. Reported rates of AL following TME are up to even 23%, being influenced by several patient-, tumour- and treatment related factors.<sup>1,2</sup> As a result of even

minor leakage, local contamination at the perirectal area may be the cause of extra-abdominal infection. The presence of AL is closely associated with the increased risk of pelvic abscess, peritonitis and septicemia, which commonly require additional intervention, prolong hospital stay, limit the cost-effectiveness of treatment and may result in post-operative death. It impairs late functional results and probably oncological outcomes.<sup>2</sup>

On the other hand, the recent emergence of technologies such as resorbable implants offers new possibilities to protect the anastomosis and reduce the consequences of leakage. Hence we reported the wrapping of anastomosis with the gentamicin-collagen sponge (GCS) as a potential preventive manoeuvre against the AL – probably limiting the leakage intensity and reducing its clinical symptoms.<sup>3,4</sup> It encouraged us to continue the study with more patients and longer follow-up in order to obtain more reliable and objective results as well as for more robust statistics.

The aim of this study was to evaluate the possible impact of GCS on the risk of clinically symptomatic AL and investigate association between AL and local relapse.

## Patients and methods

### Patients

A series of 158 patients with T1-T3 and N-/N+ ultra-low rectal cancer (below 8 cm from the anal verge) without distant metastases (M0) who underwent anterior resection with curative intent at the Lower Silesian Oncology Centre – Regional Comprehensive Cancer Centre in the years 2006 - 2012 was studied. None of them was in poor general condition, had anaemia or was treated with steroids. Patients underwent pre-operative bowel preparation with 4 L polyethylene glycol solution 1 day before surgery. All patients received prophylactic systemic antibiotic therapy in a perioperative intravenous injection within 30 minutes of the skin incision (cefotaxime 1000 mg i.v. followed by a supplementary dose 12 h later; metronidazole 500 mg i.v. followed by two more supplementary doses every 8 h) and anticoagulant therapy with low molecular weight heparin. All the patients underwent traditional open surgery through a midline laparotomy incision. All analysed patients fulfilled the following study inclusion criteria: the lack of intraoperative bowel perforation, total integrity of doughnuts after retrieval of the stapler and complete integrity of the anastomosis examined by transanal air insufflation with the anastomosis immersed in warm normal saline solution.

Patients data, tumour-related factors and treatment characteristics are shown in Table 1.

### Treatment

Sixty-five (41%) patients with T3 and / or N+ tumours in MRI or endorectal ultrasound received preoperative five-day scheduled high-dose radiation with a total dose of 25 Gy in a daily fractions of 5 Gy. Since in our institution the use of preoperative chemotherapy was limited to T4 tumours (combined with long-term radiation), it was not administered in the analysed group. The upper limit of all the pelvic fields was at the L5-S1 level and the lower one was 5 cm below the tumour. Radiotherapy was followed by surgery within 7 days. All patients were operated on strictly according to the TME with complete peri-rectal tissue removal by sharp dissection of pelvic fascia under the direct vision between parietal and visceral surface to the levators. Inferior mesenteric vessels were ligated high at their origin. Splenic flexure of the colon was mobilized to relieve a tension. Minimum 1 cm distal margin was achieved. Straight end-to-end anastomosis with double-stapling technique

TABLE 1. Baseline characteristics

Characteristics	n (%)
Gender	
Female / Male	92 (58) / 66 (42)
Age (years)	
Mean ± SD / median / range	67.1 ± 9.8 / 68 / 34-85
Comorbidity	
Diabetes / Cardiovascular disease	13 (8) / 40 (25)
Smoking	
Yes / No	87 (55) / 71 (45)
Obesity	
Yes / No	31 (20) / 127 (80)
Preoperative radiotherapy	
Yes / No	65 (41) / 93 (59)
Operating time (minutes)	
Mean ± SD / median / range	118.9 ± 24.8 / 120 / 45-190
Level of anastomosis (cm)	
Mean ± SD / median / range	5.4 ± 1.1 / 5.0 / 3-7
Blood transfusion	
Yes / No	24 (15) / 134 (85)
Postoperative fever	
Yes / No	9 (6) / 149 (94)
T stage	
T1T2 / T3	95 (60) / 63 (40)
N status	
N- / N+	91 (58) / 67 (42)

was constructed. Although routine pelvic drainage in colorectal surgery has not been justified in randomised controlled trials, it is routinely used in our institution after anterior resection because we believe it may act as an early detector of anastomotic leakage. Thus, a silastic pelvic drainage was placed in all of the analysed patients using a closed, gravitational no-suction method.

### GCS implantation

Technique of GCS implantation has already been presented by us in details elsewhere.<sup>5</sup> Briefly, anastomosis was wrapped with 10 x 10 x 0.5 cm sponge containing 130 mg of gentamicin sulfate and 280 mg purified bovine tendon type I collagen which was applied deeply into pre-sacral area to the levators level. GCS was formed and pressed to the bowel wall (Figure 1). Special effort was made for its adequate location and stability.<sup>5</sup> During the all postoperative hospital stay a close patient examination was performed several times a day in order to identify any clinical symptoms suspicious of the leakage. AL was considered to be present if any of the following features were noticed: the presence of peritonitis caused by anastomotic dehiscence, the presence of feculent substances and gas from the pelvic drain or the presence of pelvic abscess with the demonstration of leakage by transrectal examination, endoscopy, contrast enema, endorectal ultrasound or CT scanning.

### Follow-up

During the postoperative follow-up physical examination (with digital rectal examination and CEA measuring) was scheduled every three months for the first two years, at 6-months intervals for the next three years, and once a year thereafter. Abdominal and pelvic imaging was performed every six months. Colonoscopy was performed after 1 year and then every three years. Any symptoms potentially related to LR were a subject of investigation with colonoscopy and CT or MRI. LR was defined as local cancer recurrence regardless of the presence or absence of distant metastases.

### Statistical analysis

Data was collected in a prospective manner and then retrospectively analysed. In each case following parameters were recorded: patient age, gender, comorbidity (diabetes and cardiovascular disease), obesity (body mass index > 30 kg/m<sup>2</sup>), smoking

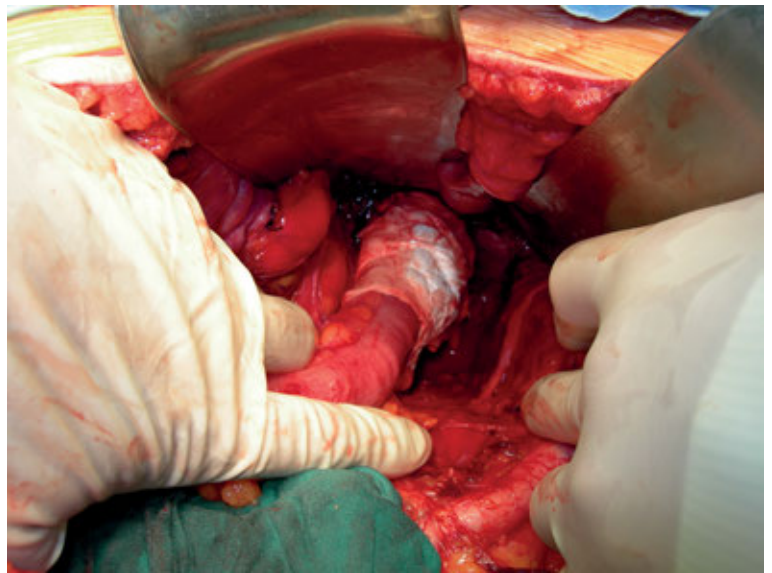


FIGURE 1. Anastomosis wrapping with GCS.

status, preoperative radiotherapy, level of anastomosis from the anal verge (cm), blood transfusion, presence of postoperative fever (> 37.5 Celsius degrees), T stage and N status. The median and range values as well as the mean values with their standard deviations were calculated when appropriate. Incidence and rates of AL and LR were calculated. Correlation between categorical variables was assessed using chi-square test with correction for continuity while between continuous variables using *T*-test. Multivariate analysis was performed with the use of multiple logistic regression. The statistical significance was assumed at *p* value < 0.05. Statistical analysis was performed by a professional statistician (PB) using R-software ver. 3.2 (free environment for statistical computing and graphics).

The study was conducted in accordance with the Declaration of Helsinki and approved by the Institutional Review Board. This research was financed through a statutory subsidy by the Minister of Science and Higher Education as a part of the research grant ST.C280.17.010 (record number in the Simple System).

### Results

GCS was applied without any technical difficulties and was well tolerated. Neither sponge-related adverse reaction nor drain blockage were noticed. AL developed in 5 patients giving the AL rate of 3.2%

TABLE 2. Uni – and multivariate analysis of anastomotic leakage incidence

Variables	Patients with leakage n (%)	Univariate analysis P - value	Multivariate analysis P - value
Gender			
Female	2 (2.2)	0.4010	-
Male	3 (4.5)		
Age			
≥ 75	4 (12.5)	0.0007	0.0004
< 75 years	1 (0.8)		
Diabetes			
Yes	1 (7.7)	0.3303	-
No	4 (2.8)		
Cardiovascular disease			
Yes	1 (2.5)	0.7811	-
No	4 (3.4)		
Smoking			
Yes	5 (5.7)	0.0401	0.043
No	0 (0)		
Obesity			
Yes	2 (6.5)	0.2435	-
No	3 (2.4)		
Preoperative radiotherapy			
yes	3 (4.6)	0.4053	-
no	2 (2.2)		
Level of anastomosis			
> 5	1 (1.5)	0.3289	-
≤ 5 cm	4 (4.3)		
Blood transfusion			
yes	1 (4.2)	0.7607	-
no	4 (3.0)		
Postoperative fever			
yes	0 (0)	0.5765	-
no	5 (3.4)		
T stage			
T1T2	3 (3.1)	0.9953	-
T3	2 (3.2)		
N status			
N-	3 (3.3)	0.9119	-
N+	2 (3.0)		

(5/158). In all the cases it was associated with clinical symptoms: peritonitis and pelvic abscess in one patient each, and gas or feculent discharge from pelvic drain in three patients. The median time to the diagnosis of AL was 5 days (range: 3-15) following surgery. Two patients (one with peritonitis and one with abscess) underwent surgical re-intervention: peritoneal lavage and defunctioning transversostomy. Three remaining patients had only minor AL without peritonitis and abscess and were effectively treated with pelvic lavage through the drain, total parenteral nutrition and antibiotic therapy. There was no leakage-related mortality. All resolution of AL was confirmed by endoscopy or contrast enema.

Univariate analysis demonstrated that patient age > 75 years and smoking were significantly related to the increased AL rate: 12.5% *vs.* 0.8% ( $p = 0.0007$ ) and 5.7% *vs.* 0 ( $p = 0.0401$ ), respectively. Influence of patient gender, diabetes and cardio-

vascular disease, obesity, preoperative radiotherapy, operating time, level of the anastomosis, blood transfusion, postoperative fever, T stage and N status on AL rate did not reach statistical significance. In multivariate analysis patient age > 75 years was identified as the most important independent risk factor for clinical AL ( $p = 0.0004$ ). However, the negative impact of smoking was also significant ( $p = 0.043$ ). Results are presented in Table 2.

Twenty-three patients were lost from follow-up. In the remaining 135 patients median follow-up (mean  $\pm$  SD; range) was 61 months ( $64.8 \pm 32.5$ ; 16-134). LR developed in 12% of patients (16/135). In 12 cases was resectable, in 5 patients with curative intent. Median interval (mean  $\pm$  SD; range) to LR was 14 months ( $15.9 \pm 6.3$ ; 7-28). 25% of patients (4/16) with LR had AL after TME while just 0.8% in non-recurrent group (1/119). 88% of LR (14/16) developed in 24 months. LR was observed in 80% of patients with postoperative AL (4/5) while only 9% of patients without AL (12/130); the difference was highly significant ( $p = 0.00001$ ). Time to LR was significantly shorter in AL group when compared with patients without leakage; median (mean  $\pm$  SD; range): 8.5 ( $9.1 \pm 2.1$ ; 7-12) *vs.* 17 ( $18.9 \pm 6.1$ ; 10-28) months ( $p = 0.014$ ).

## Discussion

Due to high risk of long duration of procedure, bacteria migration, toxin translocation, possibility of contamination and the presence of malignancy, effective antibiotics in colorectal cancer surgery are needed for the prophylaxis and treatment. Gentamicin is the one of the most often used antimicrobial agents. However, recent studies clearly show that systemic administration of gentamicin results in only borderline effectiveness and does not achieve levels above minimum inhibitory concentration in serum, subcutaneous tissue, epiploic fat and bowel wall.<sup>6</sup> In addition, although blood transfusions are not often required in modern colorectal surgery (as observed in our series), intravenously administered fluids can strongly decrease gentamicin concentrations. Local application of gentamicin provides sufficient drug dosage that can reduce the incidence of infections, lowers the risk of antibiotic resistance by reducing the need for long-term systemic therapy and carries a low risk of toxicity.<sup>7</sup> Collagen seems to be one of the most favourable matrix for controlled local drug delivery because of its bio-compatibility and well-established safety profile.<sup>8</sup> Its usage as a carrier has

positive effect on wound healing and eliminates the need of re-operation because the implant is fully resorbable. Collagen causes faster coagulation to stop bleeding and reduces the risk of hematoma or seroma formation that can in turn accelerate bacterial proliferation. The breakdown of the GCS by macrophage collagenases increases the number of collagen fibres released, which attracts fibroblasts and stimulates the fibroblasts to proliferate and lay down new collagen in the healing process.<sup>9</sup> Drugs are released from a collagen matrix by a combination of diffusion and natural enzymatic breakdown of the collagen matrix, which provides rapid (diffusion) and prolonged (breakdown of the matrix) drug release.<sup>10</sup> Moreover, immune response against collagen implants are uncommon.<sup>11,12</sup> Hence, GCS is used to improve wound healing and for prophylaxis of infections following surgery, including gastrointestinal operations.<sup>3</sup>

Features affecting AL rates in our series are not surprising. Older age is mentioned among the most frequent factors.<sup>1</sup> Negative impact of smoking is also well documented. It increases a risk of AL mainly by affecting small vessels and causing tissue hypoxia, which compromises the healing of anastomosis.<sup>2</sup> The other factors, including preoperative radiotherapy and anastomosis level did not reach statistical significance in our series. The use of covering stoma remains controversial and more individual approach is needed. However, our findings suggest that it still can be worth considering in well-selected high-risk cases, such as older and smoking patients.

Interestingly, the incidence of AL among the patients in our group seems to be relatively low when compared to the 10 - 13.7% incidence reported by others.<sup>14-18</sup> Only few papers concerning the use of GCS in colorectal surgery have been published as yet. In the recent multi-centre randomized trial enrolling 602 patients, Bennett-Guerrero and co-workers from a SWIPE 2 trial group found GCS not effective at preventing surgical-site infection, either superficial or deep: 20.3% *vs.* 13.6% ( $p = 0.03$ ) and 8.3% *vs.* 6.0% ( $p = 0.26$ ), respectively.<sup>19</sup> On the other hand, there is a growing body of data, including findings from randomized studies that support the use of GCS following high-risk colorectal procedures in order to reduce post-operative morbidity rate, wound healing time and length of hospital stay. Rutten and Nijhuis observed that the application of systemic antibiotics plus GCS *vs.* systemic antibiotics alone significantly decreased the incidence of abdominal wound infections (5.6% *vs.* 18.4%;  $p = 0.01$ ) as well as the median hospital

stay (13.8 *vs.* 16.3 days;  $p = 0.015$ ).<sup>20</sup> Nowacki *et al.* reported a lower post-operative complications rate at 30 days (20.7% *vs.* 37.5%;  $p < 0.05$ ). Sub-group analysis also revealed that the difference was maintained in high-risk patients, i.e. those with surgery exceeded 3 hours and those who experienced intra-operative bowel perforation: 19.2% *vs.* 40.8% ( $p = 0.03$ ) and 20.0% *vs.* 57.9% ( $p = 0.01$ ), respectively.<sup>21</sup> Multicenter trial by Gruessner and colleagues demonstrated significantly decreased rate of perineal wound infections and secondary complications with infection after abdomino-perineal excision if GCS was used: 6.1% *vs.* 20.8% and 6% *vs.* 21%, respectively. In addition, patients with GCS had a much greater reduction in the number of pathogens in the post-operatively obtained wound secretion samples ( $p = 0.013$ ).<sup>22</sup> De Bruin *et al.* studied the effect of GCS on postoperative outcome in patients undergoing abdomino-perineal excision following short-term neoadjuvant radiotherapy (5 Gy x 5 days to a total dose 25 Gy). They demonstrated lower rates of total and deep wound infection rates as well as higher rates of primary wound healing when GCS was applied: 16% *vs.* 57% ( $p = 0.01$ ), 5% *vs.* 29% ( $p = 0.05$ ), and 84% *vs.* 43% ( $p = 0.01$ ), respectively. The patients with GCS also had significantly shorter mean hospital stay, i.e. 15 *vs.* 25 days.<sup>23</sup>

Discrepancies in AL rates among the series of patients following anterior resection with TME and GCS implantation may be caused by many reasons. Firstly, a distribution of AL risk factors could substantially differ. Secondly, the site of GCS implantation is not standardized: wound, upon the closed fascia or pelvic cavity, around the anastomosis (as in the present study).<sup>19, 20, 21</sup> The other possible reason may be the different definition of clinical AL.<sup>24</sup> However, still little is known about the impact of GCS on anastomosis healing. Although some studies suggest positive effect of local gentamicin on collagen content and metabolism, there are conflicting data regarding this subject. Quicker mucosal, muscular and extra-cellular matrix repair was noticed in experimental study by Mutter and colleagues.<sup>25</sup> Binnebosel *et al.* reported that intra-abdominal application of gentamicin can enhance the healing of anastomosis and increase the collagen type I/III in rats.<sup>26</sup> On the other hand, Vaneerdeweg *et al.* did not observe any significant influence of GCS on symptomatic AL rate in animal models.<sup>27</sup> This topic warrants further investigation.

A meta-analysis of the recent studies demonstrates that the cumulative risk of local recurrence following curative R0 anterior resection with TME

varies from 1% to 13.5%. The risk mainly depends on the tumour stage, histological differentiation, nodal status, and the circumferential resection margin.<sup>28</sup> We observed much higher incidence of LR in AL group. However, number of patients with AL was too small to obtain a robust statistics and draw a significant conclusion. Possible association between AL and colorectal cancer recurrence is a subject of intensive research. Sammour *et al.* did not notice a significant difference in LR as well as 5-year overall and cancer-specific survival with regard to AL after rectal cancer resection.<sup>29</sup> In contrast, a negative impact of AL on LR and overall survival was reported by others.<sup>30</sup> Mirnezami *et al.* reviewed 21 studies (21,902 patients) and found that LR as well as cancer specific mortality was significantly higher after AL.<sup>31</sup> Similar findings were reported by Lu *et al.*<sup>32</sup> In the meta-analysis of 14 studies (11,353 patients) made by Wang and colleagues AL was significantly related to increased LR rates and decreased both overall and cancer-specific survival.<sup>33</sup> Postulated mechanism of LR after AL is associated with the fact that leakage may lead to the penetration and implantation of extraluminal tissue by previously exfoliated rectal cancer cells which still may be present in the lumen of the bowel despite routine rectal wash out. In addition, AL causes pelvic infection, which may enhance proliferation, migration and invasion capacities of cancer cells.<sup>33</sup>

Our study has some important limitations. Firstly, a severe weakness of this paper is an incomplete investigation of oncological outcomes. Only local recurrence analysis was completed. Survival analysis was not performed and, as a consequence, neither 5-year overall survival nor disease-free survival rates were demonstrated. Secondly, due to low AL rate some findings are based on the comparison of small groups. Even if the results are significant, their statistical power is low and conclusive statement cannot be drawn. Thirdly, this is just an observational study and a single-institution case series. Consequently, one cannot be certain that our results will be repeatable in another setting. Moreover, during the study period, GCS wrapping of an anastomosis in patients that have undergone restoration of bowel continuity after ultra-low rectal cancer resection was considered standard management and in accordance with the department policy. Therefore, it is not possible to compare these results to a control group operated on in the same time period without the use of GCS. We previously observed an anastomosis failure in 10.6%-12.6% of patients after sphincter-preserv-

ing TME.<sup>34</sup> Present results look favourable when compared to this historical cohort operated on by the same surgical team at the same institution. However, comparisons to historical series have no statistical power and no significant conclusion can be drawn. Ultimately, we will never be certain if these superior results are a consequence of the usage of GCS or whether they can be attributed to the impact of surgical technique or patient selection.

Our findings suggest that low rate of symptomatic AL might be at least partially influenced by GCS application following TME. GCS can reduce tissue exudation and fluids accumulation at the pelvis cavity and has a local anti-bacterial and haemostatic activity. Hence, it is possible that GCS can secure the anastomosis area. On the other hand, potential benefit from GCS may also be associated with the ability to diminish dehiscence range and its severe consequences, limit pelvic abscess formation, peritonitis and septicemia without the impact on sub-clinical failure. That may be the possible reason of favourable clinical course of the leakage occurred in analysed group.

Based on our previous studies and recent findings the wrapping of an anastomosis with GCS remains the standard management after low anterior rectal cancer resection in our institution. Keeping the risk of AL at the lowest possible level improves local cancer control and the patient's quality of life.<sup>31-33</sup> However, there are still some interesting points waiting to be explored. Nowacki *et al.* observed in a randomised trial a significantly reduced rate of distant metastases in patients with GCS after TME with preoperative radiotherapy compared to a control group without GCS.<sup>21</sup> These surprising findings were also demonstrated in a confirmatory study from the same institution with the median follow-up of 80 months.<sup>36</sup> These results are difficult to explain, in particular, the fact that there were no significant differences in overall and disease-free survival rates. Apart from the assessment of oncological outcomes, a detailed cost-effectiveness analysis as well as a long-term evaluation of conceivable late side effects (anastomosis stricture, persistent anterior resection syndrome) are other interesting topics worth to be explored in the future.<sup>37-40</sup>

## Acknowledgements

Authors would like to thank Mr Jacob Bronowicki for his kind assistance in revising the English of this manuscript.

## References

- Gessler B, Eriksson O, Angenete E. Diagnosis, treatment, and consequences of anastomotic leakage in colorectal surgery. *Int J Colorectal Dis* 2017; **32**: 549-56. doi: 10.1007/s00384-016-2744-x
- Tafampas P, Christodoulakis M, Tsiptsis DD. Anastomotic leakage after low anterior resection for rectal cancer: facts, obscurity, and fiction. *Surg Today* 2009; **39**: 183-8. doi: 10.1007/s00595-008-3835-2
- Szynglarewicz B, Matkowski R, Forgacz J, Pudelko M, Grzebieniak Z. Anastomosis wrapping with gentamicin-containing collagen sponge in rectal cancer patients following sphincter-preserving total mesorectal excision without defunctioning stoma. *Case Rep Clin Pract Rev* 2006; **7**: 267-71.
- Szynglarewicz B, Matkowski R, Gisterek I, Włodarska-Polińska I, Kasprzak P, Sydor D, et al. Implantation of gentamicin-containing collagen sponge following anterior resection for rectal carcinoma: can it decrease the leakage risk? *Colorectal Dis* 2007; **9** (Suppl 3): O19.
- Szynglarewicz B, Ekiert M, Forgacz J, Matkowski R. Can gentamicin-containing collagen sponge be used for the protection against leakage following low anterior resection with total mesorectal excision? *Tech Coloproctol* 2014; **18**: 767-8. doi: 10.1007/s10151-014-1139-7
- Markantonis SL, Kostopanagiotou G, Panidis D, Smirniotis V, Voros D. Effects of blood loss and fluid volume replacement on serum and tissue gentamicin concentrations during colorectal surgery. *Clin Ther* 2004; **26**: 271-81. doi: 10.1016/S0149-2918(04)90025-2
- Moore RD, Lietman PS, Smith CR. Clinical response to aminoglycoside therapy: importance of the ratio of peak concentration to minimal inhibitory concentration. *J Infect Dis* 1987; **155**: 93-9. doi: 10.1093/infdis/155.1.93
- Ruszczak Z, Friess W. Collagen as a carrier for on-site delivery of antibacterial drugs. *Adv Drug Deliv Rev* 2003; **55**: 1679-98. doi: 10.1016/j.addr.2003.08.007.
- Chvapil M. Collagen sponge: theory and practice of medical application. *J Biomed Mater Res* 1977; **11**: 721-41. doi: 10.1002/jbm.820110508
- Waldvogel FA. Future perspective of aminoglycoside therapy. *J Antimicrob Chemother* 1984; **13**: 75-8. doi: 10.1093/jac/13.suppl\_A.73
- Anselme K, Bacques C, Charriere G, Hartmann DJ, Herbage D, Garrone R. Tissue reaction to subcutaneous implantation of collagen sponge. A historical, ultrastructural, and immunological study. *J Biomed Mater Res* 1990; **24**: 689-703. doi: 10.1002/jbm.820240605
- Kinel FA, Ciaccio LA, Henderson SB. Sustained release preparations, XVI: Collagen as a drug carrier. *Arch Pharm* 1984; **317**: 657-61. doi: 10.1002/ardp.19843170802
- De Bruin AFJ, Gosselink MP, van der Harst E, Rutten HJT. Local application of gentamicin collagen implants in the prophylaxis of surgical site infections following gastrointestinal surgery: a review of clinical experience. *Tech Coloproctol* 2010; **14**: 301-10. doi: 10.1007/s10151-010-0593-0
- Frouws MA, Snijders HS, Malm SH, Liefers GJ, Van de Velde CJH, Neijenhuis PA, et al. Clinical relevance of a grading system for anastomotic leakage after low anterior resection: analysis from a National Cohort Database. *Dis Colon Rectum* 2017; **60**: 706-13. doi: 10.1097/DCR.0000000000000800
- Rutkowski A, Olesiński T, Zajac L, Bednarczyk M, Szpakowski M. The risk of anastomotic leakage after anterior resection – retrospective analysis of 501 rectal cancer patients operated on without protective stoma. *Minerva Chir* 2017; **72**: 491-8. doi: 10.1001/2013.jamasurg.2
- Snijders HS, van den Broek CB, Wouters MW, Meershoek-Klein Kranenburg E, Wiggers T, Rutten H, et al. An increasing use of defunctioning stomas after low anterior resection for rectal cancer. Is this the way to go? *Eur J Surg Oncol* 2013; **39**: 715-20. doi: 10.1016/j.ejso.2013.03.025
- Wang L, Gu J. Risk factors for symptomatic anastomotic leakage after low anterior resection for rectal cancer with 30 Gy/10 f/2 w preoperative radiotherapy. *World J Surg* 2010; **34**: 1080-5. doi: 10.1007/s00268-010-0449-9
- Kang CY, Halabi WJ, Chaudhry OO, Nguyen V, Pigazzi A, Carmichael JC, et al. Risk factors for anastomotic leakage after anterior resection for rectal cancer. *JAMA Surg* 2013; **148**: 65-71. doi: 10.1001/2013.jamasurg.2
- Bennett-Guerrero E, Pappas TN, Koltun WA, Fleshman JW, Lin M, Garg J, et al. Gentamicin-collagen sponge for infection prophylaxis in colorectal surgery. *N Engl J Med* 2010; **363**: 1038-49. doi: 10.1056/NEJMoa1000837
- Rutten HJ, Nijhuis PH. Prevention of wound infection in elective colorectal surgery by local application of a gentamicin-containing collagen sponge. *Eur J Surg Suppl* 1997; **578**: 31-5. PMID: 9167147
- Nowacki MP, Rutkowski A, Oledzki J, Chwalinski M. Prospective, randomized trial examining the role of gentamicin-containing collagen sponge in the reduction of postoperative morbidity in rectal cancer patients: early results and surprising outcome at 3-year follow-up. *Int J Colorectal Dis* 2005; **20**: 114-20. doi: 10.1007/s00384-004-0632-2
- Gruessner U, Clemens M, Pahlplatz PV, Sperling P, Witte J, Rosen HR; Septocoll Study Group. Improvement of perineal wound healing by local administration of gentamicin-impregnated collagen fleeces after abdominoperineal excision of rectal cancer. *Am J Surg* 2001; **182**: 502-9. doi: org/10.1016/S0002-9610(01)00762-0
- De Bruin AFJ, Gosselink MP, Wijffels NAT, Coene PP, van der Harst E. Local gentamicin reduces perineal wound infection after radiotherapy and abdominoperineal resection. *Tech Coloproctol* 2008; **12**: 303-7. doi: 10.1007/s10151-008-0440-8
- Rahbari NN, Weitz J, Hohenberger W, Heald RJ, Moran B, Ulrich A, et al. Definition and grading of anastomotic leakage following anterior resection of the rectum: a proposal by the International Study Group of Rectal Cancer. *Surgery* 2010; **147**: 339-51. doi: 10.1016/j.surg.2009.10.012
- Mutter D, Aprahamian M, Tiollier J, Sonzini P, Marescaux J. Evaluation of human collagen biomaterials in the healing of colonic anastomoses in dogs. *Eur J Surg* 1997; **163**: 287-95. PMID: 9161827
- Binnebose M, Junge K, Kaemmer DA, Krones CJ, Titkova S, Anurov M, et al. Intraperitoneally applied gentamicin increases collagen content and mechanical stability of colon anastomosis in rats. *Int J Colorectal Dis* 2009; **24**: 433-40. doi: 10.1007/s00384-008-0614-x
- Vaneerdeweg W, Hendriks JM, Lauwers PR, Ieven M, Eyskens EJ. Effect of gentamicin-containing sponges on the healing of colonic anastomosis in a rat model of peritonitis. *Eur J Surg* 2000; **166**: 959-62. doi: 10.1080/110241500447137
- Wang XT, Li DG, Li L, Kong FB, Pang LM, Mai W. Meta-analysis of oncological outcome after abdominoperineal resection or low anterior resection for lower rectal cancer. *Pathol Oncol Res* 2015; **21**: 19-27. doi: 10.1007/s12253-014-9863-x
- Sammour T, Hayes IP, Jones IT, Steel MC, Faragher I, Gibbs P. Impact of anastomotic leak on recurrence and survival after colorectal cancer surgery: a BioGrid Australia analysis. *ANZ J Surg* 2018; **88**: E6-E10. doi: 10.1111/ans.13648
- Du P, Burke JP, Khoury W, Lavery IC, Kiran RP, Remzi FH, et al. Factors associated with the location of local rectal cancer recurrence and predictors of survival. *Int J Colorectal Dis* 2016; **31**: 825-32. doi: 10.1007/s00384-016-2526-5
- Mirnezami A, Mirnezami R, Chandrakumaran K, Sasapu K, Sagar P, Finan P. Increased local recurrence and reduced survival from colorectal cancer following anastomotic leak: systematic review and meta-analysis. *Ann Surg* 2011; **253**: 890-9. doi: 10.1097/SLA.0b013e3182128929
- Lu ZR, Rajendran N, Lynch AC, Heriot AG, Warrier SK. Anastomotic leak after restorative resections for rectal cancer compromise cancer outcomes and survival. *Dis Colon Rectum* 2016; **59**: 236-44. doi: 10.1097/DCR.0000000000000554
- Wang S, Liu J, Wang S, Zhao H, Ge S, Wang W. Adverse effect of anastomotic leakage on local recurrence and survival after anterior resection for rectal cancer: a systematic review and meta-analysis. *World J Surg* 2017; **41**: 277-84. doi: 10.1007/s00268-016-3761-1
- Szynglarewicz B, Grzebieniak Z, Forgacz J, Pudelko M, Rapala M. Anastomotic leakage following anterior resection and total mesorectal excision in case of rectal carcinoma- prospective evaluation of the incidence, risk factors and protective methods. *Pol Przegl Chir* 2006; **78**: 1-12.
- Szynglarewicz B, Matkowski R, Maciejczyk A, Piotr Kasprzak, Daniel Sydor, Józef Forgacz, et al. Neoadjuvant radiotherapy and anastomosis dehiscence after total mesorectal excision for stage II and III rectal cancer. *Rep Pract Oncol Radiother* 2007; **12**: 87-93. doi: org/10.1016/S1507-1367(10)60044-2
- Rutkowski A, Pietrzak L, Krynski J, Zajac L, Bednarczyk M, Olesiński T, et al. The gentamicin-collagen implant and the risk of distant metastases of rectal cancer following short-course radiotherapy and curative resection: the long-term outcomes of a randomized study. *Int J Colorectal Dis* 2018; **33**: 1087-96. doi: 10.1007/s00384-018-3045-3

37. Lee SY, Kim CH, Kim YJ, Kim HR. Anastomotic stricture after ultralow anterior resection or intersphincteric resection for very low-lying rectal cancer. *Surg Endosc* 2018; **32**: 660-6. doi: 10.1007/s00464-017-5718-3
38. Ekkarat P, Boonpipattanapong T, Tantiphlachiva K, Sangkhathat S. Factors determining low anterior resection syndrome after rectal cancer resection: A study in Thai patients. *Asian J Surg* 2016; **39**: 225-31. doi: 10.1016/j.asjsur.2015.07.003
39. Chen TY, Wiltink LM, Nout RA, Meershoek-Klein Kranenbarg E, Laurberg S, Marijnen CA, et al. Bowel function 14 years after preoperative short-course radiotherapy and total mesorectal excision for rectal cancer: report of a multicenter randomized trial. *Clin Colorectal Cancer* 2015; **14**: 106-14. doi: org/10.1016/j.clcc.2014.12.007
40. Emmertsen KJ, Laurberg S. Low anterior resection syndrome score: development and validation of a symptom-based scoring system for bowel dysfunction after low anterior resection for rectal cancer. *Ann Surg* 2012; **255**: 922-8. doi: 10.1097/SLA.0b013e31824f1c21

# Molecular biomarkers and histological parameters impact on survival and response to first- line systemic therapy of metastatic colorectal cancer patients

Martina Rebersek, Tanja Mesti, Marko Boc, Janja Ocvirk

Department of Medical Oncology, Institute of Oncology Ljubljana, Ljubljana, Slovenia

Radiol Oncol 2019; 53(1): 85-95.

Received 30 August 2018

Accepted 20 September 2018

Correspondence to: Assoc. Prof. Janja Ocvirk, M.D., Ph.D., Department of Medical Oncology, Institute of Oncology Ljubljana, Zaloska 2, SI-1000 Ljubljana, Slovenia. Phone: +386 1 5879 285; E-mail: jocvirk@onko-i.si

Disclosure: No potential conflicts of interest were disclosed.

**Background.** Histological parameters of primary tumour and nodal metastases are prognostic factors for survival of operable colorectal (CRC) patients, but not predictive for response rate of systemic therapy. *KRAS* mutations in codons 12 and 13 were first recognized as a predictive factor for resistance to anti-EGFR monoclonal antibodies. Not all patients with wild-type *KRAS* (wt*KRAS*) respond to anti-EGFR antibody treatment. Additional mechanisms of resistance may activate mutations of the other main EGFR effectors pathway, such as other mutations in *RAS* gene, mutations in *P13K* and *PTEN* expression.

**Patients and methods.** In the prospective study prognostic and predictive impact of histological parameters of primary tumour, *KRAS* and *BRAF* mutations on overall survival (OS) and objective response (OR) rate of metastatic CRC (mCRC) patients treated with 1<sup>st</sup> line systemic therapy were analysed. We additionally retrospectively analysed other mutations in *RAS* genes and their impact on survival and time to progression.

**Results.** From November 2010 to December 2012, we enrolled 154 patients in the study, 95 men and 59 women. Mutations in *KRAS* gene and *V600E BRAF* gene were found in 42% and in 3% of patients, respectively. Median OS of the patients with T1, T2 and T3 tumour was 65.4 months (95% CI, 55.7–75.6) while in patients with T4 tumour, lymphangiosis, vascular and perineural invasion it has not been reached yet. Median OS of the patients with G1, G2 and G3 of tumour differentiation was 65.6 (95% CI, 53.7–77.5) and 25.3 months (95% CI, 16.6–34.1), respectively. Median OS of the patients with stage N0, N1 and N2 was 65.6 (95% CI, 56.4–74.8) and 58.0 months (95% CI, 21.9–94.2), respectively. Median OS of wt*KRAS* and mutated *KRAS* patients was 56.5 (95% CI, 48.2–64.9) and 58 months (95% CI, 52.6–63.4), respectively. Median OS of mutated codon 12 and codon 13 patients was 57 (95% CI, 50.9–64.4) and 44 months (95% CI, 40.1–48.4), respectively. Median OS of wt*BRAF* and of mutated *BRAF* patients was 59.2 (95% CI, 52.5–65.9) and 27.6 months (95% CI, 12.6–42.5), respectively. wt*KRAS* significantly affected the response to the first systemic therapy ( $p = 0.028$ ), while other parameters did not affected it,  $p = 0.07$ . In 14 patients (17%), additional mutations in *NRAS* gene, codon 61 and codon 146 were found. Median OS of wt*NRAS*, codon 61 and 146 patients was 67.1 months (50.3–67.6) while median OS of mutated *NRAS* patients has not been reached yet ( $p = 0.072$ ). Median time to progression of wt*NRAS*, codon 61 and 146 patients was 11.7 months (10.4–14.5) while median time to progression of mutated *NRAS* patients was 7.9 months (6.1–11.0), ( $p = 0.025$ ).

**Conclusions.** Mutated *BRAF*, N2 and G3 of primary tumour were poor prognostic factors for OS in mCRC patients. wt*KRAS* significantly affected the response to the first line systemic therapy. Histological parameters included in the analysis and mutated *BRAF* did not affect significantly the efficacy of 1<sup>st</sup> line systemic therapy in mCRC patients.

Key words: metastatic colorectal cancer; chemotherapy; targeted therapy; histological parameters; biomarkers

## Introduction

Colorectal cancer (CRC) is one of the most common cancer and one of the leading causes of cancer death in the world. It is one of the most common cancers in Slovenia and, according to the Cancer Registry of Slovenia, 1353 new patients were diagnosed with CRC in 2015.<sup>1</sup> Metastatic disease is still incurable, with 5% five-year overall survival (OS) without treatment. With the introduction of new chemotherapy, using oxaliplatin and irinotecan in the current management of metastatic disease, in combination with biologicals, targeting epidermal growth factor-mediated growth regulatory pathway and the vascular endothelial growth factor-mediated angiogenesis pathway we can prolong the progression-free survival (PFS) and OS of these patients.<sup>2-10</sup> In selected patients with appropriate combination of therapy and surgery we can achieve approximately a 50% five-year OS.

The development of CRC is a multistep process, which accumulates different gene mutations, chromosomal abnormalities and epigenetic changes.<sup>11</sup> The mutations within *KRAS* proto-oncogene, predominately within codons 12 and 13, activate RAS/RAF signalling and are thought to occur early in carcinogenesis of CRC. The *KRAS* status is the first molecular marker to predict the response to anti-EGFR monoclonal antibodies cetuximab and panitumumab in metastatic CRC (mCRC) patients, and it needs to be determined before deciding in favour of treatment with anti-EGFR antibodies. As the *KRAS* mutations occur early in CRC formation, there is a high concordance between the *KRAS* mutations of primary tumour and metastases, which was confirmed in previous studies.<sup>11</sup> In the retrospective study, de Roock *et al.* raised the possibility that the patients with the *KRAS* mutation in codon 13 might have benefited from anti-EGFR antibodies treatment.<sup>12,13</sup> The mutations in *KRAS* gene were found in approximately 30 to 40% of mCRC patients, reported in previous literature, but, only 40 to 60% of these patients with wt*KRAS* will respond to anti-EGFR antibodies treatment. Therefore, other molecular markers downstream of EGFR in the RAS/RAF/MAPK pathway and other effector pathways were found to be involved to predict the response to specific systemic therapy.

The *BRAF* gene encodes a serine/threonine protein kinase of the RAS/RAF/MEK/ERK kinase pathway and it is also involved in CRC carcinogenesis.<sup>11,14,15</sup> The most common mutation of the *BRAF* gene is V600E which is found in approximately 5 to 9% of mCRC.<sup>15,16</sup> The same was reported in our

previous study carried on Slovenian patients with CRC where the *BRAF* V600E mutation was found in 5.1% of patients.<sup>16</sup> Previous retrospective studies suggested that mutated *BRAF* was a marker of resistance to anti-EGFR therapy and that the patients with mutated *BRAF* had significantly shorter PFS and OS than the patients with wt*BRAF* tumours.<sup>14,15</sup> The mutations in the *KRAS* and *BRAF* genes have been reported to be mutually exclusive. In the retrospective analysis by Fariña-Sarasqueta *et al.*, it was also shown that the *BRAF* V600E mutation was an independent prognostic factor for the OS of patients with CRC in stages II and III, while the *KRAS* mutations did not have any effect on the OS of these patients.<sup>17</sup> They concluded that the prognostic role of the *KRAS* mutations in an adjuvant setting had to be determined. In published clinical studies the *BRAF* V600E mutation in mCRC is conferred to a poor prognosis regardless of treatment, but these patients may have some benefit from the treatment with cetuximab in combination with chemotherapy as the first-line therapy, except for the patients in whom the disease has progressed after the first-line therapy.<sup>15,17</sup> The status of mutations in the *RAS* gene is a new molecular predictive factor for response to treatment with EGFR inhibitors in mCRC. These mutations in the *RAS* gene, in the codons 12, 13, 61 and 146, according to the literature data, are about 15%, and they are determined from autumn 2013 at our Institute of Oncology.<sup>3,4,9</sup>

The aim of this prospective study was to analyse overall response rate (ORR), time to progression (TTP) and OS of the patients with mCRC treated with first-line systemic therapy in respect of histological parameters of primary tumour *KRAS* and *BRAF* status. We additionally retrospectively analysed other mutations in *RAS* genes and their impact on OS and TTP.

## Patients and methods

### Patients and treatment

In the study, 154 patients with histologically confirmed mCRC, primarily metastatic or progressed during or after adjuvant therapy were prospectively analysed. They were treated according to the national, ESMO and NCCN guidelines, including performance status of patients and comorbidity. They were treated with chemotherapy, including fluoropyrimidins, capecitabine or 5-fluorouracil (5-FU), oxaliplatin or irinotecan in combination with biologicals, bevacizumab or cetuximab in respect of previously determined *KRAS* status. The treat-

ment was continued according to the RECIST criteria, until the planned operation or until the progression of disease or toxicity occurred.

All relevant data from medical files were collected and entered into the data base. Baseline data was analysed with regard to age, sex, primary site (colon and rectum), number and location of metastases. Efficacy was evaluated according to the response evaluation criteria in solid tumours (RECIST, version 1.1) by using computed tomography (CT) scans, magnetic resonance scans, abdominal ultrasound, chest X-ray, bone scans, clinical examination and laboratory tests.<sup>17</sup> Toxicity was assessed according to the National Cancer Institute common toxicity criteria for adverse events (NCI-CTCAE), version 4.03. The study was approved by the Institutional Review Board Committee and was carried out according to the Declaration of Helsinki.

## Hystology

From the histological findings, data on the tumour size, the radical nature of the primary tumour operation, the presence of vascular and perineural invasion, carcinogenic lymphangiosis, the degree of differentiation, the presence of outbreaks of malignant cells and the number and severity of regional lymph nodes were collected.

## Biomarker analysis

DNA for molecular analysis was extracted from formalin-fixed, paraffin-embedded tumour tissue of primary tumours or metastases with at least 70% of tumour cells. TheraScreen KRAS Mutation Kit® (Roche Applied Science, Mannheim, D) was used to determine seven most common mutations in codons 12 and 13 of the *KRAS* gene. The V600E mutation in *BRAF* was detected by end-point genotyping using the TaqMan MGB probes (Applied Biosystems, Warrington, UK) as described previously.<sup>16</sup> The mutation V600E in *BRAF* in positive tumour samples was confirmed by direct sequencing after amplification of the exon 15 of the *BRAF* gene.<sup>16</sup> Retrospectively additional mutations in *NRAS* gene, in *KRAS* codon 61 and 146 were determined with the same method as mutations in *KRAS* codon 12 and codon 13.

## Statistical methods

The primary end-points of the analysis were overall response rate (ORR), based on RECIST criteria,

OS and time to progression (TTP) according to the *KRAS* and *BRAF* status.

The  $\chi^2$ -test was used to compare ORR, OS and TTP between groups, with 95% confidence intervals (CI) calculated for the medians. OS and TTP were estimated by using Kaplan-Meier Estimates and compared using the log-rank test. TTP was measured in all patients from the beginning of the first-line systemic chemotherapy to the first evidence of progression. The duration of OS was calculated from the beginning of systemic treatment until the date of death. P value < 0.05 was considered statistically significant. Statistical data were obtained using the SPSS software package PASW statistics 18.0.

The relationship between treatment efficacy and mutations in *KRAS* and *BRAF* gene and histological characteristics of the tumour (tumour size, presence of vascular and perineural invasion, lymphangiosis, degree of differentiation, number of affected regional lymph nodes) were evaluated by the method of the nominal logistic regression. With the Cox proportional hazards model, we evaluated the impact of histological factors, the number of affected nodes, and mutations in *KRAS* and *BRAF* gene on OS or TTP. Survival was calculated by Kaplan-Meier method to compare groups of patients, and we used the log-rank test. We marked statistically significant differences at  $p < 0.05$ . The same statistical methods were used for OS and TTP in the case of retrospectively determined additional mutations in RAS gene.

## Results

### Patient's characteristics

In total, 154 patients with mCRC who received first-line therapy between November 2010 and December 2012 were included in this prospective analysis. The cut-off date for the present analysis was April 2011. All patients were treated at the Institute of Oncology Ljubljana, all were Caucasian. The median age was 62 years (range 27–86) and the majority of the patients were males (61%). Most of the patients had mCRC (71.4%). One hundred and four patients had primary metastatic disease (59.1%). The most common sites of metastases were liver and lung. The most common therapies the patients received were irinotecan, capecitabine with bevacizumab (29.5%) and oxaliplatin, capecitabine with cetuximab (22.1%). Twenty-four patients (13.6%) were treated only with chemotherapy, capecitabine in monotherapy, or with fluoro-

TABLE 1. Patient's baseline characteristics

Patient's characteristics	Number (%)
Medium age (years)	62
Gender	
female	59 (38)
male	95 (62)
WHO performance status	
0	36 (23)
1	109 (71)
2	9 (6)
Tumour location	
colon	112 (73)
rectum	42 (27)
Primary metastatic	89 (58)
Liver metastases	68 (44)

TABLE 2. Disease characteristics

Disease characteristics	Number (%)
pT4 of primary tumour	35 (23)
Affected regional lymph nodes (N)	
N0 (no affected regional lymph nodes)	34 (22)
N1 (1 to 3 affected regional lymph nodes)	61 (40)
N2 (more than 3 affected regional lymph nodes)	59 (38)
Vascular invasion	22 (14)
Perineal invasion	25 (16)
Lymphangiogenesis	27 (17)
Grade of differentiation	
G1 (well)	10 (6)
G2 (medium)	131 (85)
G3 (poorly)	13 (8)
KRAS gen	
non-mutated (wild-type)	89 (58)
mutated	65 (42)
KRAS mutation	
codon 12	48 (73)
codon 13	17 (27)
BRAF gen	
non-mutated (wild-type)	150 (97)
mutated	4 (3)

pyrimidines in combination with oxaliplatin or irinotecan. Patients' baseline characteristics and are shown in Table 1, disease characteristics are shown in Table 2.

Median follow-up was 15 months. Of the enrolled patients, 71% had WHO performance status 1, and 73% of them the CRC primary metastatic disease was confirmed in 58% of patients. Median time to first progression after primary treatment of operable disease was 20 months. Because of a small number of R1 resections of the primary tumour (in 4 patients), perforations of the primary tumour during surgery (in 5 patients) and extramural tumour deposits (in 4 patients), these three parameters were excluded from the analysis. In 42% of

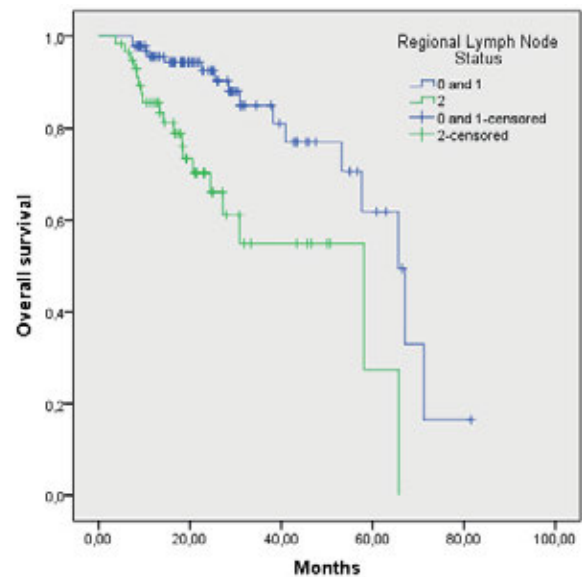
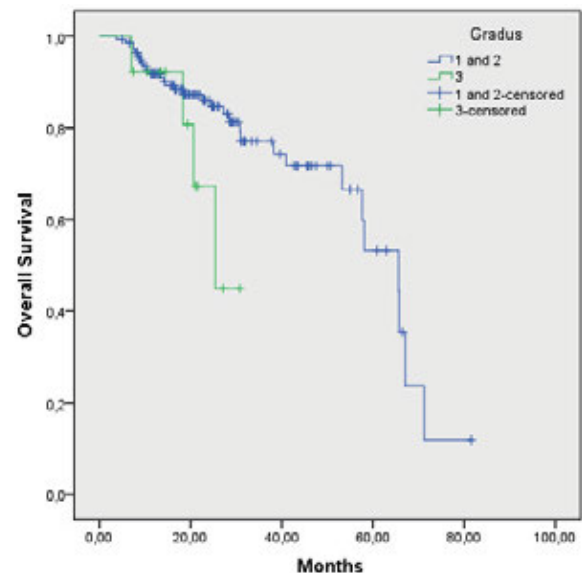
FIGURE 1. Overall survival of patients according to regional lymph node status ( $p = 0.000$ ).

FIGURE 2. Overall survival of patients according to tumour grade of differentiation G1 and G2 versus G3.

patients, the mutations in the *KRAS* gene were found, most frequently in codon 12 (73%), whereas the V600E mutation in the *BRAF* gene was found in 3%. The mutations of the *KRAS* or *BRAF* gene were detected in total in 76 patients (43.4%).

Medium OS of the patients with T1, T2 and T3 primary tumour was 65.4 months (55.7–75.6), while in the patients with T4 primary tumour, it has not been reached yet ( $p = 0.08$ ). Median OS of the patients without vascular invasion was 65.6 months

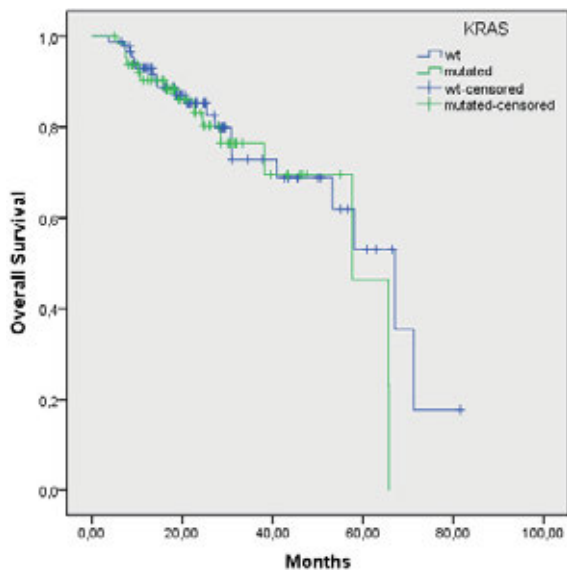


FIGURE 3. Overall survival of wtKRAS and mutated KRAS gene patients ( $p = 0.47$ ).

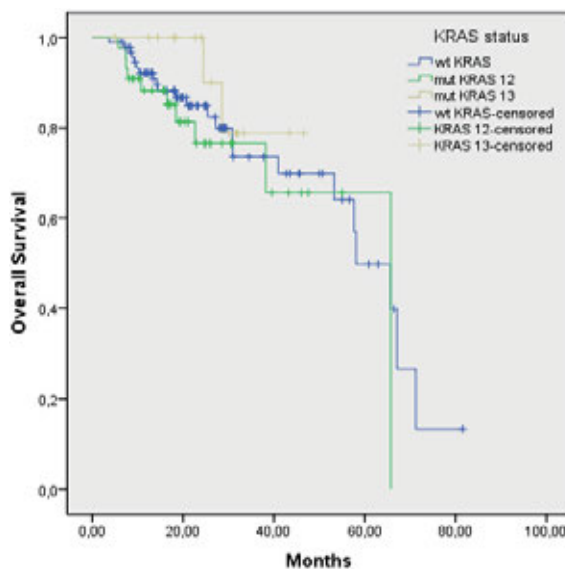


FIGURE 4. Overall survival of mutated KRAS patients in codon 12 and 13 ( $p = 0.40$ ).

(53.5–77.7), and in the patients with vascular invasion, it has not been reached yet. Median OS of the patients without perineural invasion was 65.6 months (47.9–83.3), and in the patients with perineural invasion, it has not been reached yet. Median OS of the patients without lymphangiosis was 65.6 months (53.5–77.6), and in the patients with lymphangiosis, it has not been reached yet. Median OS of the patients with grade 1 and 2 of tumour differentiation was 65.6 months (53.7–77.5), and of the patients with grade 3 of tumour differentiation, it was 25.3 months (16.6–34.1) ( $p = 0.069$ ). Median OS of the patients without affected regional lymph nodes or less than 3 of them (N0 and N1) was 65.6 months (56.4–74.8), and of the patients with more than 3 affected regional lymph nodes (N2), it was 58.0 months (21.9–94.2); the difference was statistically significant ( $p = 0.000$ ). OS of the patients according to regional lymph nodes and according to the grade of tumour differentiation are shown in Figure 1 and 2, respectively.

Median time to first progression after primary treatment of operable disease in the patients with the wtKRAS gene was 20 months (14.7–26.1), and in the patients with the mutated KRAS gene, it was 21 months (17.1–25.4) ( $p = 0.88$ ). In the patients with the mutations in codon 12, it was 21 months (14.3–28.3), and in the patients with the mutations in codon 13, it was 16 months (11.5–20.7) ( $p = 0.53$ ). Median time to first progression after primary treatment of operable disease in the patients with the wtBRAF gene was 20 months (16.7–24.1), and

in the patients with the mutated BRAF gene, it was 12 months (1.8–23.1) ( $p = 0.14$ ).

Median OS of the patients with the wtKRAS gene was 56.5 months (48.2–64.9), and in the patients with the mutated KRAS gene, it was 58 months (52.6–63.4 months;  $p = 0.47$ ) (Figure 3). In the patients with the mutation in codon 12, the median OS was 57 months (50.9–64.4), and in the patients with the mutation in codon 13, it was 44 months (40.1–48.4 months;  $p = 0.40$ ) (Figure 4). Median OS of the patients without mutation in the BRAF gene was 59.2 months (52.5–65.9), and in the patients with the mutated BRAF gene, it was 27.6 months (12.6–42.5), the difference was statistically significant ( $p = 0.05$ ) (Figure 5). The wtKRAS gene statistically significantly affected the response to the systemic therapy ( $p = 0.028$ ). Histological parameters included in the analysis and the BRAF gene mutation did not affect significantly the efficiency of first line systemic treatment.

Of 154 patients, 85 patients were wtKRAS and wtBRAF available for additional analysis, for 3 patients there was not possible to determine additional biomarker analysis from tumour tissue.

In 14 patients (17%) additional mutations in RAS gene were determined. Two patients were NRAS mutated, in 8 patients KRAS codon 61 mutation was determined, 4 patients were KRAS codon 146 mutated.

Median OS of 68 wtRAS patients was 27 months, median OS of 14 mutated RAS patients was 15 months. Median OS of wtNRAS, codon 61 and

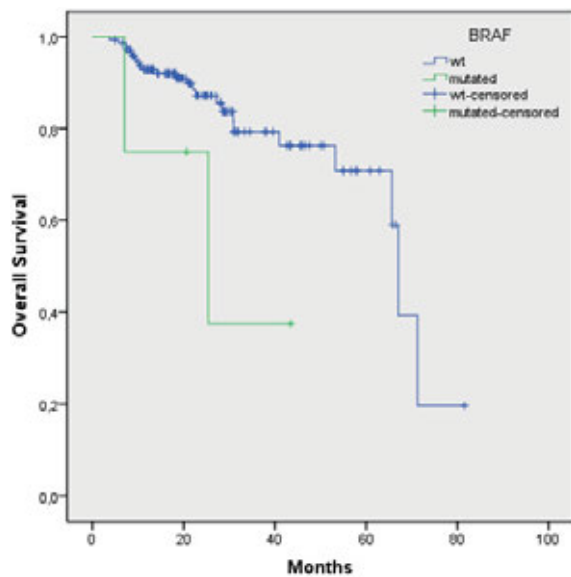


FIGURE 5. Overall survival of wtBRAF and mutated BRAF gene patients ( $p = 0.05$ ).

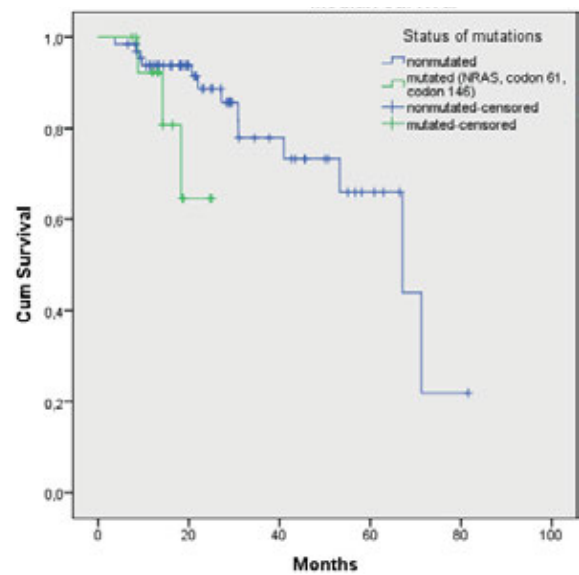


FIGURE 6. Median overall survival of wtNRAS, codon 61 and 146 patients and mutated NRAS, codon 61 and 146 patients ( $p = 0.072$ ).

TABLE 3. Response rate according to systemic treatment

Response rate	Systemic chemotherapy+ cetuximab, number (%)	Systemic chemotherapy+ bevacizumab, number (%)
Complete response	7 (13)	6 (17)
Partial response	18 (34)	8 (23)
Stable disease	21 (40)	19 (54)
Progression of disease	7 (13)	2 (6)

TABLE 4. Response rate according to mutations in codon 12 and 13

Response rate	Codon 12 mutations, number (%)	Codon 13 mutations, number (%)
Complete response	6 (12)	2 (12)
Partial response	5 (11)	6 (35)
Stable disease	23 (49)	7 (41)
Progression of disease	13 (28)	2 (12)

146 patients was 67.1 months (50.3–67.6), in mutated NRAS, codon 61 and 146 patients, it has not been reached yet ( $p = 0.072$ ) (Figure 6). Median TTP of wtNRAS, codon 61 and 146 patients, was 11.7 months (10.4–14.5), of mtNRAS, codon 61 and 146 patients, was 7.9 months (6.1–11.0 months;  $p = 0.025$ ) (Figure 7).

## Efficacy

In the patients with the wtKRAS gene, the objective response was achieved in 47% of the patients treated with chemotherapy and cetuximab and in 40%

of the patients treated with chemotherapy and bevacizumab. Stable disease was achieved in 40% of the patients treated with chemotherapy and cetuximab and in 54% of the patients treated with chemotherapy and bevacizumab. The disease progressed in 13% of the patients who received chemotherapy and cetuximab, and in 6% of the patients who were treated with chemotherapy and bevacizumab.

In the patients with the mutated KRAS gene, the objective response was achieved in 23% of the patients with the mutation in codon 12, and in 47% of the patients with the mutation in codon 13. Stable disease was achieved in 49% of the patients with the mutation in codon 12 and in 41% of the patients with the mutation in codon 13. The disease progressed during first-line treatment in 28% of the patients with the mutation in codon 12 and in 12% of the patients with the mutation in codon 13. Response rate according to systemic treatment and according to mutations in codon 12 and 13 are shown in Table 3 and 4, respectively.

## Toxicity

The most common side effects according to the criteria of the National American Institute for Cancer - National Cancer Institute - common toxicity criteria (NCI - CTC, version 4.03) were of Grade 1 or 2. The adverse effects of Grade 3 were rare: diarrhea (2%), allergic reaction to cetuximab (2%), rash (1%) and thromboembolic (1%). Grade 4 adverse reactions were diarrhea (1%), leukopenia (1%), neu-

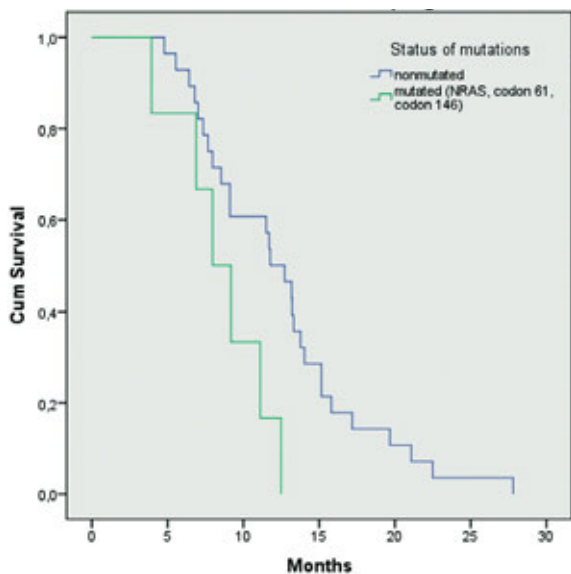


FIGURE 7. Median time to progression of wtNRAS, codon 61 and 146 patients, and mutated NRAS, codon 61 and 146 patients (p = 0.025).

tropenia (1%) and febrile neutropenia (1%). None of the patients died of adverse effects of systemic treatment (Table 5).

### Discussion

To our knowledge a prospective clinical study in patients with CRC determining the prognostic and predictive significance of the histological characteristics of primary tumours with mutations in the KRAS and BRAF gene regarding response to treatment has not yet been published. Our study was the first of that kind. The study was conducted from November 2010 to December 2012 and 154 patients were included, which was in line with the research plan. The percentage of patients with T4 tumour, G3 tumour, with more than 3 affected regional lymph nodes (N2), vascular, perineural invasion and lymphangiosis were comparable with previously published data.<sup>2,18</sup> Parameters as perforation of the primary tumour during surgery, presence of tumour deposits in subserosa, mesentery, peritonealised pericolic or perirectal mesenteric tissues and irresectability of the primary tumour, were excluded, because of the insufficient number

According to our results, poorly differentiated tumour cells and regionally advanced disease with a greater number of affected regional lymph nodes indicate a worse prognosis and a shorter survival of these patients. Other histological parameters of the primary tumour, such as the size of T4 tumour,

TABLE 5. Adverse effects of systemic treatment

	Grade 1 n (%)	Grade 2 n (%)	Grade 3 n (%)	Grade 4 n (%)
<b>Haematological</b>				
leukopenia	42 (27)	8 (5)	0	1 (1)
neutropenia	42 (27)	8 (5)	0	1+1
thrombocytopenia	33 (21)	11 (7)	0	(1+1)*
anaemia	88 (57)	10 (6)	0	0
<b>Non-haematological</b>				
alopecia	62 (40)	21 (14)	/	/
fatigue	93 (60)	11 (7)	0	/
nausea	40 (26)	10 (6)	0	/
vomiting	14 (9)	9 (6)	0	0
diarrhea	23 (15)	29 (19)	2 (2)	1 (1)
stomatitis	4 (3)	2 (2)	0	0
hand-foot syndrome	17 (11)	6 (4)	0	/
peripheral sensory neuropathy	32 (21)	8 (5)	0	0
hepatic toxicity	17 (11)	3 (2)	0	0
renal toxicity	0	0	1 (1)	0
acneiform rash	14 (9)	38 (25)	0	0
hypermagnesemia	6 (4)	0	3 (2)	0
allergic reaction to cetuximab	3 (2)	1 (1)	0	0
allergic reactions to oxaliplatin	1 (1)	0	0	0
arterial hypertension	3 (2)	9 (6)	0	/
proteinuria	20 (13)	18 (12)	0	0
bleeding	6 (4)	0	1 (1)	0
thromboembolic events	0	7 (5)	0	0
wound complications	0	0	0	/
perforation	0	0	0	0
arthralgia	17 (11)	2 (2)	0	0
bladder infection	/	3 (2)	0	0

\* 1 patient had febrile neutropenia; / = this grade of adverse effect does not exist; 0 = this grade of adverse effect was not observed in our study

carcinomatous lymphangiosis, vascular and perineural invasion, which speak of a greater biological aggressiveness of the disease and are important for decision on adjuvant systemic treatment in stages II and III, have not proved to be predictive factors of a worse outcome of the disease, although the difference in size of the primary T4 tumour was marginal (p = 0.08). We hypothesize that the cause of this could be the insufficient number of patients with such histological parameters as well as the short observation period (median observation period of 15 months), since the median OS in these patients has not yet been reached. Another possible cause may be that these histological parameters are not significantly relevant for the further course of the disease. According to the data from the literature, locally advanced primary tumour, with the infiltration of the free surface of serosa, and the incidence of a large number of regional lymph nodes, vascular invasion and carcinomatous lymphangiosis are independent prognostic factors for worse outcome of the operable disease.<sup>2,19</sup> In the case of disseminating disease this parameters also predicts aggressive course although their importance in the spread of disease is not fully defined.

The percentage of mutations in the codon 12 and 13 of the KRAS gene was found in 42% of pa-

tients, which is in accordance with the literature data in which 30 to 40% mutations are reported.<sup>20-23</sup> According to the data from the retrospective analyses of the published clinical studies the mutations in codon 12 are more frequent than mutations in codon 13, which is also confirmed by our study. Namely, 73% of the patients had mutations in codon 12, and 27% of the patients had mutations in codon 13. All the mutations analyses in our study were performed on the tumour tissue of the primary tumour. Given the proven high degree of compliance of the mutations between tumour tissue of the primary tumour and metastases, no further analysis of the status of mutations in the *KRAS* gene in operable metastases or their biopsy has been done.<sup>24</sup> In our already published retrospective analysis, which included 176 patients, *KRAS* mutations in the genes were present in 30% of the patients and more often in codon 12 than in codon 13 (84% in codon 12 vs. 16% in codon 13).<sup>24</sup>

The median OS of patients with the non-mutated *KRAS* gene was shorter in our study than in patients with mutant *KRAS* genes, but, the difference was not statistically significant ( $p = 0.47$ ), suggesting that the mutation status in the *KRAS* gene predicts response to the treatment with EGFR inhibitors, but is not a prognostic factor for survival of the patients. In some patients with a wt-*KRAS* gene the presence of the V600E mutation in the *BRAF* gene most likely can be the cause of a shorter survival, since the presence of the V600E mutation in the *BRAF* gene, according to retrospective reports of previous clinical studies, indicates a worse outcome of metastatic disease.<sup>25-28</sup> The mutation of the V600E in the *BRAF* gene was present only in patients with a non-mutated *KRAS* gene, which was expected in accordance with previous reports of mutually exclusive exclusion of the simultaneous presence of the both mutations.<sup>24</sup> The median OS of patients with mutations in codon 12 was longer than in patients with mutations in codon 13 but was not significant ( $p = 0.41$ ). According to the data from the literature, patients with mutations in codon 13 have a shorter survival than patients with mutations in codon 12. Patients with mutations in codon 13 respond to treatment with EGFR inhibitors, otherwise in a lower percentage as patients without mutations in the *KRAS* gene. The retrospective analysis of the efficacy data of these patients with mutations both in codon 12 and codon 13 treated with another EGFR panitumumab inhibitor did not confirm this.<sup>28-30</sup> In standard treatment with regard to systemic treatment recommendations, patients with mutant *KRAS* gene

do not receive a therapy with EGFR inhibitors.<sup>15</sup> In our study, we also analysed the efficacy of systemic therapy in patients with mutant *KRAS* gene with respect to the presence of mutations in codons 12 and 13, none of whom received EGFR therapy. In our analysis, however, we found that patients with mutations in codon 13 respond to a higher percentage to systemic therapy than patients with mutations in codon 12 (47% vs. 23%). The definitive conclusions of this analysis are difficult to give, given that the patients with mutations in codon 13 are in lower number than patients with mutations in codon 12 (27% vs. 73%). These mutations are less frequent in accordance with the already published data from our retrospective study (16% vs. 84%) and other published data (16–28% mutations in the codon 13 *KRAS* gene).<sup>28-30</sup> However, given that they have a shorter survival than patients with mutations in codon 12, but respond in a higher percentage to the first treatment, we believe that results of this analysis will help in the treatment of these patients, and in particular in reducing the disease burden and improving the quality of life.

In our study, we also analysed TTP of the disease in patients with operable disease. There were 64 such patients, with operable primary tumour without metastases, 16 patients with rectal cancer and 48 with colon carcinoma. Median time to recurrence of the disease in patients after primary treatment of operable disease with a non-mutated *KRAS* gene was shorter than in patients with mutated *KRAS* gene (20 vs. 21 months), but the difference was not significant ( $p = 0.88$ ). We assume that the V600E mutation in the *BRAF* gene, which was found in four patients with a non-mutated *KRAS* gene contributes for such results. With this, we confirmed the prognostic importance of the V600E mutation in the *BRAF* gene for early progression and worse outbreaks in patients with a non-mutated *KRAS* gene.<sup>31,32</sup> The TTP of the disease in patients primarily treated for operable disease with operation was longer in those who had mutations in the *KRAS* codon 12 than in those with mutations in codon 13 (21 vs. 16 months), otherwise the difference was not significant ( $p = 0.53$ ).

Regarding the presence of the V600E mutation in the *BRAF* gene in our study, as previously stated it was found in four patients, representing 3% of all patients. According to the literature, the frequency of this mutation is from 5 to 10%.<sup>2,3,9,13</sup> Also, according to our previous retrospective analysis, the V600E mutation in the *BRAF* gene was present at a higher percentage of patients, in 7.4%.<sup>24</sup> It is assumed that the specificity of the patients involved

with such primary tumour characteristics may be due to the fact that the V600E mutation was present in a lower percentage. All four patients with the V600E mutation had colon cancer, three patients were previously on adjuvant treatment, and one had a primary disseminated disease. In a retrospective analysis of the study involving 94 patients with rectal carcinoma, none of the V600E mutations in the *BRAF* gene were detected in either patient.<sup>33</sup> This suggests that this mutation is probably less important in the development of rectal cancer. The time before progression of the disease in patients after primary treatment is longer for those who did not have the V600E mutation in the *BRAF* gene than in the V600E mutation (20 to 12 months), but the difference was not significant ( $p = 0.14$ ). The cause is most likely a small number of patients with this mutation, but such result suggests a worse prognosis of these patients and an earlier recurrence of the disease. In the survival analysis, patients without V600E mutations had a significantly longer median OS than those with V600E mutation (59.2 vs. 27.6 months;  $p = 0.05$ ). In a retrospective analysis of 176 patients, 13 patients with the V600E mutation in the *BRAF* gene had a significantly lower expected median survival than patients without this mutation (44.9 vs. 107.4 months;  $p = 0.04$ ).<sup>24</sup> Both studies, both the previous retrospective and the current prospective, confirm the prognostic importance of the V600E mutation in the *BRAF* gene for predicting a worse disease outcome with shorter patient survival.

Furthermore, we examined the response rate according to the type of systemic treatment in patients with non-mutated *KRAS* gene. There were 88 such patients. Three hundred and sixty patients with a non-mutated *KRAS* gene received the first line of systemic treatment with EGFR-inhibitor cetuximab in combination with oxaliplatin or irinotecan and fluoropyrimidines, 35 patients with a non-mutated *KRAS* gene received the first line of systemic treatment with angiogenesis inhibitor bevacizumab in combination with oxaliplatin or irinotecan and fluoropyrimidines. A higher percentage of objective responses (both complete and partial), both for treatment and stability of the disease was achieved in patients with non-mutated *KRAS* gene receiving cetuximab in combination with oxaliplatin or irinotecan and fluoropyrimidines.

The definitive conclusions about this analysis cannot be made within our research, since this is a small number of patients, and the number of patients was not balanced in number. In addition, the types of systemic chemotherapy that patients

received differ. However, it was found that patients with a non-mutated *KRAS* gene had a better response to systemic first-line treatment involving cetuximab regardless of the type of systemic chemotherapy as patients with the non-mutated *KRAS* gene that received angiogenesis inhibitor bevacizumab in combination with systemic chemotherapy.

Colorectal adenocarcinoma is a heterogeneous disease. We do not know all the factors that influence the course of the disease and the response to specific systemic therapy. The determination of other mutations in the *KRAS* gene, such as mutations in codon 61 and 146, and mutations in the *NRAS* gene, has been standard in clinical practice since 2014. The frequency of mutations is about 15% and the patients with a non-mutated *RAS* gene have about 40% of this mutation. In our retrospective analysis, we found 17% of these additional mutations, which is consistent with reports from previous literature and they are predictive for response to EGFR inhibitor therapy. Patients treated with first-line anti-EGFR targeted therapy without these additional mutations in *RAS* gene, had longer survival and time to progression compared to the patients who had them. Our results confirmed predictive value of these mutations in *RAS* gene for anti-EGFR targeted therapy. However, our group of patients is moderate, but it is consisted with previously published data.<sup>33,34</sup>

Adverse effects of systemic treatment were evaluated according to NCI-CTC, version 4.03. They were mostly of Grade 1 and 2. There were 2% of G3 diarrhea and hypermagnesemia and 1% of G3 bleeding. One patient had G4 adverse effect (febrile neutropenia). In our study, adverse effects were less common than in previous published literature.<sup>35-47</sup> None of the patients died of adverse effects.

However, all patients with *RAS* non-mutated genes do not respond to treatment with anti-EGFR inhibitors. Other biomarkers have to be determined. One of them is mismatch repair deficiency (MSI-H), which is present in 3.5% to 5.0% of mCRC.<sup>48,49</sup> Immunotherapy with checkpoint inhibitors is recommended in second-line therapy in these patients. In clinical trials, there are other biomarkers in response to specific systemic therapy, such as amfiregulin and epiregulin, PI3K and PTEN mutations, but are still not recommended in regular clinical practice.<sup>50</sup> In order to made definite reasoning on this issue we need more information and more studies, both, retrospective and prospective should be performed.

## Conclusions

According to the results of our prospective study G3 of tumour differentiation (poorly differentiated adenocarcinoma) and N2 status of regional lymph nodes (more than 3 metastatic regional lymph nodes) show a greater biological aggressiveness of the disease and shorter survival after the first relapse, but do not affect the efficacy of the first-line systemic therapy.

The mutations in the *KRAS* gene have predictive value for the response to treatment with EGFR inhibitors, but do not have prognostic significance for the survival of patients with disseminated colorectal adenocarcinoma. The *KRAS* mutations in codon 12 and 13 differently affect the survival of these patients and the response rate of first-line systemic therapy.

The V600E mutation in the *BRAF* gene does not have the prognostic significance for the decision on the type of first-line systemic therapy, but it predicts a poor prognosis of the disease and shorter survival of these patients at first relapse.

According to our retrospective analysis of additional mutations in *NRAS* gene and in *KRAS* codon 61 and 146 are predictive for treatment with anti-EGFR targeted therapy.

## Acknowledgement

The research was funded by Slovenian Research Agency (ARRS), grant number P3-0321.

## References

1. *Cancer in Slovenia 2015*. Ljubljana: Institute of Oncology Ljubljana, Epidemiology and Cancer Registry, Cancer Registry of republic of Slovenia; 2018.
2. Schmoll HJ, Van Cutsem E, Stein A, Valentini V, Glimelius B, Haustermans K, et al. ESMO consensus guidelines for management of patients with colon and rectal cancer. A personalized approach to clinical decision making. *Ann Oncol* 2012; **23**: 2479-516. doi: 10.1093/annonc/mds236
3. Van Cutsem E, Cervantes A, Adam R, Sobrero A, Van Krieken JH, Aderka D, et al. ESMO consensus guidelines for the management of patients with metastatic colorectal cancer. *Ann Oncol* 2016; **27**: 1386-422. doi: 10.1093/annonc/mdw235
4. National Comprehensive Cancer Network. *NCCN clinical practice guidelines in oncology: colon cancer. V.2.2018*. [cited 2018 Jun 15]. Available at: [http://www.nccn.org/professionals/physician\\_gls/PDF/colon.pdf](http://www.nccn.org/professionals/physician_gls/PDF/colon.pdf)
5. National Comprehensive Cancer Network: NCCN clinical practice guidelines in oncology: rectal cancer. V.2.2018 [cited 2018 Aug 3]. Available at: [http://www.nccn.org/professionals/physician\\_gls/PDF/colon.pdf](http://www.nccn.org/professionals/physician_gls/PDF/colon.pdf)
6. Biagi JJ, Raphael MJ, Mackillop WJ, Kong W, King WD, Booth CM. Association between time to initiation of adjuvant chemotherapy and survival in colorectal cancer. A systematic review and meta-analysis. *JAMA* 2011; **305**: 2335-42. doi: 10.1001/jama.2011.749
7. Ocvirk J. Advances in the treatment of metastatic colorectal carcinoma. *Radiol Oncol* 2009; **43**: 1-8. doi: 10.2478/v10019-009-0004-1
8. Meyerhardt JA, Mayer RJ. Systemic therapy for colorectal cancer. *N Engl J Med* 2005; **352**: 476-87. doi: 10.1053/j.gastro.2008.02.098
9. Esin E, Yalcin S. Maintenance strategy in metastatic colorectal cancer: a systematic review. *Cancer Treat Rev* 2016; **42**: 82-90. doi: 10.1016/j.ctrv.2015.10.012
10. Advanced colorectal cancer: ESMO clinical practice guidelines for diagnosis, treatment. *Ann Oncol* 2010; **21**: v93- 7. doi: 10.1093/annonc/mdq222
11. Markowitz SD, Bertagnolli MM. Molecular basis of colorectal cancer. *N Engl J Med* 2009; **361**: 2449-60. doi: 10.1056/NEJMra0804588
12. De Roock W, Jonker DJ, Di Nicolantonio F, Sartore-Bianchi A, Tu D, Siena S, Lamba S, et al. Association of *KRAS* p.G13D mutation with outcome in patients with chemotherapy-refractory metastatic colorectal cancer treated with cetuximab. *JAMA* 2010; **304**: 1812- 20. doi: 10.1001/jama.2010.1535
13. De Roock W, Claes B, Bernasconi D, De Schutter J, Biesmans B, Fountzilas G, et al. Effect of *KRAS*, *BRAF*, *NRAS*, and *PIK3CA* mutations on the efficacy of cetuximab plus chemotherapy in chemotherapy-refractory metastatic colorectal cancer: a retrospective consortium analysis. *Lancet Oncol* 2010; **11**: 753-62. doi: 10.1016/S1470-2045(10)70130-3
14. Tol J, Nagtegaal ID, Punt CJA. *BRAF* mutation in metastatic colorectal cancer. *N Engl J Med* 2009; **361**: 98-99. doi: 10.1056/NEJMe0804588
15. Samowitz WS, Sweeney C, Herrick J, Albertsen H, Levin TR, Murtaugh MA, et al. Poor survival associated with the *BRAF* V600E mutation in microsatellite-stable colon cancer. *Cancer Res* 2005; **65**: 6063-9. doi: 10.1158/0008-5472.CCR-05-0404
16. Ličar A, Cerkovnik P, Novaković S. Distribution of some activating *KRAS* and *BRAF* mutations in Slovene patients with colorectal cancer. *Med Oncol* 2011; **28**: 1048-53. doi: 10.1007/s12032-010-9631-z
17. Fariña-Sarasqueta A, van Lijschoten G, Moerland E, Creemers GJ, Lemmens VE, Rutten HJ, et al. The *BRAF* V600E mutation is an independent prognostic factor for survival in stage II and stage III colon cancer patients. *Ann Oncol* 2010; **21**: 2396-402. doi: 10.1093/annonc/mdq258
18. Eisenhauer EA, Therasse P, Bogaerts J, Schwartz LH, Sargent D, Ford R, et al. New response evaluation criteria in solid tumors: revised RECIST guideline (version 1.1). *Eur J Cancer* 2009; **45**: 228-47. doi: 10.1016/j.ejca.2008.10.026
19. Marzouk O, Schofield J. Review of histopathological and molecular prognostic features in colorectal cancer. *Cancers* 2011; **3**: 276-81. doi: 10.3390/cancers3022767
20. Ličar A, Cerkovnik P, Ocvirk J, Novaković S. *KRAS* mutations in Slovene patients with colorectal cancer: frequency, distribution and correlation with the response to treatment. *Int J Oncol* 2010; **36**: 1137-44. doi: 10.3892/ijo.00000596
21. Artale S, Sartore- Bianchi A, Veronese SM, Gambi V, Sarnataro CS, Gambacorta M, et al. Mutations of *KRAS* and *BRAF* in primary and matched metastatic sites of colorectal cancer. *J Clin Oncol* 2008; **26**: 4217- 9. doi: 10.1200/JCO.2008.18.7266
22. Bokemeyer C, Van Cutsem E, Rougier P, Ciardiello F, Heeger S, Schlichting M, et al. Addition of cetuximab to chemotherapy as first-line treatment for *KRAS* wild-type metastatic colorectal cancer: pooled analysis of the CRYSTAL and OPUS randomised clinical trials. *Eur J Cancer* 2012; **48**: 1466-75. doi: 10.1016/j.ejca.2012.02.057
23. Artale S, Sartore- Bianchi A, Veronese SM, Gambi V, Sarnataro CS, Gambacorta M, et al. Mutations of *KRAS* and *BRAF* in primary and matched metastatic sites of colorectal cancer. *J Clin Oncol* 2008; **26**: 4217-9. doi: 10.1200/JCO.2008.18.7286
24. Rebersek M, Boc M, Škerl P, Benedik J, Hlebanja Z, Volk N, et al. Efficacy of first-line systemic treatment in correlation with *BRAF* V600E and different *KRAS* mutations colorectal cancer - a single institution retrospective analysis. *Radiol Oncol* 2011; **45**: 285-91. doi: 10.2478/v10019-011-0039-y
25. Lambrechts D, De Roock W, Prenen H, De Schutter J, Jacobs B, Biesmans B, et al. The role of *KRAS*, *BRAF*, *NRAS* and *PIK3CA* mutations as a markers of resistance of cetuximab in chemorefractory metastatic colorectal cancer. *J Clin Oncol* 2009; **27**: 9020. doi: 10.1158/1078-0432.CCR-08-2961
26. Tejpar S, De Roock W. *PIK3CA*, *BRAF* and *KRAS* mutations and outcome prediction in chemorefractory metastatic colorectal cancer (mCRC) patients treated With EGFR targeting monoclonal antibodies (MoAbs): results of a European Consortium.[abstract]. *Eur J Cancer Suppl* 2009; **7**: 322. No. 6005

27. Loupakis F, Ruzzo A, Cremolini C, Vincenzi B, Salvatore L, Santini D, et al. KRAS codon 61, 146 and BRAF mutations predict resistance to cetuximab plus irinotecan in KRAS codon 12 and 13 wild-type metastatic colorectal cancer. *Br J Cancer* 2009; **101**: 715-21. doi: 10.18632/oncotarget.13697
28. Tejpar S, Celik I, Schlichting M, Sartorius U, Bokemeyer C, Van Cutsem E. Association of KRAS G13D tumor mutations with outcome in patients with metastatic colorectal cancer treated with first-line chemotherapy with or without cetuximab. *J Clin Oncol* 2012; **30**: 3570-7. doi: 10.1200/JCO.2012.42.2592
29. Peeters M, Douillard JY, Van Cutsem E, Siena S, Zhang K, Williams R, et al. Mutant KRAS codon 12 and 13 alleles in patients with metastatic colorectal cancer: assessment as prognostic and predictive biomarkers of response to panitumumab. *J Clin Oncol* 2013; **31**: 759-65. doi: 10.1200/JCO.2012.45.1492. Epub 2012 Nov 26.
30. Roth AD, Tejpar S, Dolorezni M, Yan P, Fiocca R, Klingbiel D, et al. Prognostic role of KRAS and BRAF in stage II and III resected colon cancer: results of the translational study on the PETACC-3, EORTC 40993, SAKK 60-00 trial. *J Clin Oncol* 2010; **28**: 466-74. doi: 10.1200/JCO.2009.23.3452.
31. Fujiyoshi K, Yamamoto G, Takahashi A, Arai Y, Yamada M, Kakuta M, et al. High concordance rate of KRAS/BRAF mutations and MSI-H between primary colorectal cancer and corresponding metastases. *Oncol Rep* 2017; **37**: 785-92. doi: 10.3892/or.2016.5323.
32. Gaedcke J, Grade M, Jung K, Schirmer M, Jo P, Obermeyer C, et al. KRAS and BRAF mutations in patients with rectal cancer treated with preoperative chemoradiotherapy. *Radiother Oncol* 2010; **94**: 76-81. doi: 10.1016/j.radonc.2009.10.001
33. Pietrantonio F, Cremolini C, Petrelli F, Di Bartolomeo M, Loupakis F, Maggi C, et al. First-line anti-EGFR monoclonal antibodies in panRAS wild-type metastatic colorectal cancer: a systematic review and meta-analysis. *Crit Rev Oncol Hematol* 2015; **96**: 156-66. doi: 10.1016/j.critrevonc.2015.05.016
34. Sorich MJ, Wiese MD, Rowland A, Kichenadasse G, McKinnon RA, Karapetis CS, et al. Extended RAS mutations and anti-EGFR monoclonal antibody survival benefit in metastatic colorectal cancer: a meta-analysis of randomized, controlled trials. *Ann Oncol* 2015; **26**: 13-21. doi: 10.1093/annonc/mdu378
35. Scartozzi M, Galizia E, Chiorrini S, Giampieri G, Berardi R, Pieratoni C, et al. Arterial hypertension correlates with clinical outcome in colorectal cancer treated with first-line bevacizumab. *Clin Oncol* 2009; **20**: 227-30. doi: 10.1093/annonc/mdn637
36. Mir O, Ropert S, Alexandre J, Goldwasser F. Hypertension as a surrogate marker for the activity of anti-VEGF agents. *Ann Oncol* 2009; **20**: 967-70. doi: 10.1093/annonc/mdp206
37. Poole C, Gardiner J, Twelves C, Johnston P, Harper P, Cassidy J, et al. Effect of renal impairment on the pharmacokinetics and tolerability of capecitabine (Xeloda) in cancer patients. *Cancer Chemother Pharmacol* 2002; **49**: 225-34. doi: 10.1007/s00280-001-4808-0
38. Cassidy J, Twelves C, Van Cutsem E, Hoff P, Bajetta E, Boyer M, et al. First-line oral capecitabine therapy in metastatic colorectal cancer: a favorable safety profile compared with intravenous 5-fluorouracil/leucovorin. *Ann Oncol* 2002; **13**: 566-75. doi: 10.1200/JCO.2001.19.21.4097
39. Hoskins JM, Goldberg RM, Qu P, Ibrahim JG, McLeod HL. UGT1A1\*28 genotype and irinotecan-induced neutropenia: dose matters. *J Natl Cancer Inst* 2007; **99**: 1290-421. doi: 10.1200/JCO.2009.21.7943
40. Hoskins JM, McLeod HL. UGT1A and irinotecan toxicity: keeping it in the family. *J Clin Oncol* 2009; **27**: 2419-21. doi: 10.1200/JCO.2009.21.7943
41. Pereg D, Lishner M. Bevacizumab treatment for cancer treatment with cardiovascular disease: a double edged sword? *Eur Heart J* 2008; **29**: 2325-26. doi: 10.1093/eurheartj/ehn384.
42. Scappaticci FA, Skillings JR, Holden SN, Gerber HP, Miller K, Kabbinavar F, et al. Arterial thromboembolic events in patients with metastatic colorectal cancer treated with chemotherapy and bevacizumab. *J Natl Cancer Inst* 2007; **99**: 1232-9. doi: 10.1093/jnci/djm086
43. Lee CS, Ryan EJ, Glen A, Doherty GA. Gastro-intestinal toxicity of chemotherapeutics in colorectal cancer: the role of inflammation. *World J Gastroenterol* 2014; **20**: 3751-61. doi: 10.3748/wjg.v20.i14.3751
44. Ocvirk J, Rebersek M. Management of cutaneous side effect of cetuximab therapy with K1 creme. *Radiother Oncol* 2008; **42**: 215-24. doi: 10.1016/j.radonc.2008.0022-4
45. Ocvirk J, Cencelj S. Management of cutaneous side-effect of cetuximab therapy in patients with metastatic colorectal cancer. *JEADV* 2010; **24**: 453-9. doi: 10.1111/j.1468-3083.2009.03446.x
46. Ocvirk J, Rebersek M, Boc M, Mesti T, Ebert Moltara M. Prophylactic use of K1 cream for reducing skin toxicity during cetuximab treatment in patients with metastatic colorectal cancer (mCRC). *J Clin Oncol* 2016; **28(15 Suppl)**: V124. doi: 10.1200/JCO.2010.28.15\_suppl.e14011.
47. Siena S, Glynne-Jones R, Adenis A, Thaler J, Preusser P, Aguilar EA, et al. Reduced incidence of infusion-related reactions in metastatic colorectal cancer during treatment with cetuximab plus irinotecan with combined corticosteroid and antihistamin premedication. *Cancer* 2010; **116**: 1827-37. doi: 10.1002/cncr.24945
48. Venderbosch, ID Nagtegaal, TS Maughan, CG Smith, JP Cheadle, D Fisher, et al. Mismatch repair status and BRAF mutation status in metastatic colorectal cancer patients: a pooled analysis of the CAIRO, CAIRO2, COIN, and FOCUS studies. *Clin Cancer Res* 2014 **20**: 5322-30. doi: 10.1158/1078-0432.CCR-14-0332
49. Le DT, Uram JN, Wang H, Bartlett BR, Kemberling H, Eyring AD, et al. PD-1 blockade in tumors with mismatch-repair deficiency. *N Engl J Med* 2015; **372**: 2509-20. doi: 10.1056/NEJMoa1500596
50. Therkildsen C, Bergmann TK, Henriksen-Schnack T, Ladelund S, Nilbert M. The predictive value of KRAS, NRAS, BRAF, PIK3CA and PTEN for anti-EGFR treatment in metastatic colorectal cancer: a systematic review and meta-analysis. *Acta Oncol* 2014; **53**: 852-64. doi: 10.3109/0284186X.2014.895036

# Genetic polymorphisms in aquaporin 1 as risk factors for malignant mesothelioma and biomarkers of response to cisplatin treatment

Barbara Senk<sup>1</sup>, Katja Goricar<sup>1</sup>, Viljem Kovac<sup>2</sup>, Vita Dolzan<sup>1</sup>, Alenka Franko<sup>3</sup>

<sup>1</sup> Pharmacogenetics Laboratory, Institute of Biochemistry, Faculty of Medicine, University of Ljubljana, Ljubljana, Slovenia.

<sup>2</sup> Institute of Oncology Ljubljana, Ljubljana, Slovenia

<sup>3</sup> Clinical Institute of Occupational Medicine, University Medical Centre Ljubljana, Ljubljana, Slovenia

Radiol Oncol 2019; 53(1): 96-104.

Received 9 January 2019

Accepted 25 January 2019

Correspondence to: Assoc. Prof. Alenka Franko, M.D., Ph.D., Clinical Institute of Occupational Medicine, University Medical Center Ljubljana, Ljubljana, Poljanski nasip 58, 1000 Ljubljana, Slovenia. Phone: +386 1 5222 119; Fax: +386 1 5222 478; E-mail: alenka.franko@siol.net; ORCID ID: <https://orcid.org/0000-0001-9548-3786>

Disclosure: No potential conflicts of interest were disclosed.

**Background.** Malignant mesothelioma (MM) is an asbestos related aggressive tumor with poor prognosis. The aim of this study was to investigate if aquaporin 1 (AQP1) genetic polymorphisms influence the risk of MM and the response to cisplatin based MM treatment.

**Patients and methods.** The case-control study included 231 patients with MM and a control group of 316 healthy blood donors. All subjects were genotyped for three AQP1 polymorphisms (rs1049305, rs1476597 and rs28362731). Logistic and Cox regression were used in statistical analysis.

**Results.** AQP1 rs1049305 polymorphism was significantly associated with MM risk in dominant model adjusted for gender and age (OR = 0.60, 95% CI = 0.37–0.96,  $P_{\text{adj}}$  = 0.033). This polymorphism was also significantly associated with cisplatin based treatment related anaemia (unadjusted: OR = 0.49, 95% CI = 0.27–0.90,  $P$  = 0.021; adjusted: for CRP: OR = 0.52, 95% CI = 0.27–0.99,  $P$  = 0.046), with leukopenia (OR = 2.09, 95% CI = 1.00–4.35,  $P$  = 0.049) in dominant model and with thrombocytopenia (OR = 3.06, 95% CI = 1.01–9.28,  $P$  = 0.048) and alopecia (OR = 2.92, 95% CI = 1.00–8.46,  $P$  = 0.049) in additive model. AQP1 rs28362731 was significantly associated with thrombocytopenia (unadjusted: OR = 3.73, 95% CI = 1.00–13.84,  $P$  = 0.049; adjusted for pain: OR = 4.63, 95% CI = 1.13–19.05,  $P$  = 0.034) in additive model.

**Conclusions.** AQP1 may play a role in the risk of MM. Furthermore, AQP1 genotype information could improve the prediction of MM patients at increased risk for cisplatin toxicity.

Key words: malignant mesothelioma; AQP1; polymorphism; cisplatin

## Introduction

It is generally accepted that the risk of developing diseases and an individual's response to the treatment may also depend on their genetic characteristics. In this study, we have focused on malignant mesothelioma (MM), which is a very aggressive cancer associated with the exposure to asbestos.<sup>1-4</sup> Most frequently it arises from pleura or peritoneum, but can also arise from other serous surfaces.<sup>5,6</sup>

In Slovenia, the professional exposure to asbestos occurred mainly in asbestos cement industry,

in construction, in manufacture of machinery and insulation materials, in maintenance of various means of transport, in textile industry and in other activities.<sup>7-9</sup> Malignant mesothelioma is associated also with exposure to asbestos outside the workplace.<sup>5,8-10</sup> It is estimated that the incidence of MM will remain stable or will even increase in the near future due to the continuous presence of asbestos in buildings and to the long latent period after exposure to asbestos.<sup>11,12</sup> It is predicted that its incidence in the most industrialized countries will continue to increase until 2020,<sup>5</sup> or even later.<sup>11</sup>

Due to an increasing incidence of MM and its poor prognosis, new prognostic and predictive biomarkers are needed.<sup>13</sup> Symptoms of MM commonly occur only at late stages, therefore novel biomarkers for earlier diagnosis of MM and for establishing the response to treatment might be a promising opportunity for these patients.<sup>14</sup> Several classes of potential biomarkers of MM have been studied so far, from serum peptides to genetic and epigenetic biomarkers, however with limited success. Among serum biomarkers, soluble peptides related to mesothelin (soluble mesothelin-related peptides, SMRP),<sup>15</sup> fibulin-3,<sup>16</sup> survivin<sup>13</sup> have been studied, however none of them had sufficient predictive value as a standalone biomarker. It has been proposed, that biomarkers from two different molecular classes: protein and miRNA could be used in a combination to improve the biomarker sensitivity and specificity.<sup>14</sup>

Another approach was to investigate interindividual genetic variability in genes coding for key determinants of molecular pathogenesis of MM as potential biomarkers for prediction of the risk of MM as well as treatment response. Several studies have shown that polymorphisms in the genes involved in xenobiotic and oxidative metabolism or in DNA repair processes may play an important role in aetiology and pathogenesis of MM.<sup>17-19</sup> The most commonly studied *GSTM1* null polymorphism showed an increased risk for MM.<sup>17</sup> Similarly, two variant alleles of *XRCC1* and *XRCC3* were associated with increased risk for MM.<sup>17</sup> The carriers of at least one polymorphic *NQO1* allele (CT and TT genotypes) had an increased risk of MM compared to those with CC genotype.<sup>19</sup> A recent study showed also the association of *FTO* variability with MM susceptibility.<sup>20</sup> On the other hand, *MMP2* polymorphism was suggested to have a protective role in MM.<sup>21</sup> Furthermore, two of the investigated *MMP9* single nucleotide polymorphisms (SNPs) had significant but opposing effect on time to progression (TTP) and overall survival (OS) in MM.<sup>22</sup> *FASL-844* polymorphism could predict progression free survival (PFS) in MM patients receiving platinum based chemotherapy.<sup>23</sup> Polymorphisms in *REV1* and *REV3L* were also associated with the outcome of cisplatin based chemotherapy in MM.<sup>24</sup> The results of the study showed that DNA repair gene polymorphisms *XRCC1* may modify the response to gemcitabine-platinum combination chemotherapy in MM patients.<sup>18</sup> Despite such high numbers of genetic factors investigated, the search for potential novel genetic biomarkers continues.

Aquaporins (AQPs) are small transmembrane proteins, which facilitate an osmotically controlled passage of water. Recent research indicated a key role of AQPs in human carcinogenesis.<sup>25-27</sup> All key processes in cancer cells depend on water in the tumour microenvironment, therefore an enhanced transmembrane transmission of water is stimulated in comparison to normal cells. Overexpression of AQPs in the cell lines of the vascular endothelium and tumour cell lines suggests that AQPs may be closely related to the development and progression of a tumour.<sup>28</sup> In some cancers AQP1 expression was also shown to participate in metastatic processes.<sup>29</sup> In *AQP1*-knockout mice, xenograft tumour growth and angiogenesis were reduced, and significant necrosis occurred in the tumour tissues.<sup>30</sup>

The expression of AQP1 in MM tumour cells has been suggested to be an independent prognostic factor favouring survival in MM patients: higher levels of an AQP1 expression only in tumour cells, but not in vascular cells, predicted a better survival.<sup>31</sup> Higher levels of AQP1 expression were also associated with a better course of the disease in MM, but with worse course of the disease in some other tumours such as breast cancer, melanoma, urothelial and pharyngeal carcinoma.<sup>32-35</sup> AQP1 is of interest as a potential biomarker in MM patients as it was shown to be an independent prognostic factor<sup>11</sup> with high levels of its expression correlating with an increased survival.<sup>29,31,36</sup> AQP1 expression also correlated with improved survival rates in MM with epithelioid component in comparison to AQP1-poor MM.<sup>37</sup> Furthermore, AQP1 is also a possible new target for MM treatment,<sup>5</sup> and there are already AQP1 blockers available which could be used for therapy.<sup>38</sup>

Genetic polymorphisms were reported in *AQP1* gene, however according to our knowledge they have never been investigated in MM. A functional *AQP1* rs1476597 (-783G/C) SNP leading to transcriptional activation of the *AQP1* promoter and increased *AQP1* mRNA expression in C allele carriers was associated with better survival in glioblastoma multiform patients with GG and GC genotype.<sup>39</sup> Other *AQP1* SNPs were studied in a variety of conditions, but not in cancer. Firm evidence suggested that *AQP1* rs1049305 SNP could be involved in genetic susceptibility for development of water retention in patients with liver cirrhosis.<sup>40</sup> The study in marathon runners reported a significant association between *AQP1* rs1049305 and running performance. This study suggested that *AQP1* rs1049305 polymorphism located in 3'-UTR, in interaction with miRNAs could influence

the mRNA expression and AQP1 protein levels.<sup>41</sup> Triathletes who carried *AQP1* rs1049305 C allele had better running performance in comparison to GG genotype. This SNP was not associated with relative body weight change.<sup>41</sup> It has been suggested that *AQP1* rs10244884 could predict the risk of vaso-occlusion in sickle cell patients.<sup>42</sup>

The aim of the present study was to investigate the influence of *AQP1* genetic polymorphisms on the risk of developing MM and response to cisplatin-based treatment.

## Patients and methods

### Study population

The case-control study included patients treated for mostly MM of pleura or also peritoneum at the Institute of Oncology Ljubljana from 2007 to the end of 2016. Control group consisted of blood donors from the Institute of Transfusion Medicine in Ljubljana and were over 40 years old.

The diagnosis of MM was made by means of thoracoscopy or video-assisted thoracoscopic surgery (VATS) in patients with pleural MM and by means of laparoscopy or laparotomy in peritoneal MM. The diagnosis was confirmed histopathologically by an experienced pathologist [15].<sup>15</sup>

Demographic and clinical data (age, gender, smoking, possible other diseases) from patients with MM were obtained from the medical records of the Institute of Oncology Ljubljana.

The following clinical indicators were used to evaluate the efficacy of treatment: response to treatment according to the modified criteria RECIST (Response Evaluation Criteria in Solid Tumours),<sup>43</sup> PFS and overall survival (OS). The toxicity of the treatment was assessed according to NCI criteria (National Cancer Institute Common Terminology Criteria for Adverse Events, version 4.0).<sup>44</sup>

### Ethical approval

The study was approved by the Republic of Slovenia National Medical Ethics Committee (41/02/09) and was carried out according to the Helsinki Declaration. All the subjects included in the study have signed the written informed consent.

### Genotyping methods

DNA samples from 26 patients were isolated from peripheral venous blood with commercially avail-

able reagent sets (QIAamp DNA Mini Kit and Flexigene DNA Kit (Qiagen, Hilden, Germany)). For all other patients and controls DNA was already isolated from peripheral venous blood samples during the course of the previous studies.<sup>18,45-48</sup>

Based on the bioinformatics analysis, we selected the following SNPs: *AQP1* rs1049305 G> C in 3'-untranslated region that may affect the binding of miRNA [41], *AQP1* rs1476597 G> C in the 5'-regulatory region that may affect the binding of the transcription factors<sup>49</sup> and *AQP1* rs28362731 G> A that may affect splicing.

All the polymorphisms were genotyped using competitive allele specific PCR (KASPar) according to the manufacturer's instructions (LGC Genomics, UK).

### Statistical analysis

All statistical analyses were performed using IBM SPSS Statistics version 21.0 (IBM Corporation, Armonk, NY, USA). With the usual descriptive statistics we first described the characteristics of each variable separately. In order to assess the causal relationship between MM and the individual variables, we first used a univariate logistic regression. Both additive and dominant models were used to assess the effect of the selected *AQP1* polymorphisms. Analysis was followed by the multivariate statistical modelling, taking into account the selected *AQP1* polymorphisms and possible confounders such as age, gender, and smoking and significant clinical parameters. Hazard ratio (HR), 95% confidence interval (95% CI) and P-value were determined by Cox regression and median survival was determined by the Kaplan-Meier method.

In order to test the interactions between the selected *AQP1* polymorphisms we introduced the logistic regression models with dummy variables.

## Results

The clinical characteristics of MM patients are shown in Table 1. Among all 231 patients whose median (25%–75% range) age was 66 (58–73) years, men represented 73.6%. Epithelioid MM was present in 72.3% of patients. ECOG performance status 1 (48.1%) and 2 (39.0%) prevailed. Exposure to asbestos was confirmed in 73.8% of patients. Among all patients, 46.7% were smokers. In total 194 patients were treated with cisplatin based therapy.

In addition, 316 healthy blood donors, 235 men and 81 women, whose median (25%–75% range)

age was 49 (45-55) years were also included in the molecular-genetic part of the study.

The genotype frequency distribution for the investigated polymorphisms in 231 MM patients and in 316 controls, their minor allele frequencies (MAF) and the risk of developing MM are shown in Table 2. The genotypes' distribution was in Hardy-Weinberg equilibrium (HWE), except for the distribution of *AQP1* rs1476597 in MM patients and also in healthy controls that were not consistent with HWE and therefore we excluded this polymorphism from further statistical analysis.

In univariate analysis no polymorphism was associated with the risk of developing MM (Table 2). Higher age was associated with a higher risk of developing MM (OR = 1.21, 95% CI = 1.17–1.25,  $P < 0.001$ ) but gender (OR = 1.04, 95% CI = 0.71–1.53,  $P = 0.838$ ) was not. *AQP1* rs1049305 polymorphism was significantly associated with the risk of developing MM when adjusted for age and gender (OR = 0.59, 95% CI = 0.35–0.97,  $P_{\text{adj}} = 0.039$  in additive model; OR = 0.60, 95% CI = 0.37–0.96,  $P_{\text{adj}} = 0.033$  in dominant model). *AQP1* rs28362731 was not significantly associated with the risk of developing MM even when adjusted for age and gender (Table 2).

Clinical characteristics of MM patients treated with cisplatin based chemotherapy are presented in Table 3. The majority (68.0%) of patients were treated with gemcitabine in combination with cisplatin. In chemotherapy response a third (32.8%) of patients responded with partial response (PR) and only in few patients (3.2%) the response was complete (CR). A half (49.5%) of patients had stable disease (SD) and a few (14.5%) of them had progressive disease (PD). Median progression free survival (PFS) was 7.8 months, median overall survival (OS) 18.1 months and median follow-up from the start of chemotherapy 49.2 months.

In the survival analysis, *AQP1* rs28362731 and *AQP1* rs1049305 were not significantly associated with PFS or with OS when patients were treated with cisplatin based chemotherapy (Table 4). Even when adjusted for histological type of MM, smoking, weight loss and CRP, *AQP1* polymorphisms were not significantly associated with PFS. Likewise associations with OS remained insignificant after adjustment for the histological type of MM, smoking and CRP (data not shown). In the chemotherapy response, *AQP1* rs28362731 and *AQP1* rs1049305 were not significantly associated with response rate when patients were treated with cisplatin in combination with either gemcitabine or pemetrexed (Table 4). These associations remained

insignificant when adjusted for loss of weight and CRP (data not shown).

The association between SNPs and side effects in cisplatin based treatment is shown in Tables 5 and 6. *AQP1* rs1049305 was significantly associated with anemia grade  $\geq 2$  both in additive and dominant genetic model (additive model for genotype GC: OR = 0.40, 95% CI = 0.20–0.78,  $P = 0.007$ ; dominant model OR = 0.49, 95% CI = 0.27–0.90,  $P = 0.021$ ). The associations remained significant also when adjusted for CRP (OR = 0.46, 95% CI = 0.23–0.92,  $P = 0.029$  in additive model; OR = 0.52, 95% CI

**TABLE 1.** Description of all malignant mesothelioma (MM) patients (N = 231) and MM patients treated with cisplatin based chemotherapy (N = 194)

Characteristic	Characteristic type	All MM patients	MM patients treated with cisplatin based chemotherapy
		N (%)	N (%)
Age	Median (25%–75%)	66 (58–73)	65 (58–71.3)
Gender	Men	170 (73.6)	146 (75.3)
	Women	61 (26.4)	48 (24.7)
MM stage	I	18 (7.8)	15 (7.7)
	II	57 (24.7)	48 (24.7)
	III	69 (29.9)	62 (32.0)
	IV	66 (28.6)	50 (25.8)
	Peritoneal MM	20 (8.7)	18 (9.3)
	Undefined	1 (0.4)	1 (0.5)
Histological type	Epithelioid	167 (72.3)	147 (75.8)
	Biphasic	26 (11.3)	21 (10.8)
	Sarcomatoid	24 (10.4)	21 (10.8)
	Undefined	14 (6.0)	5 (2.6)
ECOG performance status	0	15 (6.5)	15 (7.7)
	1	111 (48.1)	100 (51.5)
	2	90 (39.0)	76 (39.2)
	3	15 (6.5)	3 (1.5)
Exposure to asbestos	No	59 (26.6) <sup>a</sup>	45 (23.3) <sup>c</sup>
	Yes	166 (73.8)	148 (76.7)
Smoking	No	120 (53.3) <sup>a</sup>	101 (52.6) <sup>d</sup>
	Yes	105 (46.7)	91 (47.4)
Treatment	Gemcitabine/Cisplatin	132 (60.0) <sup>b</sup>	132 (68.0)
	Pemetrexed/Cisplatin	62 (28.2)	62 (32.0)
	Without chemotherapy	16 (7.3)	-
	Other forms of chemotherapy	10 (4.5)	-

Data are missing for: <sup>a</sup> 6 patients, <sup>b</sup> 11 patients, <sup>c</sup> 1 patient and <sup>d</sup> 2 patients. ECOG = Eastern Cooperative Oncology Group

TABLE 2. Distribution of AQP1 genotypes in MM patients and controls and risk of MM

SNP	Role	Genotype	Patients			Controls			OR (95% CI)	P	OR (95% CI) <sub>adj</sub>	P <sub>adj</sub>
			N (%)	MAF	P <sub>HWE</sub>	N (%)	MAF	P <sub>HWE</sub>				
rs28362731 <sup>a</sup>	p.Gly165Asp	GG	210 (92.1)	0.039	0.535	288 (91.7)	0.041	0.444	Ref.	-	Ref.	-
		GA	18 (7.9)			26 (8.3)			0.95 (0.51–1.78)	0.871	0.94 (0.38–2.30)	0.885
rs1049305 <sup>b</sup>	c.*578G>C	GG	107 (46.5)	0.337	0.082	128 (40.8)	0.373	0.288	Ref.	-	Ref.	-
		GC	91 (39.6)			138 (43.9)			0.79 (0.55–1.14)	0.207	0.59 (0.35–0.97)	<b>0.039</b>
		CC	32 (13.9)			48 (15.3)			0.80 (0.48–1.13)	0.390	0.63 (0.32–1.27)	0.199
		GC+CC	123 (53.5)			186 (59.2)			0.79 (0.56–1.12)	0.181	0.60 (0.37–0.96)	<b>0.033</b>
rs1476597 <sup>c</sup>	c.-783G>C	GG	157 (68.0)	0.255	<0.001	220 (70.1)	0.247	<0.001				
		GC	30 (13.0)			33 (10.5)						
		CC	44 (19.0)			61 (19.4)						

Data are missing for: <sup>a</sup>2 controls and 3 patients, <sup>b</sup>2 controls and 1 patient, <sup>c</sup>2 controls. <sub>adj</sub> = adjusted by gender and age; MAF = minor allele frequency; P<sub>HWE</sub> = P for Hardy-Weinberg equilibrium; Ref. = reference genotype

TABLE 3. Clinical characteristics of MM patients treated with cisplatin based chemotherapy (N = 194)

Characteristic		N (%)
Chemotherapy type	Gemcitabine and cisplatin	132 (68.0)
	Pemetrexed and cisplatin	62 (32.0)
Chemotherapy response <sup>a</sup>	Complete response (CR)	6 (3.2)
	Partial response (PR)	61 (32.8)
	Stable disease (SD)	92 (49.5)
	Progressive disease (PD)	27 (14.5)
Progression of disease <sup>b</sup>	No	20 (10.5)
	Yes	171 (89.5)
Death	No	58 (29.9)
	Yes	136 (70.1)
PFS	Median (25%–75%) (month)	7.8 (5.3–13.8)
OS	Median (25%–75%) (month)	18.1 (9.4–28.7)
Follow-up from the start of chemotherapy	Median (25%–75%) (month)	49.2 (18.9–75.5)
CRP	Median (25%–75%)	20.5 (9–58)
LDH	Median (25%–75%)	2.67 (2.26–3.11)
Pain <sup>b</sup>	No	79 (41.4)
	Yes	112 (58.6)
Weight loss <sup>c</sup>	No	68 (35.8)
	Yes	122 (64.2)

Data are missing for: <sup>a</sup>8 patients, <sup>b</sup>3 patients, <sup>c</sup>4 patients. CRP = C reactive protein; LDH = lactate dehydrogenase; OS = overall survival; PFS = progression free survival

= 0.27–0.99, P = 0.046 in dominant model). AQP1 rs1049305 was also significantly associated with thrombocytopenia in additive model for genotype CC (OR = 3.06, 95% CI = 1.01–9.28, P = 0.048), but not in dominant model. AQP1 rs1049305 was also significantly associated with the risk of leukopenia (additive model for genotype CC: OR = 3.03, 95% CI = 1.10–8.38, P = 0.033; dominant model OR = 2.09, 95% CI = 1.00–4.35, P = 0.049). Furthermore, there was a significant association of AQP1 rs1049305 with alopecia in additive model for genotype CC (OR = 2.92, 95% CI = 1.00–8.46, P = 0.049), however, this SNP was not associated with neutropenia, nephrotoxicity or nausea and/or vomiting.

AQP1 rs28362731 GA genotype was significantly associated with thrombocytopenia (OR = 3.73, 95% CI = 1.00–13.84, P = 0.049). This association remained significant when adjusted for pain at diagnosis (OR = 4.63, 95% CI = 1.13–19.05, P = 0.034).

The investigated polymorphisms did not statistically significantly influence neutropenia grade  $\geq 2$ , nephrotoxicity or nausea and/or vomiting (Tables 5 and 6).

Multiplicative interaction analysis did not show any interactions between AQP1 rs28362731 and AQP1 rs1049305 polymorphisms and the risk of developing MM (OR = 1.22, 95% CI = 0.33–4.56, P = 0.771). Additionally, interactions between rs28362731 and rs1049305, rs28362731 and smok-

**TABLE 4.** Influence of AQP1 SNP on survival and chemotherapy response in MM patients

SNP	Genotype	Progress free survival			Overall survival			Chemotherapy response			
		PFS median (25%–75%) month	HR (95% CI)	P	OS median (25%–75%) month	HR (95% CI)	P	Poor response N (%)	Good response N (%)	OR (95% CI)	P
rs28362731	GG	7.7 (5.2–13.6)	Ref.	-	18.1 (9.1–28.0)	Ref.	-	112 (65.1)	60 (34.9)	Ref.	-
	GA	11.1 (7.0–14.7)	0.72 (0.39–1.33)	0.299	26.5 (14.4–47.8)	0.56 (0.26–1.19)	0.130	6 (54.5)	5 (45.5)	1.56 (0.46–5.31)	0.481
rs1049305	GG	7.9 (5.4–12.1)	Ref.	-	18.1 (9.0–26.8)	Ref.	-	55 (64.7)	30 (35.3)	Ref.	-
	GC	7.8 (5.2–15.0)	0.80 (0.58–1.11)	0.187	22.1 (10.1–29.7)	0.72 (0.50–1.05)	0.091	43 (58.1)	31 (41.9)	1.32 (0.70–2.51)	0.394
	CC	7.4 (4.8–14.1)	0.92 (0.59–1.46)	0.736	13.3 (8.1–25.4)	1.10 (0.67–1.80)	0.712	20 (76.9)	6 (23.1)	0.55 (0.20–1.52)	0.248
	GC+CC	7.8 (4.9–15.0)	0.83 (0.62–1.13)	0.233	18.2 (9.5–28.7)	0.81 (0.58–1.14)	0.220	63 (63.0)	37 (37.0)	1.08 (0.59–1.97)	0.810

SNP = single nucleotide polymorphisms; OS = overall survival; PFS = progression free survival; Ref. = reference genotype

**TABLE 5.** Association between AQP1 SNPs and haematological side effects of cisplatin based treatment (N = 176)

SNP	Genotype	Anemia grade ≥ 2 <sup>a</sup>					Thrombocytopenia <sup>b</sup>					Leukopenia grade ≥ 2 <sup>c</sup>			Neutropenia grade ≥ 2		
		N (%)	OR (95% CI)	P	OR (95% CI) <sub>adj1</sub>	P <sub>adj1</sub>	N (%)	OR (95% CI)	P	OR (95% CI) <sub>adj2</sub>	P <sub>adj2</sub>	N (%)	OR (95% CI)	P	N (%)	OR (95% CI)	P
rs28362731	GG	79 (49.4)	Ref.	-	Ref.	-	21 (13.3)	Ref.	-	Ref.	-	39 (25.2)	Ref.	-	59 (36.4)	Ref.	-
	GA	3 (27.3)	0.38 (0.10–1.50)	0.169	0.53 (0.13–2.12)	0.370	4 (36.4)	3.73 (1.00–13.84)	<b>0.049</b>	4.63 (1.13–19.05)	<b>0.034</b>	2 (18.2)	0.66 (0.14–3.19)	0.606	3 (27.3)	0.66 (0.17–2.56)	0.543
rs1049305	GG	46 (56.8)	Ref.	-	Ref.	-	10 (12.5)	Ref.	-	Ref.	-	14 (17.5)	Ref.	-	25 (30.9)	Ref.	-
	GC	23 (34.3)	0.40 (0.20–0.78)	<b>0.007</b>	0.46 (0.23–0.92)	<b>0.029</b>	8 (11.8)	0.93 (0.35–2.52)	0.892	0.71 (0.24–1.08)	0.529	18 (27.7)	1.81 (0.82–3.99)	0.144	26 (37.1)	1.32 (0.67–2.60)	0.416
	CC	13 (52.0)	0.82 (0.34–2.03)	0.674	0.74 (0.28–1.94)	0.536	7 (30.4)	3.06 (1.01–9.28)	<b>0.048</b>	2.18 (0.69–6.94)	0.185	9 (36.1)	3.03 (1.10–8.38)	<b>0.033</b>	11 (45.8)	1.90 (0.75–4.81)	0.178
	GC+CC	36 (39.1)	0.49 (0.27–0.90)	<b>0.021</b>	0.52 (0.27–0.99)	<b>0.046</b>	15 (16.5)	1.38 (0.58–3.28)	0.463	1.07 (0.43–2.69)	0.885	27 (30.7)	2.09 (1.00–4.35)	<b>0.049</b>	37 (39.4)	1.45 (0.78–2.72)	0.242

Data are missing for: <sup>a</sup>2 patients, <sup>b</sup>4 patients, <sup>c</sup>7 patients. <sub>adj1</sub> = adjusted by CRP; <sub>adj2</sub> = adjusted by pain at diagnosis; SNP = single nucleotide polymorphisms

**TABLE 6.** Associations between AQP1 SNPs and non-haematological side effects of cisplatin based treatment (N = 176)

SNP	Genotype	Alopecia <sup>a</sup>			Nephrotoxicity <sup>b</sup>			Nausea/Vomiting <sup>c</sup>		
		N (%)	OR (95% CI)	P	N (%)	OR (95% CI)	P	N (%)	OR (95% CI)	P
rs28362731	GG	60 (45.8)	Ref.	-	74 (46.8)	Ref.	-	73 (53.7)	Ref.	-
	GA	5 (55.6)	1.48 (0.38–5.76)	0.572	3 (27.3)	0.43 (0.11–1.66)	0.219	5 (55.6)	1.08 (0.28–4.19)	0.913
rs1049305	GG	30 (46.2)	Ref.	-	35 (43.8)	Ref.	-	36 (52.9)	Ref.	-
	GC	20 (35.7)	0.65 (0.31–1.35)	0.246	34 (50.0)	1.29 (0.67–2.46)	0.448	26 (44.8)	0.72 (0.36–1.46)	0.364
	CC	15 (71.4)	2.92 (1.00–8.46)	<b>0.049</b>	10 (43.5)	0.99 (0.39–2.52)	0.982	15 (71.4)	2.22 (0.77–6.41)	0.140
	GC+CC	35 (45.5)	0.97 (0.50–1.89)	0.934	44 (48.4)	1.20 (0.66–2.20)	0.547	41 (51.9)	0.96 (0.50–1.84)	0.900

Data are missing for: <sup>a</sup>33 patients, <sup>b</sup>4 patients and <sup>c</sup>28 patients. SNP = single nucleotide polymorphisms

TABLE 7. Influence of interactions on the risk of occurrence of side effects

Side effect	Interaction 1rs28362731 -rs1049305 OR (95% CI)	P <sub>1</sub>	Interaction 2 rs28362731 - smoking OR (95% CI)	P <sub>2</sub>	Interaction 3 rs1049305 - smoking OR (95% CI)	P <sub>3</sub>
Anemia grade ≥ 2 <sup>a</sup>	1.84 (0.10–32.37)	0.676	-	0.999	0.34 (0.10–1.16)	0.085
Leukopenia grade ≥ 2 <sup>b</sup>	0.95 (0.04–23.07)	0.974	-	0.999	0.92 (0.21–4.02)	0.915
Neutropenia grade ≥ 2	0.55 (0.03–9.76)	0.686	7.55 (0.39–145.1)	0.180	0.67 (0.19–2.35)	0.526
Thrombocytopenia <sup>c</sup>	1.73 (0.11–26.38)	0.693	3.06 (0.20–46.56)	0.422	0.95 (0.16–5.66)	0.955
Nephrotoxicity <sup>c</sup>	0.68 (0.04–11.98)	0.794	-	0.999	1.01 (0.30–3.43)	0.982
Alopecia <sup>d</sup>	2.06 (0.11–40.01)	0.633	-	0.999	0.60 (0.16–2.29)	0.453
Nausea/Vomiting <sup>e</sup>	2.12 (0.11–40.98)	0.620	6.83 (0.35–132.4)	0.204	0.71 (0.19–2.64)	0.608

Data are missing for: <sup>a</sup>2 patients, <sup>b</sup>7 patients, <sup>c</sup>4 patients, <sup>d</sup>33 patients and <sup>e</sup>28 patients. Interaction 1: interaction between rs28362731 and rs1049305. Interaction 2: interaction between rs28362731 and smoking. Interaction 3: interaction between rs1049305 and smoking.

ing and rs1049305 and smoking did not significantly influence the risk of occurrence of side effects (Table 7).

Haplotypes *AQP1* GG, GC and AG (5' → 3': rs28362731, rs1049305) were not significantly associated with the risk of developing MM even when adjusted for gender and age (Supplementary table).

## Discussion

In the present study we investigated the influence of *AQP1* genetic polymorphisms on the risk of developing MM as well as the associations with response to cisplatin based treatment. The important novel finding of our study is that the *AQP1* genetic variability might contribute to the risk of developing MM. Furthermore, we have shown the associations with the development of side effects of cisplatin based treatment.

*AQP1* rs1049305 polymorphism was significantly associated with the risk of developing MM, but only after adjustment for gender and age. *AQP1* rs1049305 GC heterozygotes had significantly lower risk of developing MM in the additive model, as well as the carriers of at least one polymorphic C allele in the dominant model in comparison to GG wild type. This polymorphism is located in the 3'-untranslated region, therefore it could affect the binding of miRNA and *AQP1* expression levels, however, the functionality of this polymorphism remains to be determined. On the other hand, *AQP1* rs28362731 was not significantly associated with the risk of developing MM in our study.

The statistical analyses have shown that the genotype distribution for the third investigated

polymorphism *AQP1* rs1476597 was not in accordance with HWE, so it had to be excluded from further analysis. In this polymorphism, the substitution of G for C was associated both with increased transcriptional-activation of the *AQP1*-promoter and with increased *AQP1* mRNA expression.<sup>39</sup> This is the only *AQP1* polymorphism that has been investigated in cancer so far and was associated with survival-time in glioblastoma multiforme patients.<sup>39</sup> This study used a pyrosequencing approach and reported that genotype distribution for *AQP1* rs1476597 was in accordance with HWE.<sup>39</sup> We have checked that there was no genotyping error, so deviation from HWE could be interpreted either as a potential influence of the fact, that this polymorphism may be triallelic (G/C/A) or that the polymorphisms in the proximity could affect the binding of our primers from the reaction mixture.

We have also assessed the impact of *AQP1* haplotypes, but they were not significantly associated with the risk of developing MM, not even when adjusted for age and gender.

Our study also showed that *AQP1* rs1049305 and *AQP1* rs28362731 were not significantly associated with PFS, OS or response rate when patients were treated with cisplatin in combination with either gemcitabine or pemetrexed. However, it has been suggested that *AQP1* may be an independent prognostic factor in MM, and that higher expression of *AQP1* in tumor cells, but not in vascular cells was significantly associated with better survival.<sup>31</sup> It has also been shown that *AQP1* expression significantly influenced the course of MM, regardless of the therapy or prognostic factors including histologic subtype, pathologic stage, gender, and age at time of diagnosis.<sup>31</sup>

We have also observed that *AQP1* rs1049305 was significantly associated with some of the treatment side effects such as anemia, leukopenia, thrombocytopenia and alopecia, but not with neutropenia, nephrotoxicity or nausea and/or vomiting. On the other hand, *AQP1* rs28362731 was significantly associated only with thrombocytopenia. Multiplicative interaction analysis did not show any interaction between *AQP1* rs28362731 and *AQP1* rs1049305 polymorphisms and the risk of occurrence of treatment related side effects. Similarly, side effects were not influenced by interactions between either of the studied polymorphism and smoking.

The major limitation of our study was that we had no information on asbestos exposure in healthy controls. Furthermore, MM patients were older than controls, as blood donors can only be up to 65 years old, however we accounted for that with adjustment for age in the statistical analysis. Despite the limited number of patients included in our study, all patients were monitored in the same institution and by the same oncologists, so there were no differences in the clinical assessments. Furthermore, all the patients and controls came from an ethnically homogeneous Slovenian population, so there were no differences due to genetic heterogeneity.<sup>50,51</sup>

Our study brings novel findings of the associations between *AQP1* genetic variability and the risk of developing MM that has not been previously investigated. Furthermore, it shows the impact of *AQP1* polymorphisms on the development of cisplatin treatment related side effects. It needs to be determined if the addition of these polymorphisms to previously described clinical-pharmacogenetics models could improve the prediction of treatment related side effects in MM patients [48]. Better understanding of pharmacogenetic polymorphisms would allow an individualized approach and better outcomes of cisplatin treatment in patients with MM.

In conclusion, our study suggests that the investigated *AQP1* polymorphisms may contribute to the risk of developing MM and cisplatin treatment related side effects, however our findings need to be validated in independent MM patient cohorts and in other cancers.

## Supplementary material

Supplementary table: The association between *AQP1* haplotypes and the risk of MM development.

## Acknowledgement

This work was financially supported by The Slovenian Research Agency (ARRS Grant No. P1-0170 and L3-8203).

## References

1. Wagner JC, Sleggs CA, Marchand P. Diffuse pleural mesothelioma and asbestos exposure in the North Western Cape Province. *Br J Ind Med* 1960; **17**: 260-71. PMID: 13782506
2. Zellos L, Christiani DC. Epidemiology, biologic behavior, and natural history of mesothelioma. *Thorac Surg Clin* 2004; **14**: 469-77. doi: 10.1016/j.thorsurg.2004.06.011.
3. Maule MM, Magnani C, Dalmasso P, Mirabelli D, Merletti F, Biggeri A. Modeling mesothelioma risk associated with environmental asbestos exposure. *Environ Health Perspect* 2007; **115**: 1066-71. doi: 10.1289/ehp.9900
4. Magnani C, Dalmasso P, Biggeri A, Ivaldi C, Mirabelli D, Terracini B. Increased risk of malignant mesothelioma of the pleura after residential or domestic exposure to asbestos: a case-control study in Casale Monferrato, Italy. *Environ Health Perspect* 2001; **109**: 915-9. doi: 10.1289/ehp.01109915
5. Klebe S, Griggs K, Cheng Y, Driml J, Henderson DW, Reid G. Blockade of aquaporin 1 inhibits proliferation, motility, and metastatic potential of mesothelioma in vitro but not in an in vivo model. *Dis Markers* 2015; **2015**: 286719. doi: 10.1155/2015/286719
6. Bridda A, Padoan I, Mencarelli R, Frego M. Peritoneal mesothelioma: a review. *MedGenMed* 2007; **9**: 32. PMID: 17955087
7. International Agency for Research on Cancer (IARC). IARC Working Group. Asbestos. *IARC monographs on the evaluation of carcinogenic risks to humans*. Lyon: IARC; 1972.
8. Brodtkin CA, Rosenstock L. Asbestos and asbestos-related pleural disease. In: Rosenstock L, Cullen MR, Brodtkin CA, Redlich CA, editors. *Textbook of clinical occupational and environmental medicine*. 2<sup>nd</sup> edition. Philadelphia: Elsevier Saunders; 2005. p. 364-77.
9. Wagner GR, Hearl FJ. Mineral dust: asbestos, silica, coal, manufactured fibers. In: Rosenstock L, Cullen MR, Brodtkin CA, Redlich CA, editors. *Textbook of clinical occupational and environmental medicine*. 2<sup>nd</sup> edition. Philadelphia: Elsevier Saunders; 2005. p. 1073-8.
10. Rom WN. Asbestosis, pleural fibrosis, and lung cancer. In: Rom WN, Markowitz SB, eds. *Environmental and occupational medicine*. 4<sup>th</sup> edition. Philadelphia: Wolters Kluwer, Lippincott Williams&Wilkins; 2007. p. 298-316.
11. Driml J, Pulford E, Moffat D, Karapetis C, Kao S, Griggs K, et al. Usefulness of aquaporin 1 as a prognostic marker in a prospective cohort of malignant mesotheliomas. *Int J Mol Sci* 2016; **17**(7). pii: E1041. doi: 10.3390/ijms17071041.
12. Zadnik V, Primic Zakelj M, Lokar K, Jarm K, Ivanus U, Zagar T. Cancer burden in slovenia with the time trends analysis. *Radiol Oncol* 2019; **53**(1): 96-104.7; **51**: 47-55. doi:10.1515/raon-2017-0008.
13. Gorick K, Kovac V, Franko A, Dodic-Fikfak M, Dolzan V. Serum survivin levels and outcome of chemotherapy in patients with malignant mesothelioma. *Dis Markers* 2015; **2015**: 316739. doi:10.1155/2015/316739
14. Weber DG, Casjens S, Johnen G, Bryk O, Raiko I, Pesch B, et al. Combination of MIR-103a-3p and mesothelin improves the biomarker performance of malignant mesothelioma diagnosis. *PLoS One* 2014; **9**: e114483. doi: 10.1371/journal.pone.0114483
15. Franko A, Dolzan V, Kovac V, Arneric N, Dodic-Fikfak M. Soluble mesothelin-related peptides levels in patients with malignant mesothelioma. *Dis Markers* 2012; **32**: 123-31. doi: 10.3233/DMA-2011-0866
16. Kovac V, Dodic-Fikfak M, Arneric N, Dolzan V, Franko A. Fibulin-3 as a biomarker of response to treatment in malignant mesothelioma. *Radiol Oncol* 2019; **53**(1): 96-104.5; **49**: 279-85. doi: 10.1515/raon-2015-0019

17. Neri M, Ugolini D, Dianzani I, Gemignani F, Landi S, Cesario A, et al. Genetic susceptibility to malignant pleural mesothelioma and other asbestos-associated diseases. *Mutat Res* 2008; **659**: 126-36. doi:10.1016/j.mrev.2008.02.002
18. Erculj N, Kovac V, Hmeljak J, Franko A, Dodic-Fikfak M, Dolzan V. DNA repair polymorphisms and treatment outcomes of patients with malignant mesothelioma treated with gemcitabine-platinum combination chemotherapy. *J Thorac Oncol* 2012; **7**: 1609-17. doi: 10.1097/JTO.0b013e3182653d31
19. Franko A, Kotnik N, Goricar K, Kovac V, Dodic-Fikfak M, Dolzan V. The influence of genetic variability on the risk of developing malignant mesothelioma. *Radiol Oncol* 2019; **53**(1): 96-104.8; **52**: 105-11. doi:10.2478/raon-2018-0004
20. Khella MS, Salem AM, Abdel-Rahman O, Saad AS. The association between the FTO rs9939609 variant and malignant pleural mesothelioma risk: a case-control study. *Genet Test Mol Biomarkers* 2018; **22**: 79-84. doi: 10.1089/gtmb.2017.0146
21. Strbac D, Goricar K, Dolzan V, Kovac V. Matrix metalloproteinases polymorphisms as baseline risk predictors in malignant pleural mesothelioma. *Radiol Oncol* 2019; **53**(1): 96-104.8; **52**: 160-6. doi: 10.2478/raon-2018-0005
22. Strbac D, Goricar K, Dolzan V, Kovac V. Matrix metalloproteinases polymorphisms as prognostic biomarkers in malignant pleural mesothelioma. *Dis Markers* 2017; **2017**: 8069529. doi: 10.1155/2017/8069529
23. El-Hamamsy M, Ghali RR, Saad AS, Shaheen SM, Salem AM. FAS and FASL genetic polymorphisms impact on clinical outcome of malignant pleural mesothelioma. *Onco Targets Ther* 2016; **9**: 6857-63. doi: 10.2147/OTT.S115631
24. Goricar K, Kovac V, Dolzan V. Polymorphisms in translesion polymerase genes influence treatment outcome in malignant mesothelioma. *Pharmacogenomics* 2014; **15**: 941-50. doi: 10.2217/pgs.14.14
25. Cao XC, Zhang WR, Cao WF, Liu BW, Zhang F, Zhao HM, et al. Aquaporin3 is required for FGF-2-induced migration of human breast cancers. *PLoS One* 2013; **8**: e56735. doi: 10.1371/journal.pone.0056735
26. Hwang I, Jung SI, Hwang EC, Song SH, Lee HS, Kim SO, et al. Expression and localization of aquaporins in benign prostate hyperplasia and prostate cancer. *Chonnam Med J* 2012; **48**: 174-8. doi: 10.4068/cmj.2012.48.3.174
27. Jung HJ, Park JY, Jeon HS, Kwon TH. Aquaporin-5: a marker protein for proliferation and migration of human breast cancer cells. *PLoS One* 2011; **6**: e28492. doi: 10.1371/journal.pone.0028492
28. Chen R, Shi Y, Amiduo R, Tuokan T, Suzuk L. Expression and prognostic value of aquaporin 1, 3 in cervical carcinoma in women of Uygur ethnicity from Xinjiang, China. *PLoS One* 2014; **9**: e98576. doi: 10.1371/journal.pone.0098576
29. Jagirdar RM, Apostolidou E, Molyvdas PA, Gourgoulianis KI, Hatzoglou C, Zarogiannis SG. Influence of AQP1 on cell adhesion, migration, and tumor sphere formation in malignant pleural mesothelioma is substratum- and histological-type dependent. *Am J Physiol Lung Cell Mol Physiol* 2016; **310**: L489-95. doi: 10.1152/ajplung.00410.2015
30. Saadoun S, Papadopoulos MC, Hara-Chikuma M, Verkman AS. Impairment of angiogenesis and cell migration by targeted aquaporin-1 gene disruption. *Nature* 2005; **434**: 786-92. doi: 10.1038/nature03460
31. Kao SC, Armstrong N, Condon B, Griggs K, McCaughan B, Maltby S, et al. Aquaporin 1 is an independent prognostic factor in pleural malignant mesothelioma. *Cancer* 2012; **118**: 2952-61. doi: 10.1002/cncr.26497
32. Qin F, Zhang H, Shao Y, Liu X, Yang L, Huang Y, et al. Expression of aquaporin1, a water channel protein, in cytoplasm is negatively correlated with prognosis of breast cancer patients. *Oncotarget* 2016; **7**: 8143-54. doi: 10.18632/oncotarget.6994
33. Imredi E, Toth B, Doma V, Barbai T, Raso E, Kenessey I, et al. Aquaporin 1 protein expression is associated with BRAF V600 mutation and adverse prognosis in cutaneous melanoma. *Melanoma Res* 2016; **26**: 254-60. doi: 10.1097/CMR.0000000000000243
34. Liu J, Zhang WY, Ding DG. Expression of aquaporin 1 in bladder uroepithelial cell carcinoma and its relevance to recurrence. *Asian Pac J Cancer Prev* 2015; **16**: 3973-6.
35. Lehnerdt GF, Bachmann HS, Adamzik M, Panic A, Koksai E, Weller P, et al. AQP1, AQP5, Bcl-2 and p16 in pharyngeal squamous cell carcinoma. *J Laryngol Otol* 2015; **129**: 580-6. doi: 10.1017/S002221511500119X
36. Jagirdar R, Solenov EI, Hatzoglou C, Molyvdas PA, Gourgoulianis KI, Zarogiannis SG. Gene expression profile of aquaporin 1 and associated interactors in malignant pleural mesothelioma. *Gene* 2013; **517**: 99-105. doi: 10.1016/j.gene.2012.12.075
37. Henderson DW, Reid G, Kao SC, van Zandwijk N, Klebe S. Challenges and controversies in the diagnosis of malignant mesothelioma: Part 2. Malignant mesothelioma subtypes, pleural synovial sarcoma, molecular and prognostic aspects of mesothelioma, BAP1, aquaporin-1 and micro-RNA. *J Clin Pathol* 2013; **66**: 854-61. doi: 10.1136/jclinpath-2013-201609
38. Yool AJ, Brown EA, Flynn GA. Roles for novel pharmacological blockers of aquaporins in the treatment of brain oedema and cancer. *Clin Exp Pharmacol Physiol* 2010; **37**: 403-9. doi: 10.1111/j.1440-1681.2009.05244.x
39. El Hindy N, Rump K, Lambertz N, Zhu Y, Frey UH, Bankfalvi A, et al. The functional aquaporin 1 -783G/C-polymorphism is associated with survival in patients with glioblastoma multiforme. *J Surg Oncol* 2013; **108**: 492-8. doi: 10.1002/jso.23421
40. Fabrega E, Berja A, Garcia-Unzueta MT, Guerra-Ruiz A, Cobo M, Lopez M, et al. Influence of aquaporin-1 gene polymorphism on water retention in liver cirrhosis. *Scand J Gastroenterol* 2011; **46**: 1267-74. doi: 10.3109/00365521.2011.603161
41. Saunders CJ, Posthumus M, O'Connell K, September AV, Collins M. A variant within the AQP1 3'-untranslated region is associated with running performance, but not weight changes, during an Ironman Triathlon. *J Sports Sci* 2015; **33**: 1342-8. doi: 10.1080/02640414.2014.989535
42. Elliott L, Ashley-Koch AE, De Castro L, Jonassaint J, Price J, Ataga KI, et al. Genetic polymorphisms associated with priapism in sickle cell disease. *Br J Haematol* 2007; **137**: 262-7. doi: 10.1111/j.1365-2141.2007.06560.x
43. Therasse P, Arbusck SG, Eisenhauer EA, Wanders J, Kaplan RS, Rubinstein L, et al. New guidelines to evaluate the response to treatment in solid tumors. European Organization for Research and Treatment of Cancer, National Cancer Institute of the United States, National Cancer Institute of Canada. *J Natl Cancer Inst* 2000; **92**: 205-16. PMID: 10655437
44. National Cancer Institute Common Terminology Criteria for Adverse Events, version 4.0. [cited 2018 Feb 15] Available at: [https://ctep.cancer.gov/protocoldevelopment/electronic\\_applications/ctc.htm](https://ctep.cancer.gov/protocoldevelopment/electronic_applications/ctc.htm).
45. Erculj N, Kovac V, Hmeljak J, Franko A, Dodic-Fikfak M, Dolzan V. The influence of gemcitabine pathway polymorphisms on treatment outcome in patients with malignant mesothelioma. *Pharmacogenet Genomics* 2012; **22**: 58-68. doi: 10.1097/FPC.0b013e32834e3572
46. Erculj N, Kovac V, Hmeljak J, Dolzan V. The influence of platinum pathway polymorphisms on the outcome in patients with malignant mesothelioma. *Ann Oncol* 2012; **23**: 961-7. doi: 10.1093/annonc/mdr324
47. Goricar K, Kovac V, Dolzan V. Polymorphisms in folate pathway and pemetrexed treatment outcome in patients with malignant pleural mesothelioma. *Radiol Oncol* 2019; **53**(1): 96-104.4; **48**: 163-72. doi: 10.2478/raon-2013-0086
48. Goricar K, Kovac V, Dolzan V. Clinical-pharmacogenetic models for personalized cancer treatment: application to malignant mesothelioma. *Sci Rep* 2017; **7**: 46537. doi: 10.1038/srep46537
49. Dimasi DP, Burdon KP, Hewitt AW, Savarirayan R, Healey PR, Mitchell P, et al. Candidate gene study to investigate the genetic determinants of normal variation in central corneal thickness. *Mol Vis* 2010; **16**: 562-9. PMID: 20360993
50. Vidan-Jeras B, Jurca B, Dolžan V, Jeras M, Breskvar K, Bohinjec M. »Caucasian slovenian normal«, *HLA 1998*. In: Terasaki PI, Gjerston DW, editors. *Lenexa: American Society for Histocompatibility and Immunogenetics*; 1998. p. 180-1.
51. Mizzi C, Dalabira E, Kumuthini J, Dzimir N, Balogh I, Basak N, et al. Correction: a European spectrum of pharmacogenomic biomarkers: implications for clinical pharmacogenomics. *PLoS One* 2017; **12**: e0172595. doi: 10.1371/journal.pone.0162866.]

# Potential of osteopontin in the management of epithelial ovarian cancer

Katarina Cerne<sup>1</sup>, Benjamin Hadzialjevic<sup>1</sup>, Erik Skof<sup>2</sup>, Ivan Verdenik<sup>3,4</sup>, Borut Kobal<sup>3,4</sup>

<sup>1</sup> Institute of Pharmacology and Experimental Toxicology, Faculty of Medicine, University Ljubljana, Ljubljana, Slovenia

<sup>2</sup> Department of Medical Oncology, Institute of Oncology Ljubljana, Ljubljana, Slovenia

<sup>3</sup> Department of Gynaecology, Division of Gynaecology and Obstetrics, University Medical Centre Ljubljana, Ljubljana, Slovenia

<sup>4</sup> Department of Gynaecology and Obstetrics, Faculty of Medicine, University Ljubljana, Ljubljana, Slovenia

Radiol Oncol 2019; 53(1): 105-115.

Received 7 September 2018  
Accepted 27 December 2018

Correspondence to: Prof. Borut Kobal, M.D., Ph.D, Department of Gynaecology and Obstetrics, Faculty of Medicine, University Ljubljana, Šlajmarjeva 3, SI-1000 Ljubljana, Slovenia. Phone: +386 1 522 6060; E-mail: borut.kobal1@siol.net

Disclosure: No potential conflicts of interest were disclosed.

**Background.** Osteopontin (sOPN) is a promising blood tumour marker for detecting epithelial ovarian cancer (EOC). However, other clinical uses of sOPN as a tumour marker in EOC are still lacking. Since sOPN concentrations in serum are not associated with those in ascites, we compared clinical value of sOPN concentrations in the two body fluids.

**Patients and methods.** The study included 31 women with advanced EOC and 34 women with benign gynaecological pathology. In the EOC group, serum for sOPN analysis was obtained preoperatively, after primary debulking surgery and after chemotherapy. In the control group, serum was obtained before and after surgery. Ascites and peritoneal fluid were obtained during surgery. sOPN concentrations were determined by flow cytometry bead-based assay.

**Results.** The sensitivity and specificity of sOPN in detecting EOC was 91.2% and 90.3% (cut-off = 47.4 ng/ml) in serum, and 96.8% and 100% (cut-off = 529.5 ng/ml) in ascites. Kaplan-Meier analysis showed a significant association between higher serum sOPN concentration and overall survival ( $p = 0.018$ ) or progression free survival ( $p = 0.008$ ). Higher ascites sOPN concentrations were associated with suboptimally debulked tumour and unresectable disease. Higher serum sOPN concentrations were associated with refractory disease or incomplete response to platinum-based chemotherapy.

**Conclusions.** The study showed that ascites sOPN level mirrors present disease and is superior to serum level for diagnostic purposes and surgical planning, although the end result of treatment is the response of the whole body in fighting the disease. The preoperative sOPN concentration in serum thus better reflects disease outcome.

Key words: advanced ovarian cancer; osteopontin; serum; ascites

## Introduction

Osteopontin (OPN) is an important signalling agent in the development and progression of cancers.<sup>1-4</sup> As a soluble protein, sOPN is one of the promising blood tumour markers for detecting epithelial ovarian cancer (EOC).<sup>5-8</sup> However, practical clinical use of sOPN as a tumour marker in EOC awaits further evaluation.

Although there are encouraging reports on sOPN as a serum tumour marker for detecting primary and recurrent EOC<sup>5,9-12</sup>, we have not found any published report on the prognostic value of preoperative serum sOPN level in EOC. It has been reported that increased expression of OPN in peritoneal metastatic lesion of EOC is associated with poor survival.<sup>13</sup> Additionally, we found that detecting the preoperative serum sOPN level is helpful

in assessing the prognosis of other cancer patients (*e.g.*, breast, neck, gastric).<sup>1,14</sup> It would therefore be worth also exploring the prognostic value of preoperative serum sOPN level in EOC patients.

Another attribute of a tumour marker is to help in selecting the best treatment for cancer patients. Treatment for advanced EOC patients consists of cytoreductive surgery and platinum-based chemotherapy.<sup>15-17</sup> Because of the significant survival benefit associated with successful cytoreductive surgery for advanced-stage EOC and the lack of benefit associated with an incomplete resection, attention has been directed toward developing preoperative models to predict surgical outcome. In addition to radiographic images, extent of ascites and gene expression, some of these models incorporate serum tumour marker levels, primarily cancer antigen 125 (CA125) as approved standard tumour marker in EOC.<sup>18,19</sup> Since OPN expression in metastasis is significantly increased compared to the primary tumour<sup>13</sup>, including OPN in such a model may improve the accuracy of determining the extent of intra-abdominal disease for surgical planning. The clinical usefulness of pre-treatment sOPN levels for predicting the response to chemotherapy is another field for further evaluation. A faster response to chemotherapy is an independent predictor of survival for patients with advanced EOC, regardless of debulking status.<sup>20</sup>

The results of our previous published study showed that the increase of sOPN baseline concentration in EOC patients in comparison to patients with non-malignant gynaecological pathology was much higher for local fluid (27-fold) ascites *vs* peritoneal fluid taken from the cavum Douglasi than for serum (3-fold).<sup>21</sup> It is therefore worth discovering whether determination of sOPN concentrations in ascites gives additional or more accurate information about the disease than the determination of serum sOPN concentration alone. In addition to the sOPN retention tendency in local fluid, which is potentiated in malignant compared to benign conditions, we found that sOPN concentrations in serum were not associated with concentrations in ascites or peritoneal fluid.<sup>21</sup> It would thus be reasonable to set separate control values of this marker in the blood and in the local fluid. Determination of sOPN concentrations in local fluid may be useful in combination with cytology in order to obtain more accurate results, especially in the classification of early stage disease.

Since OPN plays a significant role in carcinogenesis, the objective of our study was further to

evaluate the clinical usefulness of sOPN as a tumour marker in advanced EOC patients. The main aim of this study was to elucidate the prognostic value of preoperative serum and ascites sOPN levels. Furthermore, the usefulness of determining preoperative sOPN levels for surgical planning purposes and response to standard chemotherapy were investigated. To this end, we determined the kinetic pattern of sOPN serum concentrations after primary surgery and chemotherapy. Additionally, we examined the relationship of sOPN concentrations with various clinicopathological variables. Since sOPN concentrations in serum are not associated with concentrations in ascites, we compared the clinical usefulness of sOPN as a tumour marker in both body fluids of EOC patients.

## Patients and methods

### Patients

The study included 31 patients with advanced EOC [FIGO III-IV] and 34 patients with benign gynaecological pathology as a control group, who were operated between December 2011 and December 2013 at the Department of Gynaecology, University Medical Centre Ljubljana. Family, general, gynaecological and obstetric history, indication for surgery, other relevant diseases and current therapy were collected from medical records. Early-stage (FIGO I, II) and absence of ascites were exclusion criteria for enrolling patients with ovarian malignancy. The control group enrolled patients with common non-malignant gynaecological indications for surgery (*e.g.*, benign ovarian cyst, uterine myoma). Patients with malignancies and elevated standard tumour marker CA125 were excluded from the control group. The purpose of the study was explained to all patients and written informed consent was obtained prior to enrolment. The study was approved by the Commission of the Republic of Slovenia for Medical Ethics (No. 82/01/11) and in accordance with the Helsinki Declaration.

All EOC patients were intended for primary debulking surgery (PDS), but resectability was evaluated through imaging methods and diagnostic laparoscopy performed by an experienced oncologic surgeon. A patient was considered a candidate for neoadjuvant chemotherapy (NACT) in the case of wide spread of the disease in the abdominal and pelvic cavity (unresectable massive peritoneal involvement, widespread infiltrating carcinomatosis of diaphragm, mesenteral retraction, miliary car-

cinomatosis of the bowel, liver and stomach metastases). On the basis of these criteria, 13 patients underwent PDS and 18 patients underwent NACT, and 10 of the patients in the latter group also underwent interval debulking surgery (IDS). The extent of residual disease after debulking surgery was based on the diameter of the single largest lesion. Complete response to chemotherapy was defined by a normal serum CA125 level. The applied cut-off value for CA125 was 35 U/ml. A partial response was defined by a decrease of at least 50% in CA125 level. Patients with a smaller decrease or any increase in CA125 during chemotherapy were defined as non-responders. All available dimensions of the ovarian tumour were measured using imaging methods and, in the case of PDS, from the pathology report. All patients were followed to disease recurrence or death. Overall survival (OS) was measured from diagnosis until death from any cause. Progression-free survival (PFS) was defined as the time from diagnosis to first tumour recurrence.

### Collection and storage of samples

In the OC group, venous blood samples for determination of sOPN concentrations were obtained preoperatively, one week after PDS, and 3-6 months after the last cycle of chemotherapy. In the control group, venous blood samples were obtained prior to surgery, and 3-6 months after surgery, when the patients were healthy and non-pregnant. Four ml of peripheral blood was collected into a vacutainer, without anticoagulant or other additives. Serum was separated by centrifugation at  $2000 \times g$  for 15 minutes at  $4^\circ\text{C}$ . In both groups of patients, blood for analysis of standard tumour marker CA125 was collected at the same time as for sOPN analysis. Additionally, in the group of EOC patients, blood for CA125 measurement was obtained after each cycle of chemotherapy. Samples of ascites from patients with EOC were aspirated immediately after entry to the abdominal cavity, using a 50 ml syringe. In controls, samples of peritoneal fluid were collected during laparoscopy using a standard sampling protocol as previously described.<sup>22</sup> Samples of local fluids were transferred into a tube, which was kept on ice until centrifugation at  $1000 \times g$  for 10 min at  $4^\circ\text{C}$  within 30 minutes. Sera and supernatants of ascites and peritoneal fluid were stored in aliquots at  $-80^\circ\text{C}$ . Samples of serum, ascites and peritoneal fluid for total protein measurement were obtained at the

same time, and prepared and stored in the same manner as for sOPN analysis.

### Analysis of sOPN and total proteins

Concentrations of sOPN were measured using a FlowCytomix Simplex Kit (eBioscience, Vienna). The kit consisted of fluorescent microspheres with an emission wavelength of 700 nm. Microspheres were coated with specific antibodies raised against each of the analytes. They also contained a biotin-conjugated second antibody and streptavidin-phycoerythrin emitting at 575 nm. Samples were run on a Cell Lab Quanta™ SC-MPL (Beckman Coulter). Samples were acquired by Cell Lab Quanta™ SC-MPL software (Beckman Coulter) and analysed using FlowCytomix™ Pro 3.0 software (eBioscience). Total protein concentration was determined using the Bradford method.

### Statistical analysis

The prognostic value of sOPN concentration was examined in terms of OS and PFS, using the 50<sup>th</sup> percentile (median value) as the optimal cut-off. Surviving patients were censored at the date of last contact. Survival curves were generated using Kaplan-Meier, and the difference between the curves was analyzed by the Breslow test. Receiver operating characteristic (ROC) curve analysis was used to find the cut-off level of sOPN with optimal sensitivity and specificity. Cut-off values were calculated by Youden's index (as a criterion for selecting the optimum cut-off point). The areas under the ROC curve (AUCs) were calculated to evaluate diagnostic accuracy and to compare AUCs between sOPN in serum and in ascites. Pearson's and Spearman's correlation coefficients were used to calculate the direction and strength of the relationship between variables, as required in terms of the normality of variables. Data were compared by independent samples t-test. A *p*-value of  $< 0.05$  was considered significant. All data are presented as mean  $\pm$  standard error of mean (SEM). Statistical analysis was performed using software statistical package SPSS, version 19 (IBM Statistics, USA).

## Results

The clinical characteristics of the investigated EOC and control patients are summarized in Table 1 and 2, respectively.

**TABLE 1.** Comparison between ovarian cancer patients' characteristics who underwent primary debulking surgery and those considered candidates for neoadjuvant chemotherapy (= diagnostic laparoscopy as primary event)

Parameters	Data	
	Primary event: Debulking surgery	Primary event: Diagnostic laparoscopy
Number of patients	13	18
Age (years, value ± SEM)	57.61 ± 3.27	62 ± 2.45
Age range (years)	41-76	45-85
<b>Elevated CA125 (U/mL)</b>		
n (%)	13 (100 %)	18 (100 %)
Value (mean ± SEM)	3936 ± 1568	3904 ± 1972
<b>sOPN (ng/mL)</b>		
Serum (mean ± SEM)	70.48 ± 9.95	102 ± 11.53
Ascites (mean ± SEM)	2154 ± 479.7	4515 ± 657.3
<b>Histological type, n (%)</b>		
Serous	10 (77 %)	17 (94 %)
Endometrioid	2 (15 %)	1 (6 %)
Serous + clear cell	1 (8 %)	0 (0 %)
<b>FIGO stage, n (%)</b>		
IIIB	1 (8 %)	0 (0 %)
IIIC	11 (84 %)	11 (61 %)
IV	1 (8 %)	7 (39 %)
<b>Histological grade, n (%)</b>		
G1	0 (0 %)	2 (11 %)
G2	5 (38 %)	7 (39 %)
G3	8 (62 %)	9 (50 %)
<b>Ascites (mL)</b>		
Volume (mean ± SEM)	1779 ± 728.4	3916 ± 614.7
<b>Resection, n (%)</b>		*
R0	5 (38 %)	9 (50 %)
R1	5 (38 %)	1 (6 %)
R2	3 (24 %)	0 (0 %)
Unresectable	0 (0 %)	8 (44 %)

\* Results of interval debulking surgery.

CA125 = cancer antigen 125; FIGO = International Federation of Gynecology and Obstetrics; G = gradus; R0 = no macroscopic residual disease; R1 = < 1 cm residual disease; R2 = > 1 cm residual disease; SEM = standard error of the mean; sOPN = soluble osteopontin

### Diagnostic value of sOPN

The mean concentrations of sOPN in serum (88.92 ± 8.28 ng/ml) and ascites (3525 ± 475.1 ng/ml) were both significantly higher in EOC patients than in serum of patients in the control group (28.12 ± 2.15 ng/ml) and the peritoneal fluid (132.0 ± 7.85 ng/ml) of patients in the control group ( $p < 0.001$ ). To identify the diagnostic power of sOPN in

**TABLE 2.** Characteristics of control patients

Parameters	Data
	Control group
Number of patients	34
Age (years, value ± SEM)	41.97 ± 1.68
Age range (years)	21-69
<b>Elevated CA125 (U/mL)</b>	
n (%)	0
Value (mean ± SEM)	NA
<b>sOPN (ng/mL)</b>	
Serum (mean ± SEM)	28.12 ± 2.10
Peritoneal fluid (mean ± SEM)	132.02 ± 7.85
<b>Benign diagnosis, n (%)</b>	
Benign ovarian cyst	6 (17 %)
Myoma of uterus	21 (62 %)
Pelvic pain, sterilisation	5 (15 %)
Preventive adnexectomy	2 (6 %)
<b>Peritoneal fluid (mL)</b>	
Volume (mean ± SEM)	8.04 ± 1.22

CA125 = cancer antigen 125; SEM = standard error of the mean; sOPN = soluble osteopontin

serum and ascites, sensitivity and specificity were calculated at various cut-off points of sOPN level. The optimum cut-off value in the diagnosis of EOC was found to be 47.4 ng/ml for serum sOPN and 529.5 ng/ml for ascites sOPN. The sensitivity and specificity of these cut-off levels were lower for serum sOPN (91.2% and 90.3%; Figure 1A) than for ascites sOPN (96.8% and 100%; Figure 1B). The AUC for sOPN in serum (Figure 1A) and in ascites (Figure 1B) were 0.964 (95% CI: 0.926 - 1.00) and 0.998 (95% CI: 0.993 - 1.00), respectively. Preoperative concentrations of sOPN in serum and ascites were not correlated with concentrations of standard tumour marker CA125 in serum (serum:  $r = -0.117$ ,  $p = 0.530$ ; ascites:  $r = 0.083$ ,  $p = 0.658$ ).

### Prognostic value of sOPN

Patients were followed to disease recurrence and death. Survival status was updated in June 2016. The median follow-up was 34 months (range 0.7 - 59.2 months). During this time, 26 patients (83.8%) had developed documented disease progression and 20 (64.5%) had died.

Based on sOPN median serum concentration, patients were divided into 2 groups: group 1 = sOPN ≤ 75.39 ng/ml ( $n = 16$ ) and group 2 = sOPN

> 75.39 ng/ml ( $n = 15$ ). The OS curves of sOPN serum groups differed significantly ( $p = 0.018$ ). The estimate median OS was 40.2 months for patients in group 1 and 14.3 months for patients in group 2 (Figure 2A). In addition, PFS curves of sOPN serum groups differed significantly ( $p = 0.008$ ). The estimate median PFS was 17.7 months for patients in group 1 and 12.1 months for patients in group 2 (Figure 3A).

Based on sOPN median ascites concentration, patients were divided into 2 groups: group 1 = sOPN  $\leq 2729$  ng/ml ( $n = 16$ ) and group 2 = sOPN  $> 2729$  ng/ml ( $n = 15$ ). The estimated median OS was longer (40.2 months) for patients in group 1 than for patients in group 2 (11.5 months). However, the OS curves of sOPN ascites groups did not differ significantly ( $p = 0.051$ ) (Figure 2B). PFS curves of sOPN ascites groups were also not significantly different ( $p = 0.109$ ). The estimated median PFS was 16 months for patients in group 1 and 6.5 months for patients in group 2 (Figure 3B).

Furthermore, we evaluated the prognosis of patients with sOPN levels in ascites and/or serum below the diagnostic cut-off value. Patients with an sOPN concentration in ascites below the cut-off value had no relapse during the follow-up period of 43.3 months. Two out of three patients with an sOPN concentration in serum below the cut-off value also had no relapse during follow-up periods of 43.3 and 56.1 months. The third patient with serum below the cut-off value had progression while receiving the last line of platinum dose. However, this patient had the highest ascites to serum ratio in the study group (205-fold). The mean ascites to serum ratio in EOC patients was 46-fold (range: 3 - 205).

### Usefulness of preoperative sOPN level for surgical planning

After evaluation of resectability through imaging methods and diagnostic laparoscopy performed by an experienced oncologic surgeon, 13 patients underwent PDS and 18 patients underwent NACT; 10 of the patients in the latter group also underwent IDS (Table 1).

The mean preoperative serum sOPN level for patients who underwent PDS ( $70.45 \pm 9.95$  ng/ml) was significantly lower ( $p = 0.031$ ) than that of patients who underwent NACT, with or without IDS ( $102 \pm 11.53$  ng/ml). The mean preoperative ascites sOPN level for patients who underwent PDS ( $2154 \pm 479.7$  ng/ml) was also significantly lower ( $p = 0.018$ ) than that of patients who underwent NACT,

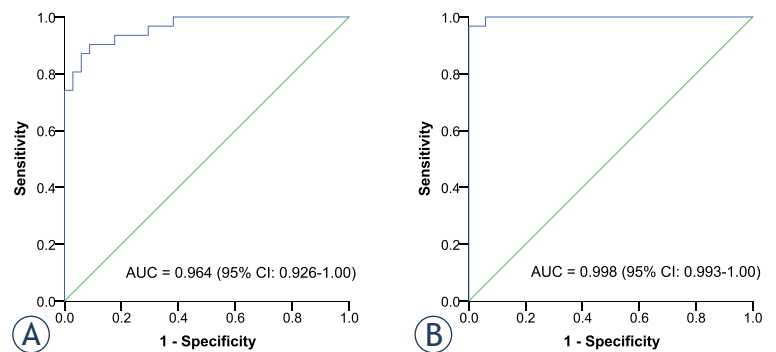


**FIGURE 1.** Receiver operating characteristic (ROC) curve for the diagnosis of ovarian cancer. The predictive performance of preoperative serum soluble osteopontin (sOPN) concentration (A) and ascites sOPN concentration (B).

AUC = area under the curve

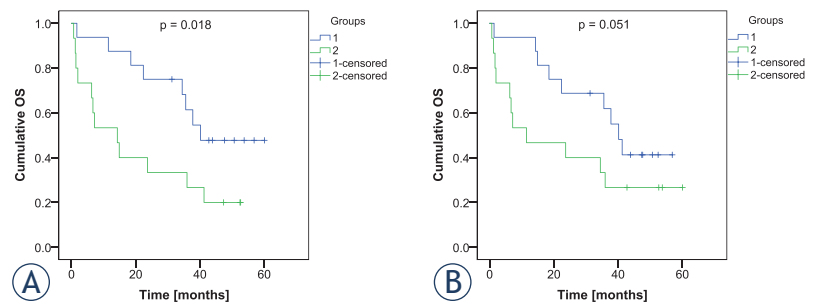


**FIGURE 2.** Kaplan-Meier survival curves. Overall survival (OS) according to preoperative soluble osteopontin (sOPN) concentrations in serum (A) and in ascites (B). Serum sOPN concentrations: group 1  $\leq 75.39$  ng/ml (blue line) and group 2  $> 75.39$  ng/ml (green line). Ascites sOPN concentrations: group 1  $\leq 2729$  ng/ml (blue line) and group 2  $> 2729$  ng/ml (green line).

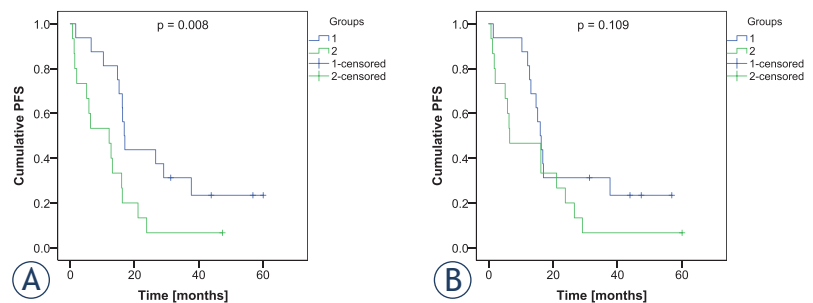


**FIGURE 3.** Progression-free survival (PFS) according to preoperative soluble osteopontin (sOPN) concentrations in serum (A) and in ascites (B). Serum sOPN concentrations: group 1  $\leq 75.39$  ng/ml (blue line) and group 2  $> 75.39$  ng/ml (green line). Ascites sOPN concentrations: group 1  $\leq 2729$  ng/ml (blue line) and group 2  $> 2729$  ng/ml (green line).

with or without IDS ( $4515 \pm 657.3$  ng/ml) (Table 1). However, there was no significant difference ( $p > 0.05$ ) in mean serum CA125 concentrations between the groups ( $3936 \pm U/ml$  vs  $3904 \pm U/ml$ ) (Table 1).

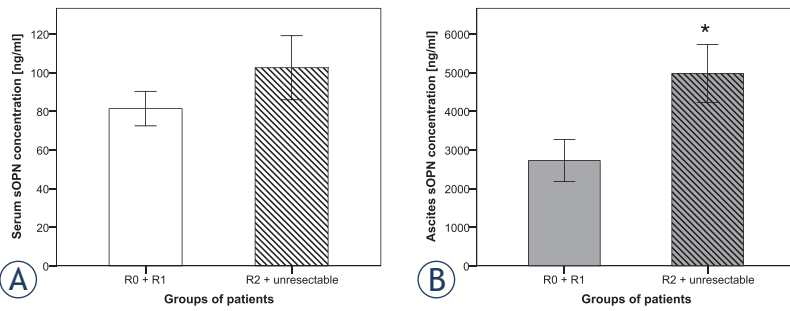


**FIGURE 4.** Association of surgical outcome and soluble osteopontin (sOPN) concentrations in serum (A) and ascites (B) at primary operation. Group 1: patients with complete (R0) and optimal (R1) cytoreduction. Group 2: patients with suboptimal (R2) cytoreduction and unresectable disease.

\* $p < 0.05$

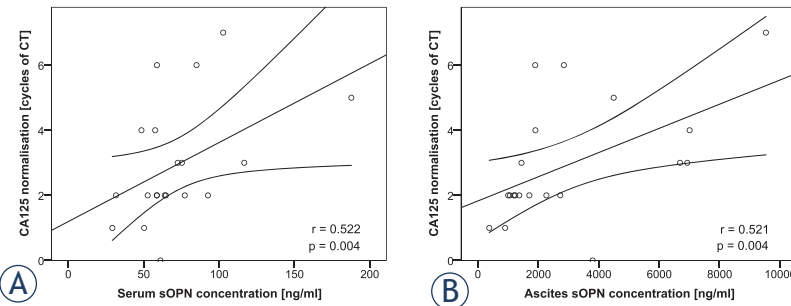


**FIGURE 5.** Correlation between serum cancer antigen 125 (CA125) normalisation after platinum-based chemotherapy and soluble osteopontin (sOPN) concentrations in preoperative serum (A) and ascites (B).

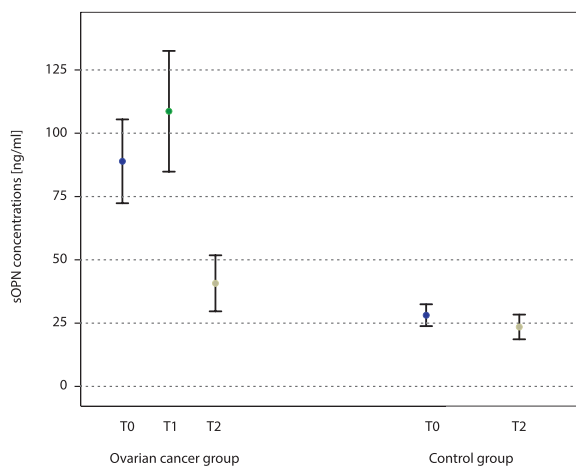


**FIGURE 6.** Comparison of soluble osteopontin (sOPN) concentrations in serum during treatment. Epithelial ovarian cancer (EOC) group - sOPN concentration: T0-preoperative, T1-after primary (debulking) surgery and T2-3 to 6 months after systemic chemotherapy. Control group (patients with benign gynaecological pathology) - sOPN concentrations: T0-preoperative and T2-3 to 6 months after surgery.

We also examined whether the preoperative sOPN level in serum and ascites can predict cytoreductive surgical outcome. Residual disease was assessed after PDS and after IDS. Complete cytoreduction of all macroscopic disease was achieved in 14 patients, optimal cytoreduction ( $< 1$  cm) in 6 patients and suboptimal ( $> 1$  cm) in 3 patients, while 8 patients had bulky unresectable disease. Due to the small numbers, patients were divided into 2 groups: group 1 = complete cytoreduction and optimal cytoreduction ( $n = 20$ ) and group 2 = suboptimal cytoreduction or unresectable disease ( $n = 11$ ). There was no significant difference ( $p = 0.086$ ) in mean serum sOPN concentrations between the groups ( $73.91 \pm 7.82$  ng/ml vs  $102.6 \pm 16.5$  ng/ml) (Figure 4A). In contrast to serum, the ascites sOPN concentration in group 1 ( $2783 \pm 542.3$  ng/ml) was significantly lower ( $p = 0.023$ ) than in group 2 ( $4980 \pm 748.2$  ng/ml) (Figure 4B).

Due to the retention tendency of sOPN in ascites, attention should be paid to a high ascites to serum ratio, as already previously mentioned. A high ratio may indicate unresectable disease in spite of a low detected serum sOPN level in such patients. Of two patients with an extremely high ascites ratio (144 and 205), one had unresectable disease and the second had suboptimal cytoreduction after PDS.

### Usefulness of preoperative sOPN level for prediction of response to chemotherapy

Twenty-nine (93%) patients received platinum-based chemotherapy and 2 died from EOC before chemotherapy was started. Thirteen patients who had PDS received a median number of 6 cycles (range 5-7) of chemotherapy with carboplatin and paclitaxel. The median number of cycles of chemotherapy in the NACT group was also 6. However, ten patients in this group who had IDS received a median number of 8 cycles (6-10) of chemotherapy with carboplatin and paclitaxel and eight patients who remained inoperable after NACT were treated with a median number of 3 cycles (range 1-6) of therapy with carboplatin/paclitaxel (4 patients), carboplatin monotherapy (1 patient), and carboplatin/pegylated liposomal doxorubicin (1 patient).

Faster CA125 normalisation was significantly associated with lower preoperative sOPN concentrations in serum ( $r = 0.522$ ,  $p = 0.004$ ) (Figure 5A) and ascites ( $r = 0.521$ ,  $p = 0.004$ ) (Figure 5B). Nine (31%) patients were partial/non-responders. The serum sOPN mean concentration in patients with an inadequate response ( $119.1 \pm 15.24$  ng/ml) was

significantly higher ( $p = 0.005$ ) than in responders ( $72.35 \pm 7.72$  ng/ml). In contrast to serum, mean ascites sOPN concentrations in patients with an inadequate response ( $4440 \pm 798.3$  ng/ml) did not differ significantly ( $p = 0.123$ ) when compared to responders ( $3022 \pm 575.8$  ng/ml).

On the basis of platinum-free interval, we divided our patients into two groups; group 1 = patients relapsing in less than 6 months (platinum-resistant disease), and group 2 = patients relapsing after more than 6 months or with no relapse during the follow-up period (platinum-sensitive disease). The mean concentration of sOPN in the preoperative serum of 8 patients in group 1 ( $104.5 \pm 8.32$  ng/ml) was not significantly different ( $p = 0.39$ ) from the serum sOPN in group 2 ( $79.49 \pm 8.34$  ng/ml). In contrast, patients in group 1 had significantly higher ( $p = 0.014$ ) ascites sOPN concentrations ( $54011 \pm 836.1$  ng/ml) than patients in group 2 ( $2881 \pm 562.9$  ng/ml).

### Kinetic pattern of sOPN concentrations in serum

In the group of EOC patients, the kinetic patterns of sOPN serum levels were determined one week after PDS ( $n = 13$ ) and 3-6 month after chemotherapy ( $n = 22$ ) to ensure an adequate recovery time of patients from the adverse effects of cytotoxic drugs (Figure 6). We found no significant difference ( $p = 0.786$ ) between mean serum sOPN concentrations in preoperative ( $88.56 \pm 9.03$  ng/ml) and postoperative ( $84.25 \pm 12.85$  ng/ml) samples. The mean serum sOPN concentration after chemotherapy ( $40.73 \pm 5.52$  ng/ml) was significantly lower ( $p < 0.001$ ) than the mean sOPN concentrations in preoperative and postoperative samples. Concentrations of sOPN in postoperative serum were positively correlated with concentrations in preoperative serum ( $r = 0.489$ ,  $p = 0.008$ ) and with ascites concentrations ( $r = 0.418$ ,  $p = 0.027$ ). Concentrations of sOPN in serum after chemotherapy were not correlated with any other samples.

At the time of collecting serum after chemotherapy, nine patients had died. In the remaining 22 patients, the sOPN serum concentration decreased in 21 patients (95%) and decreased below the diagnostic cut-off level in 17 patients (77%). In terms of the total number of patients in the study group, this result corresponded to 68% and 55% patients, respectively. The patient who had an increase in sOPN serum concentration after chemotherapy had the worst prognosis in terms of OS among pa-

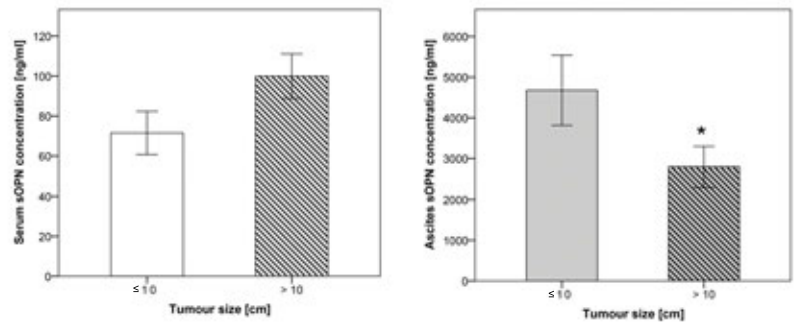


**FIGURE 7.** Association of tumour size and soluble osteopontin (sOPN) concentrations in preoperative serum (A) and ascites (B). Group 1: patients with tumour size ≤ 10 cm. Group 2: patients with tumour size > 10 cm.

\* $p < 0.05$

tients who were alive at the time of collecting serum after chemotherapy.

In the control group, kinetic patterns of sOPN serum levels were determined 6 months after surgery, when the patients were healthy (Figure 6). The mean serum sOPN concentration after treatment was  $23.49 \pm 2.46$  ng/ml.

### Biological characteristics of sOPN in different body fluids

We found that concentrations of sOPN in ascites were positively correlated with the volume of ascites ( $r = 0.431$ ,  $p = 0.013$ ) and with total proteins in the fluid ( $r = 0.985$ ,  $p < 0.001$ ). In contrast to ascites, sOPN concentrations in the peritoneal fluid of the control group were not correlated with the volume of the peritoneal fluid ( $r = -0.122$ ,  $p = 0.552$ ) and were negatively correlated with total proteins in the fluid ( $r = -0.518$ ,  $p = 0.008$ ). In serum, concentrations of sOPN were negatively correlated with total proteins ( $r = -0.372$ ,  $p = 0.033$ ) in EOC patients, whereas no correlation was found in patients of the control group ( $r = 0.227$ ,  $p = 0.537$ ).

In ascites, concentrations of sOPN were negatively correlated with tumour size ( $r = -0.371$ ,  $p = 0.044$ ), whereas serum sOPN concentrations were not correlated with tumour size (Pearson:  $r = 0.279$ ,  $p = 0.135$ ). Based on tumour size, patients were divided into two groups: group 1 = tumour size ≤ 10 cm ( $n = 12$ ) and group 2 = tumour size > 10 cm ( $n = 19$ ). There was no significant difference ( $p > 0.05$ ) in mean serum sOPN concentrations between the groups ( $71 \pm 10$  ng/ml vs  $97 \pm 11$  ng/ml) (Figure 7A). In contrast to serum, the ascites sOPN mean concentration in group 1 ( $4677 \pm 862.3$  ng/ml)

was significantly higher ( $p = 0.029$ ) than in group 2 ( $2958 \pm 530.1$  ng/ml) (Figure 7B).

## Discussion

sOPN has been intensively studied as a serum tumour marker in the diagnosis of EOC.<sup>5-8,11</sup> However, information on potential other applications of this promising tumour marker in serum and ascites in women with EOC are still lacking. One important problem with blood tumour markers is that it is questionable whether a sufficient quantity of molecules can reach the peripheral blood (a range of 0.1 to 20% of secreted protein is assumed) to detect change in the local environment of the ovaries.<sup>23</sup> The results of our previous study showed that the retention tendency of sOPN in local fluid represented by ascites is potentiated in malignant conditions and that serum sOPN concentrations were not associated with sOPN concentrations in ascites.<sup>21</sup> We thus systematically compared the clinical usefulness of serum sOPN with ascites sOPN. In addition, we evaluated whether sOPN in ascites can improve the diagnostic accuracy of serum sOPN. To the best of our knowledge, the present study is the first to indicate the usefulness of serum sOPN as a prognostic tumour marker of EOC and is also the first to demonstrate ascites sOPN usefulness in selecting the best treatment for advanced EOC patients (surgical planning and response to platinum-based chemotherapy).

The major new findings in our study were as follows: (1) The diagnostic accuracy of sOPN for detecting advanced-stage EOC was higher for sOPN in ascites than in serum. Ascites sOPN exhibited a lower false negative rate when compared to serum and no false positive rate. (2) Higher preoperative sOPN concentrations in serum were associated with significantly shorter median OS and PFS. A poor prognosis of EOC patients can thus be predicted by a high serum sOPN preoperative level. (3) Higher sOPN concentrations in ascites were associated with a worse surgical outcome and with smaller tumour size. Since high abdominal dissemination with a small primary tumour indicates biological aggressiveness, usually high-grade serous carcinoma, our findings suggest that a higher sOPN level in ascites can predict incomplete resection. (4) A very high ascites to serum sOPN ratio may identify patients who warrant further evaluation for the presence of malignant disease and also identify patients with unresectable disease and the worst prognosis, and this despite a low sOPN con-

centration in serum of the same patient. (5) Faster CA125 normalisation was positively correlated with lower preoperative sOPN levels in serum and ascites. Relapse in less than 6 months from the last date of platinum dose was associated with higher preoperative levels of sOPN in ascites. sOPN might therefore have predictive value for response to platinum-based chemotherapy in primary and recurrent EOC. (6) A significant positive association between concentrations of sOPN in ascites and ascites volume and total proteins, and no association of sOPN concentrations in peritoneal fluid of control group with peritoneal fluid volume and a negative correlation with total proteins in peritoneal fluid, indicated that an elevated sOPN concentration in ascites was related to the malignant process, especially to the production of ascites.

Our previous report showed that serum sOPN concentrations are not associated with sOPN concentrations in ascites, so we determined separate cut-off values for sOPN in serum and ascites.<sup>21</sup> The cut-off level for serum sOPN of 47.4 ng/ml was in the range of published serum cut-off values (28-60 ng/ml).<sup>11</sup> We found that the sensitivity and specificity of serum sOPN for detecting EOC were 91.2% and 90.3%, respectively. We then tried to elucidate whether the performance of sOPN as a diagnostic marker in ascites is better than in serum. We found that at a cut-off level 529.5 ng/ml, the diagnostic sensitivity and specificity were higher for ascites (96.8% and 100%) than for serum. The AUC under the sROC curve of sOPN was also higher for ascites than for serum. These data indicate that the diagnostic accuracy of sOPN for detection of advanced-stage EOC is higher for sOPN in ascites than in serum. Ascites sOPN exhibited a lower false negative rate and no false positive rate. Furthermore, one patient with serum below the cut-off value, who was diagnosed with FIGO stage IV disease, had the highest ascites to serum ratio (205-fold) in the study group (mean ratio was 46-fold; range: 3 - 205). So a very high ascites to serum sOPN ratio may identify patients who warrant further evaluation for the presence of malignant disease, in spite of a low sOPN concentration in the patient's serum. Higher false negative rates in serum are probably the consequence of the sOPN retention tendency in ascites potentiated in malignant conditions.<sup>21</sup> Moreover, sOPN levels in systemic circulation, may be influenced by noncancerous causes, which must be considered in evaluating the results.<sup>2,3</sup> A higher specificity of sOPN in ascites was expected, since tumour markers closer to the origin of disease are more specific. In

addition, our results on a significant association of sOPN concentration with ascites volume and with ascites total proteins indicated that elevated sOPN levels were disease specific. A greater volume of ascites and higher content of proteins in ascites are general signs of disease progression and/or poor prognosis.<sup>24,25</sup>

OPN mediates critical processes in cancer progression, such as cell adhesion, migration, immune response and apoptosis prevention.<sup>4</sup> It has also been demonstrated that an elevated serum sOPN concentration is associated with advanced FIGO stage, high grade, and the presence of ascites, thus suggesting a prognostic value of this marker.<sup>26,27</sup> During the median follow up of 34 months, 83% developed documented disease progression and 64.5% had died. We found that increased serum sOPN concentration was associated with significantly shorter OS and PFS when patients were grouped using an sOPN median concentration of 75.39 ng/ml. The median OS was 40.2 months for patients with sOPN of 75.39 ng/ml or less and 11.5 months for sOPN greater than 75.39 ng/ml. In addition, the median PFS was 17.7 months for patients with sOPN of 75.39 ng/ml or less and 14.3 months for sOPN greater than 75.39 ng/ml. When patients were grouped using an sOPN median concentration of 2729 ng/ml in ascites as a cut-off, the median OS was 40.2 months for patients with sOPN of 2729 ng/ml or less and 11.5 months for sOPN greater than 2729 ng/ml. In addition, the median PFS was 16 months for patients with an sOPN of 2729 ng/ml or less and 6.5 months for sOPN greater than 2729 ng/ml. A higher ascites sOPN concentration demonstrated border line statistical significance ( $p = 0.51$ ) for shorter median OS, and no association with median PFS. However, if the prognosis of patients was evaluated in relation to sOPN levels in ascites and serum below our diagnostic cut-off value, a different insight into the prognostic usefulness of the two body fluids was obtained. Patients with an sOPN concentration in ascites below the cut-off value had no relapse during a follow-up period of 43.3 months. Two out of three patients with an sOPN concentration in serum below the cut-off value also had no relapse during follow-up periods of 56.1 and 43.3 months. However, a third patient with serum sOPN below the cut-off value had progression while receiving the last line of the platinum dose. This patient had the highest ascites to serum ratio in the study group. So a very high ascites to serum sOPN ratio may identify patients with the worst prognosis, in spite of a low sOPN concentration in the patient's serum.

In the management of advanced-stage EOC, it is essential to identify patients who are more eligible for NACT and IDS, since primary complete resection cannot be achieved.<sup>18,19,28,29</sup> Laparoscopy can be used as an adjuvant procedure to assess tumour spread and resectability. Laparoscopic evaluation, however, has limitations and may, in some cases, underestimate the extent of disease.<sup>30</sup> We investigated the usefulness of sOPN for predicting surgical outcome in order to improve the preoperative treatment strategy. Significantly higher sOPN concentrations in ascites were associated with suboptimal cytoreduction or unresectable disease. Moreover, high ascites sOPN concentrations were associated with smaller tumour size. We can therefore presume that higher sOPN concentrations in ascites demonstrate a greater extent of metastatic disease and knowing this would be useful in preoperative assessment of residual disease and, potentially, in the evaluation of neoadjuvant treatment. It has already been demonstrated that OPN expression in metastasis is significantly increased compared to the primary tumour.<sup>13</sup> The different influences that determine the steady-state levels of sOPN in serum and retention of sOPN in ascites might explain why no association was found between serum sOPN concentrations and surgical outcome. Bandiera *et al.* also investigated the correlation between serum sOPN and surgical outcome, and found that elevated serum sOPN levels were associated with macroscopic residual disease. However, 28% of included patients had early stage disease, when retention of sOPN in ascites is probably less pronounced. Moreover, ascites was not present in 50% of patients.<sup>27</sup>

In EOC patients, carboplatin/paclitaxel remains the preferred combination, with docetaxel substituted for paclitaxel in patients with pre-existing neuropathy. Since EOC is a chemosensitive disease, response to therapy is an important prognostic determinant. The results of our study showed that 28% of patients with an inadequate response to primary chemotherapy had a significantly higher concentration of sOPN in serum but not in ascites, when compared to responders. However, in responders, faster CA125 normalisation was associated with lower preoperative sOPN in serum and ascites. Although EOC patients often respond (~80%) to primary therapy<sup>31</sup>, the majority of women with advanced EOC will ultimately relapse and develop drug-resistant disease.<sup>32</sup> All patients received platinum-based chemotherapy, so we used platinum-free interval to assess the usefulness of sOPN for predicting response to chemo-

therapy at relapse. The traditional definition of platinum resistance as disease relapsing within 6 months and sensitive disease as recurring beyond 6 months after chemotherapy was adopted by the Gynaecologic Oncology Group (GOG).<sup>33</sup> We found that patients relapsing in less than 6 months had a higher ascites sOPN concentration than patients relapsing after more than 6 months or who had no relapse during the follow-up period. sOPN may contribute to chemoresistance via the antiapoptotic signal, upregulation of P-gp expression, and induction of stem-like properties and thus induces chemoresistance.<sup>34-36</sup> In published studies, higher expression of OPN in lung, colorectal and oral cancer was associated with resistance to platinum-based primary chemotherapy.<sup>36-38</sup> Tumour markers for predicting response is an attractive concept, since it permits individualized treatment, so sOPN is worth further research.

The kinetic pattern of mean serum sOPN concentrations after PDS and chemotherapy showed that sOPN did not change ~ one week after PDS, although the mean sOPN concentration 3 to 6 months after completion of chemotherapy was significantly decreased. The period ~ one week after surgery was probably too short to see the effect of cytoreduction on the sOPN level. In addition, the surgical induced stress response in a patient may also influence protein distribution.<sup>39</sup> This might be why our result was not in agreement with a previously published study.<sup>10</sup> Schorge *et al.* reported significantly decreased sOPN after PDS. However sOPN was measured before the first cycle of chemotherapy.<sup>10</sup> We waited 3 to 6 months after chemotherapy before we measured sOPN, in order to ensure an adequate recovery time of patients from the adverse effects of cytotoxic drugs. At the time of collecting serum after chemotherapy, nine patients had died. In the remaining patients, the sOPN serum concentration decreased in 95% of patients and below the diagnostic cut-off level in 77% of patients. The observed decreased serum sOPN concentration after treatment supports the suggestion that sOPN in serum is correlated with tumour bulk. A similar result was observed in the Schorge *et al.* study, in which an earlier increase of sOPN compared to CA125 in patients developing recurrent disease was also shown.<sup>10</sup>

## Conclusions

Our study showed that the local fluid sOPN level, as represented by ascites, mirrors the present dis-

ease and is superior to serum sOPN level for diagnostic purposes and surgical planning, although the end result of treatment is a response of the whole body in fighting against disease and, in this respect, the preoperative sOPN concentration in systemic circulation better reflects the outcome of disease than sOPN in ascites. Nevertheless, a very high ascites to serum sOPN ratio may identify patients who warrant further evaluation for the presence of malignant, unresectable disease, and identify patients with the worst prognosis, in spite of a low sOPN concentration in the serum of the same patient.

## Acknowledgements

This work was supported by research grants from the University Medical Centre Ljubljana (Project Number: 20180033) and the Slovenian Research Agency (P3-067). The authors thank Nevenka Dolzan for technical assistance and Martin Cregeen for assistance with the English translation of the text.

## References

- Weber GF, Lett GS, Haubein NC. Osteopontin is a marker for cancer aggressiveness and patient survival. *Br J Cancer* 2010; **103**: 861-9. doi: 10.1038/sj.bjc.6605834
- Hao C, Cui Y, Owen S, Li W, Cheng S, Jiang WG. Human osteopontin: potential clinical applications in cancer (Review). *Int J Mol Med* 2017; **39**: 1327-37. doi: 10.3892/ijmm.2017.2964
- Wei R, Wong JPC, Kwok HF. Osteopontin - a promising biomarker for cancer therapy. *J Cancer* 2017; **8**: 2173-83. doi: 10.7150/jca.20480
- Zhao H, Chen Q, Alam A, Cui J, Suen KC, Soo AP, et al. The role of osteopontin in the progression of solid organ tumour. *Cell Death Dis* 2018; **9**: 356-70. doi: 10.1038/s41419-018-0391-6
- Kim JH, Skates SJ, Uede T, Wong KK, Schorge JO, Feltmate CM, et al. Osteopontin as a potential diagnostic biomarker for ovarian cancer. *Jama-Journal Am Med Assoc* 2002; **287**: 1671-9. doi: 10.1001/jama.287.13.1671
- Cramer DW, Bast RC, Berg CD, Diamandis EP, Godwin AK, Hartge P, et al. Ovarian cancer biomarker performance in prostate, lung, colorectal, and ovarian cancer screening trial specimens. *Cancer Prev Res* 2011; **4**: 365-74. doi: 10.1158/1940-6207.CAPR-10-0195
- Mor G, Visintin I, Lai Y, Zhao H, Schwartz P, Rutherford T, et al. Serum protein markers for early detection of ovarian cancer. *Proc Natl Acad Sci U S A* 2005; **102**: 7677-82. doi: 10.1073/pnas.0502178102
- Visintin I, Feng Z, Longton G, Ward DC, Alvero AB, Lai Y, et al. Diagnostic markers for early detection of ovarian cancer. *Clin Cancer Res* 2008; **14**: 1065-72. doi: 10.1158/1078-0432.CCR-07-1569
- Brakora KA, Lee H, Yusuf R, Sullivan L, Harris A, Colella T, et al. Utility of osteopontin as a biomarker in recurrent epithelial ovarian cancer. *Gynecol Oncol* 2004; **93**: 361-5. doi: 10.1016/j.ygyno.2004.01.050
- Schorge JO, Drake RD, Lee H, Skates SJ, Rajanbabu R, Miller DS, et al. Osteopontin as an adjunct to CA125 in detecting recurrent ovarian cancer. *Clin Cancer Res* 2004; **10**: 3474-8. doi: 10.1158/1078-0432.CCR-03-0365
- Lan Z, Fu D, Yu X, Xi M. Diagnostic values of osteopontin combined with CA125 for ovarian cancer: a meta-analysis. *Fam Cancer* 2016; **15**: 221-30. doi: 10.1007/s10689-015-9847-3

- 12 Hu Z-D, Wei T-T, Yang M, Ma N, Tang Q-Q, Qin B-D, et al. Diagnostic value of osteopontin in ovarian cancer: a meta-analysis and systematic review. *PLoS One* 2015; **10**: e0126444. doi: 10.1371/journal.pone.0126444
- 13 Bao LH, Sakaguchi H, Fujimoto J, Tamaya T. Osteopontin in metastatic lesions as a prognostic marker in ovarian cancers. *J Biomed Sci* 2007; **14**: 373-81. doi: 10.1007/s11373-006-9143-1
- 14 Psyrris A, Kalogerias KT, Wirtz RM, Kouvatseas G, Karayannopoulou G, Goussia A, et al. Association of osteopontin with specific prognostic factors and survival in adjuvant breast cancer trials of the Hellenic Cooperative Oncology Group. *J Transl Med* 2017; **15**: 1-11. doi: 10.1186/s12967-017-1134-7
- 15 Hacker NF. State of the art of surgery in advanced epithelial ovarian cancer. *Ann Oncol* 2013; **24**: 27-32. doi: 10.1093/annonc/mdt465
- 16 Narod S. Can advanced-stage ovarian cancer be cured? *Nat Rev Clin Oncol* 2016; **13**: 255-61. doi: 10.1038/nrclinonc.2015.224
- 17 Querleu D, Planchamp F, Chiva L, Fotopoulou C, Barton D, Cibula D, et al. European society of Gynaecological Oncology (ESGO) guidelines for ovarian cancer surgery. *Int J Gynecol Cancer* 2017; **27**: 1534-42. doi: 10.1097/IGC.0000000000001041
- 18 Bristow RE, Karlan BY. *Surgery for Ovarian Cancer: Principles and Practice*. 1st edition. Abingdon: Taylor & Francis; 2006.
- 19 Chesnaïs M, Lecuru F, Mimouni M, Ngo C, Fauconnier A, Huchon C. A pre-operative predictive score to evaluate the feasibility of complete cytoreductive surgery in patients with epithelial ovarian cancer. *PLoS One* 2017; **12**: 1-12. doi: 10.1371/journal.pone.0187245
- 20 Gupta D, Lis CG. Role of CA125 in predicting ovarian cancer survival - A review of the epidemiological literature. *J Ovarian Res* 2009; **2**: 1-20. doi: 10.1186/1757-2215-2-13
- 21 Kobal B, Jerman KG, Karo J, Verdenik I, Cerne K. Relationship of ovarian cancer tumour markers concentration between local fluid and serum: Comparison of malignant to benign condition. *Eur J Gynaecol Oncol* 2018; **5**: 743-50. doi: 10.12892/ejgo3848.2018
- 22 Jerman KG, Kobal B, Jakimovska M, Verdenik I, Cerne K. Control values of ovarian cancer tumor markers and standardisation of a protocol for sampling peritoneal fluid and performing washing during laparoscopy. *World J Surg Oncol* 2014; **12**: 1-9. doi: 10.1186/1477-7819-12-278
- 23 Lutz AM, Willmann JK, Cochran F V., Ray P, Gambhir SS. Cancer screening: A mathematical model relating secreted blood biomarker levels to tumor sizes. *PLoS Med* 2008; **5**: 1287-97. doi: 10.1371/journal.pmed.0050170
- 24 Parsons SL, Watson SA, Steele RJ. Malignant ascites. *Br J Surg* 1996; **83**: 6-14. doi: 10.1002/BJS.1800830104
- 25 Stanojevic Z, Rancic G, Radic S, Potic-Zececic N, Djordjevic B, Markovic M, et al. Pathogenesis of malignant ascites in ovarian cancer patients. *Arch Oncol* 2004; **12**: 115-8. doi: 10.2298/AOO04021155
- 26 Weber GF. The cancer biomarker osteopontin: Combination with other markers. *Cancer Genomics Proteomics* 2011; **8**: 263-88. PMID: 22086896
- 27 Bandiera E, Zanotti L, Fabricio ASC, Bucca E, Squarcina E, Romani C, et al. Cancer antigen 125, human epididymis 4, kallikrein 6, osteopontin and soluble mesothelin-related peptide immunocomplexed with immunoglobulin M in epithelial ovarian cancer diagnosis. *Clin Chem Lab Med* 2013; **51**: 1815-24. doi: 10.1515/ccm-2013-0151
- 28 Sato S, Itamochi H. Neoadjuvant chemotherapy in advanced ovarian cancer: latest results and place in therapy. *Ther Adv Med Oncol* 2014; **6**: 293-304. doi: 10.1177/1758834014544891
- 29 Skof E, Merlo S, Pilko G, Kobal B. The role of neoadjuvant chemotherapy in patients with advanced (stage IIIC) epithelial ovarian cancer. *Radial Oncol* 2019; **53**(1): 105-115. doi: 10.1515/raon-2016-0034
- 30 Rutten MJ, Leeflang MM, Kenter GG, Mol BW, Buist M. Laparoscopy for diagnosing resectability of disease in patients with advanced ovarian cancer. *Cochrane Database Syst Rev* 2014; **21**. doi: 10.1002/14651858.CD009786.pub2
- 31 Cannistra SA. Cancer of the Ovary. *N Engl J Med* 1993; **329**: 1550-9. doi: 10.1056/NEJM199311183292108
- 32 Bookman MA, Ozols RF. Factoring outcomes in ovarian cancer. *J Clin Oncol* 1996; **14**: 325-7. doi: 10.1200/JCO.1996.14.2.325
- 33 Markman M, Bookman MA. Second-line treatment of ovarian cancer. *Oncologist* 2000; **5**: 26-35. doi: 10.1634/theoncologist.5-1-26
- 34 Graessmann M, Berg B, Fuchs B, Klein A, Graessmann A. Chemotherapy resistance of mouse WAP-SVT/t breast cancer cells is mediated by osteopontin, inhibiting apoptosis downstream of caspase-3. *Oncogene* 2007; **26**: 2840-50. doi: 10.1038/sj.onc.1210096
- 35 Hsieh I-S, Huang W-H, Liou H-C, Chuang W-J, Yang R-S, Fu W-M. Upregulation of drug transporter expression by osteopontin in prostate cancer cells. *Mol Pharmacol* 2013; **83**: 968-77. doi: 10.1124/mol.112.082339
- 36 Ng L, Wan T, Chow A, Iyer D, Man J, Chen G, et al. Osteopontin overexpression induced tumor progression and chemoresistance to oxaliplatin through induction of stem-like properties in human colorectal cancer. *Stem Cells Int* 2015; **2015**: 1-8. doi: 10.1155/2015/247892
- 37 Zhang T, Zhang DM, Zhao D, Hou XM, Yang TN. Osteopontin expression is associated with platinum-based chemotherapy response and prognosis of patients with advanced non small cell lung cancer. *J BUON* 2014; **19**: 742-8. PMID: 25261661
- 38 Luo S-D, Chen Y-J, Liu C-T, Rau K-M, Chen Y-C, Tsai H-T, et al. Osteopontin involves cisplatin resistance and poor prognosis in oral squamous cell carcinoma. *Biomed Res Int* 2015; **2015**: 1-13. doi: 10.1155/2015/508587
- 39 Faça VM, Ventura AP, Fitzgibbon MP, Pereira-Faça SR, Pitteri SJ, Green AE, et al. Proteomic analysis of ovarian cancer cells reveals dynamic processes of protein secretion and shedding of extra-cellular domains. *PLoS One* 2008; **3**: e2425. doi: 10.1371/journal.pone.0002425

# Similar complication rates for irreversible electroporation and thermal ablation in patients with hepatocellular tumors

Niklas Verloh<sup>1</sup>, Isabel Jensch<sup>1</sup>, Lukas Lürken<sup>1</sup>, Michael Haimerl<sup>1</sup>, Marco Dollinger<sup>1</sup>, Philipp Renner<sup>2</sup>, Philipp Wiggermann<sup>3</sup>, Jens Martin Werner<sup>4</sup>, Florian Zeman<sup>5</sup>, Christian Stroszczyński<sup>1</sup>, Lukas Philipp Beyer<sup>1</sup>

<sup>1</sup> Department of Radiology, University Hospital Regensburg, Germany

<sup>2</sup> Department of Surgery, Robert-Bosch-Hospital, Stuttgart, Germany

<sup>3</sup> Department of Radiology, Hospital Braunschweig, Germany

<sup>4</sup> Department of Surgery, University Hospital Regensburg, Regensburg, Germany

<sup>5</sup> Center for Clinical Trials, University Hospital Regensburg, Regensburg, Germany

Radiol Oncol 2019; 53(1): 116-122.

Received 2 November 2018

Accepted 22 January 2019

Correspondence to: Lukas Philipp Beyer, M.D., Department of Radiology, University Hospital Regensburg, 93053 Regensburg, Germany. Phone: +49 941 944 17464; E-mail: lukas@lukasbeyer.com

Disclosure: No potential conflicts of interest were disclosed.

**Background.** To compare the frequency of adverse events of thermal microwave (MWA) and radiofrequency ablation (RFA) with non-thermal irreversible electroporation (IRE) in percutaneous ablation of hepatocellular carcinoma (HCC).

**Patients and methods.** We retrospectively analyzed 117 MWA/RFA and 47 IRE procedures (one tumor treated per procedure; 144 men and 20 women; median age, 66 years) regarding adverse events, duration of hospital and intensive care unit (ICU) stays and occurrence of a post-ablation syndrome. Complications were classified according to the Clavien & Dindo classification system.

**Results.** 70.1% of the RFA/MWA and 63.8% of the IRE procedures were performed without complications. Grade I and II complications (any deviation from the normal postinterventional course, e.g., analgesics) occurred in 26.5% (31/117) of MWA/RFA and 34.0% (16/47) of IRE procedures. Grade III and IV (major) complications occurred in 2.6% (3/117) of MWA/RFA and 2.1% (1/47) of IRE procedures. There was no significant difference in the frequency of complications ( $p = 0.864$ ), duration of hospital and ICU stay and the occurrence of a post-ablation syndrome between the two groups.

**Conclusions.** Our results suggest that thermal (MWA and RFA) and non-thermal IRE ablation of malignant liver tumors have comparable complication rates despite the higher number of punctures and the lack of track cauterization in IRE.

Key words: tumor ablation; interventional oncology; complications; adverse events; RFA; MWA; IRE

## Introduction

Percutaneous ablation of HCC under imaging control in focal tumor therapy has gained in importance in recent years. Besides surgical resection and liver transplantation, ablation is one of three curative therapies for the treatment of hepatocellular carcinoma (HCC).<sup>1</sup> Most ablation techniques are

so-called thermal methods, which are based on the generation of coagulation necrosis by heat. While radiofrequency ablation (RFA) and microwave ablation (MWA) are among these thermal techniques, irreversible electroporation (IRE), along with other therapies such as electrochemotherapy (ECT), is a non-thermal method for destruction of tumor tissue.<sup>2,3</sup>

IRE uses ultrashort but strong electric fields to create nanopores in the cell membrane, thereby disturbing the cellular homeostasis and subsequently causing cell death by apoptosis.<sup>4</sup> IRE is not affected by the “heat-sink-effect”<sup>5-9</sup> and can be applied in close proximity to temperature-sensitive structures such as bile ducts. Therefore, IRE is a useful technique in particular for central liver tumors in the vicinity of larger vessels and bile ducts.<sup>2</sup> However, IRE has the theoretical disadvantage compared to thermal procedures that up to six electrodes have to be put in place (*i.e.*, multiple trauma by puncture), and the puncture channel cannot be cauterized. First studies with limited number of cases have described possible complications after IRE, such as bleeding, portal vein thrombosis, infections, needle tract seeding and bile duct injuries.<sup>10-12</sup> However, larger cohort studies and systematic meta-analysis involving more than 10,000 patients exist only for thermal ablation methods.<sup>13,14</sup> To the best of our knowledge, no work systematically compares so far the complication rates between the thermal methods RFA/MWA and IRE.

This study aims to identify possible differences between complication rates and the morbidity of patients following thermal and non-thermal ablation procedures in order to guide optimal therapy decisions in the future.

## Patients and methods

### Study design and participant selection

The retrospective single-center study was approved by the Ethics Committee of the University Regensburg. It was carried out in accordance with the relevant guidelines and regulations, and informed consent was waived.

The clinical reports of all patients who underwent percutaneous tumor ablation at our interventional oncology center between 07/2010 and 05/2017 were reviewed. The indication for the percutaneous ablation was based exclusively on clinical criteria. Ablations in which more than one tumor was treated were excluded from further examination to ensure comparability between the groups.

The following parameters were assessed for both groups:

- intervention time
- length of hospital stay
- occurrence and length of intensive care unit (ICU) stay
- clinical course post intervention.

### Ablation procedures and imaging

All procedures were performed under general anesthesia and percutaneously under CT fluoroscopy guidance (CAREVision, SOMATOM Sensation 16, Siemens Healthcare).

Hematologic management was performed according to the consensus guidelines of the society of interventional radiology for procedures with a moderate risk of bleeding.<sup>15</sup> In summary, the INR was corrected to < 1.5 and the aPTT to values > 1.5. If the platelets were less than 50,000 per ml, a transfusion with platelet concentrates was performed. Clopidogrel was paused 5 days before ablation. For low molecular weight heparins, the last administration was suspended before the intervention.

IRE procedures were performed with the NanoKnife® System (Angiodynamics®) using up to six 19G electrodes. The parameters of IRE ablation were as follows: voltage, 1650 to 3000 V; pulse length, 90 µs; pulses per cycle, 70. Microwave ablation was carried out using the Acculis microwave tissue ablation system and a 14G applicator (AngioDynamics, Latham, NY, USA), which operates at 2.45 GHz with a maximum power output of 140 W. For radiofrequency ablation, the StarBurst®, RITA®, 1500X ablation system (AngioDynamics, Latham, NY, USA) with monopolar perfused 14G electrodes (StarBurst®, Talon Semi-Flex, AngioDynamics, Latham, NY, USA) was employed.

After probe placement for the ablation procedure, the parameters were adjusted depending on tumor size with the aim to gain a preferable safety margin of 1 cm.

The first follow-up imaging was routinely conducted on the first working day after the ablation through an abdominal CT and magnetic resonance imaging (MRI). Laboratory tests and physical examinations were continued until discharge of the patient.

### Complications

Complications were documented for each ablation session by evaluating medical records and radiologic images. Since during the post-interventional clinical course the patients were admitted on a surgical ward, post-interventional complications were defined according to the “Classification of Surgical Complications” according to Clavien & Dindo<sup>16</sup>, which allows a detailed insight into the grade of recorded events and even small treatment adjustments are included.

**TABLE 1.** Patient and tumor characteristics of the RFA/MWA and IRE group

	RFA/MWA (n = 117)	IRE (n = 47)	p-value
Male, n (%)	98 (83.8)	46 (97.9)	<b>0.013</b>
Age			
median (IQR)	66 (14)	71 (15)	0.239
range	45 - 82	45 - 83	
Child-Pugh-Score, n (%)			0.892
A	76 (65.0)	30 (63.8)	
B	41 (35.0)	17 (36.2)	
BCLC, n (%)			0.412
A	68 (58.1)	24 (51.1)	
B	49 (41.9)	23 (48.9)	
Tumor size, mm (mean +- SD)	22 +- 9	20 +- 8	0.186
Liver periphery, n (%)	85 (72.6)	25 (53.2)	<b>0.017</b>
Close to a major vessel, n (%)	19 (16.2)	21 (44.7)	<b>≤ 0.001</b>

BCLC = Barcelona Clinic Liver Cancer staging system; IQR = interquartile range; IRE = non-thermal irreversible electroporation; RFA/MWA = radiofrequency ablation / microwave ablation

**TABLE 2.** Intervention durations, hospital and intensive care unit (ICU) stay, occurrence of post-ablation syndrome for thermal ablation and non-thermal irreversible electroporation (IRE)

	All (164)	RFA/MWA (n = 117)	IRE (n = 47)	p-value
Intervention duration, minutes (IQR)	113 (96)	103 (103)	142 (88)	<b>0.031</b>
Hospital Stay, days				
days, median (IQR)	5 (4)	5 (4)	5 (4)	0.752
days, range	2-50	2-50	2-20	
ICU Stay, n (%)	17 (10)	14 (12)	3 (6)	0.302
days, median (IQR)	4 (5)	4 (4)	6 (-)	0.222
days, range	1-9	1-9	3-9	
Post-ablation Syndrome, n (%)	28 (17)	21 (18)	7 (15)	0.607

IQR = interquartile range; RFA/MWA = radiofrequency ablation / microwave ablation

### Post-ablation syndrome

The post-ablation syndrome is characterized by fever or flu-like symptoms following ablation treatment.<sup>17</sup> In addition, nausea, vomiting, malaise and body aches have been described.<sup>18</sup> However, in most cases the symptoms are per se self-limiting under purely symptom-oriented therapy.<sup>19</sup> In rare cases after treatment of large tumor areas, the post-ablation syndrome can last up to three weeks.<sup>19</sup> By contrast, persistent or later onset of fever may indicate a simultaneous infection or abscess.<sup>17</sup>

### Statistical analysis

All statistical analyses were performed with IBM SPSS Statistics (version 24, Chicago, IL, USA) and R 3.2.1. The data are presented as the median with the interquartile range (IQR) if not stated otherwise. The non-parametric Mann-Whitney test was used to analyze patients and tumor characteristics, the intervention time, and the length of the hospital and ICU stay. We used the Chi-Square Test of independence for comparing the observed frequencies of events (ICU-stay (y/n), post-ablation syndrome (y/n)) and examined trend of complication grades between both groups using the Cochran-Armitage test for trend. The Fisher's exact test was used to compare the in-house mortality. All tests were two-sided, and values of  $p < 0.05$  indicated a significant difference.

## Results

### Patient and tumor characteristics

In this study, 117 patients with HCC were treated with thermal ablations (microwave and radiofrequency ablation) and 47 with irreversible electroporation (IRE). Of the 164 patients, 31 (18.9%) were listed for liver transplantation and ablation was performed for bridging. The patient and lesion aspects are summarized in Table 1.

A tumor was defined as close to a major vessel if the distance to a vessel with a diameter  $> 5$  mm was less than 5 mm. A tumor was defined as peripheral if the maximum distance between all parts of the tumor and the liver capsule was 3 cm.

### Intervention time

The median intervention duration of all interventions was 113 min (IQR 96) (Table 2). A significant difference ( $p = 0.047$ ) was observed between the duration of thermal ablation (103, IQR 103) and irreversible electroporation (142, IQR 88).

### Hospital and ICU-stay

Duration of hospital stays ranged between 2 and 50 days for thermal ablation and between 2 and 20 days for irreversible electroporation, with a median of 5 days (IQR 4) for both types of interventions ( $p = 0.752$ ). There was no significant difference between thermal ablation and irreversible electroporation regarding the frequencies (12.0% (14/117) vs. 6.4% (3/47),  $p = 0.302$ ) as well as the length of ICU-stays with a median ICU stay of 4 days (IQR 4)

**TABLE 3.** Clavien & Dindo classification system with the corresponding number of events in the thermal and non-thermal irreversible electroporation (IRE) groups

Clavien-Dindo Classification		SIR Classification 2017	RFA/MWA (n = 117)	IRE (n = 47)
Grade	Description			
0	No complication	No complication	82 (70.1%)	30 (63.8%)
I	Any deviation from the normal postinterventional course without the need for pharmacological treatment or surgical, endoscopic and radiological interventions (Allowed therapeutic regimens are: drugs as antiemetics, antipyretics, analgesics, diuretics, and electrolytes, and physiotherapy. This grade also includes wound infections opened at the bedside)	Mild	11 (9.4%)	9 (19.1%)
II	Requiring pharmacological treatment with drugs other than such allowed for grade I complications. Blood transfusions and total parenteral nutrition are also included.	Moderate	20 (17.1%)	7 (14.9%)
III	requiring surgical, endoscopic or radiological intervention			
IIIa	intervention not under general anesthesia	Moderate	1 (0.9%)	0
IIIb	intervention under general anesthesia	Severe	1 (0.9%)	1 (2.1%)
IV	Life-threatening complication (including CNS complications) requiring IC/ICU-management			
IVa	single organ dysfunction (including dialysis)	Severe/Life-threatening	0	0
IVb	multi organ dysfunction	Life-threatening	1 (0.9%)	0
V	Death of a patient	Patient death	1 (0.9%)	0

ICU = intensive care unit; IQR = interquartile range; RFA/MWA = radiofrequency ablation / microwave ablation; SIR = Society of Interventional Radiology

for patients treated with thermal ablation versus 6 days for patients treated with IRE ( $p = 0.222$ ).

### Clinical course post intervention

In 17.1% of the treatments, a post-ablation syndrome occurred during the post-interventional clinical course. Significant differences between thermal ablation (17.9%) and IRE (14.9%) were not observed ( $p = 0.607$ ).

68.3% of the procedures were performed without any complication. There was no significant difference between thermal ablation and IRE regarding the occurrence and the severity of a complication ( $p = 0.864$ ).

One patient died 11 days after MWA due to multiorgan failure after an accidental puncture of the pericardium with hemopericardium and surgical overstitching (Table 3). The incidence of all documented complications is listed in Table 2. The most common complications of grade II were: blood transfusions ( $n = 10$ ), infections ( $n = 6$ ), electrolyte shifts ( $n = 4$ ).

Grade III complications were: bleeding after RFA followed by angiography without detectable source of bleeding and active monitoring on the ward ( $n = 1$ ; Figure 1), pleural drainage for reactive pleural effusion after sub-diaphragmatic MWA ( $n =$

1), HB drop after IRE with explorative laparotomy without intraoperatively visible bleeding source ( $n = 1$ ). There was one grade IVb complication with partial main portal vein thrombosis after MWA followed by an ICU stay and multi-organ dysfunction (Figure 2).

Primary efficacy, *i.e.* the percentage of target tumors successful eradicated in the 6-week follow-up imaging, was 84.3 % for RFA/MWA and 67.2 % for IRE.

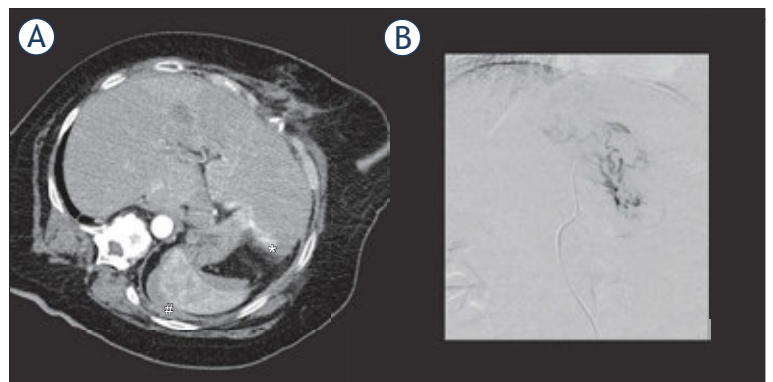


**FIGURE 1.** 68-year-old female patient with active bleeding (A) on the dorsal side of the left lobe of the liver (\*) immediately after RFA and perisplenic hematoma (#). Diagnostic angiography (B) immediately after the RFA did not show any active arterial bleeding. The patient was then monitored on a normal ward, and the bleeding ceased without further intervention.

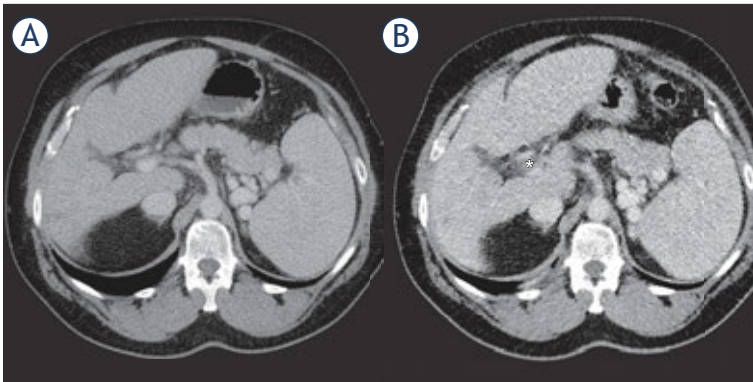


**FIGURE 2.** 57-year-old male patient with partial thrombosis (\*) of the main portal vein one day after microwave ablation (B). (A) Pre-interventional CT scan without visible thrombosis. Anticoagulation led to the regression of thrombosis without any necessary intervention.

## Discussion

Hepatocellular carcinoma (HCC) is the world's third most common cancer leading to death.<sup>20</sup> In Germany, cancer of the liver and intrahepatic bile ducts are among the top 10 deaths from cancer.<sup>21</sup> At the time of initial diagnosis, only 10–25% of patients represent candidates for surgery.<sup>22</sup>

Since early detection of cancer enables better prognosis and longer survival, it is recommended that people with the appropriate risk profile be screened for HCC.<sup>23</sup> According to EASL guidelines, half-yearly ultrasound examinations should be performed in patients with cirrhosis of the liver in stages Child-A and Child-B as well as in patients in stage Child-C if they are eligible for liver transplantation. In the case of abnormalities, additional contrast-enhanced imaging should be performed.<sup>24,25</sup>

In recent years, such observation strategies of patients with an increased risk-profile led to an earlier diagnosis of the disease and detection of HCCs at earlier stages. In addition to the higher chance of therapeutic response, early-stage patients also benefit from a broader range of different treatment options.<sup>26</sup>

Therapeutic options for hepatocellular carcinoma include surgical resection, liver transplantation, locoregional treatments, and chemotherapy. The final treatment decision depends mainly on the tumor stage, the patient performance status, and the functional liver reserve and requires a multidisciplinary approach.<sup>26</sup>

Which therapy is used in the respective case depends in particular on how far the disease has pro-

gressed at the time of diagnosis and in what condition the liver is. The patient's age and the general state of health are also considered when choosing a treatment method.<sup>27-29</sup> The effectiveness of the local-ablative therapy procedures could be proven in numerous studies of liver cancer up to a size of 3-5 cm. The use of local ablative procedures does not exclude subsequent surgical therapy. Furthermore, local-ablative procedures are often used to bridge waiting time until liver transplantation.

Irreversible Electroporation (IRE) is a novel, minimally invasive technique for the targeted destruction of cells by strong, locally limited electrical fields. Experience to date suggests that, in contrast to other local treatment methods, this technique explicitly targets the tumor cells. Other structures such as blood vessels and bile ducts are not permanently damaged. Potential disadvantages of the IRE are an increased risk of bleeding, due to the necessity of placing up to 6 electrodes in the liver and the lack of the possibility to cauterize the puncture channel.

Considering ongoing discussions which therapy should be used in respective patients, we have analyzed thermal ablation and irreversible electroporation ablation of HCC in the context of postinterventional morbidity.

In our patient cohort, the treatment decision was made by the local tumor board consisting of at least one certified hepatologist, oncologist, intervention radiologist and a highly qualified hepatobiliary surgeon with experiences in liver transplantation.

The incidence rates of the post-ablation syndrome vary significantly between studies. For example, in a prospective study of 54 patients treated with microwave ablation in liver tumors, 60% developed post-ablation syndrome.<sup>30</sup> All in all, post-ablation syndrome is seen in about one-third of patients after thermal ablation<sup>18,31</sup>. In our study, 17% of the patients had a post-ablation syndrome during the post-interventional clinical course with no differences between thermal and non-thermal ablations.

In this retrospective analysis, we report a systematical comparison between the complication rates of thermal ablation and IRE for a large patient collective.

Livraghi *et al.* reported six deaths (0.3%) and 50 other serious complications (2.2%) in a multicenter study in which more than 3,500 liver tumors were treated in 2,320 patients by thermal ablation.<sup>32</sup> Frühling *et al.* reported in a single-center study a minor complication rate of 20% (6 out of 30) and one (3.3%) major complication (bile duct dilata-

tion and stricture of the portal vein and bile duct) for IRE<sup>33</sup>, while Zeng *et al.* reports an event rate of 71.4% of minor and 7.1% of major complications for a small patient collective (n = 14).<sup>34</sup>

Comparing our results to previous studies we report a comparable rate of major complications (Grade III-V) for each procedure. However, numbers of minor complications (Grade I and II) are higher compared to previously reported studies. Of note, we used the “Classification of Surgical Complications” according to Clavien & Dindo<sup>16</sup>. In comparison to the standardized grading system of the Society of Interventional Radiology (SIR)<sup>19,35</sup>, this classification scheme offers a more detailed insight into the grade of recorded complications and especially includes events as Grade I complications that are not included in the SIR-classification. The SIR-classification only differentiates between major and minor complications; however, the classification reported in this study distinguishes five grades of complications, ranging from minor variation from the normal postinterventional course to the death of a patient.

Despite the retrospective collection of data, we were able to demonstrate that there was no significant difference in the occurrence as well as the grade of complications regarding the use of thermal versus non-thermal ablation, indicating a noninferiority of IRE in comparison to thermal ablation techniques. This is all the more remarkable because the tumors treated with IRE were significantly more frequently close to a major vessel and thus more complication-prone. In contrast, the tumors treated with RFA/MWA were significantly more frequently located in the easily accessible periphery.

We propose that the fear of a higher complication rate should not interfere with the treatment decision regarding thermal versus non-thermal ablation.

## References

- Kokudo N, Hasegawa K, Akahane M, Igaki H, Izumi N, Ichida T, et al. Evidence-based Clinical Practice Guidelines for Hepatocellular Carcinoma: The Japan Society of Hepatology 2013 update (3rd JSH-HCC Guidelines). *Hepatol Res* 2015; **45**. doi: 10.1111/hepr.12464.
- Rubinsky B, Onik G, Mikus P. Irreversible electroporation: a new ablation modality—clinical implications. *Technol Cancer Res Treat* 2007; **6**: 37-48. doi: 10.1177/153303460700600106
- Djokic M, Cemazar M, Popovic P, Kos B, Dezman R, Bosnjak M, et al. Electrochemotherapy as treatment option for hepatocellular carcinoma, a prospective pilot study. *EJSO* 2018; **44**: 651-7. doi: 10.1016/j.ejso.2018.01.090
- Davalos RV, Mir L, Rubinsky B. Tissue ablation with irreversible electroporation. *Ann Biomed Eng* 2005; **33**: 223. doi: 10.1007/s10439-005-8981-8
- Patterson EJ, Scudamore CH, Owen DA, Nagy AG, Buczkowski AK. Radiofrequency ablation of porcine liver in vivo: effects of blood flow and treatment time on lesion size. *Ann Surg* 1998; **227**: 559-65. PMID: 9563546
- Rossi S, Garbagnati F, De Francesco I, Accocella F, Leonardi L, Quaretti P, et al. Relationship between the shape and size of radiofrequency induced thermal lesions and hepatic vascularization. *Tumori* 1999; **85**: 128-32. PMID: 10363079
- Goldberg SN, Hahn PF, Tanabe KK, Mueller PR, Schima W, Athanasoulis CA, et al. Percutaneous radiofrequency tissue ablation: does perfusion-mediated tissue cooling limit coagulation necrosis? *J Vasc Interv Radiol* 1998; **9**(1 Pt 1): 101-11. PMID: 9468403
- Goldberg SN, Hahn PF, Halpern EF, Fogle RM, Gazelle GS. Radio-frequency tissue ablation: effect of pharmacologic modulation of blood flow on coagulation diameter. *Radiology* 1998; **209**: 761-7. doi: 10.1148/radiology.209.3.9844671
- Lu DS, Raman SS, Vodopich DJ, Wang M, Sayre J, Lassman C. Effect of vessel size on creation of hepatic radiofrequency lesions in pigs: assessment of the “heat sink” effect. *AJR Am J Roentgenol* 2002; **178**: 47-51. doi: 10.2214/ajr.178.1.1780047
- Dollinger M, Beyer LP, Haimerl M, Niessen C, Jung E-M, Zeman F, et al. Adverse effects of irreversible electroporation of malignant liver tumors under CT fluoroscopic guidance: a single-center experience. *Diagn Interv Radiol* 2015; **21**: 471-5. doi: 10.5152/dir.2015.14442
- Frühling P, Nilsson A, Duraj F, Haglund U, Norén A. Single-center non-randomized clinical trial to assess the safety and efficacy of irreversible electroporation (IRE) ablation of liver tumors in humans: short to mid-term results. *EJSO* 2017; **43**: 751-7. doi: 10.1016/j.ejso.2016.12.004
- Distelmaier M, Barabasch A, Heil P, Kraemer NA, Isfort P, Keil S, et al. Midterm safety and efficacy of irreversible electroporation of malignant liver tumors located close to major portal or hepatic veins. *Radiology* 2017; **285**: 1023-31. doi: 10.1148/radiol.2017161561
- Liang P, Wang Y, Yu X, Dong B. Malignant liver tumors: treatment with percutaneous microwave ablation—complications among cohort of 1136 patients. *Radiology* 2009; **251**: 933-40. doi: 10.1148/radiol.2513081740
- Bertot LC, Sato M, Tateishi R, Yoshida H, Koike K. Mortality and complication rates of percutaneous ablative techniques for the treatment of liver tumors: a systematic review. *Eur Radiol* 2011; **21**: 2584-96. doi: 10.1007/s00330-011-2222-3
- Patel U, Davidson JC, Nikolic B, Salazar GM, Schwartzberg MS, Walker TG, et al. Consensus guidelines for periprocedural management of coagulation status and hemostasis risk in percutaneous image-guided interventions. *J Vasc Interv Radiol* 2012; **23**: 727-36. doi: 10.1016/j.jvir.2012.02.012
- Dindo D, Demartines N, Clavien PA. Classification of surgical complications: a new proposal with evaluation in a cohort of 6336 patients and results of a survey. *Ann Surg* 2004; **240**: 205-13. doi: 10.1097/01.sla.0000133083.54934.ae
- Sahay A, Sahay N, Kapoor A, Kapoor J, Chatterjee A. Percutaneous image-guided radiofrequency ablation of tumors in inoperable patients - immediate complications and overall safety. *Indian J Palliat Care* 2016; **22**: 67-73. doi: 10.4103/0973-1075.173951
- Carrafiello G, Lagana D, Ianniello A, Dionigi G, Novario R, Recaldini C, et al. Post-radiofrequency ablation syndrome after percutaneous radiofrequency of abdominal tumours: one centre experience and review of published works. *Australas Radiol* 2007; **51**: 550-4. doi: 10.1111/j.1440-1673.2007.01871.x
- Goldberg SN, Grassi CJ, Cardella JF, Charboneau JW, Dodd GD, Dupuy DE, et al. Image-guided tumor ablation: standardization of terminology and reporting criteria. *J Vasc Interv Radiol* 2009; **20**(7 Suppl): S377-90. doi: 10.1016/j.jvir.2009.04.011
- Feher J, Lengyel G. [Hepatocellular carcinoma: occurrence, risk factors, biomarkers]. *Orv Hetil* 2010; **151**: 933-40. doi: 10.1556/oh.2010.28900
- Statistisches-Bundesamt. Diagnosedaten der Krankenhäuser ab 2000 zweigstelle Bonn June 2017 [updated 12. 06. 2017]. Available from: <http://www.gbe-bund.de>.
- Vauthey JN, Dixon E, Abdalla EK, Helton WS, Pawlik TM, Taouli B, et al. Pretreatment assessment of hepatocellular carcinoma: expert consensus statement. *HPB* 2010; **12**: 289-99. doi: 10.1111/j.1477-2574.2010.00181.x
- Desjardins LA. Hepatocellular carcinoma. *Clin J Oncol Nurs* 2002; **6**: 107-8. doi: 10.1188/02.cjon.107-108

24. Malek NP, Schmidt S, Huber P, Manns MP, Greten TF. The diagnosis and treatment of hepatocellular carcinoma. *Dtsch Arztebl Int* 2014; **111**: 101-6. doi: 10.3238/arztebl.2014.0101.
25. EASL Clinical Practice Guidelines: Management of hepatocellular carcinoma. *J Hepatol* 2018; **69**: 182-236. doi: 10.1016/j.jhep.2018.03.019
26. Raza A, Sood GK. Hepatocellular carcinoma review: current treatment, and evidence-based medicine. *World J Gastroenterol* 2014; **20**: 4115-27. doi: 10.3748/wjg.v20.i15.4115
27. Bruix J, Sherman M. Management of hepatocellular carcinoma. *Hepatology* 2005; **42**: 1208-36. doi: 10.1002/hep.24199
28. Ryder SD. Guidelines for the diagnosis and treatment of hepatocellular carcinoma (HCC) in adults. *Gut* 2003; **52** (Suppl 3): iii1-8. doi: 10.1016/j.jvir.2013.09.005
29. Ikai I, Kudo M, Arai S, Omata M, Kojiro M, Sakamoto M, et al. Report of the 18th follow-up survey of primary liver cancer in Japan. *Hepatol Res* 2010; **40**: 1043-59. doi: 10.1111/j.1872-034X.2010.00731.x
30. Andreano A, Galimberti S, Franza E, Knavel EM, Sironi S, Lee FT, et al. Percutaneous microwave ablation of hepatic tumors: prospective evaluation of postablation syndrome and postprocedural pain. *J Vasc Interv Radiol* 2014; **25**: 97-105. e2. doi: 10.1016/j.jvir.2013.09.005
31. Dodd GD, 3rd, Napier D, Schoolfield JD, Hubbard L. Percutaneous radiofrequency ablation of hepatic tumors: postablation syndrome. *AJR Am J Roentgenol* 2005; **185**: 51-7. doi: 10.2214/ajr.185.1.01850051
32. Livraghi T, Solbiati L, Meloni MF, Gazelle GS, Halpern EF, Goldberg SN. Treatment of focal liver tumors with percutaneous radio-frequency ablation: complications encountered in a multicenter study. *Radiology* 2003; **226**: 441-51. doi: 10.1148/radiol.2262012198
33. Fruhling P, Nilsson A, Duraj F, Haglund U, Noren A. Single-center non-randomized clinical trial to assess the safety and efficacy of irreversible electroporation (IRE) ablation of liver tumors in humans: Short to mid-term results. *Eur J Surg Oncol* 2017; **43**: 751-7. doi: 10.1016/j.ejso.2016.12.004
34. Zeng J, Liu G, Li ZH, Yang Y, Fang G, Li RR, et al. The safety and efficacy of irreversible electroporation for large hepatocellular carcinoma. *Technol Cancer Res Treat* 2017; **16**: 120-4. doi: 10.1177/1533034616676445
35. Omary RA, Bettmann MA, Cardella JF, Bakal CW, Schwartzberg MS, Sacks D, et al. Quality improvement guidelines for the reporting and archiving of interventional radiology procedures. *J Vasc Interv Radiol* 2003; **14**(9 Pt 2): S293-5. PMID: 12354820

# External beam accelerated partial breast irradiation: dosimetric assessment of conformal and three different intensity modulated techniques

Gábor Stelczer<sup>1,2</sup>, Tibor Major<sup>1</sup>, Norbert Mészáros<sup>1,3</sup>, Csaba Polgár<sup>1,3</sup>, Csilla Pesznyák<sup>1,2</sup>

<sup>1</sup> Center of Radiotherapy, National Institute of Oncology, Budapest, Hungary

<sup>2</sup> Institute of Nuclear Techniques, Budapest University of Technology and Economics, Hungary

<sup>3</sup> Department of Oncology, Semmelweis University, Budapest, Hungary

Radiol Oncol 2019; 53(1): 123-130.

Received 27 September 2018

Accepted 29 November 2018

Correspondence to: Gábor Stelczer, National Institute of Oncology, Ráth György u. 7-9, 1122 Budapest, Hungary. Phone: +36 1 224 8600 3667; E-mail: gabor.stelczer@gmail.com

Disclosure: No potential conflicts of interest were disclosed.

**Background.** The aim of the study was to evaluate and compare four different external beam radiotherapy techniques of accelerated partial breast irradiation (APBI) considering target coverage, dose to organs at risk and overall plan quality. The investigated techniques were three dimensional conformal radiotherapy (3D-CRT), "step and shoot" (SS) and "sliding window" (SW) intensity-modulated radiotherapy (IMRT), intensity-modulated arc therapy (RA).

**Patients and methods.** CT scans of 40 APBI patients were selected for the study. The planning objectives were set up according to the international recommendations. Homogeneity, conformity and plan quality indices were calculated from volumetric and dosimetric parameters of target volumes and organs at risk. The total monitor units and feasibility were also investigated.

**Results.** There were no significant differences in the coverage of the target volume between the techniques. The homogeneity indices of 3D-CRT, SS, SW and RA plans were 0.068, 0.074, 0.058 and 0.081, respectively. The conformation numbers were 0.60, 0.80, 0.82 and 0.89, respectively. The  $V_{50\%}$  values of the ipsilateral breast for 3D-CRT, SS, SW and RA were 47.5%, 40.2%, 39.9% and 31.6%, respectively. The average  $V_{10\%}$  and  $V_{40\%}$  values of ipsilateral lung were 13.1%, 28.1%, 28%, 36% and 2.6%, 1.9%, 1.9%, 3%, respectively. The 3D-CRT technique provided the best heart protection, especially in the low dose region. All contralateral organs received low doses. The SW technique achieved the best plan quality index (PQI).

**Conclusions.** Good target volume coverage and tolerable dose to the organs at risk are achievable with all four techniques. Taking into account all aspects, we recommend the SW IMRT technique for APBI.

Key words: accelerated partial breast irradiation; dosimetric evaluation; IMRT; RapidArc

## Introduction

Several previous prospective randomized trials and their meta-analysis proved that in the treatment of breast tumours, radiation therapy is an important part of breast conserving therapy. Breast conserving surgery and the subsequent irradiation of the remaining breast tissue ensure the same survival rate as radical breast surgery.<sup>1,2</sup> Nowadays,

accelerated partial breast irradiation (APBI) is becoming more and more an accepted treatment for early-stage invasive breast tumours.<sup>3-8</sup> Two main advantages are short overall treatment time (5 days) and smaller irradiated volume, which helps for the organs at risk (OAR) to be spared.

In the first external beam APBI trials the patients were treated with 3 dimensional conformal (3D-CRT) technique.<sup>9</sup> Studies with long follow up

times can be also found with brachytherapy.<sup>10,11</sup> These trials have the largest number of patients treated and the longest follow-up time. In our previous paper the dosimetric differences of the external beam and interstitial brachytherapy for APBI were evaluated.<sup>12</sup> It was found that the target volume can be appropriately irradiated by both techniques, but brachytherapy generally spares normal tissues and organs at risk better than IMRT. In 2006 a phase II sequential trial was launched at our institution.<sup>13</sup> In the first part of the trial between 2006 and 2011 forty-four patients were treated with 3D-CRT technique, while in the second part between 2011 and 2014 sixty patients were treated with image-guided “step & shoot” intensity-modulated (IMRT) technique, using 5 coplanar fields. Currently at our institution APBI treatments are carried out with “sliding window” IMRT technique according to our preliminary study.<sup>14</sup>

In current study, we conducted a dosimetric comparison of the traditional 3D-CRT, the intensity-modulated “step & shoot” (SS), “sliding window” (SW) and “RapidArc” (RA) techniques for APBI.

## Patients and methods

### Patients

For this study 40 patients were selected, who were previously treated with early-stage invasive breast cancer at our institution between 2006 and 2014 in a phase II APBI trial.<sup>13,15</sup> The study protocol was evaluated and accepted by the institutional and national ethics committees, and all patients provided written informed consent before enrolment. The trial was registered at ClinicalTrials.gov with identifier number NCT02003560. During breast-conserving surgery titanium surgical clips were placed in each patient to mark the boundaries of the excision cavity, which increased the accuracy of defining the resection cavity and consequently the planning target volume (PTV).

### Patient immobilization and CT acquisition

During planning CT scan, patients were positioned supine in a wingboard fixation device (Civco, USA). Around both breasts and on the surgical scar metal wires were placed to increase the precision of contouring. CT scans started from the mandible and included the complete volume of the lungs

and the volumes of both breasts. The most crucial part of partial breast irradiation is the exact localization of the excision cavity. Using titanium clips and the 3 mm thickness of the planning CT slices, the borders of surgical cavity could be defined in acceptable precision.

### Contouring

The contouring and 3D-CRT plans were made with Pinnacle 8.0m (Philips, The Netherlands) treatment planning system, while for the plans of SS, SW and RA the Eclipse 11 (Varian, USA) planning software was used. In the first step of target volume definition, the tumour bed was contoured by the radiation oncologist based on the seroma and the surrounding clips. In the second step, on the basis of the intact surgical margins and pathological results, it was expanded in 6 directions with margins of different size to define CTV. The minimal and maximal value of the extension between the tumour bed and the CTV was 5 and 18 mm, respectively.<sup>16</sup> The CTV was limited by the border of ipsilateral breast tissue. The safety margin between the CTV and PTV was 5 mm. As the skin is an organ at risk during partial breast irradiation, a 5 mm thick volume of the skin was cropped from PTV to create PTV<sub>eval</sub>. Heart, ipsilateral and contralateral breasts and lungs, non-target breast were contoured as organs at risk. Non-target breast was created with the extraction of PTV from ipsilateral breast.

### Planning purposes

36.9 Gy in 9 fractions was delivered on 5 consecutive days, twice a day with at least 6 hours interval between fractions. 100% of the PTV<sub>eval</sub> had to be covered with at least 95% of the prescribed dose. The allowed maximum dose was 110%. To make the techniques comparable, the same target coverage was achieved for all plans. Based on our protocol, the dose limits of the organs at risk were as follows:  $V_{100\%} < 35\%$  and  $V_{50\%} < 60\%$  for the ipsilateral breast,  $V_{30\%} < 20\%$  for the ipsilateral lung,  $V_{15\%} < 10\%$  for the heart in case of right sided tumours, while in case of left sided tumours, the value of heart  $V_{5\%}$  had to be smaller than for conventional whole breast irradiation.  $V_{xx\%}$  is the percentage of a region of interest (ROI) receiving at least the XX percent of the prescribed dose. These requirements were fulfilled in all of the plans. For contouring and for planning aims the NSABP B-39/RTOG 0413<sup>17</sup> guideline was used.

## Planning

The 3D-CRT plans were created with 4 or 5 wedged conformal non-coplanar fields from tangential directions (Figure 1). The IMRT plans were created with 5 or 6 coplanar fields covering 190°, four of these fields positioned in the medial “first” and lateral “last” 30°. The RA plans consisted of two coplanar arcs created between the most medial field of the IMRT plans and gantry angle of 180° (Figure 1). Avoidance sectors were not applied, only strict constraints were given for ipsilateral lung, heart and spine. All plans were created for linear accelerator equipped with 5 mm wide MLC and 6 MV photon energy was used. CCC algorithm in Pinnacle and AAA algorithm in Eclipse were used for dose calculations.

## Evaluation

For all techniques and all contoured organs volumes, minimum -, maximum and mean doses were recorded. Also  $V_{xx\%}$  and  $D_{xx\%}$  parameters were evaluated for all ROIs.

For the PTV<sub>eval</sub> homogeneity index and conformation number were calculated. Homogeneity index was calculated according to the ICRU83:

$$HI = \frac{D_{2\%} - D_{98\%}}{D_{50\%}}$$

And the conformation number is:

$$CN = \frac{PTV_{ref}}{V_{PTV}} \times \frac{PTV_{ref}}{V_{ref}}$$

where  $PTV_{ref}$  is the volume of PTV<sub>eval</sub> which is covered by the reference isodose,  $V_{PTV}$  is the volume of PTV<sub>eval</sub> and  $V_{ref}$  is the tissue volume encompassed by the reference isodose curve.<sup>18</sup> The plan quality index (PQI), defined by Leung *et al.*<sup>19</sup>, was calculated for all plans to include all the previous parameters in one quantity. The sum of monitor units (MU) was also recorded.

Statistical analysis was performed for all parameters with repeated measures ANOVA and Tukey post hoc test or Friedman test and Dunn post hoc test in GraphPad Instat (GraphPad Software, USA).

## Results

### Volumes

The mean volume of the tumour bed, CTV and PTV were 15.4 cm<sup>3</sup>, 80.8 cm<sup>3</sup> and 155.5 cm<sup>3</sup>, respectively. The ratios of CTV and PTV to the ipsilat-

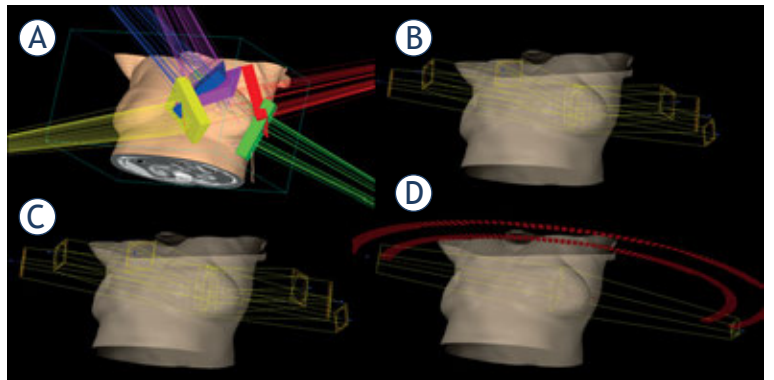


FIGURE 1: Typical beam arrangements in 3D-CRT (A), SS (B), SW (C) and RA (D) treatment plans.

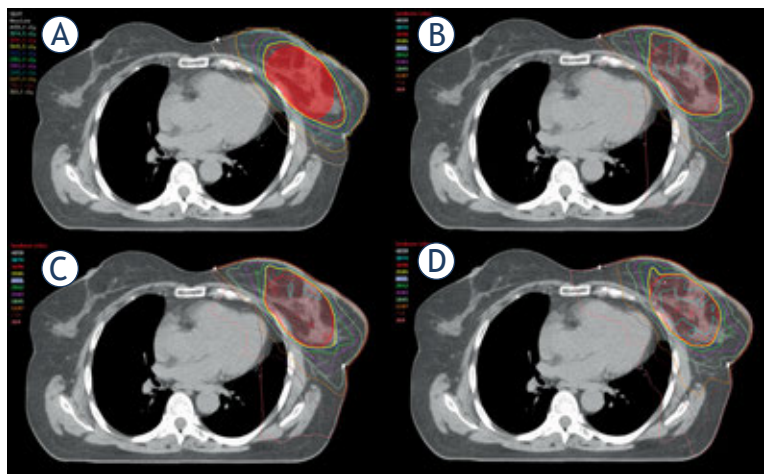


FIGURE 2: Representative dose distributions for a left sided case with 3D-CRT (A), SS (B), SW (C) and RA (D).

eral breast volume was 8.6% (range: 4–19.1%) and 16.8% (range: 8.3–40.1%), respectively.

### Target volume coverage

For each technique the  $V_{95\%}$  value of PTV<sub>eval</sub> was at least 99.5%, except for 5 cases with 3D-CRT technique. There were no significant differences between the techniques in the values of  $V_{95\%}$  and  $V_{90\%}$  (Table 1), neither for PTV<sub>eval</sub> nor for CTV. Figure 2 shows dose distributions for the four irradiation techniques in a representative case. The homogeneity index was significantly better with SW technique than with 3D-CRT, SS or RA techniques. The difference between 3D-CRT and RA technique was also significant. The average conformation numbers of 3D-CRT, SS, SW and RA were

TABLE 1. Quality indices and total number of monitor units of the four irradiation techniques

		Mean values (%)				ANOVA p value	Post hoc tests results					
		3D-CRT	SS	SW	RA		3D-CRT vs. SS	3D-CRT vs. SW	3D-CRT vs. RA	SS vs. SW	SS vs. RA	SW vs. RA
PTV eval	V <sub>95%</sub>	99.5	99.8	99.8	99.8	0.96	n.s.	n.s.	n.s.	n.s.	n.s.	n.s.
	V <sub>90%</sub>	100	100	100	100	0.875	n.s.	n.s.	n.s.	n.s.	n.s.	n.s.
CTV	V <sub>95%</sub>	99.9	100	100	100	0.001	n.s.	n.s.	n.s.	n.s.	n.s.	n.s.
	V <sub>90%</sub>	100	100	100	100	0.123	n.s.	n.s.	n.s.	n.s.	n.s.	n.s.
	HI	0.068	0.074	0.058	0.081	<0.001	n.s.	p<0.05	p<0.05	p<0.05	n.s.	p<0.05
	CN	0.6	0.8	0.82	0.89	<0.001	p<0.05	p<0.05	p<0.05	p<0.05	p<0.05	p<0.05
	PQI	0.5	0.36	0.34	0.43	<0.001	p<0.05	p<0.05	p<0.05	n.s.	p<0.05	p<0.05
	MU	677	814	1077	1136	<0.001	n.s.	p<0.05	p<0.05	p<0.05	p<0.05	n.s.

3D-CRT = three dimensional conformal radiotherapy; n.s. = not significant; RA = intensity-modulated arc therapy; SS and SW = „step and shoot“ and „sliding window“ intensity-modulated radiotherapy

TABLE 2. Dose to the organs at risk

		Mean values (%)				ANOVA p value	Post hoc tests results					
		3D-CRT	SS	SW	RA		3D-CRT vs. SS	3D-CRT vs. SW	3D-CRT vs. RA	SS vs. SW	SS vs. RA	SW vs. RA
Ipsilateral breast	V <sub>100%</sub>	14.3	13.9	12.1	12.7	<0.001	n.s.	p<0.05	p<0.05	p<0.05	p<0.05	n.s.
	V <sub>75%</sub>	31.5	26.1	25.8	21	<0.001	p<0.05	p<0.05	p<0.05	n.s.	p<0.05	p<0.05
	V <sub>50%</sub>	47.5	40.2	39.9	31.6	<0.001	p<0.05	p<0.05	p<0.05	n.s.	p<0.05	p<0.05
	D <sub>max</sub>	105.3	108.2	106.3	110.3	<0.001	p<0.05	n.s.	p<0.05	p<0.05	p<0.05	p<0.05
Ipsilateral lung	V <sub>10%</sub>	13.1	28.1	28	36	<0.001	p<0.05	p<0.05	p<0.05	n.s.	p<0.05	p<0.05
	V <sub>30%</sub>	3.9	3.6	3.6	6	<0.001	n.s.	n.s.	p<0.05	n.s.	p<0.05	p<0.05
	V <sub>40%</sub>	2.6	1.9	1.9	3	<0.001	p<0.05	p<0.05	n.s.	n.s.	p<0.05	p<0.05
	MLD	5.6	7.4	7.4	9.9	<0.001	p<0.05	p<0.05	p<0.05	n.s.	p<0.05	p<0.05
Heart (left sided tumour)	MHD	2.4	2.9	2.8	5.4	<0.001	n.s.	n.s.	p<0.05	n.s.	p<0.05	n.s.
	V <sub>5%</sub>	8.7	19.3	17.5	38.9	<0.001	n.s.	n.s.	p<0.05	n.s.	n.s.	p<0.05
	V <sub>15%</sub>	3	1.5	1.2	7.8	0.043	n.s.	n.s.	n.s.	n.s.	n.s.	p<0.05
Heart (right sided tumour)	MHD	0.8	1.6	1.6	3	<0.001	n.s.	n.s.	p<0.05	n.s.	p<0.05	p<0.05
	V <sub>5%</sub>	1.3	8.1	7.8	22.2	<0.001	p<0.05	n.s.	p<0.05	n.s.	n.s.	p<0.05
	V <sub>15%</sub>	0.6	0.1	0.2	0.5	0.711	n.s.	n.s.	n.s.	n.s.	n.s.	n.s.
Contralateral lung	V <sub>5%</sub>	0	3.4	3.2	9.6	<0.001	p<0.05	p<0.05	p<0.05	n.s.	p<0.05	p<0.05
	V <sub>10%</sub>	0	0.1	0.1	0.1	0.001	n.s.	n.s.	n.s.	n.s.	n.s.	n.s.
	D <sub>5%</sub>	0.5	4	4	5.4	<0.001	p<0.05	p<0.05	p<0.05	n.s.	p<0.05	p<0.05
	D <sub>10%</sub>	0.4	3.2	3.1	4.7	<0.001	p<0.05	p<0.05	p<0.05	n.s.	p<0.05	p<0.05
Contralateral breast	V <sub>5%</sub>	0.7	3.1	3.1	1.9	<0.001	p<0.05	p<0.05	p<0.05	n.s.	n.s.	n.s.
	V <sub>10%</sub>	0.3	0.2	0.2	0.0	0.013	n.s.	n.s.	n.s.	n.s.	n.s.	n.s.
	D <sub>5%</sub>	1.2	3.8	3.7	3.8	<0.001	p<0.05	p<0.05	p<0.05	n.s.	n.s.	n.s.
	D <sub>max</sub>	5.6	8.5	8.5	7.8	<0.001	p<0.05	p<0.05	p<0.05	n.s.	n.s.	n.s.

3D-CRT = three dimensional conformal radiotherapy; MHD = mean heart dose; MLD = mean lung dose; n.s. = non-significant; RA = intensity-modulated arc therapy; SS and SW = „step and shoot“ and „sliding window“ intensity-modulated radiotherapy

0.60, 0.80, 0.82 and 0.89, respectively, being all differences significant. The average values of homogeneity index, conformal number and PQI and the significance levels are summarized in Table 1.

### The organs at risk

Table 2 contains all the dosimetric values of the critical organs and their comparisons between different techniques.

With respect to the ipsilateral breast, the best results for dose reduction were achieved with RA technique which was also confirmed by the conformation number. The  $V_{50\%}$  values of non-target breast for 3D-CRT, SS, SW and RA were 39.6%, 29.9%, 29.6%, 19.8%, respectively. In the non-target ipsilateral breast the maximum doses were 105.1%, 105.8%, 103.8% and 106.4%, respectively.

With respect to the ipsilateral lung, we received significantly better results for dose-volume values for non-coplanar 3D-CRT in low dose ranges such as 10% of the prescribed dose, while RA resulted in the largest low dose bath ( $V_{10\%}$ ). For higher dose ranges the two static IMRT techniques achieved significantly better results for  $V_{40\%}$  than the other two.

The heart was better protected from low doses by the 3D-CRT technique. For the  $V_{15\%}$  values RA technique still provided the worst results, while the static-filed IMRTs reached the lowest doses for the heart.

Both contralateral lung and contralateral breast received low dose with all techniques. Noticeable values and differences can only be found at 5% of the prescribed dose, and only very small volume received a higher dose than 10%. For both organs the 3D-CRT had significantly better results. With 3D-CRT technique, the average maximum doses for the contralateral lung and the contralateral

breast were 0.8 Gy and 2.1 Gy, respectively. With static-field IMRT techniques the average values were 3 Gy and 3.1 Gy and with RA 3.5 Gy and 2.5 Gy, respectively.

The PQI values of 3D-CRT, SS, SW and RA techniques were 0.50, 0.36, 0.34 and 0.43. By definition, low PQI values mean high overall plan quality. The two static-field IMRT PQI values were significantly better than the ones for the other two techniques, and RA was also significantly better compared to 3D-CRT. With respect to monitor units, 3D-CRT (677 MU) and SS (814 MU) techniques were significantly lower than with SW (1077 MU) and RA (1136 MU). The difference between SW and RA was also significant.

The results of this study in comparison with other dosimetric studies in APBI can be found in Table 3<sup>20-22</sup> and Table 4 for the 3D-CRT and IMRT techniques, respectively.

### Discussion

The ratio of the target volume and the ipsilateral breast is a strict selection criteria in APBI, because good cosmetic outcomes are only achievable with the limitation of the irradiated volume. In our randomly selected 40 patients the median of tumour bed volume was 13.5 cm<sup>3</sup> (3–40 cm<sup>3</sup>). Different values can be found in the literature with respect to tumour bed sizes. Vicini *et al.*<sup>23</sup> reported similar values to ours for the average tumour bed volume (median: 14 cm<sup>3</sup> range: 3–70 cm<sup>3</sup>), while Oliver *et al.*<sup>24</sup> prepared plans with bigger surgical cavities (median: 63.5 cm<sup>3</sup> range: 12–134 cm<sup>3</sup>). Compared to our average value of 0.17 for target volume to ipsilateral breast ratio Bergom *et al.*<sup>25</sup> and Moon *et al.*<sup>26</sup> reported equal or smaller ratios, while Livi *et al.*<sup>27</sup> and Rusthoven *et al.*<sup>28</sup> reported higher ratios.

TABLE 3. Comparison between our and other 3D-CRT data published in APBI studies

	Target			Ipsilateral breast (%)		Non-target breast (%)	Heart (left-sided lesions)		Ipsilateral lung	
	$V_{PTV}$ (ccm)	$V_{PTV} / V_{IB}$	$V_{95\%}$ (%)	$V_{100\%}$	$V_{50\%}$	$V_{50\%}$	MHD (cGy)	$V_{5\%}$ (%)	MLD (cGy)	$V_{30\%}$ (%)
Patel <i>et al.</i> <sup>20</sup>	n.a.	n.a.	n.a.	26	52	n.a.	n.a.	n.a.	370	n.a.
Moon <i>et al.</i> <sup>26</sup>	n.a.	0.17	99.9	32.8	57.6	40.9	n.a.	n.a.	n.a.	n.a.
Qiu <i>et al.</i> <sup>21</sup>	236.2	n.a.	n.a.	20.3	46.8	n.a.	76.1	6.4	193.2	4.4
Essers <i>et al.</i> <sup>22</sup>	176.4	n.a.	96.4	n.a.	n.a.	23.2	200	15.9	370	n.a.
Rusthoven <i>et al.</i> <sup>28</sup>	187.5	0.243	96	19.9	47	34.5	n.a.	n.a.	n.a.	n.a.
Current work	155.5	0.168	99.5	14.3	47.5	39.6	90.3	8.7	205.3	3.9

MHD = mean heart dose; MLD = mean lung dose;  $V_{IB}$  = volume of ipsilateral breast

TABLE 4. Comparison between our and other IMRT data published in APBI studies

	Target			Ipsilateral breast (%)		Non-target breast (%)	Heart (left-sided lesions)		Ipsilateral Lung	
	V <sub>PTV</sub> (ccm)	V <sub>PTV</sub> / V <sub>IB</sub>	V <sub>95%</sub> (%)	V <sub>100%</sub>	V <sub>50%</sub>	V <sub>50%</sub>	MHD (cGy)	V <sub>5%</sub> (%)	MLD (cGy)	V <sub>30%</sub> (%)
Moon et al. <sup>24</sup>	n.a.	0.17	99.4	27.2	50.3	33.3	n.a.	n.a.	n.a.	n.a.
Qiu et al. <sup>21</sup>	236.2	n.a.	n.a.	17.3	45.3	n.a.	35.9	0.4	123.6	1.4
Livi et al. <sup>27</sup>	123	0.21	96	n.a.	n.a.	37.5	n.a.	n.a.	n.a.	9.7
Bergom et al. <sup>25</sup>	243	0.14	99.1	16.2	39.9	n.a.	n.a.	14.6	n.a.	4.6
Rusthoven et al. <sup>28</sup>	187.5	0.243	88.8	9.4	42.1	28.1	n.a.	n.a.	n.a.	n.a.
Current work	155.5	0.168	99.8	12.1	39.9	29.6	103.6	17.5	272.1	3.6
Qiu et al. <sup>21</sup>	236.2	n.a.	n.a.	18.2	44.9	n.a.	54.4	1	148	2
Essers et al. <sup>22</sup>	176.4	n.a.	98.9	n.a.	n.a.	19.7	100	4.3	190	n.a.
Current work	155.5	0.168	99.8	12.7	31.6	19.8	198.1	38.9	364.7	6

MHD = mean heart dose; MLD = mean lung dose; V<sub>IB</sub> = volume of ipsilateral breast

In order to achieve a good cosmetic result, the dose to the ipsilateral breast must be kept under a limit. According to the NSABP B-39/RTOG 0413 protocol, the V<sub>50%</sub> value of the ipsilateral breast has to be less than 60%.<sup>17</sup> However, in a retrospective study Jagsi *et al.*<sup>29</sup> found, that the threshold value for this parameter is around 40% and above this limit worse cosmetic results can occur. In our study this threshold value was exceeded by the average values of 3D-CRT plans, while the average values of the intensity modulated techniques were at or below this threshold. However, compared to other studies with the intensity modulated techniques we reached the best results, and our 3D-CRT plans were also very close to the best values with respect to ipsilateral breast protection (Table 3 and 4).

The coverage of the target volume was excellent with each technique. Based on our protocol, the V<sub>95%</sub> value of the PTV<sub>eval</sub> had to be higher than 99.5%, while the maximum dose should be less than 40.6 Gy. With 3D-CRT in case of 5 patients the coverage criterion was not fulfilled. We note that only Moon *et al.*<sup>26</sup> were able to get higher coverage with 3D-CRT technique than our results. With respect to intensity modulated techniques our study has the highest V<sub>95%</sub> coverage compared to values published in other papers.

Considering homogeneity, the best results could be achieved with the SW technique, and the difference is significant compared to the other three. With regards to the conformation number, the average value of the RA was the highest and was significantly better than for the other techniques, while in this respect the 3D-CRT was significantly the worst.

Regarding the mean dose of the ipsilateral lung in our study the 3D-CRT plans were significantly better compared to other techniques and at least as good as reported by others. As to volumes irradiated by higher doses, such as V<sub>30%</sub>, the RA resulted in the largest volumes, however these values were still in the range of the volumes published by others.

The best heart protection was achievable with 3D-CRT technique, especially in the low dose region, and our results are very similar to the data available in the literature. In this dose region (2 Gy or less) our results with intensity modulated techniques are slightly worse compared to data published by others, but well below the clinical limits. The outcome of static-field IMRT plans were better compared to RA. Other published data about dose to heart for left sided patients are also summarized in Table 3 and 4.

As for the contralateral lung and breast, each plan resulted in low doses. The 3D-CRT was significantly better as there are no fields intersecting with these organs. When applying intensity modulated techniques, only small portion of dose reaches the contralateral volumes, the average of maximum point doses varied between 2.5 and 3.5 Gy.

As for the PQI index, which takes into account the homogeneity, conformity and the dose to the organs at risk simultaneously, the two static-field IMRT techniques (SS and SW) achieved the best results; they were significantly better than the 3D-CRT and RA, but RA was significantly better compared to 3D-CRT. However, this index only takes into consideration plan quality and ignores factors, such as the overall number of MUs, treat-

ment time or the couch rotation during deliveries of the beams.

With regard to the number of monitor units, the 3D-CRT and SS technique proved to be significantly better than the SW and RA (Table 1). The table rotation applied with the 3D-CRT technique on one hand makes the treatment time longer and on the other hand can cause unintended movement of the patient, increasing the chances of intrafractional patient positioning errors, accordingly. Moreover, during planning it is difficult to take into consideration which gantry and couch angle combinations may result in collision. The RA technique provided the shortest overall treatment time, SW technique came very close to that and SS plans still could be delivered much faster than 3D-CRT plans.

## Conclusions

The advantage of the 3D-CRT technique with respect to dose to majority of OAR arises from its non-coplanar tangential beams arrangement which in the same time causes its biggest disadvantage, the long treatment time with higher uncertainty of patient positioning. Owing to its high conformality, the RA technique minimizes the potential side-effects for the ipsilateral breast, provides the shortest treatment time, however, higher volumes of organs at risk are irradiated with low doses. The two static-field IMRT techniques have a relatively short treatment time, excellent homogeneity, good conformity and the doses to the organs at risk are well below the protocol constraints. The technique with the best outcome for a specific case can be anatomy, tumour bed shape, -size and -location dependent, but taking all aspects into consideration, the SW IMRT is our recommended technique for accelerated partial breast irradiations.

## References

- Veronesi U, Cascinelli N, Mariani L, Greco M, Saccozzi R, Luini A, et al. Twenty-year follow-up of a randomized study comparing breast-conserving surgery with radical mastectomy for early breast cancer. *N Engl J Med* 2002; **347**: 1227-32. doi: 10.1056/NEJMoa020989
- Fisher B, Anderson S, Bryant J, Margolese RG, Deutsch M, Fisher ER, et al. Twenty-year follow-up of a randomized trial comparing total mastectomy, lumpectomy, and lumpectomy plus irradiation for the treatment of invasive breast cancer. *New Engl J Med* 2002; **347**: 1233-41. doi: 10.1056/NEJMoa022152
- Smith BD, Arthur DW, Buchholz TA, Haffty BG, Hahn CA, Hardenbergh PH, et al. Accelerated partial breast irradiation consensus statement from the American Society for Radiation Oncology (ASTRO). *J Am Coll Surg* 2009; **209**: 269-77. doi: 10.1016/j.jamcollsurg.2009.02.066
- Arthur DW, Vicini FA. Accelerated partial breast irradiation as a part of breast conservation therapy. *J Clin Oncol* 2005; **23**: 1726-35. doi: 10.1200/JCO.2005.09.045
- Njeh CF, Saunders MW, Langton CM. Accelerated partial breast irradiation using external beam conformal radiation therapy: a review. *Crit Rev Oncol Hematol* 2012; **81**: 1-20. doi: 10.1016/j.critrevonc.2011.01.011
- Polgár C, Van Limbergen E, Pötter R, Kovács G, Polo A, Lyczek J, et al. Patient selection for accelerated partial-breast irradiation (APBI) after breast-conserving surgery: recommendations of the Groupe Européen de Curiothérapie-European Society for Therapeutic Radiology and Oncology (GEC-ESTRO) breast cancer working group based on clinical evidence (2009). *Radiother Oncol* 2010; **94**: 264-73. doi: 10.1016/j.radonc.2010.01.014
- Coles CE, Brunt AM, Wheatley D, Mukesh MB, Yarnold JR. Breast radiotherapy: less is more? *Clin Oncol (R Coll Radiol)* 2013; **25**: 127-34. doi: 10.1016/j.clon.2012.10.013
- Livi L, Meattini I, Marrazzo L, Simontacchi G, Pallotta S, Saieva C, et al. Accelerated partial breast irradiation using intensity-modulated radiotherapy versus whole breast irradiation: 5-year survival analysis of a phase 3 randomised controlled trial. *Eur J Cancer* 2015; **51**: 451-63. doi: 10.1016/j.ejca.2014.12.013
- Rodríguez N, Sanz X, Dengra J, Foro P, Membrive I, Reig A, et al. Five-year outcomes, cosmesis, and toxicity with 3-dimensional conformal external beam radiation therapy to deliver accelerated partial breast irradiation. *Int J Radiat Oncol Biol Phys* 2013; **87**: 1051-7. doi: 10.1016/j.ijrobp.2013.08.046
- Polgár C, Major T, Fodor J, Sulyok Z, Somogyi A, Lövey K, et al. Accelerated partial-breast irradiation using high-dose-rate interstitial brachytherapy: 12-year update of a prospective clinical study. *Radiother Oncol* 2010; **94**: 274-9. doi: 10.1016/j.radonc.2010.01.019
- Strnad V, Ott OJ, Hildebrandt G, Kauer-Dorner D, Knauerhase H, Major T, et al. 5-year results of accelerated partial breast irradiation using sole interstitial multicatheter brachytherapy versus whole-breast irradiation with boost after breast-conserving surgery for low-risk invasive and in-situ carcinoma of the female breast: a randomised, phase 3, non-inferiority trial. *Lancet* 2016; **387**: 229-38. doi: 10.1016/S0140-6736(15)00471-7
- Major T, Stelczer G, Pesznyák C, Mészáros N, Polgár C. Multicatheter interstitial brachytherapy versus intensity modulated external beam therapy for accelerated partial breast irradiation: A comparative treatment planning study with respect to dosimetry of organs at risk. *Radiother Oncol* 2017; **122**: 17-23. doi: 10.1016/j.radonc.2016.08.003
- Móza E, Mészáros N, Major T, Fröhlich G, Stelczer G, Sulyok Z, et al. Accelerated partial breast irradiation with external beam three-dimensional conformal radiotherapy. Five-year results of a prospective phase II clinical study. *Strahlenther Onkol* 2014; **190**: 444-50. doi: 10.1007/s00066-014-0633-1
- Stelczer G, Major T, Mészáros N, Polgár C, Pesznyák C. [Dosimetric comparison of different techniques for external beam accelerated partial breast irradiation]. [Hungarian]. *Magy Onkol* 2016; **60**: 305-11. PMID: 27898749
- Mészáros N, Major T, Stelczer G, Zaka Z, Móza E, Pukancsik D, et al. Implementation of image-guided intensity-modulated accelerated partial breast irradiation: three-year results of a phase II clinical study. *Strahlenther Onkol* 2017; **193**: 70-9. doi: 10.1007/s00066-016-1074-9.
- Major T, Gutiérrez C, Guix B, van Limbergen E, Strnad V, Polgár C, et al. Recommendations from GEC ESTRO Breast Cancer Working Group (II): Target definition and target delineation for accelerated or boost partial breast irradiation using multicatheter interstitial brachytherapy after breast conserving open cavity surgery. *Radiother Oncol* 2016; **118**: 199-204. doi: 10.1016/j.radonc.2015.12.006
- Vicini F, White J, Julian T, Parda D, Arthur D, Kuske R, et al. NSABP protocol B-39/RTOG protocol 0413: a randomized Phase III study of conventional whole breast irradiation (WBI) versus partial breast irradiation (PBI) for women with Stage 0, I or II breast cancer. Version March 13, 2007. [cited 2018 Sep 15]. Available at [https://www.rtog.org/Portals/0/RTOG%20Broadcasts/Attachments/RTOG\\_0413\\_Trial\\_updates\\_5.22.12.pdf](https://www.rtog.org/Portals/0/RTOG%20Broadcasts/Attachments/RTOG_0413_Trial_updates_5.22.12.pdf)
- van't Riet A, Mak AC, Moerland MA, Elders LH, van der Zee W. A conformation number to quantify the degree of conformality in brachytherapy and external beam irradiation: application to the prostate. *Int J Radiat Oncol Biol Phys* 1997; **37**: 731-6. doi: 10.1016/S0360-3016(96)00601-3
- Leung LH, Kan MW, Cheng AC, Wong WK, Yau CC. A new dose-volume-based Plan Quality Index for IMRT plan comparison. *Radiother Oncol* 2007; **85**: 407-17. doi: 10.1016/j.radonc.2007.10.018

20. Patel RR, Becker SJ, Das RK, Mackie TR. A dosimetric comparison of accelerated partial breast irradiation techniques: multicatheter interstitial brachytherapy, three-dimensional conformal radiotherapy, and supine versus prone helical tomotherapy. *Int J Radiat Oncol Biol Phys* 2007; **68**: 935-42. doi: 10.1016/j.ijrobp.2007.03.005
21. Qiu JJ, Chang Z, Horton JK, Wu QR, Yoo S, Yin FF. Dosimetric comparison of 3D conformal, IMRT, and V-MAT techniques for accelerated partial-breast irradiation (APBI). *Med Dosim* 2014; **39**: 152-8. doi: 10.1016/j.meddos.2013.12.001
22. Essers M, Osman SO, Hol S, Donkers T, Poortmans PM. Accelerated partial breast irradiation (APBI): are breath-hold and volumetric radiation therapy techniques useful? *Acta Oncol* 2014; **53**: 788-94. doi: 10.3109/0284186X.2014.887226
23. Vicini FA, Chen P, Wallace M, Mitchell C, Hasan Y, Grills J, Kestin L, et al. Interim cosmetic results and toxicity using 3D conformal external beam radiotherapy to deliver accelerated partial breast irradiation in patients with early-stage breast cancer treated with breast-conserving therapy. *Int J Radiat Oncol Biol Phys* 2007; **69**: 1124-30. doi: 10.1016/j.ijrobp.2007.04.033
24. Oliver M, Chen J, Wong E, Van Dyk J, Perera F. A treatment planning study comparing whole breast radiation therapy against conformal, IMRT and tomotherapy for accelerated partial breast irradiation. *Radiother Oncol* 2007; **82**: 317-23. doi: 10.1016/j.radonc.2006.11.021
25. Bergom C, Prior P, Kainz K, Morrow NV, Ahunbay EE, Walker A, et al. A phase I/II study piloting accelerated partial breast irradiation using CT-guided intensity modulated radiation therapy in the prone position. *Radiother Oncol* 2013; **108**: 215-9. doi: 10.1016/j.radonc.2013.05.039
26. Moon SH, Shin KH, Kim TH, Yoon M, Park S, Lee DH, et al. Dosimetric comparison of four different external beam partial breast irradiation techniques: three-dimensional conformal radiotherapy, intensity-modulated radiotherapy, helical tomotherapy, and proton beam therapy. *Radiother Oncol* 2009; **90**: 66-73. doi: 10.1016/j.radonc.2008.09.027
27. Livi L, Buonamici FB, Simontacchi G, Scotti V, Fambrini M, Compagnucci A. Accelerated partial breast irradiation with IMRT: new technical approach and interim analysis of acute toxicity in a phase III randomized clinical trial. *Int J Radiat Oncol Biol Phys* 2010; **77**: 509-15. doi: 10.1016/j.ijrobp.2009.04.070
28. Rusthoven KE, Carter DL, Howell K, Kercher JM, Henkenberns P, Hunter KL, et al. Accelerated partial-breast intensity-modulated radiotherapy results in improved dose distribution when compared with three-dimensional treatment-planning techniques. *Int J Radiat Oncol Biol Phys* 2008; **70**: 296-302. doi: 10.1016/j.ijrobp.2007.08.047
29. Jagsi R, Ben-David MA, Moran JM, Marsh RB, Griffith KA, Hayman JA, et al. Unacceptable cosmesis in a protocol investigating intensity-modulated radiotherapy with active breathing control for accelerated partial-breast irradiation. *Int J Radiat Oncol Biol Phys* 2010; **76**: 71-8. doi: 10.1016/j.ijrobp.2009.01.041

Radiol Oncol 2019; 53(1): 1-5.  
doi: 10.2478/raon-2018-0035

## Bolezen osrčnika po obsevanju zaradi raka dojk

Marinko T

**Izhodišča.** Rak dojk je drugi najpogostejši rak na svetu. Moderni načini onkološkega zdravljenja izboljšujejo preživetje bolnic z rakom dojk in število tistih, ki so raka prebolele se povečuje. Vedno več pozornosti namenjamo ugotavljanju in spremljanju neželenih učinkov onkološkega zdravljenja. O ishemični bolezni srca, ki je lahko posledica zdravljenja raka dojk z obsevanjem, je objavljeno že veliko literature, nasprotno pa je o incidenci in kliničnem pomenu bolezni osrčnika po obsevanju malo podatkov.

**Zaključki.** Čeprav je vnetje osrčnika najzgodnejša oblika bolezni srca, ki nastane po obsevanju v področju srca, je v klinični praksi malokrat prepoznano, saj večinoma poteka brez simptomov, še posebno ob uporabi modernih obsevalnih tehnik. V posameznih primerih, navadno v povezavi s sistemskim onkološkim zdravljenjem in pozno po zaključenem zdravljenju, se lahko razvije resna bolezen osrčnika, ki je lahko tudi življenjsko ogrožujoča. Načini zdravljenja so enaki kot za bolnike, ki niso bili zdravljeni z obsevanjem, vendar je kirurško zdravljenje pri obsevanih bolnikih lahko težje izvedljivo.

Radiol Oncol 2019; 53(1): 6-14.  
doi: 10.2478/raon-2019-0006

## Pregled zviševanja obsevalne doze pri lokalno napredovalem nedrobnoceličnem pljučnem raku

Ma L, Men Y, Feng L, Kang J, Sun X, Yuan M, Jiang W, Hui Z

**Izhodišča.** Osnovna terapija za lokalno napredovali nedrobnocelični rak pljuč je sočasna kemoradioterapija. Lokoregionalna ponovitev predstavlja prevladujoč vzorec neuspeha. Dosedanje raziskave so potrdile povezavo med povečanimi biološko ekvivalentnimi odmerki in izboljšanim splošnim preživetjem. Vendar pa velika randomizirana raziskava III. faze, RTOG 0617, ni uspela dokazati koristi povečanja doze na 74 Gy s preprostim povečanjem števila frakcij v primerjavi s 60 Gy. Zato je raziskovanje varnih in učinkovitih metod za povečanje odmerka obsevanja upravičeno.

**Zaključki.** Navkljub proučevanju zviševanja efektivne obsevalne doze, vključno s spremenjenim frakcioniranjem, personaliziranim režimom radioterapije in novim tehnikam obsevanja še nismo soglasni, katero obsevanje je najbolj učinkovito in varno.

Radiol Oncol 2019; 53(1): 15-24.  
doi: 10.2478/raon-2019-0004

## Magnetnoresonančna difuzijska preiskava s koeficientom sploščenosti in konvencionalna magnetnoresonančna difuzijska preiskava pri oceni odziva na zdravljenje z elektrokemoterapijo pri lokalno napredovalem raku trebušne slinavke

Granata V, Fusco R, Venanzio Setola S, Palaia R, Albino V, Piccirillo M, Grimm R, Petrillo A, Izzo F

**Izhodišča.** Namen raziskave je bil primerjati ocene diagnostične učinkovitosti konvencionalnega mono-eksponentnega magnetnoresonančnega (MR) difuzijskega slikanja (ang. *diffusion weighted imaging*, DWI) in MR difuzijskega slikanja s koeficientom sploščenosti (ang. *diffusion kurtosis imaging*, DKI). Ocenjevali smo odziv na zdravljenje z elektrokemoterapijo (ECT) pri napredovalem raku trebušne slinavke.

**Bolniki in metode.** V klinično raziskavo smo vključili 21 bolnikov z lokalno napredovalim žleznim rakom trebušne slinavke, ki smo jih zdravili z ECT. Preiskavo MR pred in po ECT smo naredili pri 13/21 (61,9 %) bolnikih. Opravili smo jo z napravo jakosti magnetnega polja 1,5 T; podatke smo zajemali ob prostem dihanju v aksialni ravnini. Zajeli smo sekvence DWI s sedmimi vrednostmi b:  $b = 0, 50, 100, 150, 400, 800, 1000 \text{ s / mm}^2$ . Po preiskavi smo iz zajetih podatkov izračunali navidezni difuzijski koeficient s konvencionalnim mono-eksponentnim pristopom ter povprečje difuzijskega koeficienta in povprečje difuzijske sploščenosti s tehniko DKI. Opravljena je bila analiza krivulje ROC in določena senzitivnost, specifičnost ter pozitivna in negativna napovedna vrednost difuzijskih parametrov.

**Rezultati.** Med preiskovanimi difuzijskimi parametri so se pred in po zdravljenju pomembno spremenile le vrednosti povprečja difuzijskega koeficienta s tehniko DKI ( $p = 0,02$ , Wilcoxonov test). Pri istem parametru so bile prisotne statistično pomembne razlike v deležu sprememb med pacienti, ki so se odzvali in tistimi, ki se niso odzvali na zdravljenje. ( $p = 0,01$  test Kruskal Wallis). Povprečje difuzijskega koeficienta je pokazalo dobro diagnostično učinkovitost z občutljivostjo 80 %, specifičnostjo 100 % in površino pod ROC 0,933.

**Zaključki.** Povprečje difuzijskega koeficienta pridobljenega s tehniko DKI omogoča razlikovanje med pacienti, ki se odzovejo in pacienti, ki se ne odzovejo na zdravljenje z ECT. Povprečje difuzijskega koeficienta ima višjo diagnostično moč za oceno odziva na ECT v primerjavi s konvencionalnimi parametri DWI.

Radiol Oncol 2019; 53(1): 25-30.  
doi: 10.2478/raon-2018-0048

# Napovedna vrednost CT perfuzijskih parametrov jedra infarkta pri bolnikih s hemoragično transformacijo po zdravljenju sveže ishemične možganske kapi z intravensko trombolizo

Langel C, Šurlan Popović K

**Izhodišča.** Intravenska tromboliza je izbor zdravljenja za bolnike s simptomi in znaki ishemične možganske kapi, ki traja manj kot 4,5 ure. Hemoragične transformacije je resen zaplet intravenske trombolize in se pojavlja v 4,5–68,0 % kliničnih primerov ishemične možganske kapi. Namen raziskave je bil določiti CT perfuzijski parameter jedra infarkta, ki najzanesljiveje napove nastanek hemoragične transformacije.

**Bolniki in metode.** V retrospektivno opazovalno klinično raziskavo smo vključili 75 bolnikov z akutno ishemično možgansko kapjo, ki so bili zdravljeni z intravensko trombolizo v skladu z veljavnimi smernicami. Bolnike, pri katerih se je po intravenski trombolizi pojavila hemoragična transformacija, smo razporedili v opazovano skupino. V kontrolno skupino pa smo razporedili bolnike, pri katerih se hemoragična transformacija ni pojavila. Vsakemu bolniku opazovane skupine smo poiskali bolnika, ki se je z njim skladal po kriteriju časa od pojava simptomov ishemične možganske kapi do zdravljenja z intravensko trombolizo  $\pm 0.5$  h. Naknadno smo zaradi tehničnih neustreznosti slikovnih študij (npr. premik pacienta) iz opazovane skupine izločili pet bolnikov. Izmerili smo naslednje CT perfuzijske parametre: pretok krvi skozi možgane (*ang. cerebral blood flow - CBF*), volumen krvi v enoti mase možganovine (*ang. cerebral blood volume - CBV*), srednji čas pretoka volumna bolusa kontrasta skozi enoto volumna možganovine (*ang. mean transit time - MTT*), relativni CBF in relativni CBV. Z dvosmernim Mann-Whitneyjevim U-testom smo ugotavljali, ali med obema proučevanima skupinama bolnikov obstaja statistično pomembna razlika med izhodiščnimi vrednostmi CT perfuzijskih parametrov. Iz AUC krivulje ROC smo določili sposobnost razlikovanja posameznega CT perfuzijskih parametrov med nastankom in nenastankom hemoragične transformacije. S krivuljami ROC smo določili mejne vrednosti CT perfuzijskih parametrov, pri katerih lahko z največjo hkratno občutljivostjo in specifičnostjo pričakujemo nastanek hemoragične transformacije.

**Rezultati.** Ugotovili smo statistično pomembno razliko med opazovano in kontrolno skupino za CBF ( $p = 0,004$ ), CBV ( $p = 0,009$ ), relativni CBF ( $p < 0,001$ ) in relativni CBV ( $p = 0,001$ ). Analiza krivulj ROC je pokazala, da relativni CBF  $< 4,5$  % srednje vrednosti kontralateralne hemisfere možgan (AUC = 0,736) najbolje od vseh proučevanih CT perfuzijskih parametrov napoveduje nastanek hemoragične transformacije. Občutljivost je bila 71,0 %, specifičnost 52,5 %.

**Zaključki.** Perfuzijski CT ima pomembno vlogo pri napovedi nastanka hemoragične transformacije, saj je v pomoč pri izbiri bolnikov, ki jim intravenska tromboliza koristi. Nastanek hemoragične transformacije najbolje napoveduje perfuzijski parameter relativni CBF.

Radiol Oncol 2019; 53(1): 31-38.

doi: 10.2478/raon-2019-0005

## Napoved preživetja pacientov s perifernim T celičnim limfomom glede na znake CT. Preliminarna raziskava

Yang W, Jiang S, Lin J, Li Y

**Izhodišča.** Periferni T-celični limfom (PTCL) je redka bolezen s slabim kliničnim izidom. Radioloških poročil o preživetju bolnikov s PTCL je malo. Namen raziskave je bil preučiti prognostične vrednosti znakov CT za napoved kliničnega izida pri 51 bolnikih s histološko dokazanim PTCL.

**Bolniki in metode.** Retrospektivno smo pregledali klinične podatke in znake CT. Ocenjevali smo: število prizadetih področij, velikosti lezij, obliko, rob, gostoto, obtumorsko invazijo, znotraj tumorsko nekrozo, prizadetost bezgavk in stopnjo privzemanja kontrastnega sredstva. Uporabili smo univariatno in multivariatno logistično regresijsko analizo za določitev povezave med kliničnim izidom in radiološkimi znaki.

**Rezultati.** Večje število prizadetih lokacij, nejasni robovi z obtumorsko invazijo, nehomogena gostota in znotraj tumorska nekroza so bili povezani s slabšim izidom pri univariatni analizi ( $P < 0,05$ ). Nejasni robovi z obtumorsko invazijo pa so predstavljali neodvisno tveganje pri nadaljnji multivariatni logistični regresijski analizi ( $P < 0,05$ ). Področje pod krivuljo ROC teh CT značilnosti bilo 0,745 ( $P < 0,05$ ).

**Zaključki.** Nejasni robovi z obtumorsko invazijo so pomemben prognostični dejavnik za napoved slabšega kliničnega izida pri bolnikih s PTCL.

Radiol Oncol 2019; 53(1): 39-48.

doi: 10.2478/raon-2019-0010

## Vloga MR difuzijskega in perfuzijskega slikanja za napoved preživetja bolnikov z rakom glave in vratu, zdravljenih z radiokemoterapijo

Garbajs M, Strojjan P, Šurlan-Popovič K

**Izhodišča.** Namen raziskave je bil oceniti, ali izhodiščne vrednosti parametrov, pridobljenih z magnetno-rezonančnim (MR) difuzijskim in perfuzijskim slikanjem, in njihove spremembe zgodaj med zdravljenjem napovedujejo preživetje brez bolezni in celokupno preživetje bolnikov z lokalno in regionalno napredovalimi ploščatoceličnimi raki glave in vratu, zdravljenih s sočasno radiokemoterapijo (RT-KT) s cisplatinom.

**Bolniki in metode.** Pri 20 bolnikih z napredovalimi ploščatoceličnimi raki glave in vratu smo naredili MR difuzijsko in perfuzijsko slikanje pred zdravljenjem in po prejetih 10 Gy RT-KT. V vsaki časovni točki smo v primarnem tumorju izmerili vrednosti navideznega difuzijskega koeficienta (ADC) in MR perfuzijskih parametrov (konstanta prostorninskega prenosa med zunajceličnim zunajžilnim prostorom [ZPP] in krvno plazmo [ $K_{trans}$ ], prostornino ZPP na enoto prostornine tkiva [ $V_e$ ] in prostornino krvne plazme na enoto prostornine tkiva [ $V_p$ ]). Izračunali smo relativne spremembe parametrov po 10 Gy glede na izhodiščne vrednosti. Za določitev napovednih dejavnikov DFS in OS smo uporabili univariatno in multivariatno Coxovo regresijsko analizo. Da bi določili parameter z najvišjo diagnostično zanesljivostjo, smo analizirali krivulje ROC (receiver operating characteristic).

**Rezultati.** Nobeden izmed parametrov se ni pokazal kot napovedni dejavnik za preživetje brez bolezni. Nižje vrednosti ADC ( $p = 0,012$ ) in višje vrednosti  $K_{trans}$  ( $p = 0,026$ ) pred zdravljenjem ter večje znižanje  $K_{trans}$  ( $p = 0,014$ ) po 10 Gy (glede na izhodiščne vrednosti) so se v univariatni analizi pokazali kot pomembni napovedni dejavniki za celokupno preživetje. V multivariatni analizi smo ugotovili, da je neodvisen napovedni kazalec celokupnega preživetja samo višja vrednost  $K_{trans}$  pred zdravljenjem ( $p = 0,026$ ; 95% interval zaupanja [CI]: 0.000 – 0.132). Najvišjo diagnostično zanesljivost (krivulje ROC) s 93,3 % občutljivostjo in 80,0 % specifičnostjo je imela vrednost  $K_{trans}$  pred zdravljenjem (področje pod krivuljo [AUC] = 0,95).

**Zaključki.** V naši skupini bolnikov s ploščatoceličnimi raki glave in vratu, zdravljenih z RT-KT s cisplatinom, se je izhodiščna vrednost  $K_{trans}$  pokazala kot dober napovedovalec celokupnega preživetja.

Radiol Oncol 2019; 53(1): 49-56.  
doi: 10.2478/raon-2019-0012

## Magnetno resonančni napovedni dejavniki pri raku jezika. Možni napovedovalci zasevkov v bezgavkah na vratu

Mourad MAF, Higazi MM

**Izhodišča.** Namen raziskave je bil oceniti pomembnost treh magnetnoresonančnih slikovnih parametrov za napoved zasevkov v bezgavkah na vratu pri bolnikih z rakom jezika. Ocenjevali smo debelino tumorja, objezično razdaljo in vrednosti difuzijske konstante (ADC).

**Bolniki in metode.** Petdeset bolnikov s histološko potrjenim rakom jezika je opravilo magnetnoresonančno slikanje. Uporabili smo T1 in T2 utežene posnetke MR, difuzijsko utežene posnetke in pokontrastne sekvence T1 s supresijo maščobe.

**Rezultati.** Bolnike smo razvrstili v dve skupini glede na prizadetost bezgavk, kot jih je prikazalo magnetnoresonančno slikanje. Statistično pomembne razlike med skupinama s pozitivnimi in negativnimi bezgavkami smo ugotovili pri debelini tumorja in pri objezični razdalji (p-vrednosti 0,998 in 0,003). Prizadetosti bezgavk sta glede na analizo krivulj ROC (angl. *receiver operating characteristics*, karakteristika delovanja sprejemnika) napovedovali razmejitveni vrednosti > 13,8 mm (debelina tumorja) in ≤ 3,3 mm objezične razdalje. Med bolniki z zasevki in brez zasevkov v bezgavkah na vratu ni bilo najti statistično pomembnih razlik v vrednostih ADC (p-vrednost = 0,518).

**Zaključki.** Objezična razdalja in debelina tumorja sta dejavnika, ki bi lahko vplivala na predoperativno presojo in napoved poteka bolezni pri bolnikih z rakom jezika. Vrednost ADC tumorja se sama po sebi ne kaže zanesljiv kazalec napredovanja raka v področne bezgavke.

Radiol Oncol 2019; 53(1): 57-68.  
doi: 10.2478/raon-2019-0007

## Povišan nivo cistatina F je povezan z zmanjšano citotoksičnostjo citotoksičnih celic T

Prunk M, Perišić Nanut M, Sabotič J, Švajger U, Kos J

**Izhodišča.** Cistatin F je proteinski zaviralec cisteinskih peptidaz, ki se izraža predvsem v imunskih celicah in ga najdemo v endosomih/lizosomih. V citotoksičnih imunskih celicah cistatin F zavira obe glavni pro-grancimski konvertazi, katepsina C in H, ki aktivirata grancime, ter katepsin L, ki je udeležen pri aktivaciji perforina. Perforin in grancimi so pomembne molekule, ki citotoksičnim limfocitom omogočajo ubijanje tarčnih celic, zato lahko pomanjkljivosti ali napake pri aktivaciji bodisi perforina ali grancimov vplivajo na njihov citotoksični potencial.

**Materiali in metode.** S prenosom western smo določili nivo cistatina F, medtem ko smo interakcije cistatina F s katepsini C, H in L proučili z imunoprecipitacijo in konfokalno mikroskopijo. V celicah TALL-104 smo določili specifične aktivnosti katepsinov ter grancima B z uporabo peptidnih substratov.

**Rezultati.** Vzpostavili smo dva modela zmanjšane T-celične citotoksičnosti z uporabo celične linije TALL-104, ki smo jo tretirali z ionicinom ali imunosupresivnim citokinom transformirajočim rastnim dejavnikom beta. Zmanjšana citotoksičnost TALL-104 celic je povezana s povišanimi nivoji cistatina F in z zmanjšanimi specifičnimi aktivnostmi katepsinov C, H in L ter grancima B. Potrdili smo kolokalizacijo cistatina F s katepsini C, H in L ter interakcijo cistatina F s katepsinom C in H.

**Zaključki.** Cistatin F bi lahko nadzoroval, podobno kot pri naravnih celicah ubijalkah, citotoksičnost citotoksičnih celic T.

Radiol Oncol 2019; 53(1): 69-76.  
doi: 10.2478/raon-2019-0002

## Inhibitor NADPH oksidaz VAS2870 preprečuje s stavrosporinom inducirano celično smrt podganjih astrocitov

Šimenc J, Mojca Jurič D, Lipnik-Štangelj M

**Izhodišča.** Astrociti vzdržujejo homeostazo v osrednjem živčnem sistemu in so sorazmerno odporni na celično smrt. Disfunkcija mehanizmov, ki vodijo v smrt celice, je osnova za nastanek glioblastomov in njihove odpornosti na zdravljenje, zato je za oblikovanje učinkovitega zdravljenja potrebno natančno razumevanje načinov propadanja astrocitov. Namen dela je ugotoviti vpliv VAS2870, ki je pan-NADPH oksidazni inhibitor, na smrt astrocitov, povzročeno s stavrosporinom.

**Materiali in metode.** Astrocitne kulture novorojenih podgan smo izpostavili VAS2870 in/ali stavrosporinu, ki je povzročil celično smrt. S pomočjo pretočne citometrije smo določili živost celic, tvorbo reaktivnih kisikovih vrst (ROS) in mitohondrijski potencial. S pomočjo kemiluminiscence smo analizirali aktivnost kaspaze 3/7 ter količino celičnega ATP.

**Rezultati.** Ugotovili smo, da VAS2870 preprečuje s stavrosporinom sproženo celično smrt. Stavrosporin izvaja svoj strupen učinek s povečano proizvodnjo ROS, medtem ko VAS2870 njegov učinek zmanjša. Poleg tega VAS2870 delno obnovi mitohondrijski membranski potencial in količino ATP v celicah, izpostavljenih stavrosporinu.

**Zaključki.** Stavrosporin z oksidativnim stresom inducira celično smrt gojenih astrocitov. Tvorba ROS, mitohondrijski membranski potencial in energijsko stanje celice so občutljivi na VAS2870, kar nakazuje, da imajo NADPH oksidaze pomembno vlogo pri procesu celične smrti. Aktivacijska pot NADPH oksidaz bi zato lahko bila pomemben cilj za modulacijo smrti astrocitov.

Radiol Oncol 2019; 53(1): 77-84.  
doi: 10.2478/raon-2019-0008

## Nizka sprednja resekcija raka danke z implantacijo gentamicinske kolagenske gobice in brez razbremenilne stome. Puščanje anastomoze in lokalna ponovitev

Michalik T, Matkowski R, Biecek P, Forgacz J, Szynglarewicz B

**Izhodišča.** Sprednja resekcija s popolno mezorektalno ekscizijo pri zelo nizkem raku danke lahko povzroči povečano tveganje za anastomotično puščanje. Cilj raziskave je bil oceniti uporabnost gentamicinske kolagenske gobice za zaščito pred simptomatskim puščanjem anastomoze in raziskati povezavo med puščanjem anastomoze in lokalno ponovitvijo bolezni.

**Bolniki in metode.** Raziskali smo skupino 158 bolnikov z zelo nizkim rakom danke. Pri vseh bolnikih smo izvedli TME R0 s ščitjenjem sfinktra in zavijanjem anastomoze z gentamicinsko kolagensko gobico. V nobenem primeru ni bila narejena začasna zaščitna stoma.

**Rezultati.** Stopnja puščanja anastomoze je bila 3,2 % (5/158), srednji čas do diagnoze puščanja anastomoze pa je bil 5 dni po operaciji (razpon 3–15). Pooperativne in umrljivosti zaradi puščanja nismo zabeležili. Starost bolnika > 75 let in kajenje sta bila neodvisna dejavnika tveganja, povezana z znatno povečano stopnjo puščanja anastomoze: 12,5 % v primerjavi z 0,8 % ( $p = 0,0004$ ) oziroma 5,7 % v primerjavi z 0 % ( $p = 0,043$ ). Lokalno ponovitev bolezni smo ugotovili pri 12 % bolnikov. Ponovitev je bila izrazito pogostejša pri bolnikih s puščanjem anastomoze in je nastala prej kot v skupini brez anastomotičnega puščanja: 80 % proti 9 % ( $p = 0,00001$ ) in 8,5 proti 17 mesecev ( $p = 0,014$ ).

**Zaključki.** Zavijanje anastomoze z gentamicinsko kolagensko gobico po sprednji resekciji s mezorektalno ekscizijo je varen postopek, ki ima za posledico majhno incidenco anastomotičnega puščanja, ki je lahko povezana tudi z zmanjšanim tveganjem za lokalno ponovitev raka.

Radiol Oncol 2019; 53(1): 85-95.  
doi: 10.2478/raon-2019-0013

# Vpliv molekularnih označevalcev in histoloških parametrov na preživetje in odgovor na zdravljenje s prvim redom sistemske terapije pri bolnikih z metastatskim rakom debelega črevesa in danke

Reberšek M, Mesti T, Boc M, Ocvirk J

**Izhodišča.** Histološki parametri primarnega tumorja in bezgavčni status v regionalnih bezgavkah so napovedni dejavniki za preživetje bolnikov z operabilnim rakom debelega črevesa in danke. Nimajo pa napovednega pomena za odgovor na zdravljenje s sistemske terapijo. Mutacije v genu *KRAS* v kodonih 12 in 13 so prvi napovedni dejavnik za odpornost na zdravljenje z anti-EGFR monoklonalnimi protitelesi. Vsi bolniki z nemutiranim genom *KRAS* ne odgovorijo na zdravljenje z anti-EGFR monoklonalnimi protitelesi. Vzrok so lahko drugi mehanizmi odpornosti, ki lahko aktivirajo mutacije vzdolž signalne poti EGFR, kot so druge mutacije v genu *RAS*, mutacije v *PK13*, povečana ekspresija *PTEN*.

**Bolniki in metode.** Namen prospektivne raziskave je bil določiti vpliv histoloških parametrov primarnega tumorja in mutacij v genu *KRAS* in *BRAF* na celokupno preživetje bolnikov po prvem razsoju adenokarcinoma debelega črevesa in danke ter objektivni odgovor na zdravljenje s prvim redom sistemske terapije. Retrospektivno pa ugotoviti še vpliv drugih mutacij, kot so mutacije v genu *NRAS* in mutacije v kodonu 61 in 146 gena *KRAS*.

**Rezultati.** V raziskavo smo med novembrom 2010 in decembrom 2012 vključili 154 bolnikov, 95 moških in 59 žensk. Pri 42 % bolnikov smo ugotovili mutacijo v genu *KRAS*, pogosteje v kodonu 12 (73 %); mutacijo v genu *BRAF* pa smo ugotovili pri 3 % vseh bolnikov. Srednje preživetje bolnikov s primarnim tumorjem T1, T2 in T3 je bilo 65,4 (55,7–75,6) mesecev; pri bolnikih s primarnim tumorjem T4, karcinomsko limfangiozo, vaskularno in perinevralno invazijo pa še ni bilo doseženo. Srednje preživetje bolnikov s stopnjo diferenciacije tumorja 1 in 2 je bilo 65,6 (53,7–77,5) mesecev, pri bolnikih s stopnjo diferenciacije tumorja 3 pa 25,3 mesecev (16,6–34,1);  $p = 0,06$ . Srednje preživetje bolnikov s statusom N0 in N1 je bilo 65,6 (56,4–74,8) mesecev, pri bolnikih z N2 pa 58,0 (21,9–94,2) mesecev, razlika je bila statistično značilna ( $p = 0,000$ ). Srednje preživetje pri bolnikih z nemutiranim genom *KRAS* je bilo 56,5 (48,2–64,9) mesecev, pri bolnikih z mutiranim genom *KRAS* pa 58 (52,6–63,4) mesecev;  $p = 0,47$ . Pri bolnikih z mutacijo v kodonu 12 je bilo srednje preživetje 57 (50,9–64,4) mesecev, pri bolnikih z mutacijo v kodonu 13 pa 44 (40,1–48,4) mesecev;  $p = 0,40$ . Srednje preživetje bolnikov brez mutacije v genu *BRAF* je bilo 59,2 (52,5–65,9) mesecev, pri bolnikih z mutiranim genom *BRAF* pa 27,6 (12,6–42,5) mesecev, razlika je bila značilno pomembna ( $p = 0,05$ ). Samo nemutiran gen *KRAS* je značilno vplival na odgovor na prvi red sistemske terapije ( $p = 0,028$ ), drugi analizirani parametri pa ne ( $p = 0,07$ ). Od 85 bolnikov s *KRAS* in *BRAF* nemutiranim genom je 14 bolnikov imelo še prisotne mutacije v genu *NRAS* ter kodonu 61 in 146 gena *KRAS*. Srednje preživetje bolnikov brez prisotne mutacije v genih *KRAS*, *NRAS* in *BRAF* je bilo 67,1 (50,3–67,6) mesecev, pri bolnikih s prisotno mutacijo v genu *NRAS*, kodonu 61 in kodonu 146 gena *KRAS* pa še ni bilo doseženo ( $p = 0,072$ ). Srednji čas do ponovitve bolezni pri bolnikih brez prisotnih mutacij v genih *KRAS*, *NRAS* in *BRAF* je bilo 11,7 (10,4–14,5) mesecev, pri bolnikih s prisotno mutacijo v genu *NRAS*, kodonu 61 in kodonu 146 gena *KRAS* pa 7,9 (6,1–11,0) mesecev; ( $p = 0,025$ ).

**Zaključki.** Mutacije v genu *BRAF*, status N2 (več kot tri metastatske regionalne bezgavke) in stopnja diferenciacije 3 (slabo diferenciran adenokarcinom) so slabi napovedni dejavniki za celokupno preživetje bolnikov z metastatskim rakom debelega črevesa in danke. Mutacije v genih *KRAS* in *NRAS* imajo napovedno vrednost za odgovor na zdravljenje z zaviralci EGFR, nimajo pa napovedne vrednosti za preživetje bolnikov z metastatskim rakom debelega črevesa in danke. Histološki parametri, vključeni v analizo, in mutacije v genu *BRAF* nimajo napovednega pomena na učinkovitost odgovora na prvi red sistemskega zdravljenja teh bolnikov.

Radiol Oncol 2019; 53(1): 96-104.

doi: 10.2478/raon-2019-0009

## Genetski polimorfizmi akvaporina 1 kot dejavniki tveganja za maligni mezoteliom in označevalci odgovora na zdravljenje s cisplatinom

Šenk B, Goričar K, Kovač V, Dolžan V, Franko A

**Izhodišča.** Maligni mezoteliom (MM) je agresiven tumor, ki je povezan z azbestom in ima slabo napoved poteka bolezni. Namen raziskave je bil raziskati, ali genetski polimorfizmi akvaporina 1 (AQP1) vplivajo na tveganje za nastanek MM in na odgovor na zdravljenje, ki je temeljilo na cisplatinu.

**Bolniki in metode.** Raziskava primerov s kontrolami je zajela 231 bolnikov z MM in kontrolno skupino 316 zdravih krvodajalcev. S postopki genotipizacije smo vsem preiskovancem določili genotip za tri polimorfizme AQP1 (rs1049305, rs1476597 in rs28362731). V statistični analizi smo uporabili logistično in Coxovo regresijo.

**Rezultati.** Polimorfizem AQP1 rs1049305 je statistično značilno vplival na tveganje za MM v dominantnem modelu, prilagojeno za spol in starost (RO = 0,60; 95 % IZ = 0,37–0,96;  $P_{\text{adj}}$  = 0,033). Ta polimorfizem je v dominantnem modelu statistično značilno vplival tudi na nastanek anemije (neprilagojeno: RO = 0,49; 95 % IZ = 0,27–0,90; P = 0,021; prilagojeno za CRP: RO = 0,52; 95 % IZ = 0,27–0,99; P = 0,046) in levkopenije (RO = 2,09; 95 % IZ = 1,00–4,35; P = 0,049). V aditivnem modelu je bil ta polimorfizem povezan tudi z nastankom trombocitopenije (RO = 3,06; 95 % IZ = 1,01–9,28; P = 0,048) in alopecije (RO = 2,92; 95 % IZ = 1,00–8,46; P = 0,049). AQP1 rs28362731 je bil statistično značilno povezan s trombocitopenijo (neprilagojeno: RO = 3,73; 95 % IZ = 1,00–13,84; P = 0,049; prilagojeno za bolečino: RO = 4,63; 95 % IZ = 1,13–19,05; P = 0,034) v aditivnem modelu.

**Zaključki.** AQP1 lahko igra vlogo pri tveganju za MM. Poleg tega bi lahko informacije o genotipu AQP1 izboljšale napoved poteka bolezni pri bolnikih z MM, ki imajo večje tveganje za toksičnost cisplatinu.

Radiol Oncol 2019; 53(1): 105-115.

doi: 10.2478/raon-2019-0003

## Pomen osteopontina pri obravnavi epitelnega raka jajčnikov

Černe K, Hadžialjević B, Škof E, Verdenik I, Kobal B

**Izhodišča.** Osteopontin (sOPN) je obetaven tumorski označevalec za diagnostiko epiteljskega raka jajčnikov, medtem ko njegov pomen pri napovedi poteka bolezni in izbiri načina zdravljenja še ni bil proučen. Ker koncentracije sOPN v serumu in ascitesu niso medsebojno povezane, smo ločeno proučevali klinično uporabnost sOPN v obeh telesnih tekočinah.

**Bolnice in metode.** V raziskavo smo vključili 31 bolnic z napredovalim epiteljskim rakom jajčnikov in 34 preiskovank z benigno ginekološko patologijo. Bolnicam smo odvzeli vzorec seruma predoperativno, po primarni citoreduktivni operaciji in po kemoterapiji. Preiskovankam smo odvzeli vzorec seruma pred in po operaciji. Ascites in peritonealno tekočino smo pridobili med operacijo. Koncentracije sOPN smo izmerili s pretočno citometrijo na osnovi fluorescentnih kroglic.

**Rezultati.** Občutljivost in specifičnost sOPN sta bili 91,2 % in 90,3 % pri mejni vrednosti 47,4 ng/ml za serum ter 96,8 % in 100 % pri mejni vrednosti 529,5 ng/ml za ascites. Kaplan-Meierjeva analiza je pokazala statistično značilno povezovalno med višjo serumsko koncentracijo sOPN in krajšim skupnim preživetjem ( $p = 0,018$ ) ter krajšim časom do ponovitve bolezni ( $p = 0,008$ ). Višje koncentracije sOPN v ascitesu so bile povezane s suboptimalno resekcijo tumorja in inoperabilnim tumorjem. Višje serumske koncentracije sOPN so bile povezane s refraktarno boleznijo in nepopolnim odzivom na kemoterapijo s platinovimi spojinami.

**Zaključki.** Raziskava je pokazala, da ascites kot lokalna tekočina natančneje odraža trenutno stanje bolezni in je zato sOPN v ascitesu boljši za diagnostiko in načrtovanje kirurškega zdravljenja. Nenezadnje je končni izid zdravljenja odziv celotnega telesa na bolezen, zato je pri oceni napovedi poteka bolezni imel večjo moč serumski sOPN. ver

Radiol Oncol 2019; 53(1): 116-122.  
doi: 10.2478/raon-2019-0011

## Podobna stopnja stranskih pojavov termalne ablacije ter ireverzibilne elektroporacije pri bolnikih z rakom jetrnih celic

Verloh N, Jensch I, Lürken L, Haimerl M, Dollinger M, Renner P, Wiggermann P, Werner JM, Zeman F, Stroszczyński C, Beyer LP

**Izhodišča.** Namen raziskave je bil primerjati stranske pojave termalne mikrovalovne ablacije (MWA) in radiofrekvenčne ablacije (RFA) z ireverzibilno elektroporacijo (IRE) pri perkutanem zdravljenju raka jetrnih celic (HCC).

**Bolniki in metode.** Retrospektivno smo analizirali 117 MWA/RFA in 47 IRE postopkov (en tumor na postopek, 144 moških in 20 žensk; srednje starosti 66 let). Analizirali smo stranske pojave, dolžino hospitalizacije in bivanje v enoti intenzivne terapije ter pojavnost post-ablacijskega sindroma. Stranske pojave smo klasificirali po sistemu Clavien & Dindo.

**Rezultati.** Brez komplikacij smo izvedli 70.1 % postopkov RFA/MWA in 63.8% postopkov IRE. Komplikacije 1. in 2. stopnje (vsakršno odstopanje od standardnih postopkov zdravljenja, kot na primer zdravljenje z analgetiki) so se pojavile v 26,5 % (31/117) pri MWA/RFA in 34,0 % (16/47) po IRE. Resne komplikacije, to je 3. in 4. stopnje, so se pojavile v 2,6 % (3/117) pri MWA/RFA in 2,1 % (1/47) pri IRE. Ni bilo statistično značilnih razlik ( $p = 0.864$ ) med skupinama bolnikov pri dolžini hospitalizacij in bivanju v enoti intenzivne terapije ter pri pojavu post-ablacijskega sindroma.

**Zaključki.** Rezultati nakazujejo na primerljivo stopnjo komplikacij med skupino bolnikov, ki so imeli MWA/RFA ali IRE, kljub temu da pri IRE naredimo večje število vbodov in ne kauteriziramo trajektorij pri izvleku igle.

Radiol Oncol 2019; 53(1): 123-130.  
doi: 10.2478/raon-2019-0001

## Pospešeno delno obsevanje dojke s teleradioterapijo. Dozimetrična ocena konformalne tehnike in treh različnih intenzitetno modulirajočih tehnik

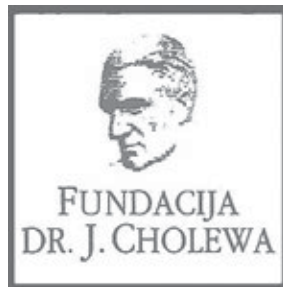
Stelczer G, Major T, Mészáros N, Polgár C, Pesznyák C

**Izhodišča.** Namen raziskave je bil oceniti in primerjati štiri različne teleradioterapevtske tehnike pospešenega delnega obsevanja dojke (*angl. accelerated partial breast irradiation*, APBI), upoštevajoč pokritost tarče, dozo na kritične organe in celokupno kakovost načrta obsevanja. Preučevane tehnike so bile tridimenzionalna konformna radioterapija (3D-CRT), tehniki »ustavi in proži« (*angl. step and shoot*, SS) in »drsečega okna« (*angl. sliding window*, SW) intenzitetno modulirane radioterapije (IMRT) in intenzitetno modulirana ločna terapija (*angl. rapid arc*, RA).

**Bolniki in metode.** Za potrebe raziskave smo izbrali posnetke 40 bolnic z APBI. Cilje načrtovanja obsevanja smo zastavili v skladu z mednarodnimi priporočili. Homogenost, konformnost in kazalce kakovosti obsevalnega načrta smo izračunali iz volumetričnih in dozimetričnih dejavnikov tarčnih volumnov in kritičnih organov. Preučevali smo tudi celokupno število monitorskih enot in izvedljivost.

**Rezultati.** Med tehnikami ni bilo statistično značilnih razlik v pokritosti tarčnega volumna. Indeksi homogenosti načrtov 3D-CRT, SS, SW in RA so bili 0,068, 0,074, 0,058 in 0,081. Konformacijska števila so bila 0,60, 0,80, 0,82 in 0,89. Vrednosti V50 % istostranske dojke za 3D-CRT, SS, SW in RA so bile 47,5 %, 40,2 %, 39,9 % in 31,6 %. Povprečne vrednosti V10 % in V40 % za pljuča na isti strani so bile 13,1 %, 28,1 %, 28 % in 36 % oz. 2,6 %, 1,9 %, 1,9 % in 3 %. Najboljšo zaščito srca smo dosegli s tehniko 3D-CRT, še posebej v nizkodoznem področju. Vsi nasprotnostranski organi so prejeli nizke doze. Najboljši indeks kakovosti načrta obsevanja (*angl. plan quality index*, PQI) smo dosgli s tehniko SW.

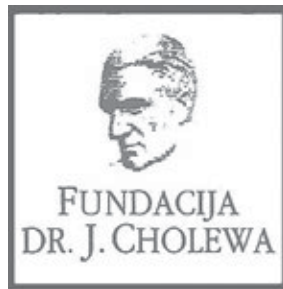
**Zaključki.** Z vsemi štirimi tehnikami dosežemo dobro pokritost tarčnega volumna in sprejemljive doze na kritične organe. Ko upoštevamo vse aspekte, za APBI priporočamo tehniko SW IMRT.



FUNDACIJA "DOCENT DR. J. CHOLEWA"  
JE NEPROFITNO, NEINSTITUCIONALNO IN NESTRANKARSKO  
ZDRUŽENJE POSAMEZNIKOV, USTANOV IN ORGANIZACIJ, KI ŽELIJO  
MATERIALNO SPODBUJATI IN POGLABLJATI RAZISKOVALNO  
DEJAVNOST V ONKOLOGIJI.

DUNAJSKA 106  
1000 LJUBLJANA

IBAN: SI56 0203 3001 7879 431



## Activity of "Dr. J. Cholewa" Foundation for Cancer Research and Education - a report for the first quarter of 2019

Doc. Dr. Josip Cholewa Foundation for cancer research and education continues with its planned activities in the first quarter of 2019 and is commencing to prepare for the activities the whole year. Its primary focus remains the provision of grants and scholarships and other forms of financial assistance for basic, clinical and public health research in the field of oncology. An analysis of the ongoing activities in the last year was made in order to make an assessment of the impact of Foundation's activities, thus providing a basis for developing new strategies and approaches in its scope of fight against cancer.

The Foundation continues to provide support for »Radiology and Oncology«, a quarterly scientific magazine with a respectable impact factor that publishes research and review articles about all aspects of cancer. The magazine is edited and published in Ljubljana, Slovenia. »Radiology and Oncology« is an open access journal available to everyone free of charge. Its long tradition represents a guarantee for the continuity of international exchange of ideas and research results in the field of oncology for all in Slovenia that are interested and involved in helping people affected by many different aspects of cancer.

The Foundation makes great efforts to provide financial and other kinds of support for the organisation of various forms of meetings to extend and broaden the knowledge about prevention of cancer, early detection of various types of cancer, its treatment and rehabilitation of cancer patients. The advances in knowledge of all aspects of dealing with cancer should be in Foundation's opinion available to all the professionals that treat cancer patients, to the patients themselves and their closest relatives and friends, and finally also to the general public.

The problems associated with cancer affect more and more people and their relatives in Slovenia and elsewhere. The Foundation will therefore continue with its activities in the years to come. Treatment of cancer is ever more successful with many patients surviving decades after the start of their treatment and many new problems and challenges have thus come into place. Longer survival of an increasing number of patients with previously incurable cancer conditions adds many new dimensions to their life and to the life of their families. It also confronts cancer specialists, all the other experts and lay public dealing with cancer with new challenges and new goals to achieve.

Borut Štabuc, M.D., Ph.D.  
Tomaž Benulič, M.D.  
Andrej Plesničar, M.D., M.Sc.  
Viljem Kovač M.D., Ph.D.



# ENA SAMA 30-MINUTNA INFUZIJA ZAGOTOVI CELOVITO ZDRAVLJENJE ABSSSI<sup>1</sup>

## Enostavno odmerjanje

Odrasli pacienti z ABSSSI: 1500 mg z enkratnim infundiranjem ali 1000 mg prvi teden, naslednji teden pa 500 mg.

# Xydalba<sup>TM</sup>

dalbavancin



**Xydalba**  
(dalbavancin)



30-minutna i.v. infuzija



**Xydalba**  
(dalbavancin)



en teden kasneje  
30-minutna i.v. infuzija



30-minutna i.v. infuzija



### SKRAJŠAN POVZETEK GLAVNIH ZNAČILNOSTI ZDRAVILA

Xydalba<sup>TM</sup> 500 mg prašek za koncentrat za raztopino za infundiranje

▼ Za to zdravilo se izvaja dodatno spremljanje varnosti. Tako bodo hitreje na voljo nove informacije o njegovi varnosti. Zdravstvene delavce naprošamo, da poročajo o katerem koli domnevnem neželenem učinku zdravila. Sestava: Ena viala vsebuje dalbavancinjev klorid, kar ustreza 500 mg dalbavancina. Po rekonstituciji en ml vsebuje 20 mg dalbavancina. Razredčena raztopina za infundiranje mora imeti končno koncentracijo od 1 do 5 mg/ml dalbavancina. **Terapevtske indikacije:** Zdravilo Xydalba je indicirano za zdravljenje akutnih bakterijskih okužb kože in kožnih struktur (ABSSSI – acute bacterial skin and skin structure infections) pri odraslih. Pozornost je treba nameniti uradnim navodilom o ustrezni uporabi protibakterijskih zdravil. **Odmerjanje in način uporabe: Odmerjanje:** Priporočeni odmerek in trajanje zdravljenja pri odraslih: Priporočeni odmerek dalbavancina pri odraslih pacientih z ABSSSI je 1500 mg z enkratnim infundiranjem 1500 mg ali 1000 mg prvi teden, naslednji teden pa 500 mg. **Starejše osebe:** Prilagoditev odmerka ni potrebna. **Okvara delovanja ledvic:** Pri pacientih z blago ali zmerno okvaro delovanja ledvic prilagoditve odmerka niso potrebne (kreatininski očistek je < 30 do 79 ml/min). Pri pacientih, ki redno prejemajo hemodializo (3-krat tedensko), prilagoditve odmerka niso potrebne, dalbavancin se lahko uporablja ne glede na čas hemodialize. Pri pacientih s kronično okvaro delovanja ledvic, katerih kreatininski očistek je < 30 ml/min in ki ne prejemajo redno hemodialize, je priporočen odmerek dalbavancina zmanjšan na 1000 mg z enkratnim infundiranjem ali 750 mg, ki mu sledi 375 mg v naslednjem tednu. **Okvara delovanja jeter:** Pri pacientih z blago okvaro delovanja jeter (Child–Pugh A) prilagoditev odmerka dalbavancina ni potrebna. Previdnost je potrebna pri predpisovanju dalbavancina pacientom z zmerno ali hudo okvaro delovanja jeter (Child–Pugh B & C), ker ni ustreznih podatkov za določitev primerne odmerjanja. **Otroci:** Varnost in učinkovitost dalbavancina pri otrocih v starosti od rojstva do < 18 let še nista ugotovljeni. Priporočila o odmerjanju ne moremo podati. **Način uporabe:** Zdravilo Xydalba mora biti rekonstituirano in potem še razredčeno pred dajanjem intravenske infuzije, ki traja 30 minut. **Kontraindikacije:** Preobčutljivost na učinkovino ali katerokoli pomožno snov. **Posebna opozorila in previdnostni ukrepi:** Preobčutljivostne reakcije: Posebej pazljivo se mora zdravilo Xydalba uporabljati pri pacientih, za katere je znano, da so preobčutljivi na druge glikopeptide, saj se lahko pojavi navzkrižna preobčutljivost. Če se pojavi alergijska reakcija na zdravilo Xydalba, je treba njegovo uporabo prekiniti in uvesti ustrezno terapijo za alergijsko reakcijo. **Driska zaradi bakterije Clostridium difficile:** Kolitis, povezan s protibakterijskimi zdravili, in psevdomembranski kolitis sta bila zabeležena pri uporabi skoraj vseh antibiotikov in sta lahko blaga pa vse do smrtno ogrožajoča. Zato je pri pacientih z drisko med ali po zdravljenju z dalbavancinom pomembno upoštevati tudi to diagnozo. V takšnih okoliščinah je treba razmisliti o prekinitvi zdravljenja z dalbavancinom in uvesti podpirne ukrepe skupaj z jemanjem posebnega zdravila proti bakteriji Clostridium difficile. Takih pacientov nikoli ne smemo zdraviti z zdravili, ki zavirajo peristaltiko. **Reakcije, povezane z infuzijo:** Zdravilo Xydalba se uporablja z intravenskim infundiranjem, ki traja skupaj 30 minut, da se zmanjša tveganje za z infuzijo povezano reakcijo. Hitre intravenske infuzije glikopeptidnih protibakterijskih zdravil lahko povzročijo reakcijo, ki je podobna "sindromu rdečeličneža", z rdečico na zgornjem delu telesa, z urtikarijo, prurituisom in/ali izpuščajem. S prekinitvijo ali upočasnitvijo infundiranja lahko te reakcije izginejo. **Okvara delovanja ledvic:** Podatki o učinkovitosti in varnosti dalbavancina pri pacientih s kreatininskim očistkom, manjšim od 30 ml/min, so omejeni. Na podlagi simulacij je prilagoditev odmerjanja potrebna pri pacientih s kronično okvaro delovanja ledvic, katerih kreatininski očistek je manjši od 30 ml/min in ki redno ne prejemajo hemodialize. **Mešana okužba:** Pri mešanih okužbah, kjer obstaja sum na Gram–negativne bakterije, se morajo pacienti zdraviti tudi z ustreznimi protibakterijskimi zdravili oz. zdravili, proti Gram–negativnim bakterijam. **Neobčutljivi organizmi:** Uporaba antibiotikov lahko pospeši prekomerno rast neobčutljivih mikroorganizmov. Če pride med zdravljenjem do superfekcije, je treba ustrezno ukrepati. **Omejitve kliničnih podatkov:** Podatki o varnosti in učinkovitosti dalbavancina pri uporabi več kot dveh odmerkov (v razmiku enega tedna) so omejeni. V večjih preskušanjih pri ABSSSI so bile vrste zdravljenih infekcij omejene samo na celulitis/sen, abscese in okužbe ran. Izkušnje z dalbavancinom pri zdravljenju pacientov s hudo oslabljenim imunskim sistemom ni. **Medsebojno delovanje z drugimi zdravili in druge oblike interakcij:** Dalbavancin se ne presnavlja z encimi CYP in vitro, zato sočasni CYP induktorji ali inhibitorji malo verjetno vplivajo na farmakokinetiko dalbavancina. Ni znano, ali je dalbavancin substrat za prenašalce jetrnega prvizema in efliksa. Uporaba skupaj z inhibitorji teh prenašalcev lahko poveča izpostavljenost dalbavancinu. Primeri takšnih inhibitorjev prenašalcev so okrepjeni inhibitorji proteaze, verapamil, kinidin, itrakonazol, klaritromicin in ciklosporin. Pričakovana je majhna verjetnost interakcije dalbavancina z zdravili, ki se presnavljajo z encimi CYP, saj ni niti inhibitor niti induktor encimov CYP in vitro. Podatki o dalbavancinu kot inhibitorju CYP2C8 niso na voljo. Ni znano, ali je dalbavancin inhibitor prenašalcev. Povečane izpostavljenosti substratom prenašalcev, občutljivim na inhibicijo aktivnosti prenašalcev, kot so statini in digoksin, ni mogoče izključiti, če so kombinirani z dalbavancinom. **Plođnost, nosečnost in dojenje:** Nosečnost: O uporabi dalbavancina pri nosečnicah ni podatkov. Studije na živalih so pokazale vpliv na sposobnost razmnoževanja. Uporaba zdravila Xydalba med nosečnostjo ni priporočljiva, razen kadar je to nujno. **Dojenje:** Ni znano, ali se dalbavancin izloča v mleko pri človeku. Potrebno je sprejeti odločitev o nadaljevanju/prekinitvi dojenja ali o nadaljevanju/prekinitvi zdravljenja z zdravilom Xydalba, pri tem pa pretehtati koristi dojenja za otroka in koristi zdravljenja za doječo žensko. **Plođnost:** Studije na živalih so pokazale zmanjšano plođnost. Potencialno tveganje za ljudi ni znano. **Vpliv na sposobnost vožnje in upravljanja s strojevi:** Zdravilo Xydalba ima lahko blag vpliv na sposobnost vožnje in upravljanja s strojevi, pri majhnem številu pacientov so namreč zabeležili omotico. **Neželeni učinki:** Pogosti: glavobol, navzea, driska. **Občasni:** vulvovaginalna glivična okužba, okužba sečil, glivična okužba, kolitis zaradi razrasta Clostridium difficile, oralna kandidiaza, anemija, trombocitopenija, nevtropenija, zmanjšan apetit, insomnija, dizgevizija, omotica, vročinski oblivi, flebitis, kašelj, zaprtost, bolečine v trebuhu, dispepsija, neprijeten občutek v trebuhu, bruhanje, pruritus, urtikarija, izpuščaji, vulvovaginalni pruritus, z infuzijo povezana reakcija, zvišana laktat–dehidrogenaza v krvi, zvišana alanin–aminotransferaza, zvišana aspartat–aminotransferaza, zvišana raven sečne kisline v krvi, neobičajni rezultati testne jetrne funkcije, zvišane vrednosti transaminaz, zvišane vrednosti alkalne fosfataze v krvi, povečano število krvnih ploščic, zvišana telesna temperatura, zvišana raven jetrnih encimov, zvišane vrednosti gama–glutamil transferaze. **Redki:** anafilaktoidna reakcija, bronhospazem. **Način in režim predpisovanja in izdaje:** H – Zdravilo se izdaja le na recept, uporablja pa se samo v bolnišnicah. **Imetnik dovoljenja za promet:** Allergan Pharmaceuticals International Ltd., Clonsburgh Industrial Estate, Coolock, Dublin 17, Irsko. **Data zadnje revizije besedila:** 14. december 2018. **Lokalni predstavnik:** Angelini Pharma d.o.o., Koprška ulica 108 A, Ljubljana.

Pred predpisovanjem se seznanite s celotnim Povzetkom glavnih značilnosti zdravila.

Samo za strokovno javnost.

Datum priprave informacije: 12. februar 2019

Vir:

1. Xydalba<sup>TM</sup> (dalbavancin), Povzetek glavnih značilnosti zdravila





# Moj čas je dragocen

## Potrebujem dober načrt

### Skrajšan povzetek glavnih značilnosti zdravila

▼ Za to zdravilo se izvaja dodatno spremljanje varnosti. Tako bodo hitreje na voljo nove informacije o njegovi varnosti. Zdravstvene delavce naprošamo, da poročajo o katerem koli domnevnem neželenem učinku zdravila.

**Cyramza 10 mg/ml koncentrat za raztopino za infundiranje** En mililiter koncentrata za raztopino za infundiranje vsebuje 10 mg ramucirumaba. Ena 10-mililitrska viala vsebuje 100 mg ramucirumaba. **Terapevtske indikacije** Zdravilo Cyramza je v kombinaciji s paklitakselom indicirano za zdravljenje odraslih bolnikov z napredovalim rakom želodca ali adenokarcinomom gastro-efozagealnega prehoda z napredovalo boleznijo po predhodni kemoterapiji, ki je vključevala platino in fluoropirimidin. Monoterapija z zdravilom Cyramza je indicirana za zdravljenje odraslih bolnikov z napredovalim rakom želodca ali adenokarcinomom gastro-efozagealnega prehoda z napredovalo boleznijo po predhodni kemoterapiji s platino ali fluoropirimidinom, za katere zdravljenje v kombinaciji s paklitakselom ni primerno. Zdravilo Cyramza je v kombinaciji s shemo FOLFIRI indicirano za zdravljenje odraslih bolnikov z metastatskim kolorektalnim rakom (mCRC), z napredovanjem bolezni ob ali po predhodnem zdravljenju z bevacizumabom, oksaliplatinom in fluoropirimidinom. Zdravilo Cyramza je v kombinaciji z docetakselom indicirano za zdravljenje odraslih bolnikov z lokalno napredovalim ali metastatskim nedrobnoceličnim pljučnim rakom, z napredovanjem bolezni po kemoterapiji na osnovi platine. **Odmerjanje in način uporabe** Zdravljenje z ramucirumabom morajo uvesti in nadzirati zdravniki z izkušnjami v onkologiji. **Odmerjanje Rak želodca in adenokarcinomom gastro-efozagealnega prehoda** Priporočeni odmerek ramucirumaba je 8 mg/kg 1. in 15. dan 28-dnevnega cikla, pred infuzijo paklitaksela. Priporočeni odmerek paklitaksela je 80 mg/m<sup>2</sup> in se daje z intravenskim infundiranjem, ki traja približno 60 minut, 1., 8. in 15. dan 28-dnevnega cikla. Pred vsakim infundiranjem paklitaksela je treba pri bolnikih pregledati celotno krvno sliko in izvide kemičnih preiskav krvi, da se oceni delovanje jeter. Priporočeni odmerek ramucirumaba kot monoterapije je 8 mg/kg vsaka 2 tedna. **Kolorektalni rak** Priporočeni odmerek ramucirumaba je 8 mg/kg vsaka 2 tedna, dan z intravensko infuzijo pred dajanjem sheme FOLFIRI. Pred kemoterapijo je treba bolnikom odvzeti kri za popolno krvno sliko. **Nedrobnocelični pljučni rak (NSCLC)** Priporočeni odmerek ramucirumaba je 10 mg/kg na 1. dan 21-dnevnega cikla, pred infuzijo docetaksela. Priporočeni odmerek docetaksela je 75 mg/m<sup>2</sup>, dan z intravensko infuzijo v približno 60 minutah na 1. dan 21-dnevnega cikla. **Premedikacija** Pred infundiranjem ramucirumaba je priporočljiva premedikacija z antagonistom histaminskih receptorjev H1. **Način uporabe** Po redčenju se zdravilo Cyramza daje kot intravenska infuzija v približno 60 minutah. Zdravila ne dajate v obliki intravenskega bolusa ali hitre intravenske injekcije. Da boste dosegli zahtevano trajanje infundiranja približno 60 minut, največja hitrost infundiranja ne sme preseči 25 mg/minuto, saj morate sicer podaljšati trajanje infundiranja. Bolnika je med infundiranjem treba spremljati glede znakov reakcij, povezanih z infuzijo, zagotoviti pa je treba tudi razpoložljivost ustrezne opreme za oživiljanje. **Kontraindikacije** Pri bolnikih z NSCLC je ramucirumab kontraindiciran, kjer gre za kavitacijo tumorja ali prepletenost tumorja z glavnimi žilami. **Posebna opozorila in previdnostni ukrepi** Trajno prekinite zdravljenje z ramucirumabom pri bolnikih, pri katerih se pojavijo resni arterijski tromboembolični dogodki, gastrointestinalne perforacije, krvavitve stopnje 3 ali 4, če zdravstveno pomembne hipertenzije ni mogoče nadzirati z antihipertenzivnim zdravljenjem ali če se pojavi fistula, raven beljakovin v urinu > 3 g/24 ur ali v primeru nefrotskega sindroma. Pri bolnikih z neuravnano hipertenzijo zdravljenja z ramucirumabom ne smete uvesti, dokler oziroma v kolikor obstoječa hipertenzija ni uravnana. Pri bolnikih s ploščatocelično histologijo obstaja večje tveganje za razvoj resnih pljučnih krvavitve. Če se pri bolniku med zdravljenjem razvijejo zapleti v zvezi s celjenjem rane, prekinite zdravljenje z ramucirumabom, dokler rana ni povsem zaceljena. V primeru pojava stomatitis je treba takoj uvesti simptomatsko zdravljenje. Pri bolnikih, ki so prejeli ramucirumab in docetaksel za zdravljenje napredovalnega NSCLC z napredovanjem bolezni po kemoterapiji na osnovi platine, so opazili trend manjše učinkovitosti z naraščajočo starostjo. **Medsebojno delovanje z drugimi zdravili in druge oblike interakcij** Med ramucirumabom in paklitakselom niso opazili medsebojnega delovanja. Na farmakokinetiko irinotekana in njegovega aktivnega presnovka, SN 38, sočasno dajanje ramucirumaba ni vplivalo. Na farmakokinetiko docetaksela sočasno dajanje ramucirumaba ni vplivalo. **Plodnost, nosečnost in dojenje** Ženskam v rodni dobi je treba svetovati, naj se izogibajo zanositvi med zdravljenjem z zdravilom Cyramza in o možnosti nosečnosti z možnim tveganjem za nosečnost in plod. Ni znano, ali se ramucirumab izloča v materino mleko. **Neželeni učinki Zelo pogosti (≥ 1/10)** nevtropenija, levkopenija, trombocitopenija, hipokaliemija, hiponatriemija, hipertenzija, epistaksa, gastrointestinalne krvavitve, stomatitis, driska, proteinurija, utrujenost/astenija, periferni edem, bolečina v trebuhu. **Pogosti (≥ 1/100 do < 1/10)** hipokaliemija, hiponatriemija, glavobol. **Rok uporabnosti** 3 leta **Posebna navodila za shranjevanje** Shranjujte v hladilniku (2 °C–8 °C). Ne zamrzujte. Vialo shranjujte v zunanji ovojnini, da zagotovite zaščito pred svetlobo. **Pakiranje** 2 viali z 10 ml **IMETNIK DOVOLJENJA ZA PROMET Z ZDRAVILOM** Eli Lilly Nederland B.V., Papendorpseweg 83, 3528 BJ Utrecht, Nizozemska **DATUM ZADNJE REVIZIJE BESEDILA** 20.09.2018 Režim izdaje: Predpisovanje in izdaja zdravila je le na recept, zdravilo pa se uporablja samo v bolnišnicah. Pred predpisovanjem zdravila natančno preberite celoten povzetek glavnih značilnosti zdravila.

### Pomembno obvestilo:

Pričujoče gradivo je namenjeno **samo za strokovno javnost**. Zdravilo Cyramza se predpisuje in izdaja le na recept, zdravilo pa se uporablja samo v bolnišnicah. Pred predpisovanjem zdravila Cyramza vas v ljudo prosimo, da preberete celotni Povzetek glavnih značilnosti zdravila Cyramza. Podrobnejše informacije o zdravilu Cyramza in o zadnji reviziji besedila Povzetka glavnih značilnosti zdravila so na voljo na sedežu podjetja Eli Lilly (naslov podjetja in kontaktni podatki spodaj) in na spletni strani European Medicines Agency (EMA): [www.ema.europa.eu](http://www.ema.europa.eu), in na spletni strani European Commission <http://ec.europa.eu/health/documents/community-register/html/alfregister.htm>.

Eli Lilly farmacevtska družba, d. o. o., Dunajska cesta 167, 1000 Ljubljana,  
telefon: (01) 5800 010, faksa: (01) 5691 705.

PP-RB-SI-0020, 19.11.2018

**CYRAMZA**<sup>®</sup>  
(ramucirumab)

# PODALJŠAJTE JI PREŽIVETJE<sup>1</sup>



DVOJNA BLOKADA HER2

Literatura:

1. Povzetek glavnih značilnosti zdravila Perjeta, dostopano maja 2018 na [http://www.ema.europa.eu/docs/sl\\_SI/document\\_library/EPAR\\_-\\_Product\\_Information/human/002547/WC500140980.pdf](http://www.ema.europa.eu/docs/sl_SI/document_library/EPAR_-_Product_Information/human/002547/WC500140980.pdf)



# AKTIVIRA IMUNSKI SISTEM. PREPOZNA. REAGIRA.

**IMFINZI™**  
durvalumab  
50 mg/ml koncentrat za raztopino za infundiranje



## SKRAJŠAN POVZETEK GLAVNIH ZNAČILNOSTI ZDRAVILA

▼ Za to zdravilo se izvaja dodatno spremljanje varnosti. Tako bodo hitreje na voljo nove informacije o njegovi varnosti. Zdravstvene delavce naprošamo, da poročajo o katerem koli domnevnem neželenem učinku zdravila. Imfinzi 50 mg/ml koncentrat za raztopino za infundiranje

**SESTAVA:** 1 ml koncentrata za raztopino za infundiranje vsebuje 50 mg durvalumaba. Ena viala z 2,4 ml koncentrata vsebuje 120 mg durvalumaba. Ena viala z 10 ml koncentrata vsebuje 500 mg durvalumaba.

**INDIKACIJE:** Zdravilo Imfinzi je kot samostojno zdravljenje indicirano za zdravljenje lokalno napredovalega, neoperabilnega nedrobnoceličnega raka pljuč (NSCLC – "non small cell lung cancer") pri odraslih, ki imajo tumorje z  $\geq 1\%$  izraženošči PD-L1 na tumorskih celicah in pri katerih bolezen ni napredovala po kemoradioterapiji na osnovi platine.

**ODMERJANJE IN NAČIN UPORABE:** Zdravljenje mora uvesti in nadzorovati zdravnik, ki ima izkušnje na področju zdravljenja raka. Bolnike z lokalno napredovalim nedrobnoceličnim rakom pljuč je treba za zdravljenje izbrati na podlagi izraženošči PD-L1, ugotovljene z validirano testno metodo. Omerjanje: Priporočeni odmerek zdravila Imfinzi je 10 mg/kg v intravenski infuziji v 60 minutah vsaka 2 tedna do napredovanja bolezni ali nesprejemljive toksičnosti oziroma največ 12 mesecev. Pri klinično stabilnih bolnikih z začetnimi znaki napredovanja bolezni je priporočeno z zdravljenjem nadaljevati, dokler napredovanje bolezni ni potrjeno. Povečevanje ali zmanjševanje odmerka ni priporočljivo. Če se stanje ne izboljša ali se poslabša, pride v poštev povečanje odmerka kortikosteroidov in/ali dodatna uporaba sistemskih imunosupresivov. Po izboljšanju na  $\leq 1$ . stopnjo je treba začeti s postopnim zmanjševanjem kortikosteroida in ga zmanjševati v obdobju vsaj 1 meseca. Po odložitvi uporabe je mogoče zdravilo Imfinzi znova začeti uporabljati v času 12 tednov, če se neželeni učinki izboljšajo na  $\leq 1$ . stopnjo in je odmerek kortikosteroida zmanjšan na  $\leq 10$  mg prednizona ali ekvivalenta na dan. Če se imunsko pogojeni neželeni učinki 3. ali 4. stopnje (močno izraženi ali življenjsko nevarni) ponavljajo, je treba zdravilo Imfinzi dokončno ukiniti. Pri ne imunsko pogojenih neželenih učinkih velja v primeru 2. ali 3. stopnje izraženošči razmisli o odložitvi uporabe zdravila Imfinzi do izboljšanja neželenih učinkov na  $\leq 1$ . stopnjo ali na izhodiščno raven. Z uporabo zdravila Imfinzi je treba prenehati v primeru neželenih učinkov 4. stopnje (razen v primeru laboratorijskih nepravilnosti 4. stopnje, pri katerih naj odložitve o prekinitvi uporabe zdravila temelji na spremljajočih kliničnih znakih oziroma simptomih in na klinični presoji zdravnika).

Zdravilo Imfinzi je namenjeno za intravensko uporabo. Dati ga je treba kot raztopino za intravensko infundiranje v obdobju 60 minut.

**KONTRAINDIKACIJE:** Preobčutljivost na učinkovino (učinkovine) ali katero koli pomožno snov.

**OPOZORILO IN PREVIDNOSTNI UKREPI:** Za izboljšanje sledljivosti bioloških zdravil je treba jasno zabeležiti lastniško ime in številko serije uporabljenega zdravila. Imunsko pogojeni pnevmonitis: Pri bolnikih, ki so prejeli zdravilo Imfinzi, sta se pojavila imunsko pogojeni pnevmonitis ali intersticijska bolezen pljuč, opredeljeno kot potreba po uporabi sistemskih kortikosteroidov in brez jasne druge etiologije. Pri bolnikih, zdravljenih z radioterapijo pljuč, je pogost radiacijski pnevmonitis in radiacijskega pnevmonitisa je zelo podobna. V študiji PACIFIC sta se pri bolnikih, ki so opravili zdravljenje z najmanj 2 cikloma sočasne kemoradioterapije od 1 do 42 dni pred začetkom preizkušanja, pnevmonitis ali radiacijski pnevmonitis pojavila pri 161 (33,9 %) bolnikih v skupini z zdravilom Imfinzi in pri 58 (24,8 %) bolnikih v skupini s placebom, vključno s 3. stopnjo (3,4 % in 3,0 %) in 5. stopnjo (1,1 % in 1,7 %). Bolnike je treba spremljati glede znakov in simptomov pnevmonitisa ali radiacijskega pnevmonitisa. Imunsko pogojeni hepatitis: Pri bolnikih, ki so prejeli zdravilo Imfinzi, se je pojavila imunsko pogojeni hepatitis, opredeljen kot potreba po sistemskih kortikosteroidih in brez jasne druge etiologije. Imunsko pogojeni kolitis: Pri bolnikih, ki so prejeli zdravilo Imfinzi, sta se pojavila imunsko pogojeni kolitis ali driska, opredeljeno kot potreba po sistemskih kortikosteroidih in brez jasne druge etiologije. Imunsko pogojeni hipotiroizem in hipertiroizem: Pri bolnikih, ki so prejeli zdravilo Imfinzi, sta se pojavila imunsko pogojeni hipotiroizem (vključno s tiroditisom), hipertiroizem in hipotiroizem. Bolnike je treba spremljati glede nenormalnih izvidov delovanja ščitnice pred zdravljenjem in redno med zdravljenjem ter kot je potrebno glede na klinično oceno. Imunsko pogojeni hipotiroizem in hipertiroizem (vključno s tiroditisom) je treba obravnavati, in ukrepati, kot je priporočeno v povzetku glavnih značilnosti zdravila. Adrenalna insuficienca: Pri bolnikih, ki so prejeli zdravilo Imfinzi, se je pojavila imunsko pogojena adrenalna insuficienca. Bolnike je treba spremljati glede kliničnih znakov in simptomov adrenalne insuficienca. Sladkorna bolezen tipa 1: Pri bolnikih, ki so prejeli zdravilo Imfinzi, se je pojavila imunsko pogojena sladkorna bolezen tipa 1. Bolnike je treba spremljati glede kliničnih znakov in simptomov sladkorne bolezni tipa 1. Hipofizitis/hipopituitarizem: Pri bolnikih, ki so prejeli zdravilo Imfinzi, sta se pojavila imunsko pogojena hipofizitis ali hipopituitarizem. Bolnike je treba spremljati glede kliničnih znakov in simptomov hipofizitisa ali hipopituitarizma. Imunsko pogojeni nefritis: Pri bolnikih, ki so prejeli zdravilo Imfinzi, se je pojavil imunsko pogojeni nefritis, opredeljen kot potreba po sistemskih kortikosteroidih in brez jasne druge etiologije. Pri bolnikih, ki so bili zdravljeni z zaviralci PD-1, so poročali o pojavljanju Stevens Johnsonovega sindroma ali toksične epidermalne nekroze. Drugi imunsko pogojeni neželeni učinki: Glede na mehanizem delovanja zdravila Imfinzi se lahko pojavijo še drugi potencialno imunski pogojeni učinki. Naslednji imunski neželeni učinki so bili zabeleženi v kliničnih preizkušanjih (n = 1889) pri manj kot 1 % bolnikov, ki so prejeli samostojno zdravljenje z zdravilom Imfinzi: miokarditis, miozitis, polimiozitis. V programu kliničnih študij so pri bolnikih poročali o primerih pankreatitisa. Bolnike je treba spremljati glede znakov in simptomov in ukrepati, kot je priporočeno za imunske pogojene neželene učinke. Z infundiranjem povezane reakcije: Bolnike je treba spremljati glede znakov in simptomov z infundiranjem povezanih reakcij. Pri bolnikih, ki so prejeli zdravilo Imfinzi, so bile opisane hude z infundiranjem povezane reakcije. Bolniki, ki niso bili vključeni v klinična preizkušanja: V študiji PACIFIC niso bili vključeni bolniki z naslednjimi značilnostmi: izhodiščno oceno zmogljivosti ECOG  $\geq 2$ ; aktivno ali predhodno dokumentirano avtoimunsko bolezenje v 2 letih pred začetkom študije; anamnezo imunske pomanjkljivosti; anamnezo hudih imunsko pogojenih neželenih učinkov, boleznih, ki so zahtevale sistemsko imunosupresijo, razen fiziološkega odmerka sistemskih kortikosteroidov ( $\leq 10$  mg na dan prednizona ali ekvivalenta); aktivno tuberkulozo ali okužbo s hepatitisom B ali C ali HIV; bolniki, ki so prejeli živo oslabljeno cepivo v 30 dneh pred začetkom zdravljenja z zdravilom Imfinzi ali v 30 dneh po začetku. Dokler takšnih podatkov ni, je treba durvalumab v teh skupinah bolnikov uporabljati previdno ter po skrbnem individualnem pretehtanju možnih koristi in tveganj za posameznega bolnika.

**MEDESEBOJNO DELOVANJE Z DRUGIMI ZDRAVILI:** Razen fizioloških odmerkov sistemskih kortikosteroidov ( $\leq 10$  mg na dan prednizona ali ekvivalenta) pred uvedbo durvalumaba ni priporočljivo uporabljati sistemskih kortikosteroidov ali imunosupresivov, ker lahko vplivajo na farmakodinamično aktivnost in učinkovitost durvalumaba. Vendar pa je mogoče kortikosteroide ali druge imunosupresive uporabiti po začetku zdravljenja z durvalumabom za zdravljenje imunske pogojene neželene učinke. Z durvalumabom niso izvedli formalnih farmakokinetičnih (PK študij) medsebojnega delovanja zdravil. Primarni opitni odstranjevanja durvalumaba sta katabolizem beljakovin preko retikuloendotelijskega sistema oziroma tarčno posredovano odstranjevanje, zato ni pričakovati presnovnih medsebojnih delovanj med zdravili.

**NEZELENI UČINKI: VARNOST ZDRAVILA IMFINZI (10 mg/kg) SO OVRDNOTILI V ŠTUDIJU PACIFIC (n = 475) PRI BOLNIKI Z lokalno napredovalim neoperabilnim NSCLC, ki so opravili zdravljenje z najmanj 2 cikloma sočasne kemoradioterapije od 1 do 42 dni pred vključitvijo v študijo. V tej populaciji bolnikov so bili najbolj pogosti neželeni učinki: kašelj (40,2 % v primerjavi s 30,3 % pri uporabi placeba), okužbe zgornjih dihal (26,1 % v primerjavi s 11,5 % pri uporabi placeba) in izpuščaji (21,7 % v primerjavi s 12,0 % pri uporabi placeba). Najbolj pogost neželeni učinek 3. - 4. stopnje je bila pljučnica (6,5 % v primerjavi s 5,6 % pri uporabi placeba). Pojavnost vseh neželenih učinkov 3. ali 4. stopnje je bila 12,8 % v skupini z zdravilom Imfinzi v primerjavi z 9,8 % v skupini s placebom. Zelo pogosti neželeni učinki: okužbe zgornjih dihal, pljučnica, hipotiroizem, kašelj/productiven kašelj, pnevmonitis, driska, bolečine v trebuhu, izpuščaji, srbenje, zvišana telesna temperatura. Pogosti neželeni učinki: zorne okužbe in okužbe ušstnih mehkih tkiv, oralna kandidoza, gripa, hipertiroizem, distonija, kolitis, zvišane vrednosti aspartat aminotransferaze ali zvišanje vrednosti alanin aminotransferazek, nočno znojenje, dermatitis, mialgija, zvišanje vrednosti kreatinina v krvi, disurija, periferni edemi, z infundiranjem povezane reakcije. Občasni neželeni učinki: adrenalna insuficienca, sladkorna bolezen tipa 1, intersticijska bolezen pljuč, hepatitis, miozitis, nefritis. Redki neželeni učinki: hipofizitis / hipopituitarizem, diabetes insipidus, polimiozitis.**

**VRSTA IN VSEBINA OVOJNINE:** 2,4 ml koncentrata v stekleni viali iz stekla tipa 1 z elastomernim zamaškom in belo snemno aluminjsko zaporo; viala vsebuje 120 mg durvalumaba. Pakiranje vsebuje 1 vialo.

10 ml koncentrata v stekleni viali iz stekla tipa 1 z elastomernim zamaškom in belo snemno aluminjsko zaporo; viala vsebuje 500 mg durvalumaba. Pakiranje vsebuje 1 vialo.

**NAČIN IZDAJANJA ZDRAVILA:** samo na recept DATUM REVIZIJA BESEDE: september 2018 (SI-0376) IMETNIK DOVOLJENJA ZA PROMET: AstraZeneca AB, S-151 85, Soderatelj, Švedska

Pred predpisovanjem, prosimo, preberite celoten povzetek glavnih značilnosti zdravila. Zdravilo v Sloveniji še ni razvrščeno na listo. Dodatne informacije so na voljo pri družbi AstraZeneca UK Limited, Podružnica v Sloveniji, Verovškova 55, Ljubljana. Samo za strokovno javnost. Informacija pripravljena: oktober 2018.

AstraZeneca

SI-4409

Zdravilo za predhodno že zdravljene bolnike z mKRR

# Več časa za trenutke, ki štejejo

  
trifluridin/tipiracil

## Spremeni zgodbo predhodno že zdravljenih bolnikov z mKRR

LONSURF® (trifluridin/tipiracil) je indiciran za zdravljenje odraslih bolnikov z metastatskim kolorektalnim rakom (mKRR), ki so bili predhodno že zdravljeni ali niso primerni za zdravljenja, ki so na voljo. Ta vključujejo kemoterapijo na osnovi fluoropirimidina, oksaliplatinina in irinotekana, zdravljenje z zaviralci žilnega endotelijskega rastnega dejavnika (VEGF) in zaviralci receptorjev za epidermalni rastni dejavnik (EGFR).

Družba Servier ima licenco družbe Taiho za zdravilo Lonsurf®. Pri globalnem razvoju zdravila sodelujeta obe družbi in ga tržita na svojih določenih področjih.

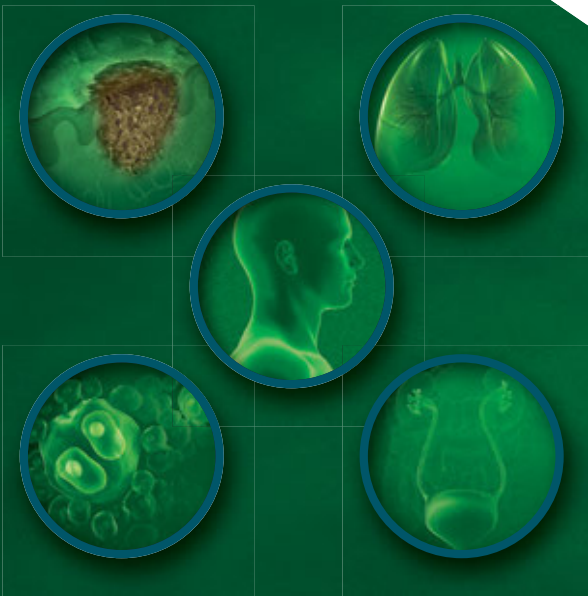


TAIHO PHARMACEUTICAL CO., LTD.



### Skrajšan povzetek glavnih značilnosti zdravila: Lonsurf 15 mg/6,14 mg filmsko obložene tablete in Lonsurf 20 mg/8,19 mg filmsko obložene tablete

▼ Za to zdravilo se izvaja dodatno spremljanje varnosti. **SESTAVA\***: Lonsurf 15 mg/6,14 mg: Ena filmsko obložena tableta vsebuje 15 mg trifluridina in 6,14 mg tipiracila (v obliki klorida). Lonsurf 20 mg/8,19 mg: Ena filmsko obložena tableta vsebuje 20 mg trifluridina in 8,19 mg tipiracila (v obliki klorida). **TERAPEVTSKE INDIKACIJE\***: Zdravilo Lonsurf je indicirano za zdravljenje odraslih bolnikov z metastatskim kolorektalnim rakom, ki so bili predhodno že zdravljeni ali niso primerni za zdravljenja, ki so na voljo. Ta vključujejo kemoterapijo na osnovi fluoropirimidina, oksaliplatinina in irinotekana, zdravljenje z zaviralci žilnega endotelijskega rastnega dejavnika (VEGF - Vascular Endothelial Growth Factor) in zaviralci receptorjev za epidermalni rastni dejavnik (EGFR - Epidermal Growth Factor Receptor). **ODMERJANJE IN NAČIN UPORABE\***: Priporočeni začetni odmerek zdravila Lonsurf pri odraslih je 35 mg/m<sup>2</sup>/odmerek peroralno dvakrat dnevno na 1. do 5. dan in 8. do 12. dan vsakega 28-dnevnega cikla zdravljenja, najpozneje 1 uro po zaključku jutranjega in večernega obroka. Odmerjanje, izračunano glede na telesno površino, ne sme preseči 80 mg/odmerek. Možne prilagoditve odmerka glede na varnost in prenašanje zdravila: dovoljena so največ 3 zmanjšanja odmerka na najmanjši odmerek 20 mg/m<sup>2</sup> dvakrat dnevno. Potem ko je bil odmerek zmanjšan, povečanje ni dovoljeno. **KONTRAINDIKACIJE\***: Preobčutljivost na zdravilni učinkovini ali katero koli pomožno snov. **OPAZORILA IN PREVIDNOSTNI UKREPI\***: Supresija kostnega mozga: Pred uvedbo zdravljenja, pred vsakim ciklom zdravljenja in po potrebi je treba pregledati celotno krvno sliko. Zdravljenja ne smete začeti, če je absolutno število nevtrofilcev < 1,5 x 10<sup>9</sup>/l, če je število trombocitov < 75 x 10<sup>9</sup>/l ali če se je pri bolniku zaradi predhodnih zdravljenj pojavila klinično pomembna hematološka toksičnost 3. ali 4. stopnje, ki še traja. Bolnike je treba skrbno spremljati zaradi morebitnih okužb, uvesti je treba ustrezne ukrepe, kot je klinično indicirano. **Toksičnost za prebavila**: Potrebna je uporaba antiemetikov, antidiaroidov ter drugih ukrepov, kot je klinično indicirano. **Ledvična okvara**: Zdravilo Lonsurf ni primerno za uporabo pri bolnikih s hudo ledvično okvaro ali končno stopnjo ledvične okvare. Bolnike z zmerno ledvično okvaro je treba zaradi hematološke toksičnosti bolj pogosto spremljati. **Jatna okvara**: Uporaba zdravila Lonsurf pri bolnikih z obstoječo zmerno ali hudo jetno okvaro ni priporočljiva. **Proteinurija**: Pred začetkom zdravljenja in med njim je priporočljivo spremljanje proteinurije z urinskimi testnimi lističi. **Pomožne snovi**: Zdravilo vsebuje laktozo. **INTERAKCIJE\***: Zdravila, ki medsebojno delujejo z nukleozidnimi prenašalci CNT1, ENT1 in ENT2, zaviralci OCT2 ali MATE1, substrati humane timidin-kinaze (npr. zidovudinom), hormonskimi kontraceptivi. **PLODNOST\*, NOSEČNOST IN DOJENJE\***: Ni priporočljivo. **KONTRACEPCIJA\***: Ženske in moški morajo uporabljati učinkovito metodo kontracepcije med zdravljenjem in do 6 mesecev po zaključku zdravljenja. **VPLIV NA SPOSOBNOST VOZNIJE IN UPRAVLJANJA S STROJI\***: Med zdravljenjem se lahko pojavijo utrujenost, omotica ali splošno slabo počutje. **NEZELENI UČINKI\***: **Zelo pogosti**: nevtropenija, levkopenija, anemija, trombocitopenija, zmanjšan apetit, diareja, navzea, bruhanje, utrujenost. **Pogosti**: okužba spodnjih dihal, okužba zgornjih dihal, febrilna nevtropenija, limfopenija, monocitoza, hipalbuminemija, nespečnost, disgevizija, periferna nevropatija, omotica, glavobol, vročinski oblivi, dispneja, kašelj, bolečina v trebuhu, zaprtje, stomatitis, boleznj ustne votline, hiperbilirubinemija, sindrom palmarne plantarne eritrodisezije, izpuščaj, alopecija, pruritus, suha koža, proteinurija, pikeksija, edem, vnetje sluznice, splošno slabo počutje, zvišanje jetrnih encimov, zvišanje alkalne fosfataze v krvi, zmanjšanje telesne mase. **Občasni**: septični šok, infektivni enteritis, pljučnica, okužba žolčevoda, gripa, okužba sečil, vnetje dlesni, herpes zoster, tinea pedis, kandidiaza, bakterijska okužba, okužba, bolečina zaradi raka, pancitopenija, granulocitopenija, monocitopenija, eritropenija, levkocitoza, dehidracija, hiperpigmentacija, hiperkalemija, hipofosfatemija, hipernatriemija, hiponatremija, hipokalciemija, protin, anksioznost, nevtrotoksičnost, disestezijska, hiperestezijska, hipostezijska, sinkopa, parestezijska, pekoč občutek, letargija, zmanjšana ostrina vida, zamajen vid, diplopija, katarakta, konjunktivitis, suho oko, vrtoglavica, neugode v ušesu, angina pectoris, aritmija, palpitanje, embolija, hipertenzija, hipotenzija, pljučna embolija, pleuralni izliv, izcedek iz nosu, distonija, orofaringealna bolečina, epistaksa, hemoragični enterokolitis, krvavitev v prebavilih, akutni pankreatitis, ascites, ileus, subileus, kolitis, gastritis, refluksni gastritis, ezofagitis, moteno praznjenje želodca, abdominalna distenzija, analno vnetje, razjede v ustih, dispnejska, gastrozofagealna refluksna bolezen, proktalgija, bukalni polip, krvavitev dlesni, glositis, parodontalna bolezen, bolezen zob, siljenje na bruhanje, flatulenca, slab zadah, hepatotoksičnost, razširitev žolčnih vodov, luščenje kože, urtikarija, preobčutljivostne reakcije na svetlobo, eritem, akne, hiperhidroza, žulj, boleznj nohtov, otekanje sklepov, artralgija, bolečina v kosteh, mialgija, mišično-skeletna bolečina, mišična oslabelost, mišični krči, bolečina v okončinah, občutek teže, ledvična odpoved, neinfektivni cistitis, motnje mikcije, hematurija, levkociturija, motnje menstruacije, poslabšanje splošnega zdravstvenega stanja, bolečina, občutek spremembe telesne temperature, kseroza, zvišanje kreatinina v krvi, podaljšanje intervala QT na elektrokardiogramu, povečanje mednarodnega umerjenega razmerja (INR), podaljšanje aktiviranega parcialnega trombolastinskega časa (aPTC), zvišanje sečnine v krvi, zvišanje laktatne dehidrogenaze v krvi, znižanje celokupnih proteinov, zvišanje C-reaktivnega proteina, zmanjšan hematokrit. **Post-marketingne izkušnje**: pri bolnikih, zdravljenih z zdravilom Lonsurf na Japonskem, so poročali o primerih intersticijske boleznj pljuč. **PREVELIKO ODMERJANJE\***: Neželeni učinki, o katerih so poročali v povezavi s prevelikim odmerjanjem, so bili v skladu z uveljavljenim varnostnim profilom. Glavni pričakovani zaplet prevelikega odmerjanja je supresija kostnega mozga. **FARMAKODINAMIČNE LASTNOSTI\***: Farmakoterapevtska skupina: zdravila z delovanjem na novotvorbe, antimetaboliti, oznaka ATC: L01BC59. Zdravilo Lonsurf sestavlja antineoplastični timidinski nukleozidni analog, trifluridin, in zaviralec timidin-fosforilaze (TPaze), tipiraciljev klorid. Po prizemu v rakave celice timidin-kinaza fosforilira trifluridin. Ta se v celicah nato presnovi v substrat deoksiribonukleinske kisline (DNA), ki se vgradi neposredno v DNA ter tako preprečuje celično proliferacijo. TPaza hitro razgradi trifluridin in njegova presnova po peroralni uporabi je hitra zaradi učinka prvega prehoda, zato je v zdravilo vključen zaviralec TPaze, tipiraciljev klorid. **PAKIRANJE\***: 20 filmsko obloženih tablet. **NAČIN PREDPISOVANJA IN IZDAJE ZDRAVILA**: Rp/Spec. **Imetnik dovoljenja za promet**: Les Laboratoires Servier, 50, rue Camot, 92284 Suresnes cedex, Francija. **Številka dovoljenja za promet z zdravilom**: EU/1/16/1096/001 (Lonsurf 15 mg/6,14 mg), EU/1/16/1096/004 (Lonsurf 20 mg/8,19 mg). **Datum zadnje revizije besedila**: avgust 2017. \* Pred predpisovanjem preberite celoten povzetek glavnih značilnosti zdravila. Celoten povzetek glavnih značilnosti zdravila in podrobnejše informacije so na voljo pri: Servier Pharma d.o.o., Podmiščakova ulica 24, 1000 Ljubljana, tel: 01 563 48 11, www.servier.si.



- Melanoma<sup>1</sup>
- Non-small cell lung carcinoma<sup>1</sup>
- Urothelial carcinoma<sup>1</sup>
- Classical Hodgkin Lymphoma<sup>1</sup>
- Head and neck squamous cell carcinoma<sup>1</sup>

References: 1. Keytruda EU SmPC

**ABBREVIATED PRESCRIBING INFORMATION Before prescribing please read full Summary of Product Characteristics!**

▼ This medicinal product is subject to additional monitoring.

**Name of the product:** KEYTRUDA 25 mg/mL concentrate for solution for infusion. • **Therapeutic indications:** KEYTRUDA as monotherapy is indicated for the treatment of advanced (unresectable or metastatic) melanoma in adults; for the adjuvant treatment of adults with Stage III melanoma and lymph node involvement who have undergone complete resection; for the first-line treatment of metastatic non-small cell lung carcinoma (NSCLC) in adults whose tumours express PD-L1 with a  $\geq 50\%$  tumour proportion score (TPS) with no EGFR or ALK positive tumour mutations; for the treatment of locally advanced or metastatic NSCLC in adults whose tumours express PD-L1 with a  $\geq 1\%$  TPS and who have received at least one prior chemotherapy regimen. Patients with EGFR or ALK positive tumour mutations should also have received targeted therapy before receiving KEYTRUDA; for the treatment of adult patients with relapsed or refractory classical Hodgkin lymphoma (cHL) who have failed autologous stem cell transplant (ASCT) and brentuximab vedotin (BV), or who are transplant-ineligible and have failed BV; for the treatment of locally advanced or metastatic urothelial carcinoma in adults who have received prior platinum-containing chemotherapy; for the treatment of locally advanced or metastatic urothelial carcinoma in adults who are not eligible for cisplatin-containing chemotherapy and whose tumours express PD-L1 with a combined positive score (CPS)  $\geq 10$ ; for the treatment of recurrent or metastatic head and neck squamous cell carcinoma (HNSCC) in adults whose tumours express PD-L1 with a  $\geq 50\%$  TPS and progressing on or after platinum-containing chemotherapy. KEYTRUDA in combination with pemtrexed and platinum chemotherapy, is indicated for the first-line treatment of metastatic non-squamous NSCLC in adults whose tumours have no EGFR or ALK positive mutations. • **Posology and method of administration:** PD-L1 testing for patients with NSCLC, urothelial carcinoma or HNSCC: Testing for PD-L1 tumour expression using a validated test is recommended for patients with NSCLC. Patients with previously untreated urothelial carcinoma or HNSCC should be selected for treatment based on the tumour expression of PD-L1 confirmed by a validated test. Posology: The recommended dose of KEYTRUDA is 200 mg administered as an intravenous infusion over 30 minutes every 3 weeks. When administering KEYTRUDA as part of a combination with pemtrexed and platinum chemotherapy, KEYTRUDA should be administered first. Patients should be treated with KEYTRUDA until disease progression or unacceptable toxicity. For the adjuvant treatment of melanoma, KEYTRUDA should be administered until disease recurrence, unacceptable toxicity, or for a duration of up to one year. In elderly patients, patients with mild or moderate renal impairment, patients with mild hepatic impairment no dose adjustment is needed. Dose delay or discontinuation: When KEYTRUDA should be withheld until adverse reactions recover to Grade 0-1 and when KEYTRUDA should be permanently discontinued please consult full Summary of Product Characteristics of Keytruda.

• **Contraindications:** Hypersensitivity to the active substance or to any of the excipients. • **Special warnings and precautions for use:** Immune-related adverse reactions: (pneumonitis, colitis, hepatitis, nephritis, endocrinopathies, skin adverse reactions and other) including severe and fatal cases, have occurred in patients receiving pembrolizumab. Most immune-related adverse reactions occurring during treatment with pembrolizumab were reversible and managed with interruptions of pembrolizumab, administration of corticosteroids and/or supportive care. Immune-related adverse reactions have also occurred after the

last dose of pembrolizumab, affecting more than one body system can occur simultaneously. For suspected immune-related adverse reactions, adequate evaluation to confirm aetiology or exclude other causes should be ensured. Based on the severity of the adverse reaction, pembrolizumab should be withheld and corticosteroids administered- for detail information please read full Summary of Product Characteristics of Keytruda. Treatment with pembrolizumab may increase the risk of rejection in solid organ transplant recipients. Severe infusion-related reactions, including hypersensitivity and anaphylaxis, have been reported in patients receiving pembrolizumab. Please read full Summary of Product Characteristics of Keytruda. Since pembrolizumab is cleared from the circulation through catabolism, no metabolic drug-drug interactions are expected. The use of systemic corticosteroids or immunosuppressants before starting pembrolizumab should be avoided because of their potential interference with the pharmacodynamic activity and efficacy of pembrolizumab. However, systemic corticosteroids or other immunosuppressants can be used after starting pembrolizumab to treat immune-related adverse reactions. Women of childbearing potential should use effective contraception during treatment with pembrolizumab and for at least 4 months after the last dose of pembrolizumab and pembrolizumab should not be used during pregnancy and breast-feeding. Safety of pembrolizumab as monotherapy has been evaluated in 4,948 patients with advanced melanoma, resected Stage III melanoma (adjuvant therapy), NSCLC, cHL, urothelial carcinoma, or HNSCC across four doses (2 mg/kg every 3 weeks, 200 mg every 3 weeks, or 10 mg/kg every 2 or 3 weeks) in clinical studies. In this patient population, the median observation time was 7.3 months (range: 1 day to 31 months) and the most frequent adverse reactions with pembrolizumab were fatigue (34.1%), rash (22.7%), nausea (21.7%), diarrhoea (21.5%), and pruritus (20.2%). The majority of adverse reactions reported for monotherapy were of Grade 1 or 2 severity. The most serious adverse reactions were immune-related adverse reactions and severe infusion-related reactions. The safety of pembrolizumab in combination with pemtrexed and platinum chemotherapy has been evaluated in 488 patients with non-squamous NSCLC receiving 200 mg, 2 mg/kg or 10 mg/kg pembrolizumab every 3 weeks, in two clinical studies. In this patient population, the most frequent adverse reactions were nausea (47%), anaemia (37%), fatigue (38%), neutropenia (22%), decreased appetite (21%), diarrhoea (20%) and vomiting (19%). Incidences of Grade 3-5 adverse reactions were 47% for pembrolizumab combination therapy and 37% for chemotherapy alone. **For the complete information on adverse reactions and their management please read full Summary of Product Characteristics.** • **Method of dispensing:** Medicinal product subject to medical prescription and can be used only in hospitals. • **Marketing Authorisation holder:** Merck Sharp & Dohme B.V., Waarderweg 39, 2031 BN Haarlem, The Netherlands. • **Marketing Authorisation Number:** EU/1/15/1024/002 • **Date of revision of the text:** 11. January 2019.



Merck Sharp & Dohme inovativna zdravila d.o.o.,  
Šmartinska cesta 140, 1000 Ljubljana  
phone: +386 1/ 520 42 01, fax: +386 1/ 520 43 50  
Prepared in Slovenia, January 2019; ONCO-1279675-0000 EXP: 01/2021

**Before prescribing please read full Summary of Product Characteristics!  
For healthcare professionals only.**

# Instructions for authors

## The editorial policy

Radiology and Oncology is a multidisciplinary journal devoted to the publishing original and high quality scientific papers and review articles, pertinent to diagnostic and interventional radiology, computerized tomography, magnetic resonance, ultrasound, nuclear medicine, radiotherapy, clinical and experimental oncology, radiobiology, radiophysics and radiation protection. Therefore, the scope of the journal is to cover beside radiology the diagnostic and therapeutic aspects in oncology, which distinguishes it from other journals in the field.

The Editorial Board requires that the paper has not been published or submitted for publication elsewhere; the authors are responsible for all statements in their papers. Accepted articles become the property of the journal and, therefore cannot be published elsewhere without the written permission of the editors.

## Submission of the manuscript

The manuscript written in English should be submitted to the journal via online submission system Editorial Manager available for this journal at: [www.radioloncol.com](http://www.radioloncol.com).

In case of problems, please contact Sašo Trupej at [saso.trupej@computing.si](mailto:saso.trupej@computing.si) or the Editor of this journal at [gsera@onko-i.si](mailto:gsera@onko-i.si)

All articles are subjected to the editorial review and when the articles are appropriated they are reviewed by independent referees. In the cover letter, which must accompany the article, the authors are requested to suggest 3-4 researchers, competent to review their manuscript. However, please note that this will be treated only as a suggestion; the final selection of reviewers is exclusively the Editor's decision. The authors' names are revealed to the referees, but not vice versa.

Manuscripts which do not comply with the technical requirements stated herein will be returned to the authors for the correction before peer-review. The editorial board reserves the right to ask authors to make appropriate changes of the contents as well as grammatical and stylistic corrections when necessary. Page charges will be charged for manuscripts exceeding the recommended length, as well as additional editorial work and requests for printed reprints.

Articles are published printed and on-line as the open access (<https://content.sciendo.com/raon>).

All articles are subject to 700 EUR + VAT publication fee. Exceptionally, waiver of payment may be negotiated with editorial office, upon lack of funds.

Manuscripts submitted under multiple authorship are reviewed on the assumption that all listed authors concur in the submission and are responsible for its content; they must have agreed to its publication and have given the corresponding author the authority to act on their behalf in all matters pertaining to publication. The corresponding author is responsible for informing the coauthors of the manuscript status throughout the submission, review, and production process.

## Preparation of manuscripts

Radiology and Oncology will consider manuscripts prepared according to the Uniform Requirements for Manuscripts Submitted to Biomedical Journals by International Committee of Medical Journal Editors ([www.icmje.org](http://www.icmje.org)). The manuscript should be written in grammatically and stylistically correct language. Abbreviations should be avoided. If their use is necessary, they should be explained at the first time mentioned. The technical data should conform to the SI system. The manuscript, excluding the references, tables, figures and figure legends, must not exceed 5000 words, and the number of figures and tables is limited to 8. Organize the text so that it includes: Introduction, Materials and methods, Results and Discussion. Exceptionally, the results and discussion can be combined in a single section. Start each section on a new page, and number each page consecutively with Arabic numerals.

*The Title page* should include a concise and informative title, followed by the full name(s) of the author(s); the institutional affiliation of each author; the name and address of the corresponding author (including telephone, fax and E-mail), and an abbreviated title (not exceeding 60 characters). This should be followed by the abstract page, summarizing in less than 250 words the reasons for the study, experimental approach, the major findings (with specific data if possible), and the principal conclusions, and providing 3-6 key words for indexing purposes. Structured abstracts are required. Slovene authors are requested to provide title and the abstract in Slovene language in a separate file. The text of the research article should then proceed as follows:

*Introduction* should summarize the rationale for the study or observation, citing only the essential references and stating the aim of the study.

*Materials and methods* should provide enough information to enable experiments to be repeated. New methods should be described in details.

*Results* should be presented clearly and concisely without repeating the data in the figures and tables. Emphasis should be on clear and precise presentation of results and their significance in relation to the aim of the investigation.

*Discussion* should explain the results rather than simply repeating them and interpret their significance and draw conclusions. It should discuss the results of the study in the light of previously published work.

### Charts, Illustrations, Images and Tables

Charts, Illustrations, Images and Tables must be numbered and referred to in the text, with the appropriate location indicated. Charts, Illustrations and Images, provided electronically, should be of appropriate quality for good reproduction. Illustrations and charts must be vector image, created in CMYK color space, preferred font "Century Gothic", and saved as .AI, .EPS or .PDF format. Color charts, illustrations and Images are encouraged, and are published without additional charge. Image size must be 2,000 pixels on the longer side and saved as .JPG (maximum quality) format. In Images, mask the identities of the patients. Tables should be typed double-spaced, with a descriptive title and, if appropriate, units of numerical measurements included in the column heading. The files with the figures and tables can be uploaded as separate files.

### References

References must be numbered in the order in which they appear in the text and their corresponding numbers quoted in the text. Authors are responsible for the accuracy of their references. References to the Abstracts and Letters to the Editor must be identified as such. Citation of papers in preparation or submitted for publication, unpublished observations, and personal communications should not be included in the reference list. If essential, such material may be incorporated in the appropriate place in the text. References follow the style of Index Medicus, DOI number (if exists) should be included.

All authors should be listed when their number does not exceed six; when there are seven or more authors, the first six listed are followed by "et al.". The following are some examples of references from articles, books and book chapters:

Dent RAG, Cole P. In vitro maturation of monocytes in squamous carcinoma of the lung. *Br J Cancer* 1981; **43**: 486-95. doi: 10.1038/bjc.1981.71

Chapman S, Nakielny R. *A guide to radiological procedures*. London: Bailliere Tindall; 1986.

Evans R, Alexander P. Mechanisms of extracellular killing of nucleated mammalian cells by macrophages. In: Nelson DS, editor. *Immunobiology of macrophage*. New York: Academic Press; 1976. p. 45-74.

### Authorization for the use of human subjects or experimental animals

When reporting experiments on human subjects, authors should state whether the procedures followed the Helsinki Declaration. Patients have the right to privacy; therefore the identifying information (patient's names, hospital unit numbers) should not be published unless it is essential. In such cases the patient's informed consent for publication is needed, and should appear as an appropriate statement in the article. Institutional approval and Clinical Trial registration number is required. Retrospective clinical studies must be approved by the accredited Institutional Review Board/Committee for Medical Ethics or other equivalent body. These statements should appear in the Materials and methods section.

The research using animal subjects should be conducted according to the EU Directive 2010/63/EU and following the Guidelines for the welfare and use of animals in cancer research (*Br J Cancer* 2010; **102**: 1555 – 77). Authors must state the committee approving the experiments, and must confirm that all experiments were performed in accordance with relevant regulations.

These statements should appear in the Materials and methods section (or for contributions without this section, within the main text or in the captions of relevant figures or tables).

### Transfer of copyright agreement

For the publication of accepted articles, authors are required to send the License to Publish to the publisher on the address of the editorial office. A properly completed License to Publish, signed by the Corresponding Author on behalf of all the authors, must be provided for each submitted manuscript.

The non-commercial use of each article will be governed by the Creative Commons Attribution-NonCommercial-NoDerivs license.

### Conflict of interest

When the manuscript is submitted for publication, the authors are expected to disclose any relationship that might pose real, apparent or potential conflict of interest with respect to the results reported in that manuscript. Potential conflicts of interest include not only financial relationships but also other, non-financial relationships. In the Acknowledgement section the source of funding support should be mentioned. The Editors will make effort to ensure that conflicts of interest will not compromise the evaluation process of the submitted manuscripts; potential editors and reviewers will exempt themselves from review process when such conflict of interest exists. The statement of disclosure must be in the Cover letter accompanying the manuscript or submitted on the form available on [www.icmje.org/coi\\_disclosure.pdf](http://www.icmje.org/coi_disclosure.pdf)

### Page proofs

Page proofs will be sent by E-mail to the corresponding author. It is their responsibility to check the proofs carefully and return a list of essential corrections to the editorial office within three days of receipt. Only grammatical corrections are acceptable at that time.

### Open access

Papers are published electronically as open access on <https://content.sciendo.com/raon>, also papers accepted for publication as E-ahead of print.



# XALKORI® - 1. linija zdravljenja napredovalega, ALK pozitivnega nedrobnoceličnega pljučnega raka<sup>1</sup>

ALK = anaplastična limfomska kinaza

## BISTVENI PODATKI IZ POVZETKA GLAVNIH ZNAČILNOSTI ZDRAVILA

### XALKORI 200 mg, 250 mg trde kapsule

▼ Za to zdravilo se izvaja dodatno spremljanje varnosti. Tako bodo hitreje na voljo nove informacije o njegovi varnosti. Zdravstvene delavce naprošamo, da poročajo o kateremkoli domnevnem neželenem učinku zdravila. Glejte poglavje 4.8 povzetka glavnih značilnosti zdravila, kako poročati o neželenih učinkih.

**Sestava in oblika zdravila:** Ena kapsula vsebuje 200 mg ali 250 mg krizotiniba. **Indikacije:** Monoterapija za: - prvo linijo zdravljenja odraslih bolnikov z napredovalim nedrobnoceličnim pljučnim rakom (NSCLC - *Non-Small Cell Lung Cancer*), ki je ALK (anaplastična limfomska kinaza) pozitiven; - zdravljenje odraslih bolnikov s predhodno zdravljenim, napredovalim NSCLC, ki je ALK pozitiven; - zdravljenje odraslih bolnikov z napredovalim NSCLC, ki je ROS1 pozitiven. **Odmerjanje in način uporabe:** Zdravljenje mora uvesti in nadzorovati zdravnik z izkušnjami z uporabo zdravil za zdravljenje rakavih bolezni. **Preverjanje prisotnosti ALK in ROS1:** Pri izbiri bolnikov za zdravljenje je treba pred zdravljenjem opraviti točno in validirano preverjanje prisotnosti ALK ali ROS1. **Odmerjanje:** Priporočeni odmerek je 250 mg dvakrat na dan (500 mg na dan), bolniki pa morajo zdravilo jemati brez prekinitev. Če bolnik pozabi vzeti odmerek, ga mora vzeti takoj, ko se spomni, razen če do naslednjega odmerka manjka manj kot 6 ur. V tem primeru bolnik pozabljenega odmerka ne sme vzeti.

**Prilaganja odmerkov:** Glede na varnost uporabe zdravila pri posameznem bolniku in kako bolnik zdravljenje prenaša, utegne biti potrebna prekinitev in/ali zmanjšanje odmerka pri bolnikih, ki se zdravijo s krizotinibom 250 mg peroralno dvakrat na dan (za režim zmanjševanja odmerka glejte poglavje 4.2 v povzetku glavnih značilnosti zdravila). Za prilaganje odmerkov pri hematološki in nehematološki toksičnosti (povečanje vrednosti AST, ALT, bilirubina; ILD/pnevmonitis; podaljšanje intervala QTc, bradikardija, boleznici oči) glejte preglednici 1 in 2 v poglavju 4.2 povzetka glavnih značilnosti zdravila. **Okvara jeter:** Pri zdravljenju pri bolnikih z okvaro jeter je potrebna previdnost. Pri blagi okvari jeter prilaganje začetnega odmerka ni priporočeno, pri zmerni okvari jeter je priporočeni začetni odmerek 200 mg dvakrat na dan, pri hudi okvari jeter pa 250 mg enkrat na dan (za merila glede klasifikacije okvare jeter glejte poglavje 4.2 v povzetku glavnih značilnosti zdravila). **Okvara ledvic:** Pri blagi in zmerni okvari prilaganje začetnega odmerka ni priporočeno. Pri hudi okvari ledvic (ki ne zahteva peritonealne dialize ali hemodialize) je začetni odmerek 250 mg peroralno enkrat na dan; po vsaj 4 tednih zdravljenja se lahko poveča na 200 mg dvakrat na dan. **Starejši bolniki (≥ 65 let):** Prilaganje začetnega odmerka ni potrebno. **Pediatrična populacija:** Varnost in učinkovitost nista bili dokazani.

**Način uporabe:** Kapsule je treba pogoltniti cele, z nekaj vode, s hrano ali brez nje. Ne sme se jih zdrobiti, raztopiti ali odpreti. Izogibati se je treba uživanju grenivk, grenivkinega soka ter uporabi šentjanževke. **Kontraindikacije:** Preobčutljivost na krizotinol ali katerokoli pomožno snov. **Posebna opozorila in previdnostni ukrepi:** **Določanje statusa ALK in ROS1:** Pomembno je izbrati dobro validirano in robustno metodologijo, da se izognemo lažno negativnim ali lažno pozitivnim rezultatom. **Hepatotoksičnost:** V kliničnih študijah so poročali o hepatotoksičnosti, ki jo je povzročilo zdravilo (vključno s primeri s smrtnim izidom). Delovanje jeter, vključno z ALT, AST in skupnim bilirubinom, je treba preveriti enkrat na teden v prvih 2 mesecih zdravljenja, nato pa enkrat na mesec in kot je klinično indicirano. Ponovite preverjanj morajo biti pogostejše pri povečanih vrednostih stopnje 2, 3 ali 4. **Intersticijska bolezen pljuč (ILD)/pnevmonitis:** Lahko se pojavi huda, življenjsko nevarna ali smrtna ILD/pnevmonitis. Bolnike s simptomi ILD/pnevmonitisa je treba spremljati,

zdravljenje pa prekiniti ob sumu na ILD/pnevmonitis. **Podaljšanje intervala QT:** Opažali so podaljšanje intervala QTc. Pri bolnikih z obstoječo bradikardijo, podaljšanjem intervala QTc v anamnezi ali predispozicijo zanj, pri bolnikih, ki jemljejo antiaritmike ali druga zdravila, ki podaljšujejo interval QT, ter pri bolnikih s pomembno obstoječo srčno boleznijo in/ali motnjami elektrolitov je treba krizotinib uporabljati previdno; potrebno je redno spremljanje EKG, elektrolitov in delovanja ledvic; preiskavi EKG in elektrolitov je treba opraviti čimbržje uporabi prvega odmerka, potem se priporoča redno spremljanje. Če se interval QTc podaljša za 60 ms ali več, je treba zdravljenje s krizotinibom začasno prekiniti in se posvetovati s kardiologom. **Bradikardija:** Lahko se pojavi simptomatska bradikardija (lahko se razvije več tednov po začetku zdravljenja); izogibati se je treba uporabi krizotiniba v kombinaciji z drugimi zdravili, ki povzročajo bradikardijo; pri simptomatski bradikardiji je treba prilagoditi odmerek. **Srčno popuščanje:** Poročali so o hudih, življenjsko nevarnih ali smrtnih neželenih učinkih srčnega popuščanja. Bolnike je treba spremljati glede pojavov znakov in simptomov srčnega popuščanja in ob pojavu simptomov zmanjšati odmerjanje ali prekiniti zdravljenje. **Nevropenija in levkopenija:** V kliničnih študijah so poročali o nevtropeniji, levkopeniji in febrilni nevtropeniji; spremljati je treba popolno krvno sliko (pogostejše preiskave, če se opazijo abnormalnosti stopnje 3 ali 4 ali če se pojavi povišana telesna temperatura ali okužba). **Perforacija v prebavilih:** V kliničnih študijah so poročali o perforacijah v prebavilih, v obdobju trženja pa o smrtnih primerih perforacij v prebavilih. Krizotinib je treba pri bolnikih s tveganjem za nastanek perforacije v prebavilih uporabljati previdno; bolniki, pri katerih se razvije perforacija v prebavilih, se morajo prenehati zdraviti s krizotinibom; bolnike je treba poučiti o prvih znakih perforacije in jim svetovati, naj se nemudoma posvetujejo z zdravnikom. **Vplivi na ledvice:** V kliničnih študijah so opazili zvišanje ravnih kreatinina v krvi in zmanjšanje čistka kreatinina. V kliničnih študijah in v obdobju trženja so poročali tudi o odpovedi ledvic, akutni odpovedi ledvic, primerih s smrtnim izidom, primerih, ki so zahtevali hemodializo in hiperkaliemiji stopnje 4. **Vplivi na vid:** V kliničnih študijah so poročali o izpadu vidnega polja stopnje 4 z izgubo vida. Če se na novo pojavi huda izguba vida, je treba zdravljenje prekiniti in opraviti oftalmološki pregled. Če so motnje vida trdovratne ali se poslabšajo, je priporočljiv oftalmološki pregled. **Histološka preiskava, ki ne nakazuje adenokarcinoma:** Na voljo so le omejeni podatki pri NSCLC, ki je ALK in ROS1 pozitiven in ima histološke značilnosti, ki ne nakazujejo adenokarcinoma, vključno s ploščatoceličnim karcinomom (SCC). **Medsebojno delovanje z drugimi zdravili in druge oblike interakcij:** Izogibati se je treba sočasni uporabi z močnimi zaviralci CYP3A4, npr. atazanavir, ritonavir, kobicistat, itraconazol, ketokonazol, posakonazol, vorikonazol, klaritromicin, telitromicin in eritromicin (razen če morebitna korist za bolnika odtehta tveganje, v tem primeru je treba bolnike skrbno spremljati glede neželenih učinkov krizotiniba), ter grenivko in grenivkinim sokom, saj lahko povečajo koncentracije krizotiniba v plazmi. Izogibati se je treba sočasni uporabi z močnimi induktorji CYP3A4, npr. karbamazepin, fenobarbital, fenitoin, rifampicin in šentjanževka, saj lahko zmanjšajo koncentracije krizotiniba v plazmi. Učinek zmernih induktorjev CYP3A4, npr. efavirenz in rifabutin, še ni jasan, zato se je treba sočasni uporabi s krizotinibom izogibati. Zdravila, katerih koncentracije v plazmi lahko krizotinib spremeni (midazolam, alfentanil, cisaprid, ciklosporin, derivati ergot alkaloidov, fentanil, pimizol, kinidin, sirolimus, takrolimus, digoksin, dabigatran, kolhicin, pravadstatin; sočasni uporabi s temi zdravili se je treba izogibati oziroma izvajati skrbni klinični nadzor; bupropion, efavirenz, peroralni kontraceptivi, raltegravir,



irinotekan, morfin, nalokson, metformin, prokinamid). Zdravila, ki podaljšujejo interval QT ali ki lahko povzročijo Torsades de pointes (antiaritmiki skupine IA (kinidin, disopiramid), antiaritmiki skupine III (amiodaron, sotalol, dofetilid, ibutilid), metadon, cisaprid, moksifloksacin, antipsihotiki) - v primeru sočasne uporabe je potreben skrben nadzor intervala QT. Zdravila, ki povzročajo bradikardijo (nedihidropiridinski zaviralci kalcijevih kanalčkov (verapamil, diltiazem), antagonisti adrenergičnih receptorjev beta, klonidin, gvanfacin, digoksin, meflokin, antiholinesteraze, pilokarpin) - krizotinib je treba uporabljati previdno. **Plodnost, nosečnost in dojenje:** Ženske v rodni dobi se morajo izogibati zanositvi. Med zdravljenjem in najmanj 90 dni po njem je treba uporabljati ustrezno kontracepcijo (velja tudi za moške). Zdravilo lahko škoduje plodu in se ga med nosečnostjo ne sme uporabljati, razen če klinično stanje matere ne zahteva takega zdravljenja. Matere naj se med jemanjem zdravila dojenju izogibajo. Zdravilo lahko zmanjša plodnost moških in žensk. **Vplivi na sposobnost vožnje in upravljanja strojev:** Lahko se pojavijo simptomatska bradikardija (npr. sinkopa, omotica, hipotenzija), motnje vida ali utrujenost; potrebna je previdnost. **Neželeni učinki:** Najresnejši neželeni učinki so bili hepatotoksičnost, ILD/pnevmonitis, nevtropenija in podaljšanje intervala QT. Najpogostejši neželeni učinki (≥ 25 %) so bili motnje vida, navzea, diareja, bruhanje, edem, zaprtje, povečane vrednosti transaminaz, utrujenost, pomanjkanje apetita, omotica in nevtropatija. Ostali zelo pogosti (≥ 1/10 bolnikov) neželeni učinki so: nevtropenija, anemija, levkopenija, disgeevzija, bradikardija, bolečina v trebuhu in izpuščaji. **Način in režim izdaje:** Predpisovanje in izdaja zdravila je le na recept, zdravilo pa se uporablja samo v bolnišnicah. Izjemoma se lahko uporabljata pri nadaljevanju zdravljenja na domu ob odpuštu iz bolnišnice in nadaljnjem zdravljenju. **Imetnik dovoljenja za promet:** Pfizer Europe MA EEEG, Boulevard de la Plaine 17, 1050 Bruxelles, Belgija. **Datum zadnje revizije besedila:** 23.10.2018.

**Pred predpisovanjem se seznanite s celotnim povzetkom glavnih značilnosti zdravila.**

**Vir:** 1. Povzetek glavnih značilnosti zdravila Xalkori, 23.10.18



Pfizer Luxembourg S.A.R.L., GRAND DUCHY OF LUXEMBOURG, 51, Avenue J.F. Kennedy, L-1855, Pfizer podružnica Ljubljana, Letališka cesta 29a, 1000 Ljubljana

